Understanding mechanisms of mitotic nuclear envelope reassembly using inducible relocalisation strategies

Laura Downie

Thesis submitted to the University of Warwick for the degree of

Doctor of Philosophy in Life Sciences (MIBTP DTP)

School of Life Sciences
University of Warwick

January 2023

Contents

List of Figures

List of Tables

List of Abbreviations

ABC	ammonium bicarbonate
ACN	acetonitrile
APC/C	Anaphase-promoting complex/cyclosome
BAF	Barrier-to-autointegration factor
Bub3	budding uninhibited by benzimidazoles 3
BubR1	budding uninhibited by benzimidazole-related 1
CAA	2-chloroacetamide
Cdc20	Cell Division Cycle protein 20
CDK	cyclin-dependent kinase
CENP-E	Centromere protein E
CENP-F	Centromere protein F
CHMP7	charged multivesicular body protein 7
CIN	Chromosome instability
CLEM	Correlative light-electron microscopy
CLIMP-63	cytoskeleton-linking membrane protein 63
CPC	Chromosomal Passenger Complex
CRISPR	clustered regularly interspaced short palindromic repeats
DAPI	4',6-diamidino-2-phenylindole
DMSO	dimethyl sulfoxide
DNA	Deoxyribonucleic acid
DTT	Dithiothreitol
ECL	enhanced chemiluminescence
EDMD	Emery-Dreifuss muscular dystrophy
EDTA	Ethylene diamine tetraacetic acid
ELYS	Embryonic large molecule derived from yolk sac
ER	endoplasmic reticulum
ESCRT	Endosomal sorting complex required for transport
EZ	Exclusion zone
FACS	Fluorescence-activated cell sorting

FKBP	FK506-binding protein
FRB	FKBP and rapamycin-binding
GFP	Green Fluorescent Protein
GO	Gene Ontology
HRP	horseradish peroxidase
INM	inner nuclear membrane
IP	Immunoprecipitation
KNL1	Kinetochore null protein 1
LAP1	Lamina associated polypeptide 1
LAP2β	Lamina-associated polypeptide 2, isoform β
LBR	lamin B receptor
LEM	LAP2-emerin-MAN1
LEMD3	LEM Domain Containing 3
LINC	Linker of Nucleoskeleton and Cytoskeleton
Mad2	mitotic arrest deficiency 2
MCC	mitotic checkpoint complex
MN	Micronuclei
MNE	Micronuclear envelope
NDC80	nuclear division cycle 80
NE	nuclear envelope
NEBD	nuclear envelope break down
NPC	nuclear pore complex
ONM	outer nuclear membrane
PCR	polymerase chain reaction
PFA	Paraformaldehyde
PKC	Protein kinase C
PLP	Periodate-lysine-paraformaldehyde
PM	plasma membrane
PMSF	phenylmethylsulfonyl fluoride
PP1γ	protein phosphatase-1 γ isoform
PP2A	protein phosphatase 2A
Rab	Ras-related protein
RCC1	Regulator of chromosome condensation 1
REEP	Receptor expression-enhancing proteins
ROI	Region of interest
RPE-1	retinal pigment epithelial-1
RT	Room temperature

SAC	Spindle Assembly Checkpoint
Samp1	spindle-associated membrane protein 1
SBF-SEM	serial block face scanning electron microscopy
SD	standard deviation
SDS-PAGE	Sodium dodecyl-sulfate polyacrylamide gel electrophoresis
SiR	silicon rhodamine
STED	stimulated emission depletion
STIM1	stroma-interacting molecule 1
SUN	Sad1p-UNC-84
TAC	tip attachment complexes
TCEP	Tris-(2-carboxyethyl) phosphine hydrochloride
TFA	Trifluoroacetic acid
TM	transmembrane
VRK1	vaccinia-related kinase 1
WT	Wild type

Acknowledgements

I would like to thank my supervisor Steve Royle for the opportunity to work on this exciting project and for continual guidance and support, and for teaching me so many skills during my PhD. Nuria, who I have learnt so much from and has gone above and beyond during the project, and has really inspired me as a scientist. To both Steve and Nuria for feedback and discussion of my thesis.

Royle lab members (past and present) for helpful discussions, feedback and making the lab a great place to do research. Alex Moore, Joe Parham, Ryan Harrison and Melissa Hampson for contributions in the project, ideas and discussion.

Members of CMCB for creating an exciting environment to work (and for the many cakes!). Past project supervisors and lab members who have who taught me so much in research.

Would also like to thank the BBSRC who have funded my project work.

The Computing and Advanced Microscopy Development Unit group members for microscopy, imaging and analysis support. University of Warwick School of Life Sciences Proteomics Research Technology Platform for mass spectrometry analysis and guidance, in particular Cleidiane Zampronio for help and guidance in preparing samples and troubleshooting.

To my parents, grandparents and Lindsay for constant support, endless encouragement and supply of tea. This would never have been possible without you. Joe, we are a team, thank you for being there for me and believing in me. Finally my friends who have always kept me going!

Declaration

This thesis is submitted to the University of Warwick in support of my application for the degree of Doctor of Philosophy. It has been composed by myself and has not been submitted in any previous application for any degree

The work presented (including data generated and data analysis) was carried out by the author except in the cases outlined below:

RPE-1 GFP-Sec61β mCherry-tagged nuclear/NE protein cell lines were generated in collaboration with Nuria Ferrandiz. Nuria then characterised the cell lines by measure of mitotic timings and western blots.

HCT116 LBR-FKBP-GFP cells were generated in collaboration with Nuria and Alex Moore. Nuria completed FACS and western blot characterisation of HCT116 LBR-FKBP-GFP cells. Alex completed genotyping PCR of HCT116 LBR-FKBP-GFP cells.

SBF SEM sample preparation was completed by Nuria.

Steve Royle prepared kymographs and assisted in analysis and figure preparation.

Joe Parham designed the cleavable mitochondrial anchor and completed initial optimisation.

Parts of data included in this thesis have been published: RPE-1 GFP-Sec61β mCherry-tagged nuclear/NE cell line characterisation (Figure 3.1) and SBF-SEM (Figure 4.1B) were published in (Ferrandiz *et al.*, 2022), included in the Appendix.

Inclusion of published work

In the Appendix is a published paper to which I contributed to generating and characterising cell lines used, and also to writing and editing sections in manuscript preparation.

"Endomembranes promote chromosome missegregation by ensheathing misaligned chromosomes" (Ferrandiz *et al.*, 2022)

Abstract

Cell division involves the accurate segregation of chromosomes to two daughter cells by the mitotic spindle. Errors in this process can lead to developmental defects or diseases, including cancers. During mitosis, the mitotic spindle is within an "exclusion zone" (EZ) from which membrane structures are mostly absent. Polar misaligned chromosomes may be positioned in the region containing densely packed endomembranes outside of the EZ. Recent work in our lab has shown that these misaligned chromosomes can become wrapped in multiple layers of endomembranes, and that this promotes aneuploidy fate and micronucleus (MN) formation.

The envelope assembled at misaligned chromosomes forming MN provides insufficient protection of the micronuclear DNA. The MN envelope is also unstable and prone to rupture, which exposes the micronuclear DNA to cytoplasmic content and can result in extensive DNA damage and propagate chromosomal instability.

Our main aim is to understand the NE reassembly mechanism, particularly the recruitment of NE proteins and membranes to chromatin, which will inform how this process is defective at missegregated chromosomes forming MN. Key to this is understanding the organisation of nuclear components after nuclear envelope breakdown in early mitosis. We have developed methods to induce the relocalisation of membrane compartments and key proteins of NE reassembly in live cells. This unexpectedly revealed distinct behaviours of different proteins originating from the NE to that of a marker of the ER during mitosis. Ultrastructural analysis of relocalised compartments provided clear evidence in support of the presence of subdomains within the ER enriched in particular profiles of NE proteins. Our functional data suggest a role for these subdomains in NE reassembly and we propose that concentrating proteins within these subdomains makes the reassembly process more efficient.

Chapter 1

Introduction

Eukaryotic cells are by definition compartmentalised by intracellular membrane-bound structures which allow activities to be contained within distinct environments inside the cell. However, this poses a challenge for cell division, where membrane-bound compartments must be broken apart and reassembled to distribute between the two daughter cells.

1.1 Interphase nuclear envelope

The nucleus encloses and protects the genome of the cell. Essential to the nuclear functions is the envelope that forms the boundary compartmentalising the nucleus, which allows regulated transport and creates an environment within the nucleus that maintains the genome and regulates gene expression. The NE also connects to cytoskeletal structures in the cytoplasm, allowing force transduction, and to underlying structures within the nucleus, organising chromatin within the nucleus.

1.1.1 Interphase nuclear envelope composition

The interphase NE consists of an outer nuclear membrane (ONM) and an inner nuclear membrane (INM) connected at nuclear pores (depicted in Figure 1.1). The ONM of the NE is contiguous with the ER and has similar composition. While the INM, despite being fused with the ONM, contains a distinct profile of proteins and lipids (Smoyer *et al.*, 2016; Romanauska and Köhler, 2018). The nuclear lamina is a meshwork of lamin intermediate filaments which underlies and supports the NE (reviewed by de Leeuw *et al.* (2018)). In interphase, several INM proteins interact with lamin proteins, chromatin or chromatin-bound

proteins. These interactions organise chromatin within the nucleus and function in regulating gene expression.

Nuclear pore complexes (NPCs) are situated within the nuclear pores connecting the ONM and INM (reviewed by Strambio-De-Castillia *et al.* (2010)). These large protein complexes are assembled from nucleoporins, that form a nucleoplasmic basket structure, cytoplasmic filaments and a central channel, through which NPCs regulate transport across the NE. Proteins, for example INM proteins (Mudumbi *et al.*, 2020), may also be transported through peripheral channels of the NPC, situated between the NPC and the membrane pore.

LINC complexes, which span both membranes of the NE, connect the nuclear lamina to the cytoplasmic cytoskeleton (recently reviewed by Lityagina and Dobreva (2021)). These complexes are formed from interaction between the INM SUN domain proteins and ONM nesprin proteins within the interlumenal space of the NE. SUN domain proteins bind to nuclear lamina proteins within the nucleus and the nesprin family proteins interact with cytoskeleton components in the cytoplasm (actin filaments, intermediate filaments or microtubules). LINC complexes therefore allow force transduction from the cytoskeleton to the nucleus and have important functions in many processes, including nuclear positioning and during cell migration.

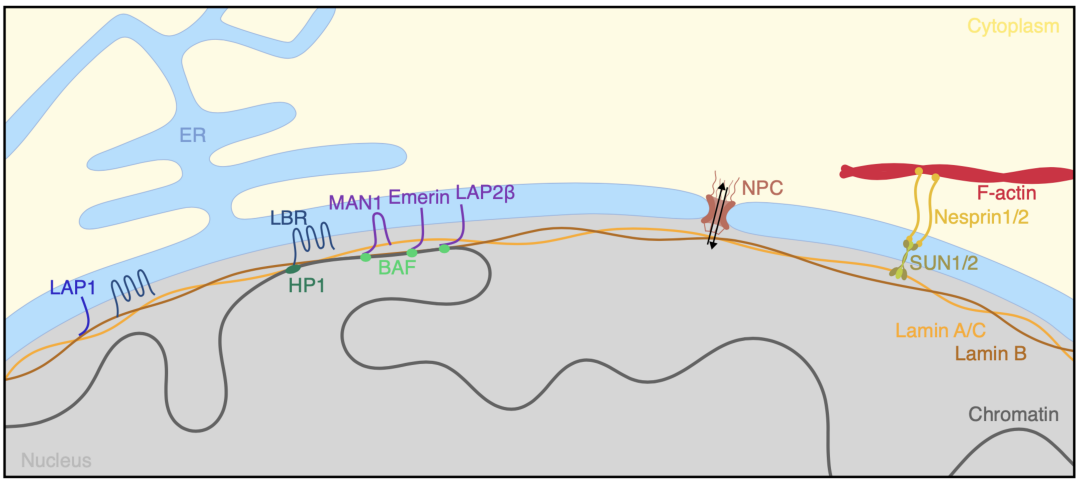

Figure 1.1. Interphase nuclear envelope structure and connections. The interphase NE is composed of an ONM and INM connected at sites of nuclear pores. The NE makes connections to chromatin or chromatin-bound protein within the nucleus through INM proteins, which include LBR and LEM domain proteins (example emerin, LAP2β and MAN1). Connections are also made between proteins within the INM and the underlying nuclear lamina, including LBR, LAP1 and LAP2β. The LINC complex spans both NE membranes and is formed between SUN proteins in the INM that interact with nuclear lamina proteins, and nesprin family proteins in the ONM that connect to cytoskeletal structures. NPCs are large protein complexes situated within pores at sites where the INM and ONM are fused. NPCs regulate transport across the NE through the central and peripheral channels.

1.1.2 Targeting of proteins to the INM

Proteins are targeted to the INM by diffusion within the ER, translocation through the NPC, and retention at the INM through interaction with chromatin or lamina proteins ("diffusion-retention" model) (reviewed by Ungricht and Kutay (2015)). This targeting mechanism is therefore influenced by the morphology and connectivity of the ER connected to the NE ONM in which the INM proteins diffuse (Pawar *et al.*, 2017).

INM proteins may use different mechanisms of translocation across the nuclear pore while present within the membrane (Zuleger *et al.*, 2011; Mudumbi *et al.*, 2020). Most of the INM proteins are proposed to use the peripheral channels of the NPC to transport across the NE, but a small proportion may use both the central and peripheral channels (Mudumbi *et al.*, 2020). For example, integral INM protein LBR can transport through the peripheral side channel of the NPC in a Ran GTPase-dependent mechanism (Zuleger *et al.*, 2011), but has also been found to use the central channel (Mudumbi *et al.*, 2020). LBR is retained at the INM through interaction of nucleoplasmic N-terminal domains with lamin B of the nuclear lamina (Worman *et al.*, 1988) and with chromatin directly (Ulbert *et al.*, 2006) or indirectly, through heterochromatin-bound histones HP1 (Ye and Worman, 1996) and H3 (Polioudaki *et al.*, 2001).

1.1.3 Subdomains at the interphase NE

INM proteins show varied distribution and dynamics within the NE. For example, the INM protein LBR forms domains within the interphase nuclear envelope in terms of localisation (Makatsori *et al.*, 2004) and dynamics (Giannios *et al.*, 2017). The domains of concentrated and less mobile LBR are proposed to be at sites of contact to underlying nuclear lamina and heterochromatin. In addition, in interphase, LBR was present within regions of a distinct profile of proteins to those proximal to emerin, another INM protein (Cheng *et al.*, 2022). This suggests that domains of different protein profiles exist within the INM and connected interphase ER.

1.1.4 Nuclear envelope defects in disease

Laminopathies are a group of disorders, which include muscular dystrophies and cardiomyopathies, that result from defects in the nuclear lamina (reviewed by Davidson and Lammerding (2014)). These disorders can result from mutations in genes encoding lamin proteins, which affect the NE stability and the transduction of signals from the cytoskeleton to the nucleus. Laminopathies can also be caused

by mutation of INM proteins that form the connections between the nuclear lamina and NE, and of LINC complex proteins connecting the nuclear lamina to the cytoskeleton.

One laminopathy is Emery-Dreifuss muscular dystrophy (EDMD), a progressive muscle weakening disorder with notable cardiac effects (reviewed by Heller *et al.* (2020)). The causative mutations that have been identified include those in the LMNA gene encoding lamin-A/C proteins (Bonne *et al.*, 1999), but also in genes encoding emerin and SUN domain proteins of the INM, among many other genes. Emerin interacts with lamin A and this interaction is important to targeting emerin to the INM and connecting the NE to the nuclear lamina (Clements *et al.*, 2000). Emerin levels around nuclei of muscle cells were reduced in EDMD patients as result of mutations (Nagano *et al.*, 1996). The nuclei of skin fibroblast cells from EDMD patients were less stable and deformed more under strain (Zwerger *et al.*, 2013), demonstrating the effects of lack of emerin at the INM and depleted connections to the underlying nuclear lamina on the NE structure.

Lamin expression is altered in many cancers, where it is proposed that the resulting changes in NE stability increase the ability to deform the nucleus, allowing the cell to move through tight spaces without compromising the nuclear compartment and therefore promoting metastasis (reviewed by Davidson and Lammerding (2014)).

1.2 Interphase endoplasmic reticulum

1.2.1 ER function

The ER functions in multiple processes within the interphase cell, including protein folding and transport, calcium storage and lipid synthesis. The ER forms contacts with other membrane-bound organelles, including mitochondria, Golgi, endosomes and the plasma membrane (reviewed by Prinz *et al.* (2020)). These membrane contacts function in, for example, lipid transfer between structures. ER membrane contacts also regulate fission and dynamics of other membrane structures.

1.2.2 ER structure and dynamics

The interphase ER is a large, continuous, dynamic network consisting of interconnected ER tubules and flattened membrane sheet (cisternae) structures. These structures show different distribution within the interphase cell and in a cell type dependent manner. In most cell types to date, ER cisternae are mostly

located close to the nucleus and the tubular network towards the cell periphery (Lu *et al.*, 2009; Puhka *et al.*, 2012). However, some cell types compared in the same study had prominent cisternae in the cell periphery (Puhka *et al.*, 2012).

Recent capture of ER structures using super resolution imaging have allowed accurate measure of the dimensions of ER structure types and revealed in more detail the properties of each structure. ER tubules have nanoscale diameter, reported in 48 nm to 144 nm range with an average of 96 ± 17 nm from stimulated emission depletion (STED) super resolution imaging of live interphase COS-7 cells (Schroeder *et al.*, 2019). ER cisternae are more consistent in dimension due to presence of spacing proteins which bridge sheet membranes (Figure 1.2D) and were measured to be 30 nm to 50 nm thick in the same study by STED imaging (Schroeder *et al.*, 2019).

Several characteristics of the ER make this organelle challenging to study. Its large and dynamic structure means that ER must be visualised with fast and 3D imaging to truly appreciate its distribution and movements in live cells. The visualisation method used is important to distinguish between ER structure types. Indeed, conflicting reports of the ER organisation in mitosis have been presented in two studies in mammalian cells. Lu *et al.* (2009) reported more cisternal than tubular structures in mitotic cells, while Puhka *et al.* (2007, 2012) observed the opposite organisation in CHO-K1 cells, with mostly tubular structures observed in mitosis. This was attributed to limitations of the visualisation method used by Lu *et al.* (2009) (Lu *et al.* (2009) by spinning disk confocal microscopy and Puhka *et al.* (2012) by high-pressure freezing and freeze substitution visualised by EM tomography). The preparation method, including temperature and use of fixatives, can also affect the preservation of ER structures (Lu *et al.*, 2009; Puhka *et al.*, 2012).

New aspects of interphase ER structure have been discovered through super resolution imaging in recent years (Nixon-Abell *et al.*, 2016; Gao *et al.*, 2019; Schroeder *et al.*, 2019), including the presence of dynamic nanoscale holes within the ER cisternae, which were previously viewed as static (Schroeder *et al.*, 2019), and the existence of domains of distinct protein profiles within ER tubules (Gao *et al.*, 2019). In addition, ER tubules have been seen to form dense matrices in multiple cell types, which could be perceived as sheets under certain visualisation methods (Nixon-Abell *et al.*, 2016), highlighting the importance of the visualisation method used to fully understand ER morphology. An example from Schroeder *et al.* (2019) demonstrating the difference in appearance of a cluster of ER tubules visualised by confocal or STED microscopy clearly demonstrates this issue. This could also potentially explain the conflicting

observations of ER structure in mitotic CHO-K1 cells in previous reports, in that Puhka *et al.* (2012) had studied ER structure in more detail by electron tomography, whereas Lu *et al.* (2009) visualised ER only by spinning disk confocal microscopy in this cell type, which is probably not sufficient to resolve these structures.

ER tubules within the network are dynamic and undergo continual reorganisation. The tubules can be tethered and fused at three-way junctions (Hu *et al.*, 2009) and can also assemble into dense matrix structures (Nixon-Abell *et al.*, 2016). ER tubule organisation and dynamics are influenced by contacts to other organelles or microtubules (reviewed by Westrate *et al.* (2015)). ER tubules can connect to microtubules through three different interaction types: connecting to microtubule motor proteins; microtubule plus tip proteins or by static interaction on microtubules. These interactions each differently affect ER tubule dynamics and organisation within the cell.

ER tubules form dynamic attachments to microtubules through binding of motor proteins kinesin or dynein, which slide the ER tubule in opposite directions along the microtubule and regulate ER tubule distribution within the cell (Woźniak *et al.*, 2009). Additional interactions between microtubules and ER tubules are formed through the transmembrane protein STIM1 (stroma-interacting molecule 1) at ER tubule ends and the microtubule plus tip protein EB1 (Waterman-Storer *et al.*, 1995) (Figure 1.2B). These interactions were shown to exert forces that extend connected ER tubules by pushing or pulling, depending on microtubule dynamics *in vitro*, linking tubule movement and distribution to the connected microtubule length and dynamics (Waterman-Storer *et al.*, 1995) (Figure 1.2B). A third type of interaction between ER and microtubules is mediated by the ER transmembrane protein CLIMP63 (cytoskeleton-linking membrane protein 63), which shapes ER cisternal sheets but is also found in ER tubules (Nixon-Abell *et al.*, 2016), and can bind along the length of microtubules (Klopfenstein *et al.*, 1998). These static interactions to the microtubules may act to tether and stabilise ER tubules, and to organise the ER within the cell.

1.2.3 ER shaping proteins

The regulation of ER shape is complex and involves multiple different proteins which function in parallel to regulate the formation or stabilisation of the different structure types. New proteins which function in ER shape regulation have been identified even in recent years (Christodoulou *et al.*, 2016, 2020) and the full complement of proteins involved may still to be discovered.

ER tubules and the ends of ER cisternae have higher curvature, and are therefore more energetically unfavourable, than the mostly flat surface of cisternae. Reticulons and REEP families proteins can shape ER membrane to form and stabilise the high curvature ER tubules and the edges of cisternal sheets (Voeltz *et al.*, 2006) (Figure 1.2 C-D). In interphase cells, Rtn4 and REEP5 function redundantly in shaping these high curvature structures (Voeltz *et al.*, 2006). Recently, reticulon proteins have also been shown to function in the formation or maintenance of nanoholes within the flat cisternae (Schroeder *et al.*, 2019).

A connected ER tubule network is formed by the tethering or fusion of tubules. The tethering of ER tubules by transmembrane atlastins (family of GTPases) (Hu *et al.*, 2009) or membrane bound CHMP7 (Chu *et al.*, 2022) (ESCRT-III complex component) forms three-way junctions that are stabilised by lunapark protein (Chen *et al.*, 2012). These three-way junctions connecting tubules in the network may persist or be subsequently fused by atlastin GTPase activity (Orso *et al.*, 2009). Atlastin proteins may also function with lunapark to stabilise the three-way junctions before their fusion (Wang *et al.*, 2016).

The transmembrane ER protein CLIMP63 functions in cisternal sheet formation through mediating spacing between membranes by forming a bridge across the ER lumen (Shibata *et al.*, 2010). CLIMP63 has also recently been discovered to have a role in regulating the dynamics of nanoholes detected within ER cisternae and therefore has a potential role in remodelling (Gao *et al.*, 2019). In addition, CLIMP63 localises at ER tubules (Nixon-Abell *et al.*, 2016), where the protein forms subdomains with a distinct protein profile to reticulon-enriched domains (Gao *et al.*, 2019).

Microtubules additionally have a role in the formation, maintenance and distribution of ER tubules (Waterman-Storer *et al.*, 1995; Woźniak *et al.*, 2009), as described in the above section.

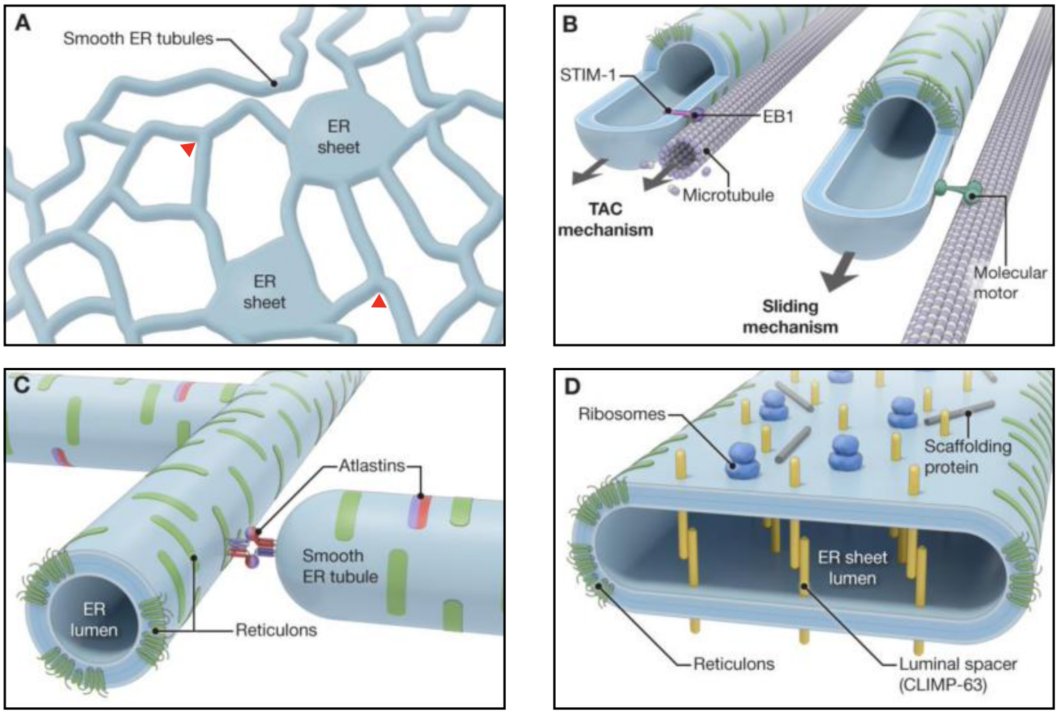

Figure 1.2. ER structures and shaping proteins. (**A**) The interphase ER is a large, dynamic and continuous structure consisting of interconnected ER tubules and flattened membrane sheets (cisternae). Red arrowheads indicate three-way junction sites forming the tubule network. ER cisternal sheets in some cell types contain nanoscale holes (not shown in this schematic) revealed by advanced imaging. (**B**) Example of ER tubule contacts to microtubules. STIM1 at ER tubule ends can bind microtubule plus tip protein EB1 to form tip attachment complexes (TACs). (**C**) Reticulon and REEP family proteins stabilise the highly curved structure of ER tubules which range in nanoscale diameter. Atlastins stabilise and fuse three-way junction sites between ER tubules. (**D**) ER cisternae are flattened sheets with large lumenal space. The curved ends of cisternae are shaped by reticulon proteins and the lumenal distance is determined by interaction of CLIMP-63 proteins which bridge the membranes. Adapted with permission from Elsevier, Goyal and Blackstone (2013), under Copyright Clearance Center License Agreement.

1.3 Mitosis

Mitosis is the dynamic process by which cells segregate chromosomes to form two daughter nuclei during cell division. Chromosome segregation is mediated by the mitotic spindle, composed of microtubules and associated proteins. The steps of mitosis are highly regulated and are coordinated with multiple other processes of cell division (including reassembly of the NE). Defects in chromosome segregation during mitosis can result in changes in chromosome number in the daughter cells, termed aneuploidy, or formation of small structures that remain separate from the main nucleus, termed micronuclei (MN).

1.3.1 Steps of mitosis

In the first stage of mitosis, prophase, the chromatin within the nucleus condenses in preparation for segregation. The microtubules, which form the mitotic spindle, begin to polymerise from the centrosomes and the two centrosomes begin to move to apart (depicted in Figure 1.3).

During prophase, contacts between proteins of the NE INM and the chromatin or nuclear lamina are lost as a result of phosphorylation events. This releases membrane from chromatin and allows for accurate segregation of chromosomes (Champion *et al.*, 2019). The nuclear envelope breaks down and fragments, which allows "compartment mixing" and chromosome capture by mitotic spindle fibres from opposite poles connecting to chromosomes via kinetochore structures at the centromere (Nabetani *et al.*, 2001; McCleland *et al.*, 2004; Cheeseman *et al.*, 2006). These attachments are formed through a "Search-and-capture" model of dynamic microtubule growth and shrinkage (Holy and Leibler, 1994), and the additional mechanisms that facilitate this process, as reviewed by Vukušić and Tolić (2022).

In metaphase, the chromosomes are aligned at the metaphase plate by the bipolar spindle. The chromosome alignment mechanism depends on chromosome position within the cell after NEBD, whether beyond or between the spindle poles (reviewed by Auckland and McAinsh (2015)). The stable attachment of kinetochores to mitotic spindle microtubules from opposite poles is assessed by the spindle assembly checkpoint (SAC), which remains active and blocks progression to the next stage if errors are detected.

Next, if the SAC is satisfied, the cell enters anaphase. During this step, the sister chromatids of each chromosome are pulled towards opposite spindle poles. The separation is facilitated by the cleavage of cohesin complexes that hold

the chromatids together along their length (Uhlmann *et al.*, 1999). Anaphase can be described in two phases: anaphase A and anaphase B. In anaphase A, kinetochore microtubules connected to the chromosomes shorten, pulling apart sister chromatids towards opposite spindle poles (Koshland *et al.*, 1988) (recently reviewed by McIntosh (2021)). In anaphase B, astral microtubules and interpolar microtubules generate forces to pull the spindle poles further apart (as recently reviewed by Vukušić and Tolić (2021)). The nuclear envelope begins to reassemble around chromatin masses.

During telophase, the NE assembles as a coat around the chromatin masses to form the two daughter nuclei and the chromosomes begin to decondense. As the cell itself enters the final stage of division, the mitotic spindle forms the midbody structure where abscission occurs to separate daughter cells (Mierzwa and Gerlich, 2014; Hu *et al.*, 2012).

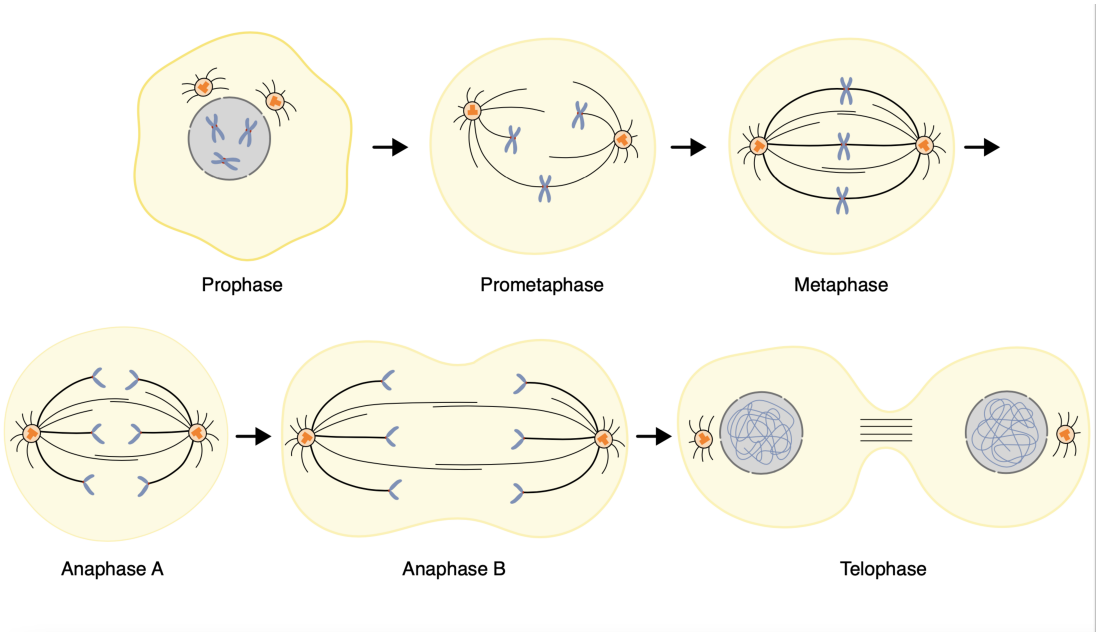

Figure 1.3. Steps in mammalian cell mitosis. Stages of mitosis are shown with the centrosomes (orange), mitotic spindle microtubules (black), chromosomes (blue), kinetochores (red) and nucleus and NE (shown in grey).

1.3.2 Regulation of mitosis

The critical drivers of early mitosis are the cyclins and cyclin-dependent kinase (CDKs), which regulate mitotic entry and progression. The activity of CDKs relies upon the availability and binding of the appropriate cyclin protein. Cyclin proteins undergo cell cycle-regulated ubiquitylation, targeting them for proteasomal degradation and causing protein levels to change through the cell division cycle (Glotzer *et al.*, 1991).

Regulation of mitotic exit is conferred, in part, through the targeting of proteins for degradation. Anaphase-promoting complex/cyclosome (APC/C) is an E3 ubiquitin ligase that modifies and targets substrate proteins for proteasomal degradation to allow chromatin separation and mitotic exit. APC/C activity levels are tightly controlled through the cell cycle and activation requires cofactor binding (Cdc20 or Cdh1). The binding of the cofactor Cdc20 is inhibited by phosphorylation of APC/C by active CDK1 in early mitosis (Zhang *et al.*, 2016) and is controlled by the SAC.

Mitotic exit is additionally regulated by dephosphorylation through inactivation of mitotic kinases and increased activity of phosphatases (recently reviewed by Vagnarelli (2021)). PP1 and PP2A are the main phosphatases identified in regulating mitotic exit. Both PP1 and PP2A require binding of additional cofactor subunits to assemble the active enzyme (Vagnarelli, 2021). In early mitosis, active CDK1 directly or indirectly (through regulating inhibitor binding) inhibits PP1 and PP2A activity (Dohadwala *et al.*, 1994; Vigneron *et al.*, 2009), which also acts in turn to further amplify CDK1 activity.

Mitotic checkpoints also act to assess accurate completion of mitotic processes before progression to the next phase. Entry into mitosis is controlled by the DNA damage checkpoint which prevents cells with damaged DNA from entering mitosis (at the G2/M transition).

Later, the SAC checks for correct bioriented attachment of chromosome kinetochores to the mitotic spindle before progression into anaphase, to prevent chromosome segregation defects (reviewed by Musacchio (2015)).

1.4 Membrane-bound structures reorganise during early mitosis

Mitosis and cell division processes involve extensive structural changes and reorganisation of the membrane-bound components of the cell (Figure 1.4). The plasma membrane remodels to accommodate shape changes during division of the cell, including cell rounding and cytokinetic abscission. The organelles also undergo major structural changes in mitosis, to ensure equal inheritance of membrane components by the two daughter cells. The NE is disassembled in early mitotic stages to allow contacts to form between the mitotic spindle machinery and the chromosome kinetochores for subsequent chromosome segregation. The ER remodels and along with Golgi fragments, mitochondria and other endomembranes, is excluded from the spindle region. Membrane contacts between

organelles are also important to mitotic membrane organisation and dynamics. The change in membrane structures in mitosis means that the cell must later correctly partition membrane components to each daughter cell during division.

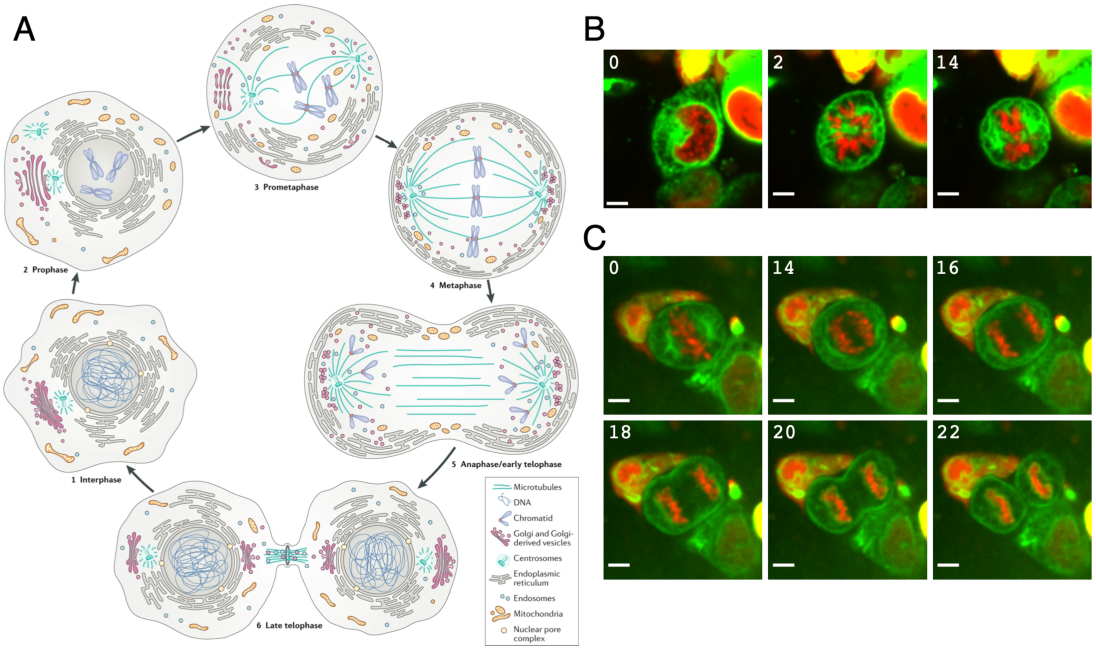

Figure 1.4. Remodelling of ER and other membrane structures in mitosis. (**A**). Remodelling of membrane compartments as a mammalian cell progresses through mitosis. (**B**) HCT116 cells transiently expressing an ER marker (FKBP-GFP-Sec61β, shown in green) and construct to visualise DNA (pmCherry-H3.2, shown in red) captured at 2 min intervals. Time is indicated in minutes. Scale bars, 5 µm. (**C**). HCT116 cells transiently expressing an ER marker and construct to visualise DNA, as the cell shown in B, and captured under the same imaging conditions. Time is indicated in minutes. Scale bars, 5 µm. A was reproduced with permission from Springer Nature, Carlton *et al.* (2020), under Copyright Clearance Center License Agreement.

1.4.1 Nuclear envelope breakdown

In mammalian cells, the nuclear envelope is fragmented during early mitosis to allow access of cytoplasmic components and formation of contacts between mitotic spindle microtubules and kinetochores of chromosomes.

Phosphorylation of several INM and nuclear proteins regulates nuclear envelope break down (NEBD) through loss of contact between the NE and the underlying nuclear lamina and chromatin. Example, BAF which binds both chromatin and LEM domain proteins at the INM (as shown in Figure 1.1) is phosphorylated by VRK1 kinase in early mitosis, which releases BAF from chromatin and therefore connections between chromatin and the NE (Nichols *et al.*, 2006). The dissociation of NE membrane from chromatin is important to allow accurate chromosome segregation (Champion *et al.*, 2019).

The interaction between LINC complexes, which span both membranes of the NE and connect the nuclear lamina to the cytoskeleton, and the nuclear lamina are dissociated by CDK1- and PLK1- mediated phosphorylation of the INM protein SUN1 (Patel *et al.*, 2014). The nuclear lamina itself is disassembled through modifications resulting in loss of connections to INM proteins and to other lamin proteins, including phosphorylation of lamin proteins by CDK1 and PKC (reviewed in Karoutas and Akhtar (2021)) and INM protein LBR. Lipid synthesis in the ER has a role in nuclear lamina disassembly through signalling events activating PKC (Mall *et al.*, 2012). NPCs are disassembled by phosphorylation of nucleoporin components which then dissociate the into the ER or cytoplasm.

Microtubule motor proteins also generate forces that promote NEBD by pulling membrane from chromatin (Beaudouin *et al.*, 2002; Salina *et al.*, 2002). The remodelling of the ER connected to the interphase NE as cells enter mitosis may also promote disassembly of the NE, as described in the following section.

1.4.2 ER remodelling in early mitosis

During interphase, the ER is arranged as a dynamic network of cisternal sheets and tubules, the distribution of which may be cell type dependent (Lu *et al.*, 2009; Puhka *et al.*, 2012). The ER undergoes extensive remodelling during mitosis, as shown with fluorescent tagged ER membrane protein Sec61β in Figure 1.4 B-C.

In early mitosis, the ER reorganises to facilitate NEBD and spindle formation. The extent to which the ER remodels (from cisternal sheets to tubules) in mitosis has been proposed to depend upon the cell type in multiple studies (Lu *et al.*, 2009; Puhka *et al.*, 2012). In some cell types, fenestrated sheets were formed in mitosis and may represent an intermediate in the remodelling from sheet to tubule structures (Puhka *et al.*, 2012). The small dynamic holes present within these fenestrated sheets are proposed to allow more efficient remodelling of the ER to tubules in response to changes in the cell, such as in early mitosis, as proteins shaping the high curvature edges of the nanoholes are already dispersed within the sheet surface (Schroeder *et al.*, 2019). The extent of ER remodelling in mitosis may also depend on the relative total amount of ER or on ribosome number (which stabilise cisternae) in different cell types (Puhka *et al.*, 2007, 2012). This variation further highlights the complexity of investigating NE protein and ER organisation in mitosis.

The remodelling of ER structures in early mitosis promotes break down of the connected NE. In *C.elegans* embryos, ER remodelling (Audhya *et al.*, 2007) and regulation of ER lipid synthesis proximal to the nucleus (Bahmanyar *et al.*,

2014) were each found to promote NEBD. The depletion of YOP-1 and RET-1 in *C. elegans* embryos (homologues of mammalian Rtn4a and REEP5/DP1), which are known to form and stabilise ER tubules and high curvature structures, disrupted the peripheral ER network and delayed NEBD in the first embryonic division (Audhya *et al.*, 2007). The loss of continuity in the peripheral ER network observed as a result of the depletion may affect forces transduced through the network to pull NE membrane from chromatin during NEBD, delaying disassembly, or the diffusion of NE components into the ER upon break down.

The protein Rab5, a small GTPase which functions in interphase trafficking of early endosomes, was first implicated in regulating ER organisation and in promoting NEBD during mitosis by observations in the same study of *C. elegans* first embryonic division (Audhya *et al.*, 2007). Rab5 depletion resulted in similar disruption in ER network morphology and NEBD delay to the depletion of YOP-1 and RET-1 described above. Rab5 has since been shown to be necessary for NE disassembly in the partially open mitosis in *Drosophila* cells (Capalbo *et al.*, 2011). Capalbo *et al.* (2011) reported that in *Drosophila* cells, Rab5 also functions in spindle assembly, and so the observed defects upon depletion in both systems may reflect indirect changes in the ER network as result of spindle defects. There may also be additional unidentified Rab5 effectors. Indeed, in mammalian cells, Rab5 has been discovered to function in chromosome congression through role in recruitment of kinetochore component Centromere protein F (CENP-F) (Serio *et al.*, 2011).

REEP family proteins REEP3 and REEP4 function redundantly in forming and stabilising curved ER structures in mitosis, but do not mediate the same function in interphase cells (Kumar *et al.*, 2019). This is the first demonstration of an ER shaping protein specifically functioning in mitosis and suggests that a different set of ER shaping proteins may function to mediate the extensive ER remodelling as cell enter mitosis. The regulation of REEP3/REEP4 mitotic function has not yet been determined. REEP4 is recruited to the INM in interphase by ELYS (Golchoubian *et al.*, 2022), which functions in initiating NPC assembly and can bind chromatin. This could act to spatially restrict REEP4 functions in interphase, although a significant proportion of REEP4 also localises to the peripheral ER (Golchoubian *et al.*, 2022).

Mitotic ER remodelling is also regulated, at least in part, by phosphorylation of other ER shaping proteins at mitotic entry. The tubular ER network is dissociated by phosphorylation of lunapark (Wang *et al.*, 2016), a protein which stabilises three-way junctions connecting tubules in interphase (Chen *et al.*, 2012). CDK1-mediated phosphorylation of CHMP7 in early mitosis is proposed to

interfere with CHMP7 oligomerisation and three-way junction tethering function (Chu *et al.*, 2022). Phosphorylation of either protein may therefore also function in the remodelling of ER tubules to cisternal sheets. In early mitosis, several of the contacts between ER and microtubules are dissociated through phosphorylation of ER proteins, including CLIMP63 (Vedrenne *et al.*, 2005) and STIM1 (Smyth *et al.*, 2012). This allows ER remodelling and facilitates the clearance of ER membranes from the spindle region.

However, ER-microtubule contacts mediated by other ER proteins, including Samp1 (Buch *et al.*, 2009) and REEP3/4 (Schlaitz *et al.*, 2013), are formed or maintained in mitosis. Example, the protein Samp1 present in the INM in interphase, a proportion of which localises to polar regions of the spindle during mitosis (Buch *et al.*, 2009). ER tubules have been observed aligned along spindle microtubules in metaphase cells (Lu *et al.*, 2009). These interactions between ER and microtubules may provide structural support of the mitotic spindle. Although, the interactions are importantly spatially restricted to the outer regions of the spindle to prevent interference of membranes with chromatin segregation, as reviewed in the next section.

1.4.3 Exclusion zone

During mitosis, the mitotic spindle and chromosomes have been found to be located within a region of the cell from which membrane structures are mostly absent, termed the "exclusion zone" (EZ). The presence of an EZ was reported in early studies in the 1950s in plant cells as a "clear space" or "clear zone" around the mitotic spindle (Bajer and Molè-Bajer, 1955; Bajer, 1957). The EZ has since been described in *Drosophila* cells (Schweizer *et al.*, 2015; Araújo *et al.*, 2023) and in multiple mammalian cell types (McCullough and Lucocq, 2005; Nixon *et al.*, 2017; Ferrandiz *et al.*, 2022). In mammalian cells, the EZ is maintained from metaphase through to early telophase, when membranes access the zone to reassemble the NE around chromatin (McCullough and Lucocq, 2005). SBF-SEM imaging and 3D segmentation of a metaphase HeLa cell highlighted the contrast between the EZ volume, which almost free of any membrane structures, and the dense area of membranes outside of this zone (Nixon *et al.*, 2017), as shown in Figure 1.5.

EZ function

The importance of maintaining the spindle within this membrane EZ for accurate chromosome segregation has been demonstrated. Chromosome segregation defects were observed when holes were introduced by membrane disruption

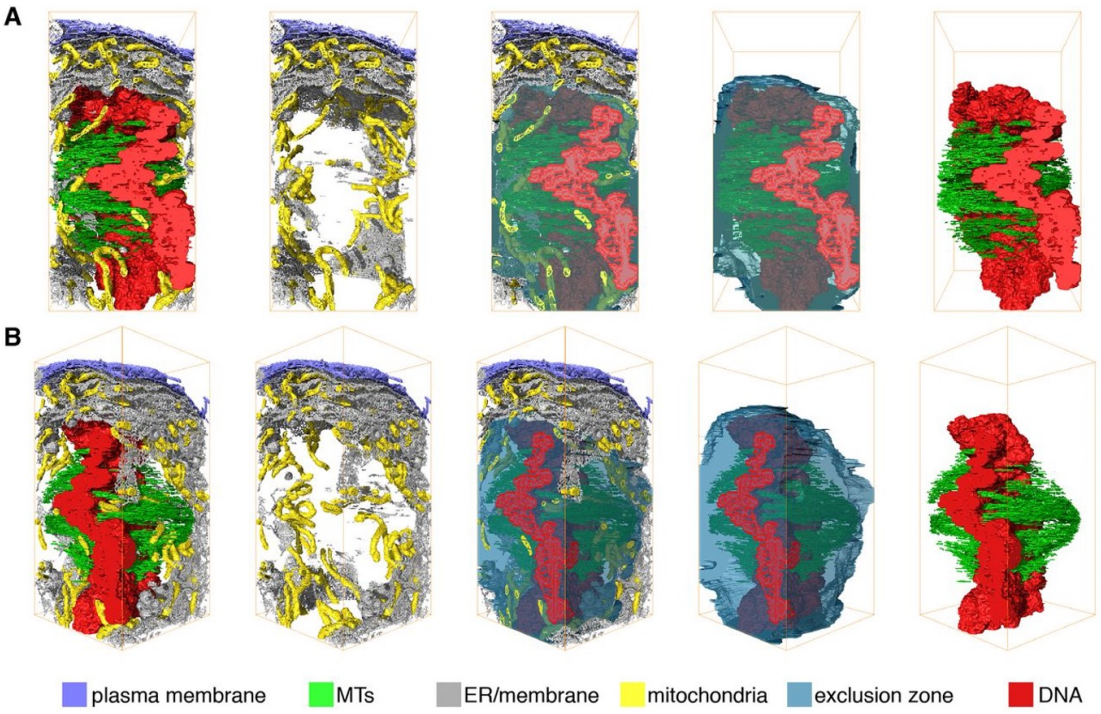

Figure 1.5. Membrane exclusion zone around the metaphase chromatin and mitotic spindle. SBF-SEM segmentation 3D model of metaphase HeLa cell, shown from two different viewing angles (the view in A is rotated 45° about the z-axis to B). The exclusion zone volume is indicated in blue. SBF-SEM segmentation reproduced with permission from Journal of Cell Science, Nixon *et al.* (2017), under Copyright Clearance Center License Agreement.

(Schweizer *et al.*, 2015), tethering membrane to chromatin (Champion *et al.*, 2019) or by maintaining membrane contacts to microtubules that are usually lost at mitotic entry (Smyth *et al.*, 2012). In addition, segregation defects were also induced when membranes were not sufficiently cleared from the spindle region to establish the EZ (Schlaitz *et al.*, 2013). ER membranes have also been shown to impair chromosome movement and promote chromosome segregation defects (Merta *et al.*, 2021). It is therefore proposed that the EZ prevents interference of these membrane structures with chromosome segregation. The EZ prevents early coating of chromatin with membrane, which can cause segregation defects and micronucleus formation, and coordinates NE reassembly with chromatin separation.

In addition to preventing the interference of membrane structures with chromosome segregation, the EZ has also been proposed to concentrate protein components for spindle assembly during early mitosis in mammalian cells (Schweizer *et al.*, 2015). Other proteins were also concentrated within the spindle region in *Drosophila* S2 cells, including SAC protein Mad2 and nucleoporin Megator (mammalian Tpr) which regulates the SAC (Schweizer *et al.*, 2015), suggesting that additional factors, such as mitotic regulatory proteins, may also

be concentrated within the EZ.

EZ formation and maintenance

REEP family proteins REEP3 and REEP4, which shape and stabilise high curvature ER structures in mitosis (Kumar *et al.*, 2019), have a role in establishing the EZ (Schlaitz *et al.*, 2013). REEP3 and REEP4 were found to function redundantly in the clearance of membrane from the spindle region in a mechanism that is proposed to involve attachment and movement of ER which is dependent on microtubules (Schlaitz *et al.*, 2013). This clearance did not rely on membrane shaping function of the proteins (Kumar *et al.*, 2019). The mechanisms regulating the mitotic specific functions of REEP3/REEP4 are not yet understood (Kumar *et al.*, 2019). The exclusion of membrane from the spindle region is also facilitated by the loss of other ER contacts to microtubules through phosphorylation events in early mitosis, as described in the above section. The mitotic spindle has also been proposed to physically exclude large ER structures from accessing the spindle region (Liu *et al.*, 2018).

F-actin at the cell cortex may also have a role in sequestering ER membrane structures away from the spindle EZ region (McCullough and Lucocq, 2005). Layers of ER cisternae around the cell cortex are seen in mitotic HeLa cells at metaphase through to early telophase, as visualised by EM (McCullough and Lucocq, 2005). These layers were lost in late telophase/G1 cells, after the NE had reformed around chromatin. This suggests that the function of these cortical ER structures is important in early mitosis. Inhibiting polymerisation of actin filaments results in loss of ER at the cortex indicating a role of F-actin in cortical ER positioning (McCullough and Lucocq, 2005). The association of ER with F-actin at the cell cortex may function to tether ER, preventing membranes from accessing the EZ and chromatin until required for NE reassembly. Tethering of ER at the cortex could also affect the remaining connected ER, pulling the structure away from the EZ region towards the cell cortex.

1.5 Nuclear envelope reassembly mechanisms

In mammalian cells, the nuclear envelope is broken down in early mitosis to allow attachment of the kinetochores to the mitotic spindle and for the subsequent chromosome separation. The cell then needs to reassemble the NE around segregated chromatin masses during mitotic exit to form two daughter nuclei. The mechanism of nuclear envelope formation involves the ordered recruitment of membrane and nuclear components to chromatin and remodelling to reform

the nuclear envelope. NPCs are reassembled to reestablish nuclear transport and the nuclear lamina reforms to support the NE membrane. The interphase NE is continuous with the ER and how the cell delineates these structures after mitosis is unclear.

The process of NE assembly must be tightly controlled to allow coordination with multiple other mitotic processes, including chromatin separation, chromatin decondensation and mitotic spindle disassembly (Liu and Pellman, 2020). This ensures a functional NE compartment is accurately assembled on the surface of chromatin masses. The role of phosphorylation and other post-translational modifications in regulating and coordinating the process of NE reassembly has been reported for many of the NE components (Wurzenberger and Gerlich, 2011). The importance of the control of the distribution and remodelling of membrane compartments at particular mitotic stages in spatial and temporal regulation has become clearer in recent years (Puhka *et al.*, 2012; McCullough and Lucocq, 2005) .

1.5.1 NE protein localisation in mitosis and reassembly mechanism

How do nuclear and nuclear envelope proteins localise after NEBD in mammalian cells?

Three models have been proposed for the organisation of proteins originating from the NE during mitosis (Collas and Courvalin, 2000). In the precursor vesicle model, NE proteins are present in vesicles formed from the NE, either by NE fusion or breakdown. Alternatively, NE proteins have been proposed to diffuse into the ER upon NEBD, freely diffusing or existing as domains that are enriched in specific subsets of proteins within the ER. Currently, the diffusion model is more widely accepted due to limited *in vivo* evidence of the presence of precursor vesicles functioning in NE reformation.

The different models for NE protein localisation in mitosis also imply the mechanism of NE assembly. During late mitosis in each model, proteins in these structures contact chromatin or chromatin-bound protein, to initiate NE reassembly. The membrane structures are then remodelled to form the NE surrounding the chromatin mass. The enrichment of proteins in structures (vesicle model) or concentration in specific regions of the ER (domain model) could act as a mechanism to prime proteins and associated membrane for efficient delivery to chromatin to assemble the NE.

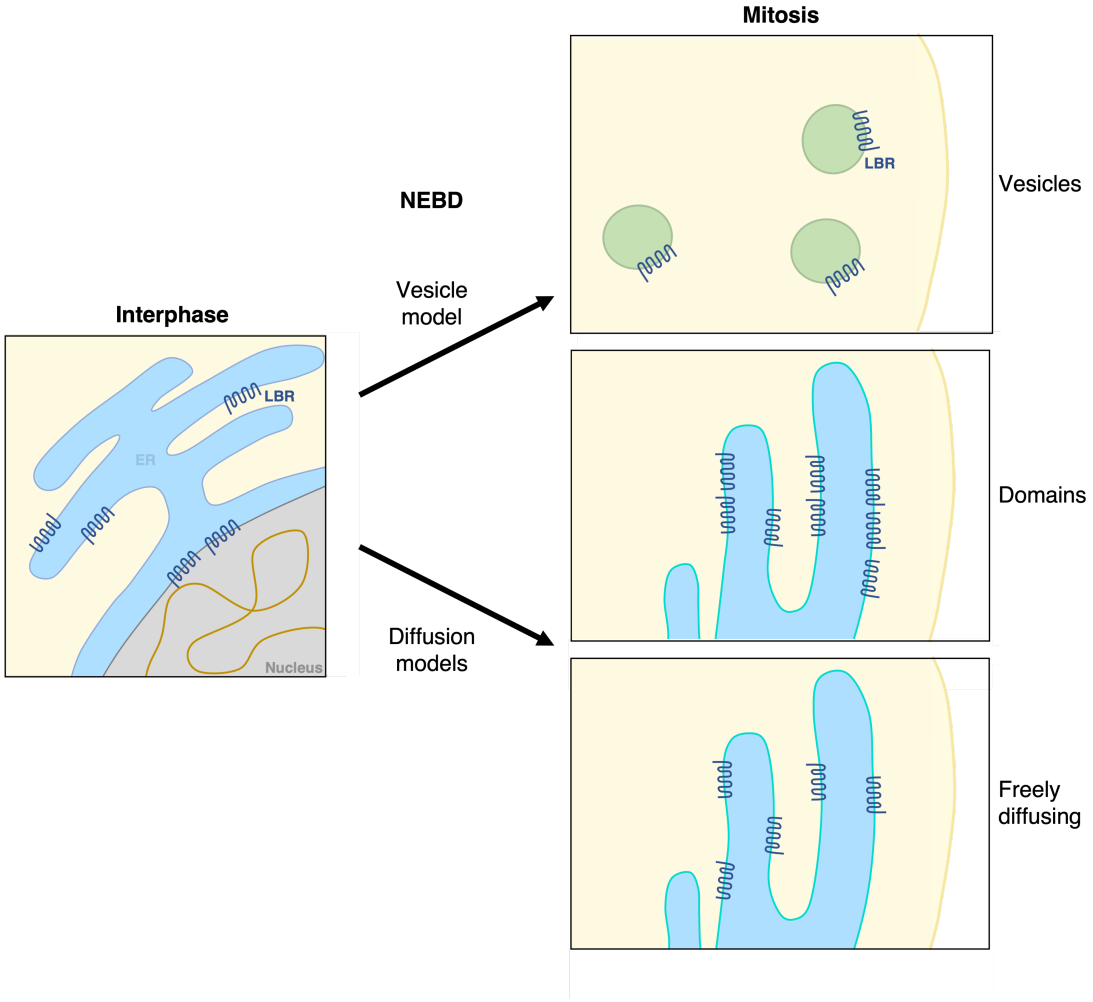

Figure 1.6. Fate of NE proteins after NEBD in mitosis. (**Vesicle model**). The vesicle model proposes that after NEBD, NE proteins are present in vesicles formed from the NE, either by fusion of the NE or fragmentation during NEBD. The vesicles formed are specifically enriched in proteins from the NE and could act as precursor structures that concentrate NE components for efficient NE reassembly. (**Diffusion models**). The diffusion models propose that NE proteins diffuse into the ER upon NEBD. Two different behaviours are proposed, NE proteins are either freely diffusing within the ER membranes or are concentrated within subdomains enriched in particular NE proteins. Although contacts are lost upon mitotic entry, some enrichment in subdomains may be maintained from sites of contact to underlying structures in interphase where these NE proteins are enriched. Similar to as proposed for the vesicle model, these subdomains could act to concentrate NE components within subregions of the expansive ER membrane structure, primed for delivery to chromatin for NE reassembly. Colour is used to indicate the distinct composition of compartment membranes to that of the ER and the membranes of the alternative model.

Vesicle model

In the precursor vesicle model, NE proteins are present in vesicles formed from the NE, either by NE fusion or fragmentation during breakdown. The model proposes that vesicles enriched in NE components act as precursors to NE reassembly. The vesicles contact chromatin through NE proteins present in the vesicle membrane, bound vesicles flatten and then fuse to form the NE on the chromatin surface.

Early *in vitro* evidence of mitotic vesicles enriched in nuclear components has been presented in several systems. These studies suggested the presence of distinct populations of mitotic vesicles with different composition, morphology (size and presence of ribosomes) and behaviour (binding, fusing ability and timing of recruitment to chromatin).

One of the earliest *in vitro* studies identified vesicle populations of distinct protein composition that function in NE reassembly in *Xenopus* egg extract (Wilson and Newport, 1988). Later, a subpopulation of mitotic vesicles isolated from mammalian cells was found to differentially associate with vimentin intermediate filaments in a phosphorylation-dependent manner *in vitro* (Maison *et al.*, 1993). Interestingly, the INM protein LBR was enriched on vesicles bound to intermediate filaments compared to those unbound, whereas ER and Golgi markers were enriched on unbound vesicles. Vesicle populations of different composition and sedimentation patterns have also been reported to be recruited to chromatin with different timing and in an ordered manner in a *Xenopus* system *in vitro* (Drummond *et al.*, 1999). Markers of the INM and ONM were found enriched in different vesicle populations in this study (Drummond *et al.*, 1999). The order of recruitment of the different vesicle populations to chromatin was then also confirmed by endogenous staining of marker proteins present in each population in *Xenopus* XLK-2 cells (Drummond *et al.*, 1999). These observations overall suggested the presence of mitotic vesicle populations enriched in NE proteins primed for reassembly of the NE in late mitosis.

Two populations of vesicles showing different morphology and binding behaviour were observed by EM from *Xenopus* egg extract system onto chromatin. Vesicle populations with ribosomes were observed bound on the surface of chromatin, whereas those devoid of ribosomes appeared only to bind to other available membrane (other vesicles or membrane already coating chromatin) (Wiese *et al.*, 1997). This also demonstrated the ability of populations of mitotic vesicles to bind chromatin and to fuse to other vesicles and membrane around chromatin, supporting the vesicle model of binding and fusion to reform the NE. Vesicle populations with different timings of recruitment to chromatin were also observed

to show different morphology by ultrastructural analysis (Drummond *et al.*, 1999). The recruitment of these NE precursor vesicles was regulated by phosphorylation events (Ito *et al.*, 2007) in *Xenopus* egg extracts and Ran-dependent recruitment to chromatin, both in *Xenopus* egg extracts (Lu *et al.*, 2012) and human cell system *in vitro* (Zhang and Clarke, 2001). Mitotic vesicle populations isolated using different protein markers from human cells had different size profiles and were seen by EM to contain differing amounts of electron dense material, suggesting their composition varies and potential for cargo (Buendia and Courvalin, 1997).

Overall, *in vitro* experiments suggested the presence of distinct populations of mitotic vesicles with different composition, density, morphology (size and presence of ribosomes) and behaviour (fusing ability). These studies also indicate that the different vesicle populations are recruited to chromatin with different timings and in an order that may be related to fusing ability. The recruitment may be regulated by phosphorylation of INM proteins present on vesicles and by the Ran-GTP gradient in mitosis. However, *in vitro* mitotic vesicles have been dismissed as an artefact of the isolation process, which may fragment the ER, forming "microsomes".

Even in recent years, more evidence supporting the vesicle model has been reported *in vivo*. The INM protein LBR was found to be enriched in a subpopulation of mitotic vesicles from homogenised mammalian cells that bound vimentin filaments *in vitro* (Maison *et al.*, 1993) and showed distinct size and sedimentation profile (Buendia and Courvalin, 1997). Similarly, LBR containing vesicles from *Xenopus* egg extracts also displayed different morphology and timing of recruitment to chromatin to other mitotic vesicle populations (Drummond *et al.*, 1999). LBR is proposed to have an important role in the recruitment of these vesicle populations to chromatin for NE reassembly (Maison *et al.*, 1995; Ma *et al.*, 2007; Lu *et al.*, 2010). Observations in mammalian cells overexpressing GFP-tagged *Xenopus* LBR suggested that vesicles containing LBR could form from the interphase NE. The stage at which LBR accumulates in the forming vesicle was not shown, so it remains unclear whether LBR is involved in forming the region or was subsequently concentrated in the forming vesicle. At high levels of overexpression, LBR-containing membrane-bound structures were observed in the cytoplasm. When visualised by EM, the vesicles were seen to be surrounded by multiple double-layered membranes which contained an ER marker, but not NPC components or lamin B (Ma *et al.*, 2007). These vesicles could be an overexpression artefact or represent an endogenous function of LBR enhanced by overexpression.

A population of mitotic vesicles containing LAP1 and showing a distinct protein profile from other NE proteins were also identified in *in vitro* isolations (Maison *et al.*, 1997). Endogenous LAP1 localises in a punctate signal during mitosis in mammalian cells, that was not observed in the interphase cytoplasm or after the NE reformed in late telophase, which suggests presence of a vesicle population containing LAP1 with a role in mitotic NE reassembly (Santos *et al.*, 2015).

Perhaps the most convincing evidence for precursor vesicles to NE assembly was presented by CLEM in HeLa cells expressing GFP-BAF, in which small vesicle structures approaching gaps in the reassembling NE around the chromatin where GFP-BAF was bound and proximal to microtubules were observed (Haraguchi *et al.*, 2008). This implied vesicle recruitment to chromatin-bound BAF for NE reassembly at the central "core" region of chromatin, after membrane coating on the peripheral ends of chromatin. Also, implies involvement of microtubules in regulating vesicle recruitment or in determining the localisation of BAF to this region. Although this was not discussed, the diameter of the vesicles visualised in this study were consistent with the range occupied by ER tubules (Schroeder *et al.*, 2019).

Diffusion models

Currently, it is more widely accepted that the NE is reassembled from NE proteins which disperse into ER structures after NEBD. Although, even within these models there are different mechanisms proposed for the mitotic distribution of NE proteins and the ER structures involved in NE reassembly.

The diffusion models state that NE proteins disperse into the ER at NEBD, with two different behaviours of NE proteins proposed, either freely diffusing within the ER membranes or concentrated within subdomains enriched in particular NE proteins. Early dynamic studies of the INM protein LBR suggested that NE proteins were diffuse within ER structures in mitosis, before binding chromatin for NE reassembly (Ellenberg *et al.*, 1997), however these studies were at low resolution and features, including subdomains, may not be resolved. Indeed, in recent years super resolution microscopy has revealed subdomains of interphase ER tubules enriched in ER proteins (Gao *et al.*, 2019), but similar has not been applied to protein dynamic studies in mitotic cells.

Although contacts between the NE and underlying structures are lost upon mitotic entry, some enrichment in subdomains may be maintained from sites of contact and persist into mitosis. Examples of distinct subdomains of the ER enriched in specific proteins have been observed in mitotic cells.

Spindle-associated membrane protein 1 (Samp1) and emerin, both localising to INM in interphase, do not completely overlap in localisation in mitosis (Buch *et al.*, 2009). Both proteins localised similarly within the majority of mitotic ER membrane in mammalian cells, but emerin was not present at spindle-associated ER membrane domains containing Samp1 (Buch *et al.*, 2009).

In terms of the ER structures functioning in NE reassembly, different models have also been proposed. Anderson and Hetzer (2008) reported that ER tubules form initial contacts to chromatin and then remodel to form sheets coating the chromatin in mammalian cells (U20S). The reduced expression of ER tubule-stabilising reticulon protein was found to delay NE assembly, whereas overexpression increased the rate of reassembly (Anderson and Hetzer, 2008), indicating the importance of tubule-to-sheet remodelling in forming the NE. However, this did not exclude a role for cisternae in NE reassembly. Other groups report that ER cisternae form the first coat at the peripheral ends of chromatin before expanding around the perimeter of the chromatin mass in two mammalian cell types (HeLa and BSC1) (Lu *et al.*, 2011). Although tubule-to-sheet remodelling may also have a function in these cells.

Mitotic ER structure has been shown to be dependent on cell type (Lu *et al.*, 2009; Puhka *et al.*, 2012), therefore the NE reassembly mechanism may also depend on the abundance of tubular relative to cisternal or intermediate structures (fenestrated sheets) in different cell types. This could influence structures contacting to form NE and the extent of remodelling from tubules required to reassemble the NE.

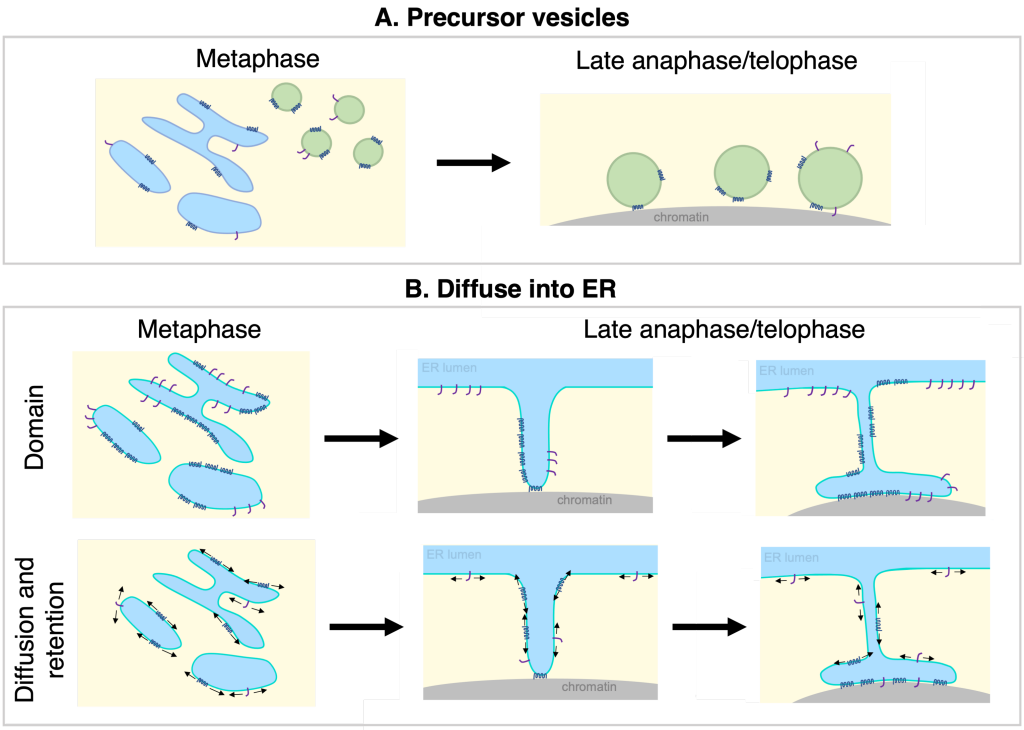

Figure 1.7. NE reassembly mechanisms. (**Vesicle model**). NE proteins are present in vesicles formed from the NE. These vesciles are enriched in NE components which contact chromatin, vesicles flatten and then fuse to form the NE on the chromatin surface. Vesicles may also fuse to other vesicles or membrane already coating the chromatin. (**Diffusion models**). NE proteins present within the ER structures interact with chromatin directly or with chromatin bound proteins, recruiting ER membranes to the chromatin for NE reassembly. ER structures involved in making initial contacts to chromatin for reassembly may involve ER tubules, which then remodel to sheets to spread and reform the NE (as shown). However, other some groups have reported that ER cisternae make the initial contacts to chromatin to form the NE. The exact mechanism may be cell type dependent, as different ratios of ER tubules and cisternae are present in mitosis.)

1.5.2 Recruitment of NE components to chromatin

The NE components are recruited to chromatin in an ordered and spatially restricted pattern for NE reassembly. Transient subdomains formed at regions of chromatin during NE reassembly, termed "core" and "non-core" (Haraguchi *et al.*, 2000), are formed by the recruitment of components to specific chromatin regions or their concentration within these regions by spatial regulating factors. Many of the interactions involved in determining the hierarchy of protein recruitment are regulated by post-translational modifications that reestablish interactions of NE proteins with chromatin or chromatin-bound protein to reassemble the NE.

Order and binding

BAF is one of the first nuclear proteins to bind chromatin after entry to anaphase and has a role in recruiting several other proteins to chromatin to initiate NE reassembly. BAF transiently localises around the chromatin mass before becoming strongly concentrated at the central "core" region of chromatin during telophase (Haraguchi *et al.*, 2008). BAF recruits INM proteins emerin, MAN1 and LAP2β, through binding to a LAP2-emerin-MAN1 (LEM) domain present in each protein, and the nuclear lamina protein lamin A to this central chromatin region (Haraguchi *et al.*, 2001; Mansharamani and Wilson, 2005). LAP2α, a nucleoplasmic protein containing a LEM domain, was also recruited to the central region of chromatin by BAF (Dechat *et al.*, 2004). Despite each containing a conserved LEM domain, through which these proteins can interact with BAF, emerin, LAP2β, MAN1 and LAP2α were each recruited to chromatin and concentrated within the "core" region with different dynamics (Haraguchi *et al.*, 2008).

After concentration of BAF at the "core" region, nuclear lamin protein lamin A and LEM domain proteins emerin (INM) and LAP2α (nucleoplasmic) were next concentrated to the "core" (Haraguchi *et al.*, 2008). LAP2β and MAN1, both transmembrane LEM proteins, were then concentrated at this central region (Haraguchi *et al.*, 2008). The INM proteins, including the LEM domain proteins described which are localised to the "core" region of chromatin, also bring membrane to the chromatin for reassembly of the NE. The initial binding of BAF to chromatin and to LEM domain proteins are regulated by PP2A- and PP4-mediated dephosphorylation of BAF (Asencio *et al.*, 2012; Zhuang *et al.*, 2014), and phosphorylation of individual LEM domain proteins (Hirano *et al.*, 2009).

Another INM protein recruiting membrane to chromatin during NE reassembly is

the INM protein LBR, which shows a different localisation pattern at chromatin to "core" localising proteins described (BAF, the LEM domain proteins and lamin A). LBR, nuclear pore proteins and lamin B initially localise to "non-core" peripheral ends of chromatin (Haraguchi *et al.*, 2008). LBR is reported to have similar recruitment timing to chromatin as LEM domain proteins also localising to the INM (emerin (Haraguchi *et al.*, 2000, 2008), LAP2β and MAN1 (Haraguchi *et al.*, 2008)), but with a distinct pattern of recruitment. LBR recruitment to chromatin is regulated, at least in part, by PP1γ (protein serine/threonine phosphatase-1 γ isoform) (Ito *et al.*, 2007). PP1γ is recruited to chromatin in early anaphase through regulatory subunit Repo-Man (Vagnarelli *et al.*, 2011) under temporal control by CDK1 inactivation (Vagnarelli *et al.*, 2006). PP1γ in complex with Repo-Man dephosphorylates histone H3 protein, restoring HP1 interaction with chromatin, and recruiting membrane for NE reassembly through interaction of INM protein LBR with HP1 (Ye and Worman, 1996) and H3 (Polioudaki *et al.*, 2001).

Later in mitosis, nuclear envelope proteins become more distributed around the chromatin (Haraguchi *et al.*, 2008). This again occurrs with different dynamics for individual proteins (Haraguchi *et al.*, 2008), suggesting difference in the mechanism of distribution or interactions of the individual proteins that affect movement of, or within, the membrane. The NE must also expand to accommodate decondensing chromatin at this stage.

Regulation of transient telophase subdomains at the reassembling NE

The nucleoporin ELYS has been found to have a role in formation of the transient "core" and "non-core" subdomains at the NE during reassembly in late mitosis (Clever *et al.*, 2012). ELYS can directly bind to chromatin, where the protein initiates NPC assembly during mitosis (Franz *et al.*, 2007). ELYS recruitment to chromatin may be regulated by RanGTP (Fernandez and Piano, 2006; Franz *et al.*, 2007), which is highest in proximity to chromatin through regulation by the guanine-nucleotide exchange factor RCC1 bound to chromatin, which promotes the GTP-bound active form (reviewed by Clarke and Zhang (2008)).

In late anaphase, ELYS is concentrated at the "non-core" peripheral ends of chromatin (Franz *et al.*, 2007). LBR is recruited to the chromatin peripheral ends by interaction with ELYS bound to this region chromatin (Clever *et al.*, 2012). This interaction is cell cycle- and phosphorylation-dependent (Clever *et al.*, 2012). In turn, ELYS also regulates LBR phosphorylation through an as yet unidentified mechanism (Mimura *et al.*, 2016). Depletion of ELYS affected the concentration of the "core" component BAF and of lamin A and

LEM domain proteins emerin and LAP2β (known to be recruited by BAF to chromatin) to the "core" region (Clever *et al.*, 2012). This suggested role for ELYS in formation of both the "core" and "non-core" subdomains during NE reassembly, although the precise mechanism remains unclear. Phosphorylated "core" component BAF has been found to concentrate at the "core" region, while total BAF was detected around the chromatin mass at this stage (Zhuang *et al.*, 2014), also suggesting the involvement of phosphoregulation in establishing the "core" subdomain. The mitotic ER shaping protein REEP4 and ELYS both localise to the "non-core" chromatin regions (Golchoubian *et al.*, 2022) which may imply a role in recruitment of highly curved ER structures, likely tubules, for reassembly in the "non-core" region. This supports the idea that there may be distinct ER structures recruited or spreading to form NE at "core" compared to "non-core sites".

Other groups have proposed a role for mitotic spindle microtubules in establishing telophase subdomain formation (Haraguchi *et al.*, 2008; Liu *et al.*, 2018). The spindle microtubules may exclude larger ER sheet structures, but not smaller ER tubule structures, from accessing the "core" region of chromatin during NE assembly (Liu *et al.*, 2018). This may also affect the NE proteins recruited to "core" and "non-core" subdomains of chromatin at telophase through their concentration in particular ER structures or differential association with spindle microtubules for delivery. Indeed in cells, BAF (Haraguchi *et al.*, 2008; Dubińska-Magiera *et al.*, 2019) and emerin (Dubińska-Magiera *et al.*, 2019) localise to the mitotic spindle. This suggests that microtubule association could have a role in delivery of components to the "core" chromatin regions for transient subdomain formation at reforming NE (Haraguchi *et al.*, 2008).

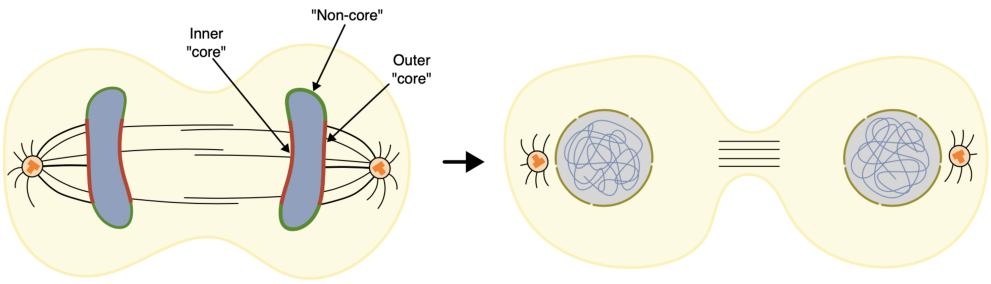

Figure 1.8. Transient subdomains during NE assembly in telophase. "Core" and "non-core" subdomains at the telophase NE described by Dechat *et al.* (2004); Haraguchi *et al.* (2008); Liu *et al.* (2018). "Core" localising proteins include BAF, LEM domain proteins (LAP2α, LAP2β, emerin and MAN1) and A-type lamins (lamin-A/C). "Non-core" proteins described include LBR, NPC components and B-type lamins. Later in NE assembly, the nuclear and NE proteins become more disperse around the NE.

1.5.3 Coordination with chromatin separation

The EZ around the mitotic spindle, described above, has an important role in preventing premature coating of chromatin with membranes during mitosis. Spindle microtubules are also proposed to physically exclude larger ER structures from the spindle region, coordinating reassembly of the NE with mitotic spindle disassembly and chromatin separation (Liu *et al.*, 2018). In addition, a phosphorylation gradient from Aurora B kinase activity within the spindle midzone regulates NE reassembly relative to extent of chromosome separation (Afonso *et al.*, 2014). As a result, the inner "core" region of chromatin (facing the opposite chromatin mass) that is exposed to the highest Aurora B activity has delayed membrane recruitment relative to the peripheral ("non-core") and outer "core" regions (Afonso *et al.*, 2014).

1.5.4 Coordination with chromatin decondensation

Chromatin decondensation is coordinated with chromosome segregation and NE reassembly. Defects can cause formation of NE invaginations commonly identified in cancer cells and in laminopathies (as reviewed in Malhas *et al.* (2011)). Chromatin decondensation is also coupled with expansion of the NE to accommodate the increasing volume occupied by the decondensing chromatin.

The mechanisms coordinating chromatin condensation and NE reassembly processes involve dephosphorylation of histone proteins, which cause structural changes in the chromatin and allow interaction with proteins for recruitment of NE components and membrane for NE reassembly, example LBR and associated membrane, as described in the above section.

BAF is one of the first proteins recruited to chromatin during the NE assembly process. BAF forms oligomers bound to DNA, crosslinking and compacting chromatin (Zheng *et al.*, 2000). This chromatin compaction acts as a barrier on the chromatin surface to prevent access of membranes within chromatin and restricting NE formation to the chromatin surface (Samwer *et al.*, 2017). Formation of dense, compact chromatin by histone deacetylation (Schneider *et al.*, 2022) and BAF (Haraguchi *et al.*, 2008) also prevent microtubules accessing within the chromatin and preventing missegregation (Schneider *et al.*, 2022).

1.5.5 Sealing holes in the NE

Finally, in the reassembly process, gaps in the NE need to be resolved. Endosomal sorting complexes required for transport (ESCRT) proteins complexes function in membrane remodelling processes, including during NE reassembly and repair,

and also membrane abscission during cytokinesis (reviewed by Gatta and Carlton (2019)). ESCRT-III functions to seal holes in the NE during reassembly left at sites of microtubule connections to chromatin. ESCRT-III components are recruited to chromatin after interaction of the CHMP7 subunit directly with membrane or with INM protein LEM2 which is concentrated at the "core" chromatin regions, proximal to microtubules, through interaction with BAF in telophase (Olmos *et al.*, 2016; Gu *et al.*, 2017; von Appen *et al.*, 2020). CHMP7 recruitment is regulated by CDK1-mediated phosphorylation during early mitosis, which inhibits interaction of CHMP7 with LEM2 (Gatta *et al.*, 2021). CHMP7 recruits other ESCRT-III components, which in turn recruit the enzyme spastin, that disassembles spindle microtubules (Vietri *et al.*, 2015). The ESCRT-III complex assembled seals the holes left in the NE at sites where microtubule connections were lost and reestablishes nuclear compartmentalisation (Vietri *et al.*, 2015).

1.6 Misaligned chromosomes and defective micronuclear envelope

Accurate chromosome segregation requires alignment of chromosomes at the metaphase plate and timely segregation through stable attachment of kinetochores to microtubules from opposite spindle poles.

Misaligned chromosomes can arise through defective or absent attachment of kinetochores to mitotic spindle microtubules (shown in Figure 1.9). The formation of attachments to spindle microtubules is error-prone (Cimini *et al.*, 2003). The kinetochore attachments formed are assessed by the SAC, which blocks separation of chromosomes with attachment defects, to prevent chromosome missegregation. In addition, misaligned chromosomes may be aligned to the metaphase plate and recued from missegregated fate by error correction mechanisms. Even during anaphase, lagging chromosomes can still be rescued to the main chromatin mass. If attachment defects are not detected by the SAC and errors are not corrected, this can lead to chromosome missegregation, and result in aneuploidy or MN formation. The existence of multiple levels of control and correction mechanisms highlights the importance of preventing this fate and ensuring accurate segregation of chromosomes.

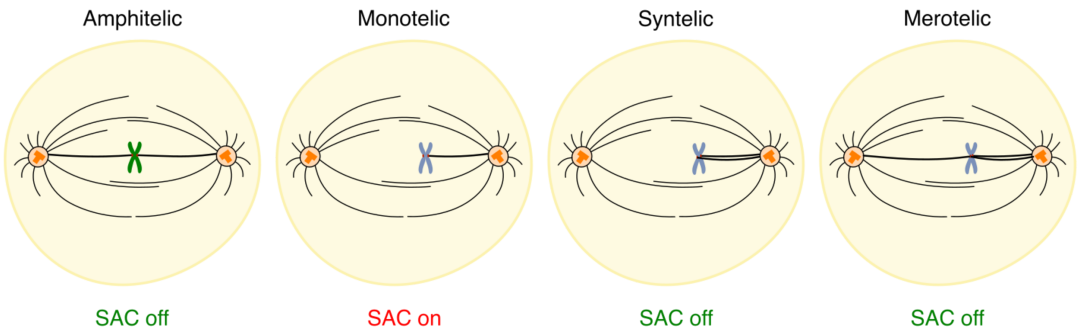

Figure 1.9. Types of kinetochore attachment error. (**Amphitelic**). Stable attachment of sister kinetochores to microtubules emanating from opposite spindle poles. (**Monotelic**). One kinetochore is attached to microtubules from one spindle pole, but the sister kinetochore remains unattached. (**Syntelic**). Sister kinetochores attached to microtubules from the same spindle pole. (**Merotelic**). Single kinetochore with attachment to microtubules from both spindle poles.

1.6.1 Error correction mechanisms

Merotelic and syntelic attachments

Merotelic attachment describes when a single kinetochore becomes attached to microtubules from both spindle poles (as shown in Figure 1.9). These errors have been found to occur often during early mitosis in mammalian cells (Cimini *et al.*, 2003). The erroneous attachments can silence the SAC at both kinetochores as chromosomes are bioriented, with tension from each pole. Merotelic attachments therefore have the potential to result in misaligned chromosomes in anaphase.

However, error correction mechanisms act to prevent chromosome missegregation from merotelic attachments through correction of attachment errors before progression to anaphase. Despite attachment to both poles, pulling forces at the incorrect attachment of the merotelic kinetochore are stronger than the force at the correctly attached sister kinetochore, due to the attachment of merotelic kinetochore to both poles, meaning a stronger pulling force is required to move towards the correct spindle pole. Tension at kinetochores has been shown to increase or to maintain the normal number of kinetochore microtubules within the attached fibre and ultimately improve the stability of the microtubule attachment at metaphase (Nicklas and Ward, 1994; King and Nicklas, 2000).

The activity of an Aurora B kinase of the chromosome passenger complex (CPC) destabilises microtubule attachments to kinetochores by phosphorylation of kinetochore protein Ndc80 (DeLuca *et al.*, 2006; Akiyoshi *et al.*, 2009). This destabilising activity is responsible for the difference in pulling force at the correct and erroneous attachments of merotelic kinetochore. Through stronger pulling force from the correct spindle pole on the merotelic kinetochore, the chromosome

may segregate correctly (Cimini *et al.*, 2003). The kinetochore attachment to the microtubule fibre from the incorrect pole, which is less stable, may also completely detach upon pulling force (Cimini *et al.*, 2003).

Specificity of destabilising the merotelic kinetochore connection to the incorrect spindle pole was originally proposed to be determined by the position of merotelic attachment to the this pole being positioned closer to Aurora B bound at centromeres than the attachment to the correct pole (opposite to the other pole to which correctly attached kinetochore is bound), which is being pulled away from the centromere (Cimini *et al.*, 2006). However, the positioning at the inner centromere has since been found to not be necessary to the error correction. Instead, the important role of tension in regulating kinetochore architecture and Aurora B destabilising activity has been shown (Auckland *et al.*, 2017; de Regt *et al.*, 2022).

The action of these correction mechanisms mean that incidence of merotelic attached chromosomes missegregating at anaphase is infrequently in normal diploid cells, despite merotelic attachment errors frequently occurring during early mitosis (Cimini *et al.*, 2003).

Syntelic attachment describes when both sister kinetochores are attached to microtubules from the same spindle pole. Syntelic attachments do not activate the SAC, as both kinetochores are attached to spindle microtubules. However, the tension on the kinetochores mean that these attachment errors can be corrected through the attachment-destablising activity of Aurora B, similar to as described for merotelic attachment correction.

Monotelic attachments

Monotelic attachment occurs when one sister kinetochore is unattached (as shown in Figure 1.9). Unlike merotelic and syntelic attachments, monotelic attachments activate the SAC, which blocks cells with these erroneous attachments progressing to anaphase (Cimini *et al.*, 2002).

Anaphase correction

The error correction mechanisms described above can correct the majority of kinetochore attachment errors prior to progression into anaphase. However, a small percentage of cells may progress into anaphase with merotelic attachments that are not detected by the SAC and not successfully corrected, forming lagging chromosomes in anaphase (Cimini *et al.*, 2002). An Aurora B phosphorylation gradient present in anaphase, with highest levels at the spindle midzone, is

generated through association with spindle microtubules (Fuller *et al.*, 2008). This gradient corrects any errors persisting in anaphase through delay of NE assembly on lagging chromosomes within the higher Aurora B activity region in the spindle midzone between the poles and on the inner "core" of the main chromatin mass that faces this region, to allow for reincorporation of the misaligned chromosome and to prevent MN formation (Afonso *et al.*, 2014; Warecki and Sullivan, 2018; Orr *et al.*, 2021).

1.6.2 Aneuploidy and MN formation

Genomic instability has been described as an "enabling characteristic" that facilitates acquisition of the properties constituting the hallmarks of cancer (Hanahan and Weinberg, 2000). Chromosome instability (CIN), a form of genomic instability, describes the situation where changes in chromosome number or structure occur at an increased rate (Tijhuis *et al.*, 2019). This is associated with poor patient prognosis through capabilities acquired or lost as a result of these chromosomal changes (Tijhuis *et al.*, 2019). CIN can occur as a consequence of aneuploidy or at micronuclear DNA.

Aneuploidy is described as chromosome content which differs from normal in a cell. This can occur by gain or loss of whole chromosomes (numerical aneuploidy) or regions of single or multiple chromosomes (structural aneuploidy) (Tijhuis *et al.*, 2019). Structural and numerical aneuploidy can both result from defects in chromosome segregation during mitosis. Aneuploidy is reported in most cancer types and in approximately 90% of tumours (Zhou *et al.*, 2020).

MN are small DNA-containing structures separate from the main nucleus. MN can form during mitosis from misaligned whole chromosomes that are not rescued to the main chromatin mass and subsequently missegregate in anaphase. MN can also form from chromosome fragments that result from DNA damage events. For example at chromatin bridges or from existing MN, which form chromosome fragments without a centromere. Missegregated chromosomes or chromosome fragments can become coated in membrane, forming a MN, and then remain separated from the main nucleus. It is also possible for MN to form during interphase, by budding from the NE, although mitotic error is the most likely source of MN (Shimizu *et al.*, 1998).

Due to defects in the surrounding nuclear envelope, which affect envelope function and stability, MN are source of DNA damage and CIN. This can include chromothripsis, which describes chromosome fragmentation within a chromosome or chromosome arm, and error-prone reassembly (Crasta *et al.*, 2012; Zhang *et al.*,

2015). Chromosomes or chromosome fragments incorporated in MN are also more likely to missegregate in the subsequent divisions (Soto *et al.*, 2018).

1.6.3 Misalignment and missegregation

Despite multiple checks and correction mechanisms, cells with misaligned chromosomes can enter anaphase under certain conditions, although this is expected to occur at low frequency, resulting in missegregation of the chromosome (Cimini *et al.*, 2003). This leads to the question as to what factors promote the missegregated fate of a misaligned chromosome. The origin and position of the misaligned chromosome within the cell is one factor proposed to affect missegregation frequency (Ferrandiz *et al.*, 2022; Vukušić and Tolić, 2022). Two types of misaligned chromosome that can arise are lagging and polar chromosomes, classified by mechanism of misalignment and resulting position within the cell. How does the position of the misaligned chromosome within the cell affect the fate of the chromosome?

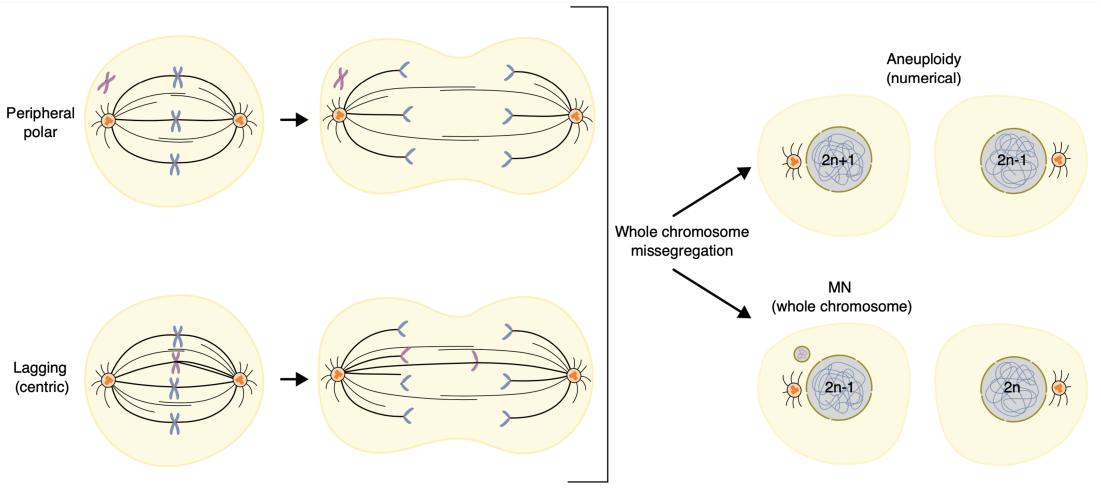

Figure 1.10. Misaligned chromosome segregation defects. Peripheral polar chromosomes are positioned beyond the spindle region and require multiple steps to align at the metaphase plate, and may be more prone to attachment errors as a result of their position relative to the spindle and the membrane EZ. These polar chromosomes may become misaligned, for example through delay in alignment or by ensheathing in membranes outside of the EZ. Lagging chromosomes are those observed in the space between the two chromatin masses as these separate in anaphase and result from mitotic defects, for example erroneous merotelic attachment of kinetochores as shown.

Lagging chromosomes

Lagging chromosomes can arise during anaphase from errors in chromosome congression and alignment to the metaphase plate that result in a misaligned chromosome positioned between the chromatin masses and lagging behind in anaphase (Fonseca *et al.*, 2019). These errors include the incorrect attachment

of kinetochores to spindle microtubules, example merotelic attachment (Figure 1.9). Lagging chromosome fragments can also form by absent attachment in acentric chromosomes fragments that can arise through unrepaired DNA damage (reviewed by Guo *et al.* (2019)).

Polar chromosomes

Polar chromosomes are those located outside of the central spindle region, often beyond the spindle pole. These chromosomes rely on several more steps for their alignment at metaphase plate than chromosomes positioned between the spindle poles after NEBD (as recently reviewed by Vukušić and Tolić (2022)). The position these chromosomes beyond the spindle pole requires the generation of a different force at each kinetochore to pull the chromosome in the direction of the spindle equator (Auckland *et al.*, 2017). The proximity to centrosomes, from which microtubules polymerise, increases chance of encountering and forming multiple attachments and erroneous attachments, as reviewed by Vukušić and Tolić (2022). Polar chromosomes may become missegregated through multiple mechanisms, which include delayed or defective alignment to the metaphase plate (Kuniyasu *et al.*, 2018; Gomes *et al.*, 2022).

Membranes promote missegregation

Polar misaligned chromosomes are situated outside of the membrane EZ that exists around the mitotic spindle. These chromosomes can become ensheathed in layers of membranes present within this region (Ferrandiz *et al.*, 2022). Ensheathing of misaligned chromosomes promotes subsequent missegregation, and represents a new mechanism of aneuploidy and MN formation (Ferrandiz *et al.*, 2022). Indeed, membranes have been demonstrated to slow or restrict chromosome movements (Merta *et al.*, 2021), which may delay or prevent rescue of misaligned chromosomes positioned outside the EZ to the metaphase plate. Kinetochore attachments were also affected by the ensheathing of chromosomes, with no stable microtubule contacts detected (Ferrandiz *et al.*, 2022). This further highlights the importance of the membrane EZ around the spindle in preventing chromosome missegregation.

1.6.4 Defective micronuclear envelope formed at misaligned chromosomes

The envelope surrounding misaligned chromosomes that form a MN is defective and this has consequences for the function and protection of the micronuclear

DNA. This includes transport across the micronuclear envelope (MNE) (Liu *et al.*, 2018), affecting processes such as DNA damage repair and DNA replication (Okamoto *et al.*, 2012). The defects affect the stability of the MNE, meaning that MN are prone to rupture, which exposes the micronuclear DNA to cytoplasmic content (Hatch *et al.*, 2013). This can result in extensive DNA damage, including at the level of chromosome fragmentation (chromothripsis), and initiate an innate immune response (Crasta *et al.*, 2012). MN disruption allows ER tubules to access within the micronuclear DNA and alters chromatin compaction (Hatch *et al.*, 2013). MN disruption occurred frequently in several mammalian cancer cell lines, reported in over 65% of MN in U2OS cells (Hatch *et al.*, 2013). This disruption may also affect the fate of the micronuclear DNA in subsequent cell divisions, further demonstrating the potential long-term consequences of MN disruption (Hatch *et al.*, 2013). Disrupted MN were identified in tumour sections from human non-small-cell lung cancers and could act as a marker for CIN (Hatch *et al.*, 2013).

MN disruption has been described to occur after mitotic exit (Hatch *et al.*, 2013), which raises the question as to what factors determine the disrupted fate. The profile of proteins incorporated at the MNE and the dynamics of their recruitment to misaligned chromosomes during mitosis could affect the function and stability of the MNE and explain the disruption. Indeed, changes in the level and coating of the nuclear lamina protein lamin B1 at MN have been identified before disruption occurs (Hatch *et al.*, 2013). This could also be true of nuclear envelope proteins, particularly the INM proteins, which provide contact to underlying nuclear lamina proteins and recruit membrane to form NE. Increased levels of the INM proteins LBR and emerin have been observed at MN formed from lagging chromosomes (Maass *et al.*, 2018), suggesting altered recruitment.

MNE formation and composition is affected by the origin or position of the misaligned chromosome within the cell. The recruitment of a subset of nuclear/NE proteins ("non-core" proteins) has been reported to be delayed or impaired at lagging chromosomes forming MN (Liu *et al.*, 2018; Orr *et al.*, 2021). The described "non-core" proteins include NPC components and therefore expect transport of DNA repair machinery and other nuclear components into MN formed to be defective, and therefore affect stability and function of the MNE assembled at these misaligned chromosomes.

The recruitment of components for MNE assembly to misaligned chromosomes is regulated by the Aurora B phosphorylation gradient in the spindle midzone in anaphase. The Aurora B phosphorylation gradient has been shown to delay recruitment of components for NE reassembly to lagging chromosomes (positioned

between the spindle poles, where higher Aurora B activity) (Warecki and Sullivan, 2018; Orr *et al.*, 2021). Polar chromosomes situated outside of the Aurora B midzone may incorporate these "non-core" proteins with normal dynamics. Microtubules are also implicated in determining the proteins recruited to form the MNE (Liu *et al.*, 2018), but their role is not well understood.

In addition to affects on the profile of proteins at the MNE, the ensheathing of polar chromosomes positioned outside of the membrane EZ may also affect the stability of MNE formed through the mechanism of assembly and properties of the envelope formed. The identity and size of the missegregated chromosome forming the MN have also been proposed to explain the stability of MNE formed (Mammel *et al.*, 2022).

1.7 Aims of PhD project

We aim to understand the fate of proteins originating from the NE after the NE breaks down in early mitosis and how this localisation relates to the mitotic ER. This will inform current models proposed for NE protein localisation and the mechanisms by which membrane structures containing these proteins coat chromatin to reassemble the NE in mitosis. We also set out to explain how the reassembly process differs at misaligned chromosomes forming a defective MN envelope.

Chapter 2

Materials and Methods

2.1 Molecular Biology

2.1.1 Cloning protocol

Cloning was by a "cut and paste" method, whereby restriction enzyme sites, one located upstream and one downstream of the region of interest in the donor vector are also found at the intended integration site within the target vector. This allowed direct ligation of the region of interest into the target site of the vector after digestion. Alternatively, primers were designed to amplify across the region by PCR and introduce restriction enzyme sites at the ends of the insert, corresponding to restriction sites within the vector at which the PCR product will be inserted.

2.1.2 Plasmids

The following plasmids were available from Addgene: EGFP-BAF (Addgene #101772); Emerin pEGFP-C1 (637) (Addgene #61993); LAP2 Full I pAcGFP-N1 monomeric GFP (1317) (Addgene #62044); LBR pEGFP-N2 (646) (Addgene #61996); mRuby2-LaminA-C-18 (Addgene #55901); pAc-GFPC1-Sec61β (Addgene #15108); pMaCTag-P05 (Addgene #120016); pMD2.G (Addgene #12259); pMGF182 (Addgene #97006); pMito-mCherry-FRB (Addgene #59352); psPAX2 (Addgene #12260); pVE13300 (Addgene #137715); pWPT-GFP (Addgene #12255); Stargazin-GFP-LOVpep (Addgene #80406). mCherry-Histone H3.2 plasmid was provided as a gift (A. Bowman, University of Warwick).

FKBP-GFP-N1 and FKBP-GFP-C1 plasmids used in cloning were constructed in the Royle lab using BamHI-AgeI or NheI-AgeI restriction enzymes, respectively,

to introduce FKBP insert into pEGFP-N1 or pEGFP-C1 plasmid (Clontech).

Plasmids encoding mCherry-tagged nuclear or nuclear envelope proteins were constructed from available plasmids encoding GFP-tagged protein. The region encoding LAP2 (rat) was cut from LAP2 Full I pAcGFP-N1 monomeric GFP (1317) plasmid using NheI-BamHI restriction enzymes and ligated into similarly digested pmCherry-N1 vector. The mCherry-emerin plasmid was generated through replacing the tag of available Emerin pEGFP-C1 (637) vector with mCherry fragment from pmCherry-C1 using AgeI-XhoI restriction sites. To construct plasmids encoding mCherry-BAF or mCherry-CHMP7, the region encoding BAF or CHMP7 was amplified by PCR from available EGFP-BAF or pMGF182 plasmids, also introducing BglII and HindIII restriction sites at the ends of the amplified region to allow insertion into pmCherry-C1 vector. Similarly, to clone LBR-mCherry, the LBR-encoding region was amplified from available LBR pEGFP-N2 (646) plasmid, introducing KpnI and BamHI sites at the ends of the region. The digested PCR product was ligated into pmCherry-N1 vector. PCR primer sequences are listed in Table 2.1.

Plasmid encoding tagged ER protein mCherry-Sec61β was constructed by digestion of pAc-GFPC1-Sec61β with EcoRI-BglII and ligation into pmCherry-C1 vector (made by substituting mCherry for EGFP in pEGFP-C1 by AgeI-XhoI digestion).

Transfer plasmids for lentiviral transduction (pWPT LAP2beta-mCherry, pWPT LBR-mCherry, pWPT mCherry-BAF, pWPT mCherry-CHMP7, pWPT mCherry-emerin) were constructed through introduction of restriction sites (using MluI-SalI sites or MluI-BstBI sites for LBR-mCherry) by PCR to allow insertion of mCherry-tagged gene in substitution of GFP encoding region in pWPT-GFP vector. The mCherry-tagged genes were amplified using primer sets listed in able 2.1

The template plasmid for C-terminal PCR tagging method (Fueller *et al.*, 2020) encoding FKBP-GFP tag, pMaCTag-P05-FKBP-GFP, was generated through amplifying the region encoding FKBP-GFP from FKBP-GFP-N1 and introducing BamHI-SpeI restriction sites (Table 2.1). The PCR product was ligated in substitution of the GFP tag present in available pMaCTag-P05 plasmid.

Plasma membrane anchor Stargazin-darkmCherry-FRB was constructed by PCR of Stargazin encoding region from Stargazin-GFP-LOVpep using primer sets listed in Table 2.1. Plasmid encoding SH4-FRB-EBFP2 was made by replacing mRFP tag of SH4-FRB-mRFP plasmid available from previous work (Wood *et al.*, 2017). and ligation into pMito-mCherry-FRB-K70N plasmid, substituting for

pMito tag, at NheI-BamHI sites. The dark mCherry Mitotrap construct was made by site-directed mutagenesis (K70N mutation) (Wood *et al.*, 2017).

FKBP-GFP-Sec61β was generated by ligating BglII-EcoRI fragment from pAc-GFP-C1-Sec61β into digested FKBP-GFP-C1 plasmid

Re-routable NE proteins could be constructed using a cut and paste method. FKBP-GFP-BAF using BglII-Acc65I enzymes to cut BAF constructed from mCherry-BAF plasmid and ligate into FKBP-GFP-C1 vector. Similarly, to clone FKBP-GFP-CHMP7, the CHMP7 encoding region was cut from mCherry-CHMP7 plasmid using BglII-Acc65I restriction sites and product ligated into FKBP-GFP-C1. To make FKBP-GFP-emerin construct, the region encoding emerin was cut from Emerin pEGFP-C1 (637) plasmid using XhoI-BamHI and product ligated into FKBP-GFP-C1. LBR-FKBP-GFP was generated by cutting LBR from LBR-mCherry using BamHI-KpnI sites and ligating into FKBP-GFP-N1 plasmid. To clone FKBP-GFP-LAP2β, BglII-SalI sites were introduced at either end and a C-terminal stop codon to LAP2β amplified by PCR from LAP2 Full I pAcGFP-N1 monomeric GFP (1317) plasmid template, using oligos as listed in Table 2.1. Digestion and ligation into FKBP-GFP-C1 vector.

2.1.3 PCR Primers

Table of primer sequences used in PCR amplification of target regions, introducing restriction enzyme sites for cloning.

Primer Name	**Sequence (5' - 3')**	**Cloning**
LD005 (F)	aagcttGGTACCcATGCCAAGTAGGAAATTTGC	LBR-mCherry
LD006 (R)	tcgagGGATCCgtGTAGATGTATGGAAATATACGG	LBR-mCherry
LD007 (F)	aagcttAGATCTTGGTCCCCGGAGCGG	mCherry-CHMP7
LD008 (R)	tcgagAAGCTTTCACAATGGCTTTAGAGTCGGTTC C	mCherry-CHMP7
LD009 (F)	aagcttAGATCTATGACAACCTCCCAAAAGC	mCherry-BAF
LD010 (R)	tcgagAAGCTTCTACAAGAAGGCATCACACC	mCherry-BAF
LD011 (F)	aagcttACGCGTcATGGTGAGCAAGGGCGAGG	pWPT- mCherry-BAF pWPT-mCherry-CHMP7 pWPT-mCherry-emerin
LD012 (R)	tcgagGTCGACCTACAAGAAGGCATCACACCACTC	pWPT mCherry-BAF
LD013 (R)	tcgagGTCGACTCACAATGGCTTTAGAGTCGG	pWPT mCherry-CHMP7
LD014 (R)	tcgagGTCGACCTAGAAGGGGTTGCCTTCTTCAG	pWPT mCherry-emerin
LD015 (F)	aagcttACGCGTcATGCCGGAGTTCCTAGAGGACC	pWPT LAP2-mCherry
LD016 (F)	aagcttACGCGTcATGCCAAGTAGGAAATTTGCC	pWPT LBR-mCherry
LD017 (R)	tcgagTTCGAATTACTTGTACAGCTCGTCCATGC	pWPT LBR-mCherry
LD018 (R)	tcgagGTCGACTTACTTGTACAGCTCGTCCATGC	pWPT LAP2-mCherry
LD031 (F)	aagcttAGATCTATGCCGGAGTTCCTAGAGG	FKBP-GFP-LAP2
LD032 (R)	tcgagGTCGACCTAgCAGTTGGATATTTTAGTATCT TGAAG	FKBP-GFP-LAP2

Primer Name	Sequence (5' - 3')	Cloning
AM03 (F)	aagcttGGATCCCCGCCACCAATGGGAGTGCAGGTGG	pMaCTag-P05 FKBP-GFP
AM04 (R)	tcgagACTAGTTTACTTGTACAGCTCGTCCATGCCGAGAGT	pMaCTag-P05 FKBP-GFP
CK003 (F)	gcggctagcATGGGGCTGTTTGATCGAGGTGTTCAAATGCTTTT	Stargazin-darkmCherry-FRB
CK007 (R)	TTTACTCATGGATCCttTACGGGCGTGGTCCGG	Stargazin-darkmCherry-FRB

Table 2.1. Sequence of PCR primer oligonucleotides used in cloning.

Table of primers designed for C-terminal PCR-tagging method of generating CRISPR knock-in HCT116 LBR-FKBP-GFP cell lines and genotyping PCR of edited cells.

Primer Name	Sequence (5' - 3')	Application
AM01 (M1)	CGTGACGAGTACCACTGTAAGAAGAAATACGGCGTGGCTTGGGAAAAGTACTGTCAGCGTGTGCCCTACCGTATATTTCCATACATCTACTCAGGTGGAGGAGGTAGTG	LBR-FKBP-GFP PCR-tagging
AM02 (M2)	TTTGCAAATGGCAGCTGGAATTGCAGGAGTATTTTGTAGAAAAGCCAGAAGAGCAAAAAAAAAGAGCATTAGTAGATGTATGATCTACACTTAGTAGAAATTAGCTAGCTGCATCGGTACC	LBR-FKBP-GFP PCR-tagging
AM11 (F)	AGAATTTGGGGGAAAGCAGG	Genotyping PCR
AM12 (R)	CATCCTTACTTGTATTTTTCCTATGTTAACTG	Genotyping PCR
AM13 (R)	CAGTGGCACCATAGGCATAA	Genotyping PCR
AM14 (F)	AAGACAATAGCAGGCATGCT	Genotyping PCR

Table 2.2. Sequence of PCR primer oligonucleotides and genotyping primers used in generating and characterising C-terminal PCR-tagging CRISPR knock-in cell line.

2.2 Cell Biology

2.2.1 Cell types and cell lines

All cell lines were kept in a humidified incubator at 37 °C and 5 % CO_2. Cell media was routinely tested for mycoplasma contamination by a PCR-based method.

HCT116 (ATCC, CCL-247) and cell lines derived from HCT116, HeLa (Health Protection Agency/European Collection of Authenticated Cell Cultures; 93021013) and HEK293T (ATCC, CRL-11268) cells were maintained in Dulbecco's Modified Eagle's Medium (DMEM) supplemented with 10 % FBS and 100 U mL^{-1} penicillin/streptomycin.

RPE-1 (Horizon Discovery) and derived cell lines were maintained in DMEM/F-12 Ham supplemented with 10 % FBS, 2 mM L-glutamine, 100 U mL^{-1}

penicillin/streptomycin and 0.26 % sodium bicarbonate ($NaHCO_3$).

RPE-1 GFP-Sec61β stable cell line was generated by Fugene-HD (Promega) transfection of pAc-GFPC1-Sec61β. Individual clones were isolated by G418 treatment (500 µg mL^{-1}) and were validated using a combination of western blot, FACS and fluorescence microscopy (Ferrandiz *et al.*, 2022).

Stable co-expression of mCherry-BAF, mCherry-emerin, mCherry-CHMP7, LBR-mCherry or LAP2β-mCherry with GFP-Sec61β in RPE-1 cells was achieved by lentiviral transduction of RPE1 cells stably expressing GFP-Sec61β. Individual cells positive for GFP and mCherry signal were sorted by FACS and single cell clones validated by fluorescence microscopy and western blot. Mitotic timings of mCherry-BAF and LBR-mCherry cell lines were measured and compared to timing of control cells (Ferrandiz *et al.*, 2022).

HeLa pMito-mCherry-FRB cell line was previously made in the lab by Liam Cheeseman. Briefly, HeLa Flp-in cells (gift from Francis Barr) were stably transfected with pEF5-FRT-V5-TOPO-pMito-mCherry-FRB and selected by hygromycin resistance.

HCT116 LBR-FKBP-GFP CRISPR knock-in cells were generated using C-terminal PCR tagging method (Fueller *et al.*, 2020). LBR-specific tagging oligonucleotides (M1 and M2) were designed using the online design tool (Fueller *et al.*, 2020). Oligonucleotide sequences are listed in the Table 2.2. PCR fragment was amplified from the template plasmid (pMaCTag-P05 FKBP-GFP) using LBR-specific tagging oligonucleotides. HCT116 cells were transfected with PCR cassette and plasmid encoding Cas12a (pVE13300). Cells were selected and maintained in media supplemented with puromycin dihydrochloride (Gibco) at 1.84 µM. Populations of cells positive for GFP signal were selected by FACS. Characterised cells through genotyping PCR (see primers in Table 2.2), western blot and immunofluorescence staining.

2.2.2 Lentiviral transduction

For lentiviral transduction, HEK293T packaging cells were incubated in DMEM supplemented with 10 % FBS, 2 mM L-glutamine, and 25 µM chloroquine diphosphate (C6628, Sigma) for 3 h. Transfection constructs were prepared at 1.3 pM psPAX2, 0.72 pM pMD2.G and 1.64 pM transfer plasmid (encoding the tagged protein to be expressed) in OptiPro SFM. Polyethylenimine (PEI) dilution in OptiPro SFM was prepared separately at 1:3 ratio with DNA (w/w, DNA:PEI) in the transfection mixture. Transfection mixes were combined, incubated at room temperature for 15 min to 20 min, and then added to the packaging cells.

Cells were incubated for 18 h, after which the media was replaced with DMEM supplemented with 10 % FBS and 100 U mL^{-1} penicillin/streptomycin. Viral particles were harvested 48 h post-transfection. Viral supernatant was centrifuged and filtered before applying to target cells. Target cells were then infected through incubation in media containing 8 µg mL^{-1} polybrene (408727, Sigma) for 16 h to 20 h. Media was replaced with complete media and cells were screened after 24 h.

2.2.3 DNA transfection

Transient transfections of DNA into HCT116, RPE-1 and HeLa were completed using Fugene-HD (Promega) or GeneJuice Transfection Reagent (Merck), following the manufacturer's protocol. Typically, a total of 1 µg of DNA was transfected per one well of 6-well plate or one fluorodish with 3 µL of transfection reagent. Example, for transfection of two plasmids, 0.5 µg of DNA of each plasmid was added to the transfection mix. Media on cells was exchanged for fresh complete media on the following day.

2.2.4 Cell synchronisation

To synchronise cells of particular stages of mitosis, cells (RPE1 GFP-Sec61β, RPE1 GFP-Sec61β LBR-mCherry, HCT116 LBR-FKBP-GFP or HeLa pMito-mCherry-FRB) were first treated with media containing thymidine at 2 mM for 16 h. After 16 h, media containing thymidine was removed, cells were washed gently three times with sterile PBS, and fresh media added. Incubated cells for a further 7 h-8 h. To block cells in early mitosis, nocodazole was then added at a final concentration of 330 nM. Incubated cells for around 16 h. To synchronise cells at G2/M boundary, after thymidine treatment and release period, RO-3306 (Sigma, SML0569) solution (prepared in DMSO), was added at 9 µM to media and applied to cells. Incubated cells for around 16 h.

2.2.5 Relocalisation

Rapamycin (J62473, Alfa Aesar) stock solution was prepared at 20 mM in 100 % ethanol. Prepared diluted aliquots at 200 µM from the stock by dilution in 100 % ethanol. The diluted aliquot (200 µM) was used to prepare solutions applied to cells.

Heterodimerisation of FKBP and FRB tags was induced through addition of rapamycin to media at a final concentration of 200 nM. For fixed cell experiments, 2 mL of 200 nM rapamycin dilution was prepared in complete media per well of a 6 well plate (2 µL of 200 µM rapamycin solution per 2 mL of media). Media was

removed from the wells, rapamycin-containing media was added, and then the plate was returned to the incubator for 30 min until fixation.

To apply rapamycin to live cells on the microscope, where media was already present in the dish. Rapamycin solution was prepared at 400 nM concentration in imaging media (Leibovitz's L-15 Medium, no phenol red, supplemented with 10 % FBS) and diluted (1:2) to final concentration 200 nM in media present in dish.

For synchronised cells, cells were washed three times with PBS to release from RO-3306 block. Rapamycin dilution was prepared at 200 nM in complete media (2 µL of 200 µM rapamycin solution per 2 mL of media) and siR-DNA (Spirochrome) added to a final concentration of 0.25 µM (0.25 µL of 1 mM stock added per 1 mL of media). The final PBS wash was removed from the dish and media containing rapamycin and dye was added. Dishes were incubated for 30 min, after which the dish was washed with PBS. Then 1 mL of imaging media was added to the dish in preparation for imaging.

2.2.6 Inducing misaligned chromosomes

To induce misaligned chromosomes in diploid RPE-1 cells or cell lines, cells were treated for 3 h with the centromere protein E (CENP-E) inhibitor GSK923295 at 150 nM, added to complete media. The 1 mM GSK923295 working solution, which was added to media, was prepared by dilution of original 50 mM stock (S7090, Selleckchem) in DMSO. After 3 h, the GSK923295 treatment was washed off the cells and fresh media added. Dishes were returned to the incubator for around 15 min, then SiR-DNA (Spirochrome) was added at 0.5 µM to the media. Dishes were incubated at least 15 min in SiR-DNA containing media before transfer to microscope for selection of cells and live imaging.

2.2.7 Immunofluorescence

For fixed-cell imaging, cells were seeded on glass coverslips (16 mm diameter and thickness number 1.5, 0.16 mm to 0.19 mm).

PFA fixation (3 % PFA/4 % sucrose in PBS) was for 15 min. PTEMF fixation (0.2 % Triton X-100, 0.02 M PIPES pH 6.8, 1 mM $MgCl_2$, 10 milliM EGTA, 4 % PFA in water) was for 10 min. For PLP fixation, cells were washed twice with 2 mL of PBS, and then fixed for 2 h at room temperature in 2 mL of freshly prepared PLP fixative (2 % [wt/vol] paraformaldehyde in 87.5 mM lysine, 87.5 mM sodium phosphate, pH 7.4, and 10.0 mM sodium periodate).

After fixation, cells were washed with PBS. Then cells were incubated in permeabilisation buffer (0.5 % v/v Triton X-100 in 1xPBS) for 10 min. Followed by two PBS washes, then 45 min to 1 h blocking (3 % BSA, 5 % goat serum in 1xPBS). Antibody dilutions were prepared in blocking solution (as in Table 2.3). After blocking, cells were incubated for 1 h with primary antibody, PBS washed (3 washes, 5 min each), incubated 1 h with secondary antibody, then 5 min each PBS wash (3 washes), mounting with Vectashield containing DAPI (Vector Labs Inc.) and then sealed.

Antibody	**Supplier**	**Dilution (IF)**
anti-LBR antibody produced in mouse (polyclonal)	SAB1400151, Sigma-Aldrich	1:300
Recombinant Anti-NUP133 antibody [EPR10808(B)] (Alexa Fluor 647) (monoclonal)	ab225215, Abcam	1:500
KDEL Polyclonal Antibody, rabbit (polyclonal)	PA1-013, Invitrogen	1:200
Anti-Pericentrin antibody - Centrosome Marker Rabbit (polyclonal)	ab4448, Abcam	1:5000
Monoclonal Anti-α-Tubulin antibody produced in mouse (monoclonal)	T6074, Sigma	1:1000
GFP-Booster ATTO488 conjugated nanobody	gba488, Chromotek	1:200
goat anti-rabbit 568	A11036, Invitrogen	1:500
goat anti-rabbit 647	A21245, Invitrogen	1:500
goat anti-mouse 647	A21235, Invitrogen	1:500

Table 2.3. Antibodies for Immunofluorescence. All antibody dilutions were prepared in blocking solution (3 % BSA, 5 % goat serum in 1xPBS).

2.3 Biochemistry

2.3.1 Harvesting mitotic cells

RPE1 GFP-Sec61β LBR-mCherry (or RPE1 GFP-Sec61β control) cells were seeded at around 1.5×10^6 cells per 150 mm dish (5 dishes per cell line). Cells were synchronised using thymidine-nocodazole treatment described above. After 16 h nocodazole treatment, media on cells was replaced with media containing rapapmycin (200 nM). Note rapamycin containing media was prepared using media removed from dishes, as a number of mitotic cells had already detached into the media. Dishes were incubated with rapamycin for 30 min before harvesting mitotic cells.

To harvest mitotic cells, mitotic shake off was used. Dishes were agitated and then the media containing mitotic cells was collected into a 50 mL tube. Collected mitotic cells were pelleted by centrifugation, washing off rapamycin treatment. Dishes were further agitated and washed with PBS to collect any remaining

mitotic cells. PBS from washes of each dish were collected into the tube containing pelleted mitotic cells from the same dish. Each dish was washed once more with PBS to collect any remaining mitotic cells, adding the PBS to the tube from the same dish. Cells were pelleted and then resuspended in 5 mL warm PBS. Cells collected from same conditions (sample or control) were combined at this stage. Centrifuged to pellet cells. Resuspended cells in 5 mL of cold PBS and transferred to 15 mL tube on ice in preparation for the next step (subcellular fraction collection or mitochondrial purification). Washed with 5 mL cold PBS to collect any remaining cells from the 50 mL tube and transferred to same 15 mL tube.

2.3.2 Subcellular fractionation

To prepare for subcellular fraction collection, all centrifuges and rotors to be used were cooled to 4 °C. All centrifugation steps were at 4 °C. Homogenisation buffer was prepared: 3 mM imidazole pH 7.2, 250 mM sucrose, adding protease inhibitor cocktail (Roche) before use. Note absence of detergents from reagents used for fraction preparation, to minimise potential disruption of membranous structures.

Pelleted cells were resuspended in 5 mL cold PBS on ice and transferred to a 15 mL tube. The original tube was washed with 5 mL cold PBS to collect any remaining cells into the same 15 mL tube. Samples were centrifuged (Eppendorf 5804R, S-4-72 rotor) to collect cells (134 g for 5 min). Then poured off supernatant. Added 7 mL cold HB and gently resuspended the pellet. Collected cells at 773 g for 7 min and then poured off supernatant. Resuspended cells in 1 mL cold HB using a 1000 µL tip, keeping the tip at the bottom of the tube.

Cells were homogenised by passing through a 23G needle. Initially, cells were passed twice (keep needle tip low, avoiding bubbles). Then checked for homogenisation under light microscope. Continued to further pass cells through needle and check for homogenisation until observed mostly released material and smooth grey nuclei. Avoided excessive number of passes, as this can rupture nuclei. At each subsequent fraction step, a small volume of fraction was visualised on a light microscope to access fraction purity.

First fraction step pelleted nuclei. Pellet at 1900 g for 12 min (Eppendorf 5417R, F-45-30-11 rotor). Carefully removed supernatant (post nuclear supernatant) and collected in a new tube on ice. Retained a small volume (75 µL) of the PNS in a separate tube for western blot. Resuspended pellet (nuclei) in (100 µL) cold IP wash buffer.

Second fraction step pelleted “heavy” membranes. Pelleted membrane fraction at

15 000 *g* for 15 min (Eppendorf 5417R). A small volume of the supernatant (light membrane and cytoplasm) was retained for western blot. Transferred remaining supernatant to ultracentrifuge tube (thickwall polycarbonate, ref 349622) on ice for next centrifuge step. Resuspended pellet ("heavy" membranes) in (100 µL) cold IP wash buffer.

Third fraction step pelleted "light" membranes. Required ultracentrifuge tubes to be around 80% full, or would require to adjusted spin speed, so additional cold HB buffer was added. Pelleted membrane fraction at 100 000 *g* for 1 h in ultracentrifuge (Optima Max-XP Tabletop Ultracentrifuge with TLA-100.3 Fixed-Angle Rotor). Supernatant (cytosol) was carefully transferred to a tube on ice. Pellet ("light" membranes) was resuspended using a 200 µL blunted pipette tip in 200 µL cold HB, harshly but avoiding bubble formation. Pipetted up and down further with a 200 µL "bevel-ended" tip to ensure pellet was fully resuspended, avoiding formation of bubbles. Samples were stored at - 20 °C.

2.3.3 Mitochondrial purification

Following harvest of mitotic cells (as described in Harvesting mitotic cells subsection), cells were lysed (50 mM Tris-HCl, pH 7.0 (at 25 °C), 150 mM NaCl, 1 mM EDTA, 1 mM DTT).

The mitochondria were then purified following manufacturer's instructions for Qproteome Mitochondria Isolation Kit (Quiagen), resuspending the mitochondrial pellet in 200 µL lysis buffer at the final step. Protease inhibitors were excluded from buffers, as PreScission protease was added at later step to cleave the tag. Important to keep samples cold at all times to prevent protein degradation.

2.3.4 PreScission protease cleavage

PreScission protease digestion was used to cut expressed tagged proteins containing the specific cleavage site recognised by the enzyme (LEVLFQ/GP). Purified mitochondria were split equally by volume into two 1.5 mL tubes. PreScission protease (GE27-0843-01, Cytivia) was added to one tube (5 µL (10 U) of protease per 100 µL of sample). All tubes were kept at 4 °C for 16 h with end on end rotation. Note protease inhibitor was excluded from any buffers used before PreScission protease cleavage.

2.3.5 Immunoprecipitation

Dilution buffer (10 mM Tris, 150 mM NaCl, 0.5 mM EDTA pH7.5) and wash buffer (dilution buffer with addition of protease inhibitor cocktail tablet (Roche) and 1 mM PMSF) were prepared.

For RFP-trap IP of cellular fractions (heavy and light membranes), the manufacturer's protocol for RFP-Trap Magnetic Agarose beads (Chromotek) was followed. Initial steps were slightly adjusted, as the membrane fractions had already been resuspended in cold wash buffer ready to input to IP and did not require lysis solution step.

For GFP-trap IP of purified mitochondrial samples, the manufacturer's protocol for GFP-Trap Magnetic Agarose beads (Chromotek) was followed.

In all IP experiments, samples were incubated with beads overnight with end on end rotation at 4 °C to maximise protein binding.

To dissociate protein from beads, beads were resuspended in 50 µL 1x Laemmli buffer. Proteins were dissociated by boiling at 95 °C for 5 min. Samples were centrifuged at around 4500 *g* for 5 min to collect beads. The tubes were then placed into a magnetic holder to separate the beads and the supernatant was transferred to a fresh tube on ice. A small volume of the IP sample was retained for western blot validation.

2.3.6 Western blot

Protein concentration was determined by Bradford assay. A solution of protein diluted in 4x Laemmli sample buffer (containing 10% β-mercaptoethanol) at the calculated volume for the protein mass was prepared. Proteins were then denatured by boiling at 95 °C for 5 min.

The protein and ladder were loaded on a precast SDS-PAGE gel (Bio-Rad). Proteins were run in PGRB buffer, initially at 40V (maximum mA) until sample was accumulated at the interface between the stacking and running gels. Then voltage was then increased (to 80-100V) and the protein run until the dye front reached close to the base of the gel. After the gel run was completed, the stacking and excess gel were removed.

Protein was transferred to a nitrocellulose membrane (0.2 µm pore size) using iBlot 2 Dry Blotting System (Invitrogen). An optional equilibration step was included prior to transfer, soaking the gel in 20% ethanol for 5 min to 10 min before adding to stack, as including this step has the potential to increase

efficiency of protein transfer. Proteins were transferred using programme P0 for 7 min (20V 1 min, 23V 4 min, 25V 2 min).

The membrane was blocked for 1 h at RT in 5% milk TBST (20 mM Tris, 150 mM NaCl, 0.1% Tween 20, pH 7.6). Primary antibody dilutions were prepared as in Table 2.4. The blot was incubated with primary antibody dilution for 1 h at RT, or overnight at 4 °C. The blot was then washed for around 10 min in TBST. Secondary antibody dilutions were prepared as specified in Table 2.4. The blot was incubated in secondary antibody dilution for around 1 h at RT. The membrane was then washed three times with PBS for 5 min before detection.

Protein was detected through development of a chemiluminescent signal. ECL start (RPN3243) or ECL prime (RPN2232) solution was prepared at 1:1 ratio just prior to adding to membrane. The ECL solution was applied to the membrane and then exposed and captured using a G-box system.

Antibody	**Supplier**	**Dilution (WB)**
Anti-mCherry antibody, rabbit polyclonal	ab183628, Abcam	1:1000 or 1:2000 in 2% milk TBST
GFP antibody [3H9], rat monoclonal [3H9] to GFP	3h9, Chromotek	1:1000 in 3% BSA TBST
Rabbit IgG HRP Linked Whole Ab (from Donkey)	NA934V, Cytiva	1:5000 in 5% milk TBST
anti-LBR antibody produced in mouse (polyclonal)	SAB1400151, Sigma-Aldrich	1:500 in 2% milk TBST
BAF Antibody (A-11), mouse monoclonal	sc-166324, Santa Cruz Biotechnology	1:500 in 2% milk TBST
HRP-conjugated mouse anti-β-Actin (C4)	sc-47778, Santa Cruz Biotechnology	1:20000 in 2% milk TBST
Anti-α-Tubulin antibody, Mouse monoclonal	T6074, Sigma-Aldrich	1:2500 in 2% milk TBST
Anti-Rat IgG (whole molecule)-Peroxidase antibody produced in goat	A9037, Sigma	1:5000 or 1:8000 in 5% milk TBST
Mouse IgG HRP Linked Whole Ab	NXA931 (from sheep), Cytiva	1:5000 in 5% milk TBST
Rabbit IgG HRP Linked Whole Ab (from donkey)	NA934, Cytiva	1:5000 in 5% milk TBST

Table 2.4. Antibodies for western blotting.

2.3.7 Mass spectrometry analysis

To prepare for "in gel" trypsin digestion, sample was loaded on a 10% SDS-PAGE gel, leaving empty lanes between samples to minimise contamination. The sample was run at 40V until protein accumulated at the interface of the stacking and

running gels, and then voltage was increased to 80V and run until proteins had migrated around 1.5 cm into the gel. The gel was then stained with InstantBlue (Abcam). Sample lanes were cut, diced into small cubes (2 mm to 4 mm), transferred to a single 1.5 mL tube per lane and covered in molecular grade water. Stored at -20 °C until collection of all sample repeats.

The gel cubes were destained for 20 min at 55 °C with shaking in 50 % ethanol 50 mM ammonium bicarbonate (ABC). This was repeated, replacing solution after each wash, until the gel cubes were destained and the solution clear. The gel was then dehydrated in 100 % ethanol for 5 min at RT with shaking. A reduction/alkylation solution was prepared by dilution of a stock solution (50 mM TCEP, 200 mM CAA in water) in 50 mM ABC. The gel cubes were incubated in the prepared buffer (10 mM TCEP, 40 mM CAA) with gentle shaking at 70 °C for 5 min. This was followed by three washes of 20 min with 50 % ethanol 50 mM ABC at RT with shaking, replacing solution after each wash. Gel cubes were again dehydrated by 5 min incubation at RT in 100 % ethanol with shaking. Solution was discarded from the gel tubes. The gel was then hydrated for 10 min at RT in trypsin solution (2.5 ng μL^{-1}) prepared by dilution of trypsin stock in 50 mM ABC. Stock trypsin (0.1 µg μL^{-1}) was prepared by resuspending 20 µg lyophilized trypsin (Promega) in 200 µL provided Trypsin Resuspension Dilution Buffer (Promega) with sonication. Buffer volume was increased by adding additional 50 mM ABC to ensure the gel in the tube was submerged and prevent dehydration. Then incubated overnight overnight at 37 °C for trypsin digestion.

After overnight trypsin digestion, the digested peptides should have released from the gel into solution. Gently centrifuged tubes to collect any condensation. The solution on the gel was collected into a new tube for each sample. Gel pieces were submerged in 25 % ACN 5 % formic acid solution and sonicated in a water bath for 10 min at RT. Solution was collected in the tube containing previously collected solution from the same sample. Sonication and solution collection was repeated three times. The collected peptide solution was then dried in a Speed-Vac at 50 °C to 60 °C until the volume was around 20 µL or less, to concentrate the solution. The peptides were then resuspended in 2 % ACN, 0.1 % TFA to a final volume of around 50 µL. When a white pellet was visible after drying, which can result from small pieces of gel being transferred during collection of solution surrounding the gel, and additional step was included after resuspending the samples in 2 % ACN, 0.1 % TFA as described. After resuspending, the sample was sonicated in a water bath for 10 min. Sample was then loaded onto a 0.22 µm filter column and centrifuged at maximum speed (21 100 *g*) for 5 min to filter the sample. Sample

was transferred into a labelled vial suitable for mass spectrometry.

Samples were analysed by mass spectrometry by the Proteomics Research Technology Platform, University of Warwick.

2.4 Microscopy

For most live cell imaging, cells were plated onto uncoated fluorodishes (23 mm diameter, 0.17 mm thickness, World Precision Instruments Ltd) and imaged in media (Leibovitz's L-15 Medium, no phenol red, supplemented with 10 % FBS) in an incubated chamber at 37 °C. Where used, dyes (SiR-DNA, SPY-555 or SiR-tubulin) were added at 0.25 µM around 30 min before selecting cells on the microscope (or in synchronised cells, dye was washed out after 30 min). Most live and fixed cell imaging was captured using a Nikon CSU-W1 spinning disc confocal system with SoRa upgrade (Yokogawa) and either a 100x, 1.49 NA, oil, CFI SR HP Apo TIRF (Nikon) or a 63×, 1.40 NA, oil, CFI Plan Apo objective (Nikon) with optional 2.3× intermediate magnification and 95B Prime sCMOS camera (Photometrics, 11 µm x 11 µm pixel size). The system has a CSU-W1 (Yokogawa) spinning disk unit with 50 µm and SoRa disks (SoRa disk used), Nikon Perfect Focus autofocus, Okolab microscope incubator, Nikon motorized xy stage and Nikon 200 µm z-piezo. Excitation was via 405 nm, 488 nm, 561 nm and 638 nm lasers with 405/488/561/640 nm dichroic and Blue, 446/60; Green, 525/50; Red, 600/52; FRed, 708/75 emission filters. Acquisition and image capture was via NiS Elements software (Nikon).

For overnight imaging to measure mitotic timings, a personal DeltaVision microscope system (Applied Precision, LLC), based on an IX-71 microscope body (Olympus) was used with a CoolSNAP HQ2 interline CCD camera (Photometrics, 6.45 µm x 6.45 µm pixel size) and a 60×, 1.42 NA, oil, PlanApo N objective. The system was equipped with Precision Control microscope incubator, Tokai Hit stage top incubator and Applied Precision motorized xyz stage. Illumination was via a Lumencor SPECTRA X light engine (DAPI, 395/25; GFP, 470/24; mCherry, 575/25; CY-5, 640/30), dichroics (Quad: Reflection 381-401:464-492:531-556:619-644 Transmission 409-456:500-523:564-611:652-700; GFP/mCh: Reflection 464-492:561-590 Transmission 500-553:598-617) and filter sets (DAPI: ex 387/11 em 457/50; GFP: ex 470/40 em 525/50; TRITC: ex 575/25 em 597/45; mCherry: ex 572/28 em 632/60; CY-5: ex 640/14 em 685/40). Image capture was by softWoRx 5.5.1 software (Applied Precision). Images were deconvolved using softWoRx 3.0 with the following settings: conservative ratio, 15 cycles and high noise-filtering.

2.5 Data Analysis

2.5.1 Exclusion zone and spindle analysis

Images were segmented using Labkit (Arzt *et al.*, 2022) in Fiji as a pixel classifier to segment the ER. The original image and the segmented mask were used in a workflow to specify: 1) manual position of centrosomes in 3D; 2) manual drawing of DNA line in the midpoint between centrosomes (saved as CSV); 3) cell outline (3 polygons drawn towards the top, middle, bottom of the cell); 4) exclusion zone (circular ROI in the centre of exclusion zone). Then using LimeSeg (Machado *et al.*, 2019), an adaptive algorithm segmented in 3D the cell and the exclusion zone using the mask, and the starting ROIs. Briefly, the cell outline is found using "skeleton" that shrinks to fit the cell exterior and the Exclusion Zone is created using "sphere" expanded from a seed ROI inside the cell until it touches the ER. This process was fully automated with a checking step at the end to correct obvious errors. These errors could be fixed by more accurate drawing of the seed ROIs. In cases where they could not, we discarded the images from the analysis (5 out of 46 images). The data were fed into a custom written Igor routine that calculated many spatial parameters of spindle positioning.

2.5.2 Nuclear envelope analysis

To measure GFP-Sec61β and NE protein recruited to the main nucleus and MN, ROIs of each structure were selected by thresholding the DNA channel after enhancing contrast by applying contrast limited adaptive histogram equalization (CLAHE) in the DNA channel only. ROIs were eroded by 1 pixel to minimise noise around the selected regions. Brightness and contrast were adjusted identically across all images in the channels being measured. Three ROIs (main nucleus, MN and background) were used to measure GFP-Sec61β and NE protein fluorescence using "Measure" in Fiji. Results were exported as plain text using a script. Plots of the ratio of background subtracted measures ((MN – background)/(main – background)) were made using ggplot2 package in RStudio.

2.5.3 Anaphase distance and kymograph

Line profiles of fluorescence were taken along the spindle axis and then a secondary profile orthogonal to this axis at the midpoint of the line. These profiles were imported into Igor where they could be reassembled into kymographs of fluorescence along the line over time. Using a manually defined anaphase time, the kymographs could be offset and averaged to represent the behaviour of all

the cells in the dataset.

The kymographs were subsequently used to retrieve the distances between the two chromosome masses. This was done using a peak finding algorithm custom-written in Igor.

2.5.4 Recoating analysis

An ImageJ macro was used to segment the DNA masses and outline them. Then measured the outline using a 3 px thick line, the values in each channel were output as a text file. These files were read into Igor and processed. Briefly, the profiles were then spatially aligned by finding the centres of each DNA mass, drawing a line between them at each time point and then finding the intersect between this line and each profile. The profiles were then "recast" from this point and resampled so that all profiles were the same length. This allowed us to average all of the recast profiles to observe the behaviour of each condition.

2.5.5 Mass spectrometry data

Raw mass spectrometry files were loaded into MaxQuant (Version number 2.0.1.0). Group-specific parameters Digestion and Modifications were maintained as default and Label-free quantification (LFQ) was selected. Uniprot Human Proteome (UP000005640) database was selected in Global Parameter. Volcano plots comparing LFQ intensities were generated, subcellular analysis conducted (selecting specific GO terms) and plots output using Igor (Igor Pro 9.01 64-bit) code available on Github (https://github.com/quantixed/VolcanoPlot). Results were thresholded using 1.5 fold-change enrichment over control samples.

GO Term	Cellular compartment
GO:0005783	endoplasmic reticulum
GO:0070971	endoplasmic reticulum exit site
GO:0005788	endoplasmic reticulum lumen
GO:0005789	endoplasmic reticulum membrane
GO:0044322	endoplasmic reticulum quality control compartment
GO:0031205	endoplasmic reticulum Sec complex
GO:0071782	endoplasmic reticulum tubular network
GO:0098826	endoplasmic reticulum tubular network membrane
GO:0005793	endoplasmic reticulum-Golgi intermediate compartment
GO:0033116	endoplasmic reticulum-Golgi intermediate compartment membrane
GO:0012507	ER to Golgi transport vesicle membrane
GO:0005791	rough endoplasmic reticulum
GO:0048237	rough endoplasmic reticulum lumen
GO:0030867	rough endoplasmic reticulum membrane
GO:0005790	smooth endoplasmic reticulum

Table 2.5. GO Terms for filtering mass spectrometry results for ER proteins.

GO Term	Cellular compartment
GO:0005639	integral component of nuclear inner membrane
GO:0016604	nuclear body
GO:0005635	nuclear envelope
GO:0042405	nuclear inclusion body
GO:0005637	nuclear inner membrane
GO:0016363	nuclear matrix
GO:0031965	nuclear membrane
GO:0005640	nuclear outer membrane
GO:0042175	nuclear outer membrane-endoplasmic reticulum membrane network
GO:0034399	nuclear periphery
GO:0005643	nuclear pore
GO:0044613	nuclear pore central transport channel
GO:0044615	nuclear pore nuclear basket
GO:0043596	nuclear replication fork
GO:0016607	nuclear speck
GO:0005730	nucleolus
GO:0005654	nucleoplasm
GO:0000786	nucleosome
GO:0005634	nucleus

Table 2.6. GO Terms for filtering mass spectrometry results for nuclear proteins.

Chapter 3

Nuclear envelope formation at misaligned chromosomes

3.1 Introduction

Chromosomes can become misaligned by the absence or loss of attachment to mitotic spindle microtubules. Two types of misaligned chromosomes, which are classified according to their position relative to the spindle, are lagging and polar misaligned chromosomes (Kuniyasu *et al.*, 2018), depicted in Figure 3.3A below. Lagging chromosomes are observed in the space between the two chromatin masses as these separate in anaphase. Polar chromosomes are situated outside of the membrane exclusion zone that exists around the spindle in mitosis. Our lab has demonstrated that these polar chromosomes can become ensheathed in multiple layers of the endomembranes that are present outside of the exclusion zone region and that this ensheathing affects chromosome fate (Ferrandiz *et al.*, 2022).

Several mechanisms exist to detect and correct chromosome alignment defects in mitosis. However, any misaligned chromosomes that are not successfully rescued and aligned at the metaphase plate can subsequently missegregate in anaphase. Missegregated chromosomes can recruit and become coated in membrane, forming a MN, separate from the main nucleus. Our lab has found that ensheathing of polar chromosomes promoted chromosome missegregation and ultimately MN formation (Ferrandiz *et al.*, 2022).

MN provide insufficient protection for the DNA, which can result in DNA damage, as extreme in some cases as chromothripsis (extensive chromosome fragmentation) (Crasta *et al.*, 2012), and initiate an immune response (Hatch *et al.*, 2013). MN

are also prone to disruption, resulting in further loss of the barrier protecting DNA and increasing the potential for extensive DNA damage. Structurally, this disruption has been seen to allow access of ER tubules within the micronuclear DNA and also to alter chromatin compaction (Hatch *et al.*, 2013). Disruption may also affect the fate of the micronuclear DNA in subsequent cell divisions, further demonstrating the potential long term consequences of MN disruption (Hatch *et al.*, 2013).

The mechanism underlying MN disruption remains unclear. It is therefore important to understand the nuclear envelope reassembly process at misaligned chromosomes, to determine why the MN envelope formed is defective. The profile of proteins recruited and the dynamics of their recruitment to misaligned chromosomes could affect the function and stability of the micronuclear envelope formed. Indeed, changes in the level and coating of the nuclear lamina protein lamin B1 at micronuclei have been identified before disruption occurs (Hatch *et al.*, 2013). This could also be true of NE proteins, particularly the INM proteins which connect the NE to the underlying lamina and chromatin, and recruit membrane to chromatin during NE reassembly in mitosis. Increased levels of the INM proteins LBR and emerin have been observed at micronuclei formed from lagging chromosomes (Maass *et al.*, 2018).

The particular set of proteins recruited and their recruitment dynamics could also vary at different types of misaligned chromosome, due to position of the chromosome within the cell and, in the case of polar misaligned chromosomes, ensheathing in membrane. It has been reported that recruitment of a subset of NE proteins (termed "non-core") is absent or impaired at lagging chromosomes, but not at misaligned chromosomes localised outside of the spindle region (Liu *et al.*, 2018), where the chromosome may become ensheathed.

In this chapter, we aimed to further investigate the defective nuclear envelope assembly at misaligned chromosomes that form MN.

3.2 Nuclear envelope assembly process

We aim to understand the NE assembly mechanism, particularly the recruitment of NE proteins, and how this process is defective at missegregating chromosomes that form MN. To investigate NE assembly, we first generated five stable diploid RPE-1 cell lines that co-expressed an mCherry-tagged nuclear/nuclear envelope protein (BAF, CHMP7, emerin, LAP2β or LBR) with tagged ER protein GFP-Sec61β by lentiviral transduction. RPE-1 cell clones expanded from fluorescence-activated cell sorting of single cells were initially

screened for fluorescence by microscopy. mCherry-BAF/GFP-Sec61β and LBR-mCherry/GFP-Sec61β cell lines used in later work were then further characterised for protein expression by western blot and mitotic timings were measured (Figure 3.1 and published in Ferrandiz *et al.* (2022)).

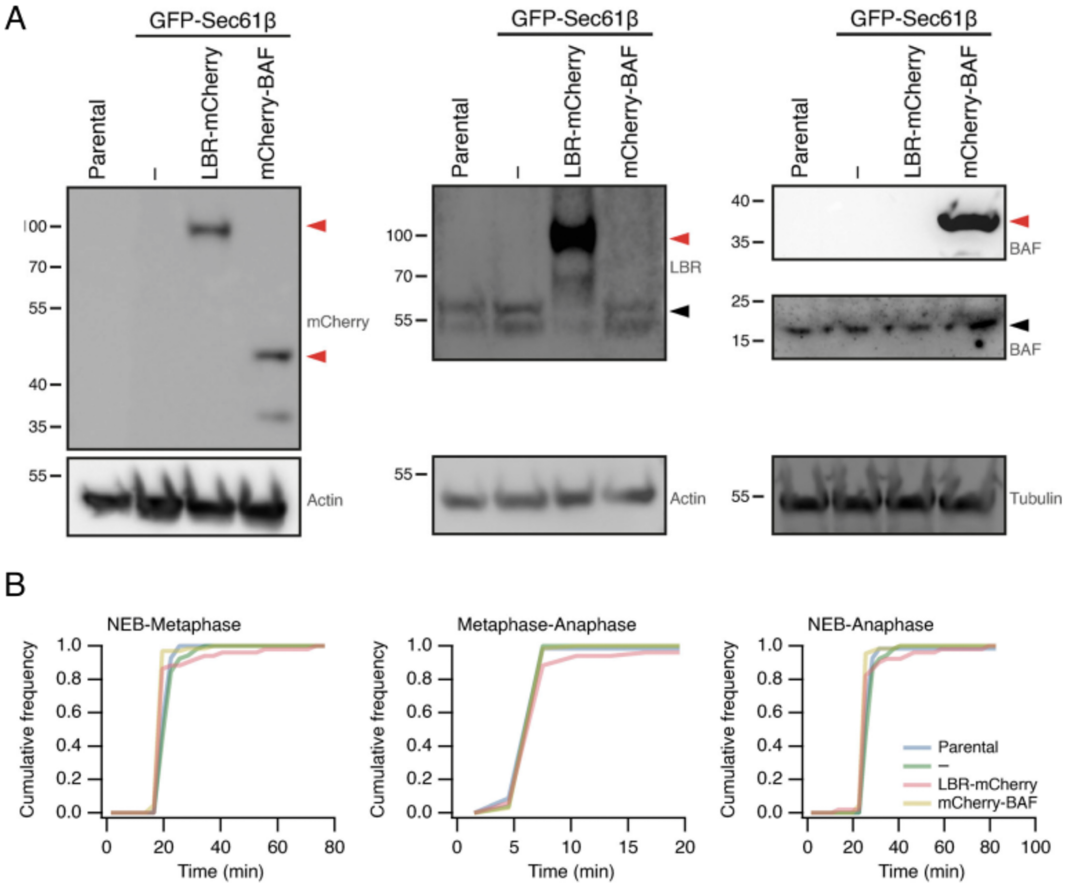

Figure 3.1. Characterisation of RPE-1 cell lines stably expressing GFP-Sec61β and mCherry-BAF or LBR-mCherry. RPE-1 cell lines stably expressing the indicated mCherry-tagged protein (BAF or LBR) and the ER marker GFP-Sec61β were made by lentiviral transduction. (**A**) Western blot of lysates collected from RPE-1 WT (parental), RPE-1 GFP-Sec61β and RPE-1 GFP-Sec61β mCherry-BAF or LBR-mCherry cell lines. Proteins were detected by antibody stain for mCherry or endogenous protein (LBR or BAF) with an actin or tubulin loading control. Red arrowheads indicate the expected mass of the mCherry-tagged protein. Black arrowheads indicate expected mass of the endogenous protein. (**B**) Mitotic timings measured of RPE-1 cell lines stably expressing constructs. Shown are cumulative frequencies for progression between mitotic stages (NEB to metaphase, metaphase to anaphase, and NEB to anaphase). Parental RPE-1, n = 69; RPE-1 GFP-Sec61β alone, n = 52; RPE-1 GFP-Sec61β LBR-mCherry, n = 66; RPE-1 GFP-Sec61β mCherry-BAF, n = 51. This work was done in collaboration with Nuria Ferrandiz.

The endogenous and mCherry-tagged proteins were detected in mCherry-BAF/GFP-Sec61β and LBR-mCherry/GFP-Sec61β cell lines by western blot (Figure 3.1A). The expression level of endogenous LBR detected appeared lower in the LBR-mCherry/GFP-Sec61β cell line than in the parental

cells, suggesting some compensation in LBR expression level. However, it should be noted that LBR is still overexpressed in this cell line.

BAF protein with an N-terminal fluorescent tag (Haraguchi *et al.*, 2008) and LBR with a C-terminal tag (Haraguchi *et al.*, 2008) are widely used constructions and each show localisation and recruitment to chromatin similar as described for the endogenous protein. In addition, we observed no gross nuclear morphological changes which would suggest erroneous function of LBR/BAF in our cell lines. The mitotic timings measured showed normal mitotic progression, which also implies that the protein fusions expressed are functional and do not interfere with mitotic processes (Figure 3.1B).

The RPE-1 cell lines made allowed the localisation of nuclear, nuclear envelope and ER proteins to be followed as single cells progressed through mitosis (Figure 3.2 and Figure 6.1). NE reformation is a highly dynamic and regulated process, and is coordinated with multiple other processes in mitosis. Visualising proteins in live cells allowed the capture of any transient changes in localisation, that may be missed in fixed samples, and the timing of localisation changes relative to other mitotic events. We were particularly interested in the dynamics and pattern of recruitment and coating of the proteins onto chromatin, comparing that of nuclear, NE and ER membrane proteins.

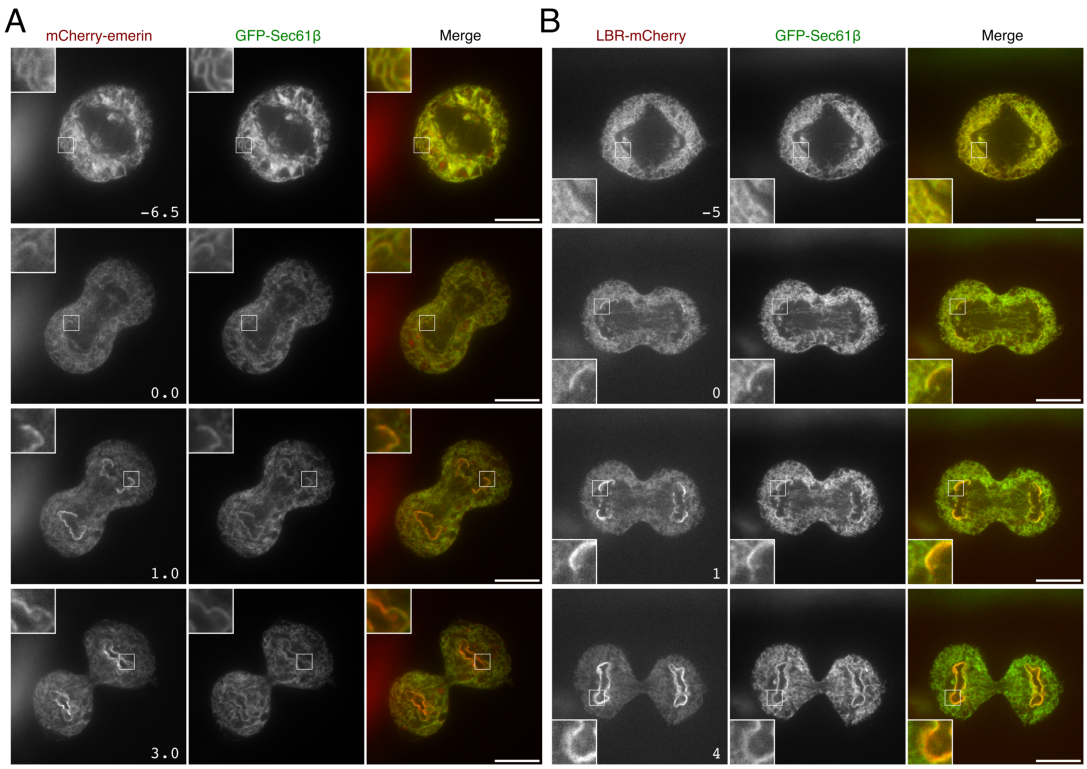

Figure 3.2. Mitotic localisation of nuclear, NE and ER proteins in RPE-1 stable cell lines. RPE-1 cell lines stably expressing the indicated mCherry-tagged inner NE protein (emerin or LBR) and the ER marker GFP-Sec61β were made by lentiviral transduction. Shown are single slices of cell lines captured live with an imaging interval of 0.5 min (emerin) or 1 min (LBR). Time is indicated in minutes. ROIs are 3 times expanded from 50 pixel region. Scale bars, 10 µm.

Individual NE proteins showed different dynamics and patterns of recruitment to chromatin, and in timing and localisation relative to the ER marker Sec61β (examples shown for two INM proteins in Figure 3.2 and for additional nuclear/NE proteins in Figure 6.1).

BAF is a small protein known to bind chromatin early in the NE reassembly process, where it recruits other NE proteins and associated membrane for NE reassembly and also has an important role in compacting chromatin. mCherry-BAF appeared diffuse in metaphase and a pool remained diffuse throughout the division. In early anaphase, a proportion of mCherry-BAF started to coat around the perimeter of the chromatin and, just one minute later, concentrated more towards the chromatin peripheral ends. Later in anaphase, mCherry-BAF strongly concentrated in the central ("core") of chromatin, then only to the outer "core" region (central chromatin surface not facing the opposite chromatin mass), before becoming more patchy within this region and more distributed around the NE of daughter nuclei (Figure 6.1A).

Emerin and LAP2β each interact with, and are recruited by, BAF to chromatin for NE reformation through a LEM domain and are present within the INM of the NE formed. LAP2β can additionally be recruited by direct interaction with chromatin through a second LEM domain. Despite sharing a recruitment mechanism, emerin and LAP2β each showed different patterns of localisation at the chromatin during NE reassembly. In the RPE-1 GFP-Sec61β mCherry-emerin cell line, mCherry-emerin showed a similar localisation pattern to the ER marker Sec61β in metaphase and early anaphase. mCherry-emerin initially coats the peripheral ends of chromatin, as GFP-Sec61β, before coating around the chromatin perimeter. Later in mitosis, mCherry-emerin then concentrated in the central ("core") region of the chromatin before becoming more distributed around the NE of the newly assembled daughter nuclei (Figure 3.2A). Whereas LAP2β-mCherry appeared to concentrate first at the peripheral ends ("non-core" region) of chromatin before coating around the newly reformed NE in late mitosis (Figure 6.1B).

We compared the localisation of the INM proteins emerin and LAP2β to LBR, another protein originating from the INM (Figure 3.2B). LBR also localises similar to GFP-Sec61β in metaphase and early anaphase. However, unlike emerin, but similar to LAP2β, LBR-mCherry appears to first coat the peripheral ends ("non-core" region) of chromatin. LBR-mCherry then concentrates at the peripheral ends, before distributing around the NE surrounding chromatin.

CHMP7 is a protein which functions later in the NE reassembly process,

recruiting components for sealing holes in the forming NE. In RPE-1 GFP-Sec61β mCherry-CHMP7 cells, the tagged CHMP7 appears punctate throughout mitosis. mCherry-CHMP7 localised to chromatin later than the other nuclear proteins studied, and in a very discontinuous pattern, only visible after much of chromatin has been coated by GFP-Sec61β, as expected from CHMP7 function (Figure 6.1C).

Overall, the localisation dynamics of the nuclear and NE proteins visualised and the ER protein GFP-Sec61β demonstrates some of the complexity in the highly ordered and spatially regulated recruitment in the reassembly of the NE in mitosis. Comparing different proteins each originating from the INM (LBR, emerin and LAP2β), we see these can be recruited with different dynamics and pattern, as has been described.

3.3 Nuclear envelope assembly at misaligned chromosomes

Next, we investigated if misaligned chromosomes recruit components of the NE, and compared the level and dynamics of this recruitment at misaligned chromosomes to that at the main nucleus.

To visualise NE and ER protein recruitment dynamics in live cells, we used our RPE-1 cell lines that stably co-expressed GFP-Sec61β with either mCherry-BAF or LBR-mCherry described in the previous section. Misaligned chromosomes were induced in the stable diploid RPE-1 cell lines by treatment with an allosteric inhibitor of CENP-E, GSK923295 (Wood *et al.*, 2010). The inhibitor was washed off and the cells were allowed time to recover before metaphase cells with polar misaligned, ensheathed chromosomes were selected to follow during imaging. Lagging chromosomes, arising at anaphase, were also observed, but at lower frequency than induced polar chromosomes. The fate of the misaligned chromosome (rescued to the main chromatin mass or remaining separate and missegregating) and the recruitment of NE protein and ER membrane to the chromosome and to the main chromatin masses were followed (Figure 3.3). This was compared at lagging and polar misaligned chromosomes, to see if we observe defects in the recruitment of LBR (described as "non-core"), but not BAF ("core"), as reported at lagging chromosomes by Liu *et al.* (2018).

In RPE-1 GFP-Sec61β mCherry-BAF cells, both mCherry-BAF and GFP-Sec61β were recruited to lagging and polar chromosomes with similar timing to the main chromatin masses (Figure 3.3B). Similarly, we observed no obvious difference

in the timing of recruitment of LBR-mCherry to lagging or polar misaligned chromosomes compared to the main chromatin masses (Figure 3.3B). The average measure of the recruitment dynamics of multiple cells revealed a potential delay in the recruitment of mCherry-BAF to both misaligned chromosome types compared to the main chromatin masses (Figure 3.3C). However, this was not a clear difference. The accuracy of our measurements are limited by the relatively slow time resolution of imaging, but even so, the difference in recruitment ($\sim$2 min) is unlikely to be biologically significant.

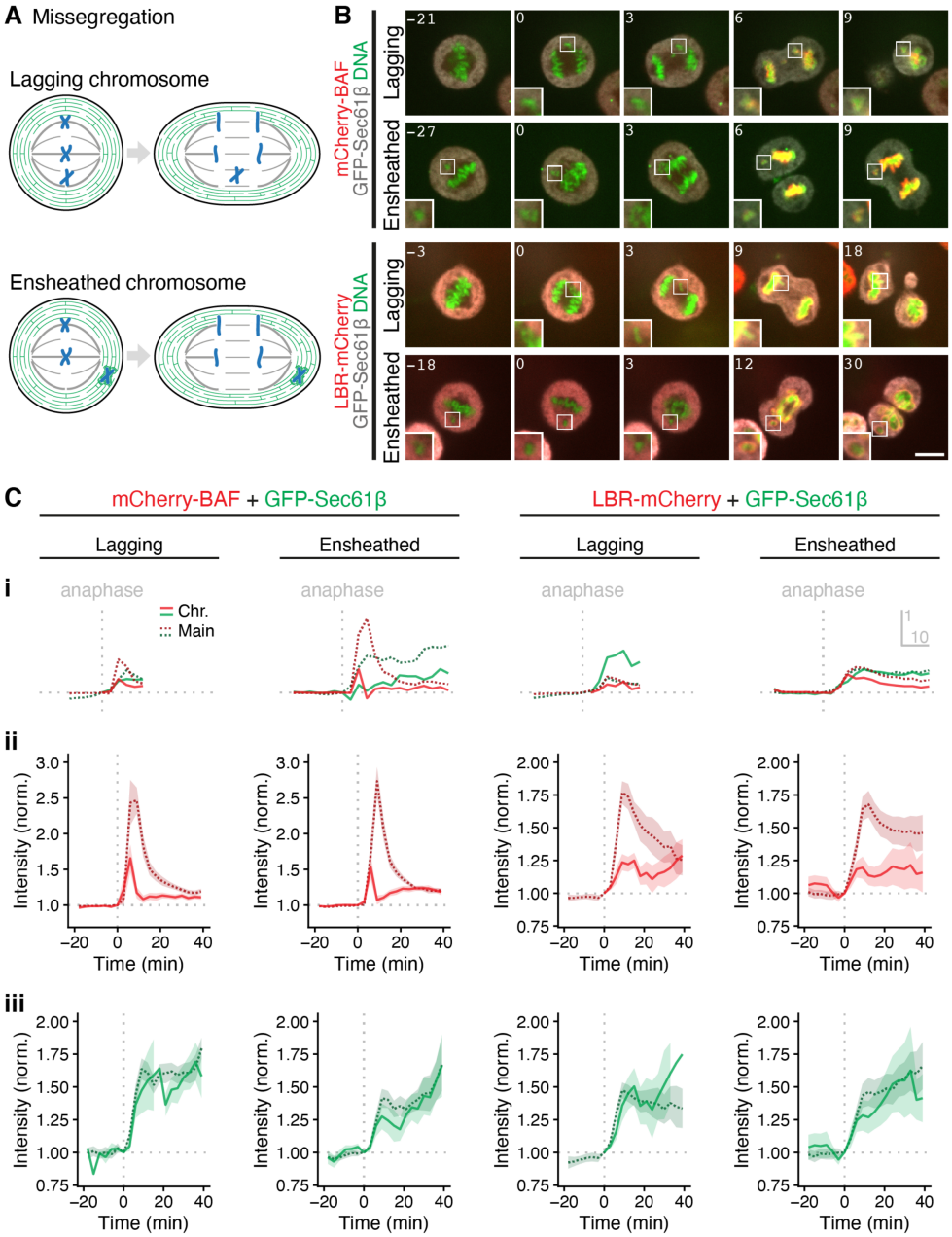

Figure 3.3. Nuclear envelope protein recruitment to misaligned chromosomes forming micronuclei. (**A**) Schematic diagram showing two types of misaligned chromosome. Lagging chromosomes are observed between the two chromatin masses in anaphase. Polar chromosomes are situated outside of the exclusion zone and can become ensheathed in endomembranes, represented in green. (**B**) Still confocal slices from videos of example mitotic cells with a lagging or ensheathed misaligned chromosome. RPE-1 cell lines stably expressing GFP-Sec61β and mCherry-tagged nuclear or NE protein (mCherry-BAF or LBR-mCherry) are shown. Time is indicated in minutes, with the first anaphase frame set as time 0 min. Scale bar, 10 µm. (**C**) Timing and level of GFP-Sec61β and mCherry-BAF (left) or LBR-mCherry (right) recruitment to lagging or ensheathed misaligned chromosomes and to the main chromatin masses. (**i**) Example traces of normalised intensity measured at the misaligned chromosome and the main chromatin masses from the representative cells shown in **B**. Scale bars show 1 unit of intensity and 10 min. (**ii**) Average intensity of mCherry-BAF (left) or LBR-mCherry (right) at misaligned chromosome (red) or main chromatin mass (dark red). (**iii**) Average intensity of GFP-Sec61β at misaligned chromosome (light green) or main chromatin mass (dark green). Traces were normalised to the intensity value at anaphase, offset and averaged. Lines show the average ± SD.

Previously, it has been reported that recruitment of a subset of NE proteins (termed "non-core") is absent or impaired at lagging chromosomes, but not at polar misaligned chromosomes (Liu *et al.*, 2018). However, other investigators have since reported recruitment, with delay, of proteins belonging to this subset ("non-core") to lagging chromosomes (Orr *et al.*, 2021). The nocodazole treatment conditions used to induce misalignment by Liu *et al.* (2018) were shown to also affect the Aurora B gradient important for NE protein recruitment and reassembly (Orr *et al.*, 2021) and may also affect ER structures (Lu *et al.*, 2009). Our results agree that proteins classed as "non-core" (LBR) are recruited to lagging misaligned chromosomes. Although, it is unclear from our results whether there is any meaningful delay in recruitment.

3.4 Defective nuclear envelope assembly at misaligned chromosomes forming micronuclei

Next, we looked at the composition and integrity of the MN envelope formed after division of a cell with a missegregated chromosome and compared this to the main nuclear envelope. RPE-1 cells stably co-expressing tagged nuclear or nuclear envelope protein (mCherry-BAF or LBR-mCherry) and ER marker GFP-Sec61β were pretreated with GSK923295 to induce polar misaligned chromosomes. Cells were released from treatment, allowed time to recover, and then fixed and stained.

We observed disruption of a proportion of MN, with ER marker GFP-Sec61β visible inside the micronuclear chromatin in the majority of MN observed in GSK923295 pretreated cells (Figure 3.4A). Similar disruption of MN has been described previously (Hatch *et al.*, 2013). In addition, disrupted MN also appeared to have increased recruitment of nuclear protein BAF and the INM protein LBR compared to the main nucleus. The intensity of BAF or LBR at the MN correlated with the GFP-Sec61β level at the same MN (Figure 3.4B). The intensity data appeared as two groups when MN were manually assigned as intact or disrupted based on the presence or absence of GFP-Sec61β inside the micronuclear DNA (Figure 3.4B). This also suggested a correlation between the level of enrichment of BAF or LBR at MN compared to the main nucleus and the disruption of MN. In a separate series of experiments, we also demonstrated that the DNA in disrupted MN was accessible to the cytosol using a histone acetylation marker (H3K27) (Ferrandiz *et al.*, 2022).

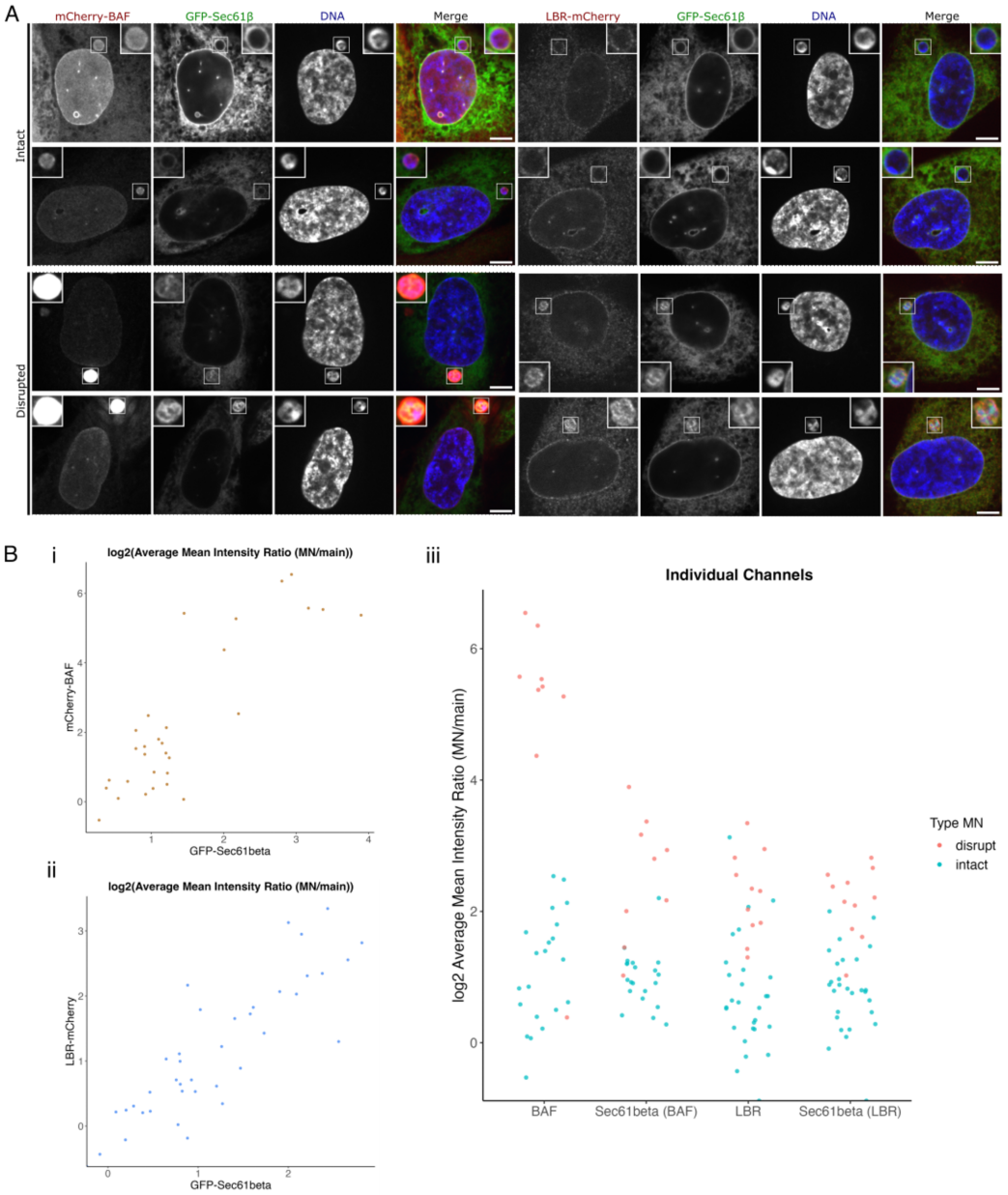

Figure 3.4. Defective nuclear envelope at micronuclei. (**A**) Single confocal slices from z-stacks of images of GSK923295 pretreated RPE-1 cells stably expressing GFP-Sec61β and mCherry-tagged protein (mCherry-BAF or LBR-mCherry, as indicated) with a micronucleus. Cells were fixed with PFA solution around 50 min after washout of the treatment. GFP signal was enhanced by antibody stain and DNA was labelled with DAPI. Insets are 2 times expanded from a 50 px region. Scale bar, 5 µm. (**B**) Intensity measure of mCherry-BAF (**i**) or LBR-mCherry (**ii**) and GFP-Sec61β at MN as a ratio of the intensity at the corresponding nucleus of the same cell, each with background subtraction. Intensity values are represented as a ratio (MN/main nucleus, log2 transformed). (**iii**). Intensity measure ratios of individual channels. Colour indicates the type of MN, classified manually by the presence or absence of GFP-Sec61β inside MN DNA. mCherry-BAF n=30 cells from 3 independent experiments; LBR-mCherry n=38 cells from 3 independent experiments.

Our results could suggest that ensheathing of induced polar chromosomes may promote MN disruption. While the origin of the observed micronuclei (from a polar or lagging chromosome) cannot be determined with certainty in these fixed samples, lagging chromosomes were observed at a much lower frequency than polar chromosomes under these treatment conditions (Ferrandiz *et al.*, 2022). Therefore, we expect a large proportion of the MN to have formed from division of cells with polar misaligned chromosomes induced by the applied treatment.

The stage at which the disruption of MN occurred is uncertain and so we cannot determine from our results whether the increase in LBR and BAF promotes or is a consequence of disruption. The level of recruitment of each protein to misaligned chromosomes forming MN was followed in live cells above (Figure 3.3), but the stability of the MNE that formed was not studied. At present, the particular defect that causes disruption of MN formed from ensheathed chromosomes is not understood.

3.5 Discussion

We have shown that lagging and polar misaligned chromosomes similarly recruit nuclear protein BAF and INM protein LBR. Since we did not detect any meaningful delay in recruitment, our results disagree with those presented by Liu *et al.* (2018) which suggest differential recruitment to each type of the misaligned chromosome. Our finding, that lagging chromosomes can similarly recruit the subset of NE proteins termed "non-core", was also reported by another group Orr *et al.* (2021).

The disruption of the micronuclear envelope suggested a defective NE assembly process at missegregating chromosomes, affecting the function and stability of the MN formed. Therefore, we next looked more generally at the NE reassembly process, to better understand how membranes and proteins involved are arranged in mitosis and recruited to chromatin for envelope formation. This will be the focus of the remainder of this thesis.

Chapter 4

Disrupting ER in mitosis and NE reassembly

4.1 Introduction

The interphase nuclear envelope structure and the arrangement of NE proteins have been widely studied (Figure 1.1). However, how the membranes derived from the NE and the proteins contained within these membranes are reorganised after nuclear envelope breakdown in mitotic human cells remains poorly understood. The mitotic distribution of NE proteins and membranes is also important when considering the mechanism of NE reassembly later in mitosis.

Currently, two models are proposed for the organisation of NE proteins during mitosis (Figure 1.6). In the precursor vesicle model (Wilson and Newport, 1988; Wiese *et al.*, 1997), NE proteins are present in vesicles formed specifically from the NE, either by NE fusion or breakdown. Alternatively, NE proteins have been proposed to diffuse into the ER upon NEBD (Ellenberg *et al.*, 1997), freely diffusing or existing as domains that are enriched in specific subsets of proteins. Currently, the diffusion model is more widely accepted due to limited *in vivo* evidence of precursor vesicles functioning in NE reassembly.

During late mitosis in each model, proteins within these structures contact chromatin or chromatin-bound proteins, to initiate NE reassembly. In the vesicle model, the vesicles formed from the NE are recruited to chromatin and then fuse to form the NE sheet. In the diffusion model, different ER structures have been proposed to be involved in initiating NE reassembly. ER tubules were first reported to form the initial contacts to chromatin and then remodel to form sheets that coat chromatin in mammalian cells (Anderson and Hetzer, 2008). However,

other groups have since observed ER cisternae first coating the peripheral ends of chromatin before expanding around the perimeter of the chromatin mass to form the NE (Lu *et al.*, 2011).

The enrichment of proteins in precursor structures (vesicle model) or concentration in specific regions of the ER (domain model) in mitosis could act as a mechanism to prime proteins and associated membrane for efficient delivery to chromatin for NE reassembly. The particular region of chromatin to which these enriched regions or structures are recruited could also explain the transient subdomains described by Haraguchi *et al.* (2000) and others during NE reassembly in live mitotic cells.

In this chapter, we set out to investigate the proposed models for the organisation of NE proteins in mitosis through visualising and disrupting ER and NE protein localisation in mitotic cells. This will also inform our understanding of the NE reassembly mechanism later in mitosis.

4.2 Effects of relocalising ER membranes in mitosis

4.2.1 System for inducible ER relocalisation

Our lab has developed a method to allow inducible relocalisation of large membrane compartments in mitosis (Ferrandiz *et al.*, 2022), as shown in Figure 4.1A. The system is based on the rapamycin-induced heterodimerisation of FRB and FKBP tags fused to key proteins. To induce relocalisation of large membrane compartments, an FKBP tag was introduced on a protein present on the compartment we aim to relocate (for example, the ER), and an FRB tag on a protein present at the target destination (for example, the plasma membrane). In each protein, the tag must be accessible to the cytoplasmic side of the membrane to allow rapamycin binding and heterodimerisation. This method has been used to induce the movement of ER membranes to the plasma membrane in mitosis, confirmed by immunofluorescent staining of multiple ER protein markers (Ferrandiz *et al.*, 2022). This inducible method of relocalising the ER in mitosis has been applied previously to disrupt ensheathing around polar misaligned chromosomes, a manipulation which allowed the rescue of the chromosome from a missegregation fate (Ferrandiz *et al.*, 2022).

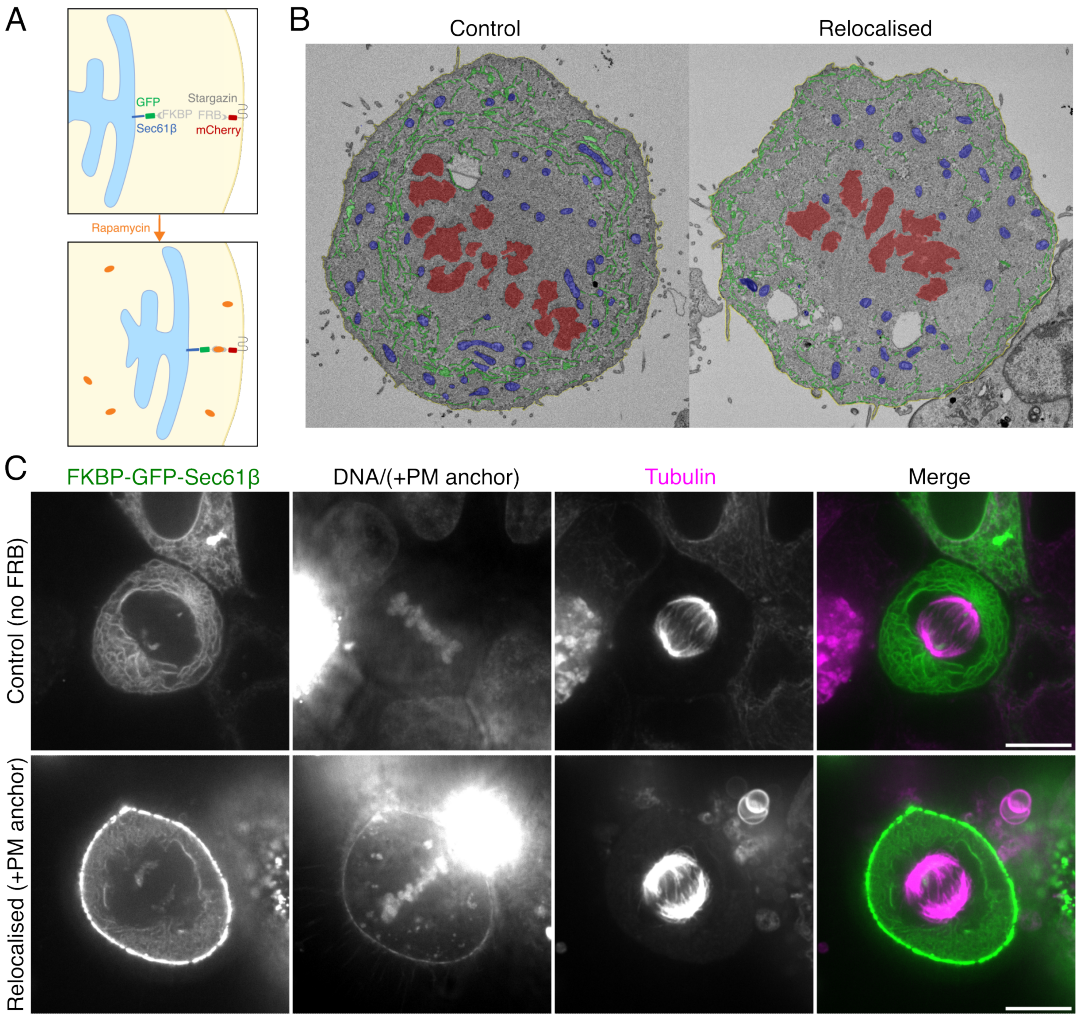

Figure 4.1. Inducible system for relocalising ER membrane compartments in mitosis. (**A**) Schematic diagram of the inducible system used to relocalise ER membranes in mitosis. Rapamycin induced heterodimerisation of expressed ER localised FKBP-GFP-Sec61β and plasma membrane anchor (Stargazin-mCherry-FRB). (**B**) SBF-SEM imaging of mitotic HCT116 cells. Shown are single sections from a stack of control (left) or an induced ER-relocalised (right) cell, with ER (green), plasma membrane (yellow), mitochondria (blue) and chromosomes (red) highlighted. SBF-SEM data and segmentation by Nuria Ferrandiz. (**C**) Single slices of live synchronised (thymidine/RO-3306) mitotic HCT116 cells expressing FKBP-GFP-Sec61β and plasma membrane anchor (Stargazin-mCherry-FRB) or control (no FRB anchor). Rapamycin (200 nM) was applied at RO-3306 washout and images captured around 1 h after washout/rapamycin addition. DNA was labelled with SPY-555 dye and tubulin with SiR-tubulin. Scale bars, 10 µm.

4.2.2 Exclusion zone expansion with ER relocalisation in mitosis

In SBF-SEM of HCT116 cells transiently expressing constructs allowing ER relocalisation, ER structures could be seen relocalised to, and making contacts with, the plasma membrane of a metaphase cell after rapamycin induced heterodimersation (Figure 4.1B). As a result of the ER relocalisation, there was a clear expansion of the exclusion zone around the mitotic spindle. Here we have applied the same system, but in live mitotic HCT116 cells (Figure 4.1C). HCT116 cells were used for these experiments, as they are near diploid and have normal division in untreated conditions. HCT116 were preferred to RPE-1 used in the previous chapter, because we find HCT116 cells to be easier to transfect, and therefore allow us to easily express the combinations of constructs needed for relocalisation. Relocalisation was induced in cells growing asynchronously, with the mitotic stage selected on the microscope. After addition of rapamycin to induce relocalisation, the ER marker FKBP-GFP-Sec61β was seen as bright fluorescent signal at the cell periphery and lower levels were visible inside the cytoplasm. Therefore, the expansion of the exclusion zone after ER relocalisation, previously observed in our lab by SBF-SEM, could also be observed when ER relocalisation was induced in live metaphase cells.

4.2.3 ER relocalisation affects mitotic spindle orientation and positioning

We have seen that relocalisation of ER protein Sec61β and associated ER membrane to the PM in mitotic cells resulted in an expansion of the EZ around the mitotic spindle, clearly visible in live cells (Figure 4.1C) and at the structural level by SBF-SEM (Figure 4.1B). We then set out to determine how the relocalisation of ER membranes to the PM in mitosis and concomitant expansion of the EZ may affect mitotic spindle assembly and function. HCT116 cells transiently expressing ER marker FKBP-GFP-Sec61β and a PM anchor (Stargazin-darkmCherry-FRB) or control (no FRB anchor) were treated with rapamycin to induce relocalisation. The cells were then fixed after 30 min incubation with rapamycin, to allow time for ER relocalisation (usually 15 min to 20 min after rapamycin addition). The cells were stained with antibodies labelling pericentrin and tubulin (Figure 4.2). Using spinning disk microscopy, we saw clear expansion of the membrane EZ volume in cells with relocalisation of ER to the PM, as observed previously by SBF-SEM and similarly treated live cells in our lab (Figure 4.1).

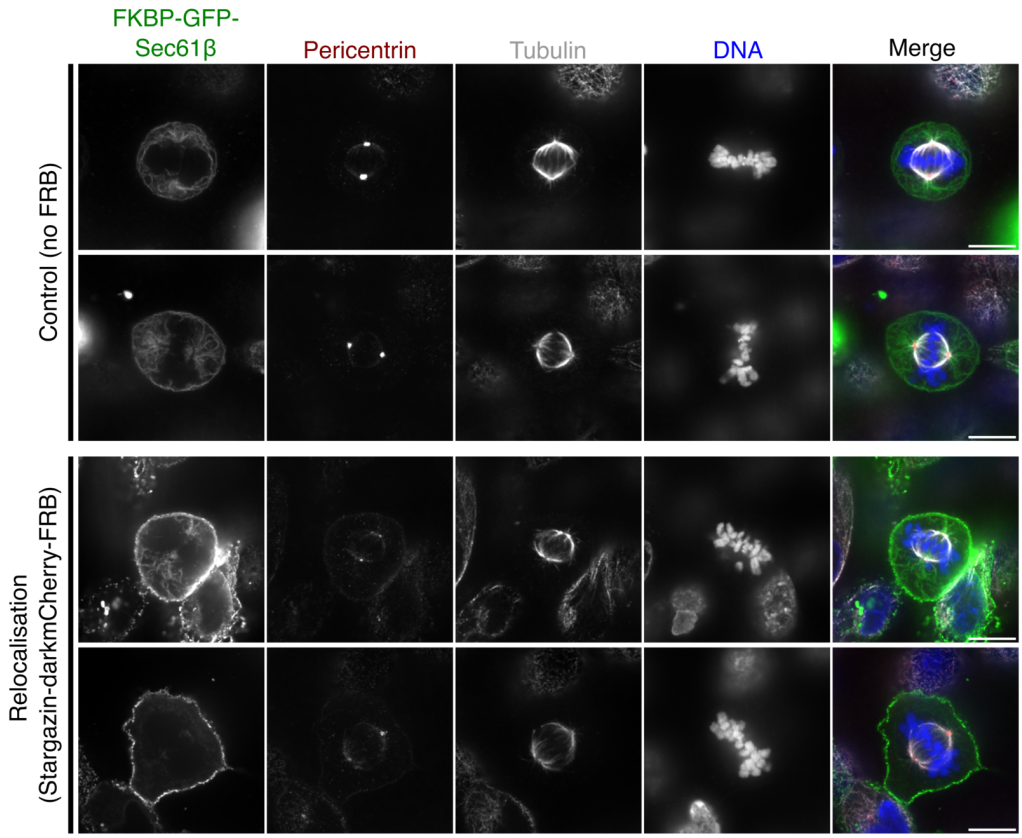

Figure 4.2. Mitotic spindle characteristics with exclusion zone expansion after ER relocalisation in mitosis. Single slices from z-stacks of confocal micrographs captured of HCT116 cells transiently expressing FKBP-GFP-Sec61β and either Stargazin-darkmCherry-FRB or no plasma membrane anchor (control), treated with rapamycin (200 nM) for 30 min before fixation. Centrosomes (pericentrin) and α-tubulin were stained using antibodies and DNA stained with DAPI. Scale bars, 10 µm.

To determine any effect of this manipulation on mitotic spindle structure, a semi-automated image analysis workflow was written to analyse these images. The mitotic spindle, cell and the EZ volume were modelled in 3D in order to derive measurements (Figure 4.3A). Spindle and cell characteristics were measured in ER relocalised and control cells (Figure 4.3B).

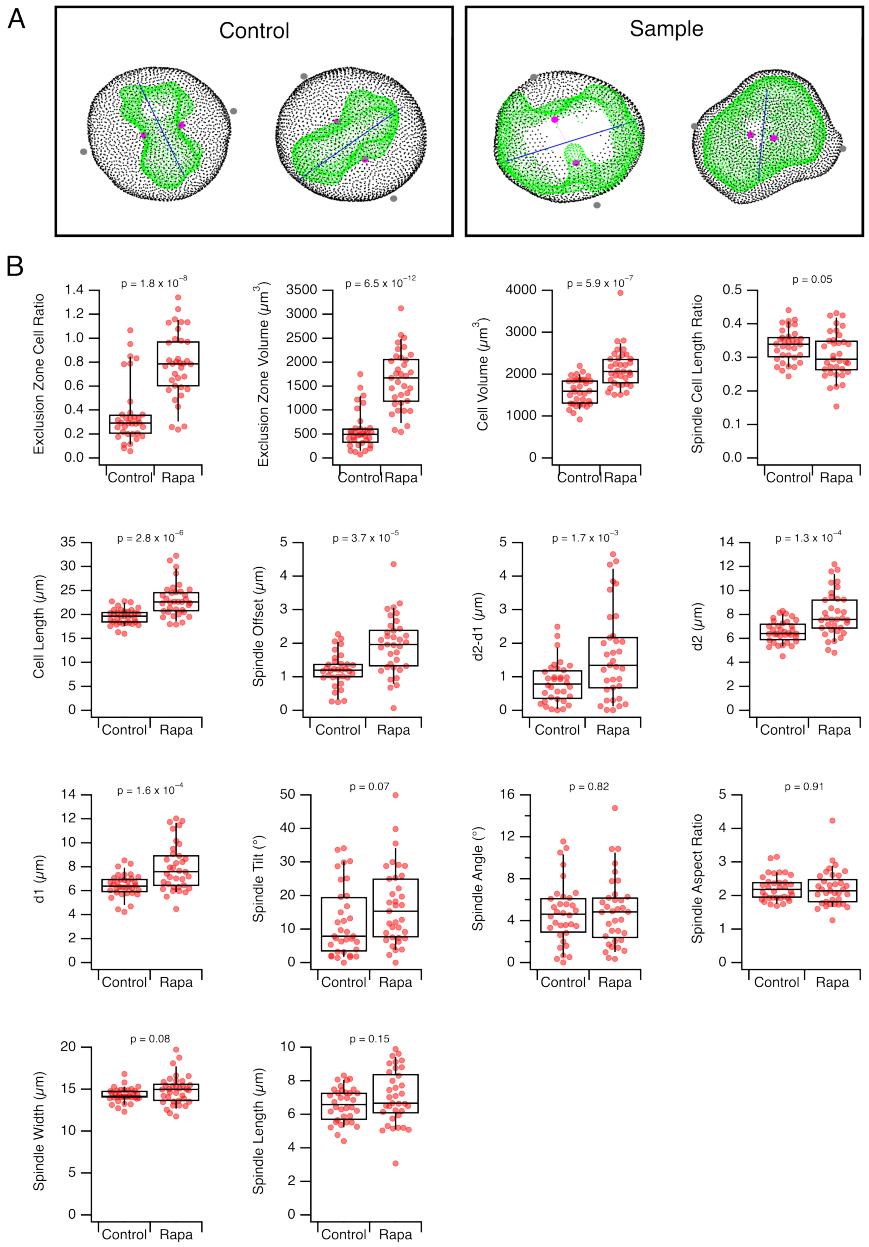

Figure 4.3. Mitotic spindle characteristics with exclusion zone expansion after ER relocalisation in mitosis. (**A**) Examples of segmented control or ER relocalised HCT116 cells represented in Figure 4.2. Normalisation, automated segmentation (EZ boundary and cell perimeter) and manual specification (centrosome position in 3D and metaphase DNA axis) were used to measure output parameters. Green dots indicate points on the exclusion zone boundary and black dots on the cell outline, both from LimeSeg segmentation. Pink circles indicate the 3D position of the centrosomes and the pink line connects these points. Grey circles indicate the points of intersection of the line extended from the pink line connecting the centrosomes with the cell perimeter. The blue line indicates the metaphase DNA axis. (**B**) Box plots to show measures of spindle and exclusion zone parameters in ER relocalised or control cells. d1 and d2 are the distances from each centrosome to the cell cortex, measured from the centrosome position to the point of intersection of the line connecting the two centrosomes with the cell cortex. The spindle offset measures position of the spindle relative to the cell perimeter. Spindle angle is the angle measured between the spindle axis and the DNA axis. Spindle tilt is the angle between the spindle axis and the coverslip. Each dot represents an individual cell, for control cells n=34, and sample cells n=35, from three independent repeats. Boxes show the IQR, horizontal bar represents the median, and whiskers indicate the 9th and 91st percentiles. A Student's T-test with Welch's Correction was used to compare mean of control to relocalised sample cells with labelled p-values.

The expansion of the EZ (increased volume and occupying a larger proportion of the overall cell volume compared to control) after relocalisation of FKBP-GFP-Sec61β was clear from these measures. The overall cell volume and aspect ratio did not show significant change in ER relocalised cells compared to control, suggesting that the ER relocalisation to the PM and subsequent EZ expansion did not expand or stretch the cell in any significant way. Similarly, the spindle aspect ratio measured was equivalent in relocalised and control cells, and the spindle does not appear to have been extended in width or length from the individual plots. This was surprising, as we expected the connections between ER and spindle during mitosis (example through Samp1 and REEP proteins) may have resulted in some pulling force on the spindle when the ER was relocated to the PM. However, we do see examples of small extensions of spindle microtubules towards the expanded EZ after relocalisation of the ER in live cells (Figure 4.1), which may have been missed in this analysis.

Changes in the orientation and position of the spindle in ER relocalised cells were the most evident from the measurements. The results indicate an effect of ER relocalisation on spindle centering within the cell (measured as the difference in distance of each centrosome to the cell cortex, d2-d1) and the spindle tilt (the angle between the spindle axis and the base of the cell). This supports a functional role of the EZ in the proper orientation and positioning of the mitotic spindle within the cell. Although we did not see any changes in the spindle dimensions, the expansion of the EZ and the pulling force which could result from the connections of ER to the mitotic spindle may have induced rotation and movement of the spindle. Observing the relocalisation event in live cells will allow us to determine the origin of the defect more clearly. The EZ is proposed to concentrate proteins to promote spindle assembly (Schweizer *et al.*, 2015). While no gross structural abnormality of the spindle in cells with mitotic ER relocalisation was clear from our analysis, relocalisation was induced after the spindle had formed, and so defects are restricted to ongoing dynamics in metaphase.

The results do not tell us if there are any effects of ER relocalisation on spindle function. For example, the observed spindle position and orientation defect may be expected to affect chromatin separation and mitotic progression. The forces generated around the cell cortex and the overall cell shape are known to adjust during late anaphase to correct problems in spindle positioning within the cell (Kiyomitsu and Cheeseman, 2013). It is possible that ER relocalised to the PM may, in addition, affect this correcting mechanism for incorrect spindle position in later mitosis, through mechanically reinforcing the membrane or through blocking

recruitment of dynein to the cell cortex or contacts between astral microtubules and dynein for positioning.

Therefore, next we wanted to determine the effect of induced ER relocalisation on mitotic progression in live cells, measuring chromosome segregation and coordinated NE reassembly process, to investigate spindle functionality.

4.2.4 Defects in chromatin segregation and coating after ER relocalisation

We hypothesised that the relocalisation of Sec61β and associated ER to the plasma membrane and clearance from the area proximal to the chromatin in mitosis may affect the recoating of the chromatin masses and NE reassembly. The observed expansion of the exclusion zone (Figures 4.1, 4.2 and 4.3) may affect EZ function and so therefore the recoating of chromatin with membranes from outside the EZ region and coordination of this recoating with chromatin separation.

To investigate, the anaphase segregation event and the subsequent coating of chromatin with ER were analysed in mitotic cells with induced ER relocalisation and compared to control cells. HCT116 cells transiently expressing constructs for the induced relocalisation of ER membranes to the PM (FKBP-GFP-Sec61β and Stargazin-darkmCherry-FRB) and to visualise DNA (pmCherry-H3.2) were prepared. Rapamycin was applied to live cells on the microscope to induce relocalisation in early mitosis and the mitotic progression of cells followed and compared to control cells with no relocalisation (Figure 4.4).

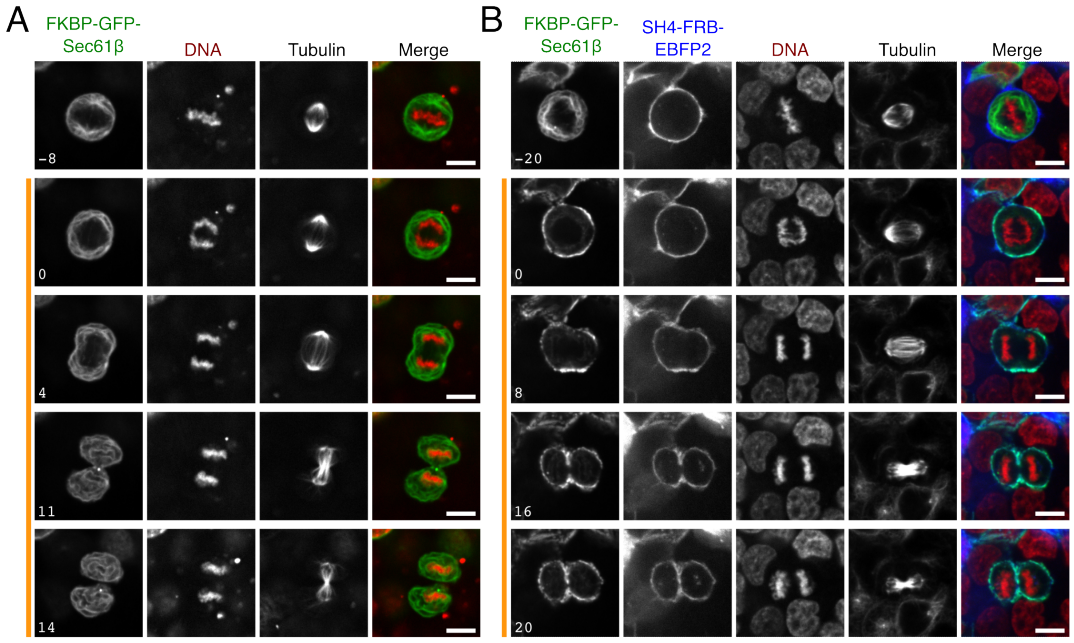

Figure 4.4. Progression of cell with inducible relocalisation of ER membrane in mitosis. Single slices from z-stacks captured over time of live HCT116 cells expressing FKBP-GFP-Sec61β and plasma membrane anchor (SH4-FRB-EBFP2) (**A**) or no anchor control (**B**). DNA was labelled with SPY-555 dye and tubulin labelled with SiR-tubulin. Rapamycin was applied shortly after capture of the first image and is indicated by orange bar. Time is indicated in minutes, with time 0 set as a similar anaphase stage in each cell. Scale bars, 10 µm.

Surprisingly, cells where ER was relocalised to the PM in early mitosis were frequently observed to progress through mitosis and reassemble the NE (Figure 4.4 and Figure 4.5A). We were interested if clearance of ER from the area proximal to chromatin may affect recoating of chromatin masses by ER membrane to reform the NE later in mitosis. The timing and completeness of chromatin recoating was therefore analysed by measuring the fluorescent profile around the perimeter of each chromatin mass at each time point, as shown in Figure 4.5B. The fluorescent intensity values around the chromatin perimeter were assigned a colour from a scale and represented as a kymograph (Figure 4.5C). Importantly, the kymographs were oriented in the same way with the start and end representing the intersection with the spindle axis. The average kymograph at each timepoint was then calculated for all cells measured (Figure 4.5D). The average result indicated a delay of approximately 6 min in the recoating of the outer and inner faces of the central "core" region of chromatin masses (but not peripheral ends) compared to control cells.

The observed changes in recoating of chromatin after ER relocalisation could be explained by a slower anaphase progression, due to the highly coordinated nature of these processes. We measured the separation of chromatin masses

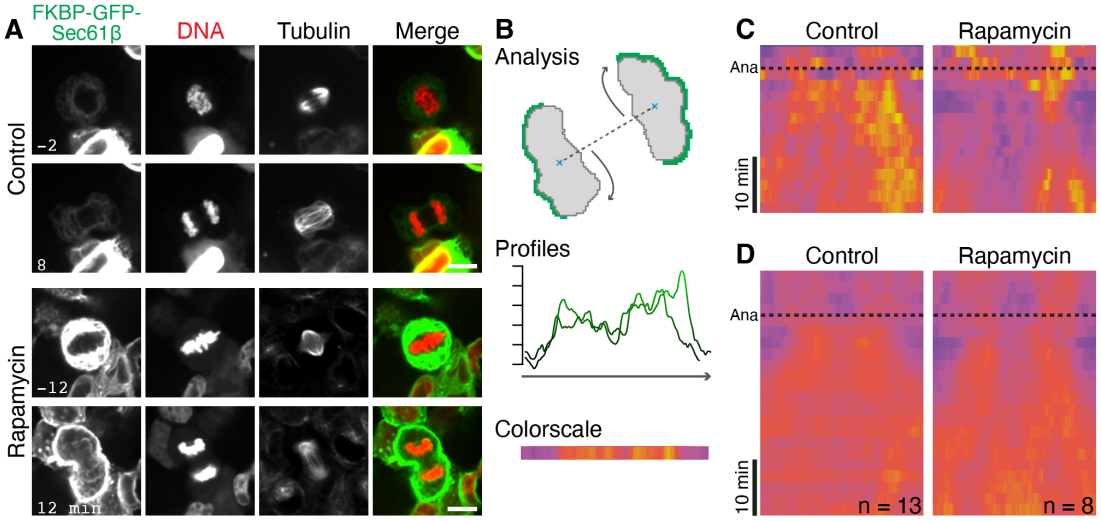

Figure 4.5. Recoating of ER around chromatin in ER relocalised mitotic cells. (**A**) Micrographs of control and rapamycin treated HCT116 cells expressing FKBP-GFP-Sec61β, Stargazin-dCherry-FRB and pmCherry-H3.2 stained with SiR-tubulin. Still images of metaphase and anaphase are shown. Time is in minutes relative to anaphase (0 min). Images were captured at 2 min intervals. Scale bar, 10 µm. (**B**) Schematic diagram of image analysis. Chromosome masses were segmented, outlined and the fluorescence profiles of their perimeter taken. Profiles were recast from the point of intersection of a line (dotted) connecting the two centroids (blue crosses). The profiles were scaled to a uniform length and averaged to produce a single profile for each time point. (**C**) Kymographs assembled from each time point for the examples shown in A. (**D**) Kymographs averaged from the indicated number of cells.

in ER relocalised cells and compared to control cells. The ER, DNA and spindle in relocalised or control cells were visualised along two axes (along the spindle axis and its perpendicular axis), and fluorescent signals were represented as kymographs. The average kymograph from multiple cells was calculated (Figure 4.6A). The separation between chromatin masses was measured between peaks at each timepoint in the kymograph (Figure 4.6B). There was no clear difference in the time between the onset and completion of anaphase in control and relocalised samples. In addition, the control and relocalised cells each showed chromatin separation of around 9 µm on average. However, we see an unexpected inward movement of the chromatin masses after their separation in anaphase in relocalised cells. This relaxation of chromatin after separation could be related to the slower coating of the "core" chromatin region we observed. Relocalised FKBP-GFP-Sec61β at the PM around the midbody could impair or slow the cytokinetic abscission event, through effects on the remodelling of the PM or forces required for furrow ingression during cytokinesis. This could also explain the observed relaxation of chromatin masses after their separation.

We have observed a delay in ER coating of the central "core" region of chromatin and a relaxation of chromatin after separation in cells with induced ER relocation in mitosis. This suggested that the relocalisation of ER had disrupted the

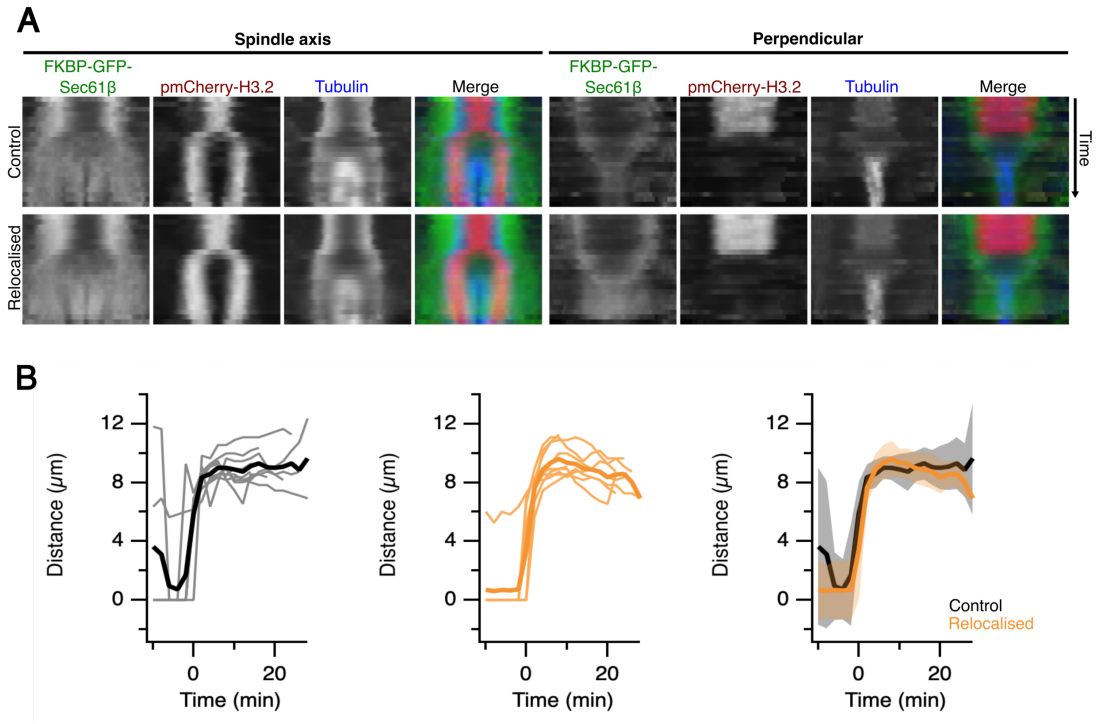

Figure 4.6. Mitotic progression and chromatin separation with induced ER relocalisation in mitosis. (**A**) Average kymographs of data represented in Figure 4.5A. FKBP-GFP-Sec61β, pmCherry-H3.2 and tubulin signal along spindle/DNA axis and perpendicular axes. (**B**) Anaphase distances of chromatin separation in data represented in Figure 4.5A. The distance was measured between peaks at each timepoint shown in the kymograph and the average taken. Thin lines show individual cells, thick lines and shading show the average ± standard deviation. Grey lines represent control cells and the orange lines show cells with ER relocalised. For control cells n=10, and sample cells n=9.

NE reassembly process at chromatin, but that it was still possible for cells to reassemble the NE even when the majority of ER was held at another location.

4.2.5 NE components show distinct pattern to ER relocalised at the plasma membrane or mitochondria

We were interested to explain the defects of chromatin separation and delay in coating of chromatin "core" region after ER relocalisation in mitotic cells in our analysis. We next asked how the relocalisation affected the distribution and recruitment of other proteins to chromatin for NE reassembly. The results could help distinguish between the proposed models of NE reassembly, as the fate and distribution of NE proteins relative to the ER after NEBD in mitosis is currently poorly understood.

We utilised the inducible ER relocalisation system, transiently expressing FKBP-GFP-Sec61β and a PM anchor (Stargazin-darkmCherry-FRB) in HCT116 cells, as in previous relocalisation experiments. The relocation of ER to the PM was induced by the addition of rapamycin and the cells were fixed. The INM protein LBR and nuclear lamin protein lamin B1 were both stained with antibodies to assess the effects of ER relocalisation on the mitotic distribution of these proteins and how this could influence their recruitment to chromatin for NE reassembly (Figure 4.7).

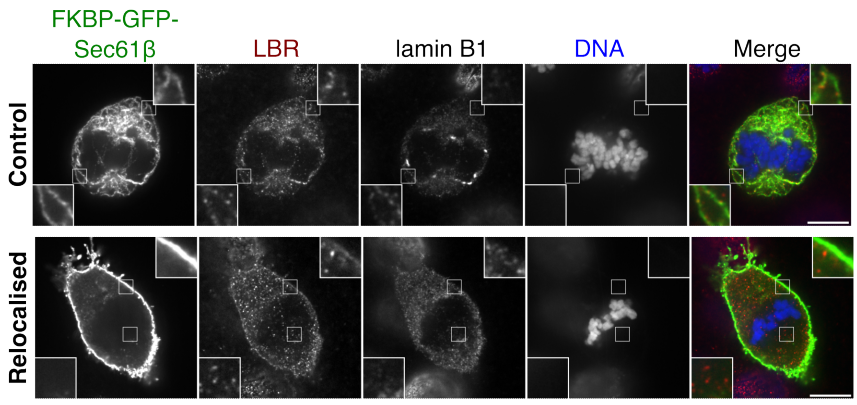

Figure 4.7. Nuclear envelope and lamin protein show different distribution to relocalised ER at the plasma membrane. Representative single slice micrographs from a z-stack of HCT116 cells transiently expressing FKBP-GFP-tagged ER protein Sec61β and PM anchor (Stargazin-darkmCherry-FRB) are shown, with control (no FRB anchor). Rapamycin was applied for 30 min before fixation with PTEMF. LBR and lamin B1 were stained using antibodies and DNA stained with DAPI. ROIs are 3 times expanded from 50 pixel region. Scale bars, 10 µm.

Lamin B1 signal was not detected with relocalised FKBP-GFP-Sec61β coating at the PM, as expected (lamin B1 loses interactions with INM proteins at the NE as a result of early phosphorylation events during mitosis). A proportion of the INM protein LBR could be observed at sites of relocalised FKBP-GFP-Sec61β at the PM. However, a proportion of LBR signal appeared to remain in the cytoplasm.

If INM components were dispersed throughout the ER after NEBD, as is proposed in the free diffusion model, we would expect these proteins to show similar behaviour to the relocalised ER. However, a proportion of LBR shows a distinct pattern to relocalised ER. This is most obvious as discrete LBR-positive puncta in metaphase cells. This would support presence of distinct subdomains of LBR enrichment in the ER, as in the domain model of NE reassembly, or of distinct structures containing LBR, as in the vesicle model. In relocalisation experiments described so far, we have induced the movement of ER to the PM. However, we have seen that when FKBP-GFP-Sec61β and associated membrane is relocalised to the PM using this system, we have incomplete relocalisation, as a portion of ER remains is able to coat the chromatin masses to assemble the NE.

To test if we can improve the extent and efficiency of mitotic ER relocalisation, we compared the relocalisation of FKBP-GFP-Sec61β to the mitochondria using our inducible system (Figure 4.8A) to the pattern observed after relocalising to the PM. We expect the proximity and increased surface area of the mitochondria as a surface for relocalisation compared to the PM could allow more efficient and complete relocalisation of ER. The mitochondria are also dynamic, and closer to the ER, so relocalisation may be more efficient due to increased probability of encounters.

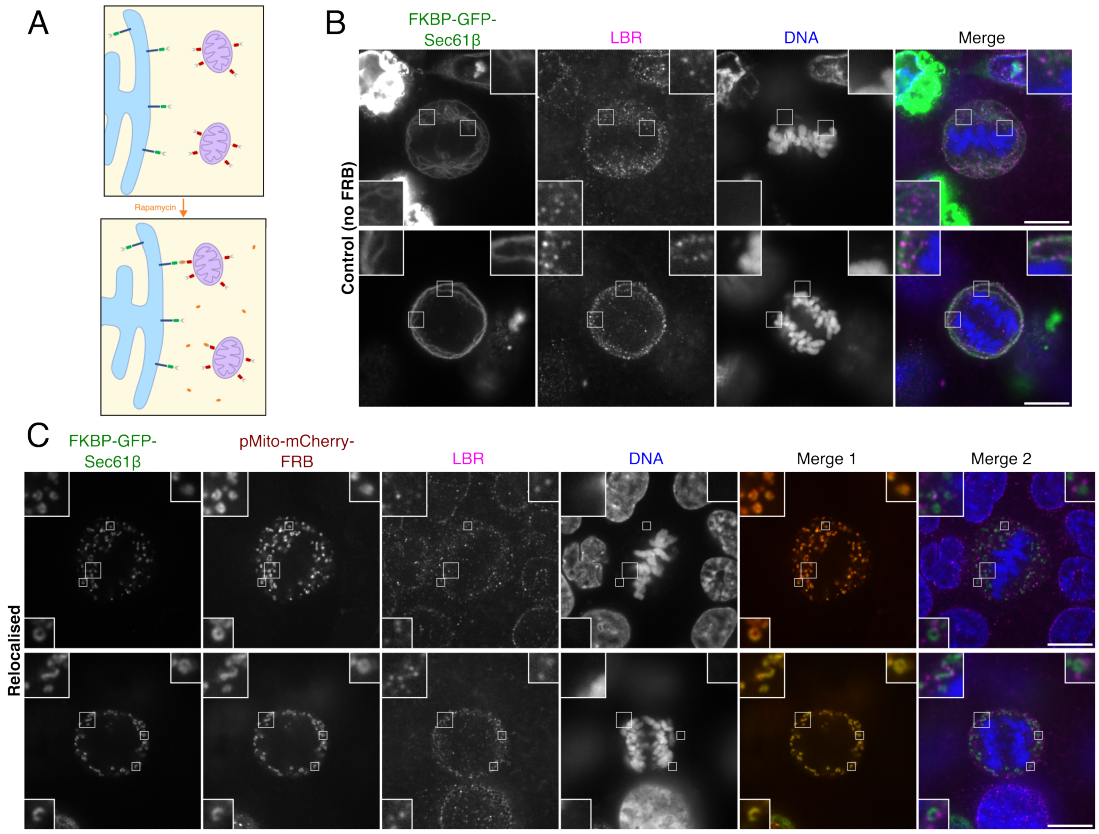

Figure 4.8. INM protein LBR shows distinct pattern to ER relocalised at the mitochondria. (**A**) Schematic of relocalisation. (**B-C**). Representative single slice micrographs from z-stack of HCT116 cells transiently expressing FKBP-GFP-tagged ER protein Sec61β and mitochondrial (pMito-mCherry-FRB) anchor are shown in **C** with control (no FRB anchor) in **B**. Rapamycin was applied for 30 min before fixation with PTEMF. LBR was stained using antibodies and DNA labelled with DAPI. ROIs are 3 times expanded from 50 pixel region or 4 times expanded from a 25 pixel region. Scale bars, 10 µm.

FKBP-GFP-Sec61β completely surrounded the mitochondria after induced relocalisation (Figure 4.8C), while endogenous LBR localised in a distinct pattern in the same cells. LBR signal was more discontinuous than Sec61β and appeared to show some preference for the ends of the relocalised Sec61β coating around mitochondria. Again, as observed when relocalising ER to the PM (Figure 4.7), a proportion of endogenous LBR remained after FKBP-GFP-Sec61β relocalisation. LBR staining also appeared more discontinuous than expressed FKBP-GFP-Sec61β in the absence of relocalisation (control in Figure 4.7A and Figure 4.8B).

Overall, ER marker FKBP-GFP-Sec61β relocalised at the PM or mitochondria showed a continuous coating of either structure. However, endogenous LBR detected at sites of relocalisation showed a more discontinuous pattern. A proportion of LBR also appeared to remain after relocalisation of FKBP-GFP-Sec61β to either structure and did not move with this ER marker. This suggested the concentration of LBR in specific subregions of the ER (supporting the domain model) or in separate structures from the ER (supporting the vesicle model), each of which may function to concentrate components for NE reassembly later in mitosis.

We were very interested to follow up this unexpected LBR localisation, as this could reveal more about the distribution of NE proteins in mitosis in relation to the ER membranes. The differing localisation and behaviour relative to the ER appear to favour the domain and vesicle models over free diffusion of LBR proteins within the ER after NEBD.

4.3 Differential behaviour of NE proteins after relocalisation in mitosis

The distinct localisation and behaviour of NE protein LBR in relation to the ER marker Sec61β in mitosis suggested that LBR was either enriched in specific subdomains of the ER or within separate compartments, supporting the domain or vesicle models of NE protein distribution. We were therefore interested to see the pattern of LBR after induced relocalisation and to compare this to the relocalisation pattern of Sec61β we have observed, to further investigate LBR localisation in relation to the ER in mitosis.

In order to put these localisations in a wider context, the relocalisation pattern of other nuclear/nuclear envelope proteins were induced. This would allow us to compare behaviours of proteins originating from different interphase locations and to determine if any observed behaviours are specific to LBR. The mitotic localisation of the NE proteins and their behaviour when relocalised, especially when compared to the ER, will inform proposed models of the fate of NE proteins after NEBD and the mode of reassembly to form the NE.

To investigate the pattern of relocalisation, HCT116 cells transiently expressing a FKBP-GFP-tagged nuclear/NE protein (FKBP-GFP-BAF, FKBP-GFP-CHMP7, FKBP-GFP-emerin, FKBP-GFP-LAP2β or LBR-FKBP-GFP) and a PM (Stargazin-darkmCherry-FRB or Stargazin-mCherry-FRB) or mitochondrial anchor (pMito-mCherry-FRB), or no anchor (control) were prepared. Rapamycin was applied for 30 min to induce relocalisation before cells were fixed (Figure 4.9).

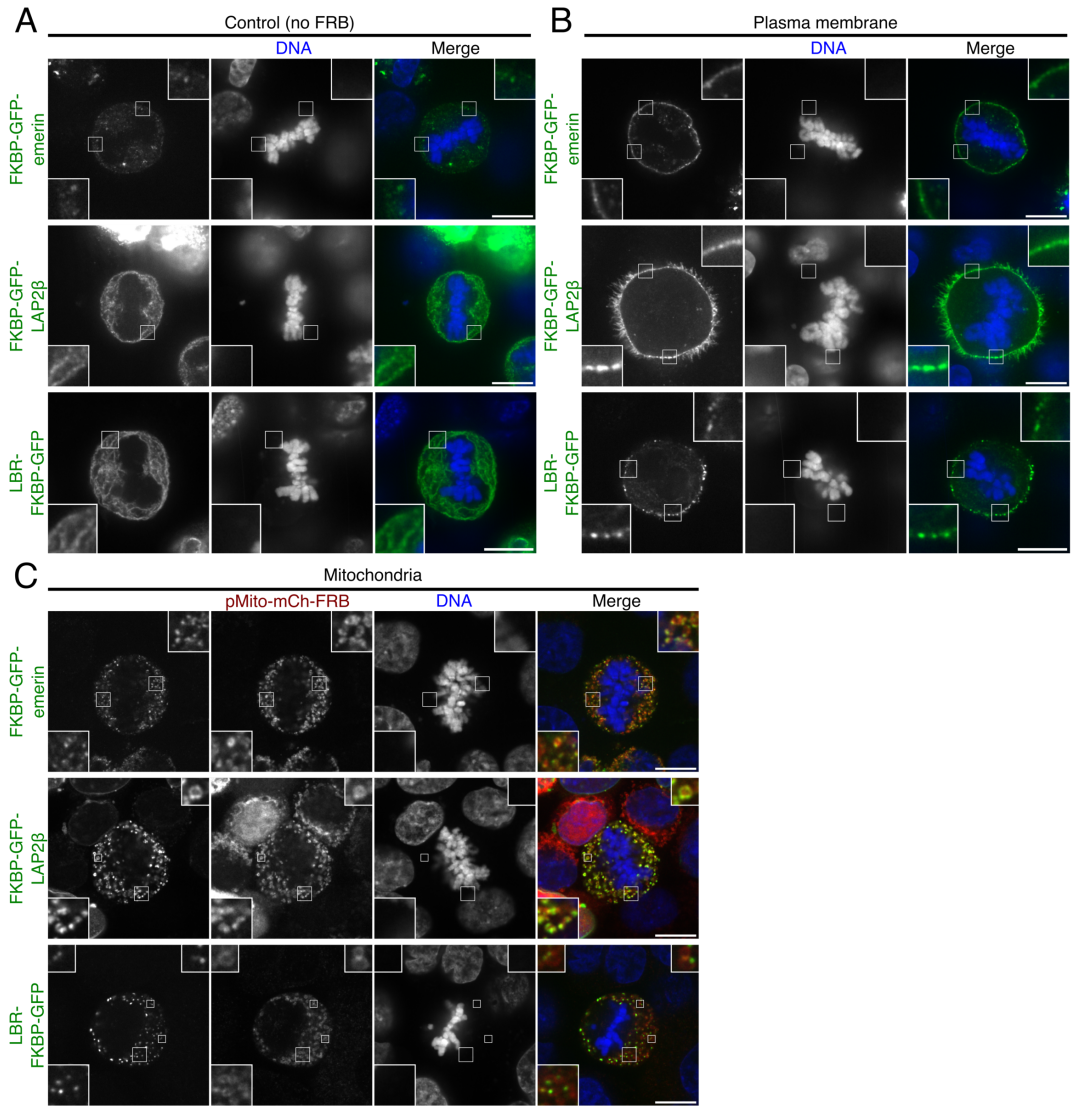

D

Relocalised protein	Plasma membrane	Mitochondria
emerin	Discontinous, almost complete coating	Large puncta, one or two per mitochondria
LAP2β	Discontinous, almost complete coating	Puncta and patches, near complete coating
LBR	Large puncta	Large puncta, one or two per mitochondria

Figure 4.9. Differing pattern of relocalisation of inner nuclear envelope proteins in mitosis. (**A-C**) Representative single slice micrographs from z-stacks of HCT116 cells transiently expressing indicated FKBP-GFP-tagged INM protein (FKBP-GFP-emerin, FKBP-GFP-LAP2β or LBR-FKBP-GFP) with no FRB anchor (control, **A**), plasma membrane anchor (Stargazin-darkmCherry-FRB or Stargazin-mCherry-FRB, **B**)) or mitochondrial anchor (pMito-mCherry-FRB, **C**). Rapamycin was applied for 30 min before PTEMF fixation and staining of DNA with DAPI. Scale bars, 10 µm. ROI are 3 times expanded from 50 pixel region, or 4 times expanded from 25 pixel region. (**D**) Summary table of relocalisation patterns of INM proteins observed in A-C.

We compared the pattern of the different nuclear/nuclear envelope proteins relocalised during mitosis (Figure 4.9 and Figure 6.2) to the pattern already observed for relocalisation of the ER marker Sec61β (Figure 4.7 and Figure 4.8). Each protein showed different relocalisation patterns, as summarised in Figure 4.9D and Figure 6.2D.

The INM proteins emerin, LAP2β and LBR each relocalised with different patterns in mitosis (FKBP-GFP-emerin, FKBP-GFP-LAP2β and LBR-FKBP-GFP in Figure 4.9). In control metaphase cells, LBR-FKBP-GFP and FKBP-GFP-LAP2β appeared to localise similar as expected for ER membrane, but in a notably discontinuous pattern. While FKBP-GFP-emerin was more distributed and puncate. When relocalised to the PM, FKBP-GFP-emerin almost completely coated the PM, but in a discontinuous pattern. Similarly, FKBP-GFP-LAP2β relocalised to the PM formed an almost complete, but discontinuous, coating. However, LBR-FKBP-GFP relocalised to the PM as large puncta which were inconsistent in size, with some larger, more patch-like structures also observed. Although, this could be the result of viewing angle in 2D. Note that a proportion of FKBP-GFP-emerin and LBR-FKBP-GFP signal remained after relocalisation to the PM, while a large proportion of the expressed FKBP-GFP-LAP2β appeared to have been relocalised to the PM. FKBP-GFP-emerin and LBR-FKBP-GFP showed similar relocalisation pattern when relocalised to the mitochondria. The relocalised puncta were variable in size and few in number, with one or two observed at an individual mitochondrion.

The relocalisation pattern of these proteins each originating from the INM was clearly different to that observed for BAF, which is not integrated within a membrane in mitosis. FKBP-GFP-BAF was mostly diffuse in the cytoplasm in control metaphase cells, with some localised to the spindle and the cell cortex (Figure 6.2). FKBP-GFP-BAF relocalised continuously around the PM or mitochondria. In contrast, CHMP7, which can associate with ER membrane and functions to seal holes late in the NE reassembly process, was present in small puncta in metaphase cells prior to relocalisation (FKBP-GFP-CHMP7 in Figure 6.2). FKBP-GFP-CHMP7 relocalised to the PM and mitochondria in a patchy pattern, but with near complete coating. This demonstrated that the punctate pattern of relocalisation observed for proteins from the INM (LBR, emerin and LAP2β) was not a result of limited availability of relocalisation sites at the PM or mitochondria.

The discontinuous and punctate pattern of relocalised INM proteins (LBR, emerin and LAP2β) was of particular interest, as we have observed a more continuous coating of the ER marker FKBP-GFP-Sec61β when relocalised to

the same structures within the cell (PM or mitochondria). This differing behaviour suggested that these NE proteins are not distributed throughout the ER during mitosis, as was proposed in the free diffusion model, and may be more concentrated in particular subdomains or in separate structures, supporting the domain or vesicle models.

4.4 Discussion

In this chapter, we have shown that ER relocalisation and subsequent expansion of the exclusion zone affect the mitotic spindle orientation and position when induced around the metaphase stage. Analysis of ER relocalisation effects in live cells indicated a delay of recoating of the outer and inner faces of the central "core" region of chromatin masses and a chromatin separation defect. This could not be explained by slower chromosome segregation in anaphase.

The defective coating of the "core" region of the chromatin mass was likely a result of delayed or insufficient recruitment of components to reform the NE within this region. We visualised the distribution of NE proteins after ER relocalisation in mitosis, to see if there is coating of nuclear components in the central "core" chromatin regions. This revealed an unexpected localisation pattern of the NE protein LBR that was distinct from the ER. We investigated this further and saw that endogenous LBR relocalised in a distinct pattern to ER marker Sec61β and to other proteins originating from the interphase INM in mitosis.

Overall, this suggested that NE proteins are not freely diffusing within the ER in mitosis, and supported the presence of precursor domains or vesicles to NE reassembly enriched in NE components. We were interested to follow up these observations by further investigating the relationship of LBR to the ER in mitosis, as this will inform the mechanism of NE reassembly.

Chapter 5

Nuclear envelope proteins and mitotic NE reassembly

5.1 Introduction

LBR is one of the principal components of the interphase NE, making connections to the underlying nuclear lamina and heterochromatin. LBR is a multipass transmembrane protein within the INM with nucleoplasmic N-terminal and C-terminal domains. During reassembly of the NE, LBR is recruited early to the peripheral ends of the chromatin mass and recruits membrane to this region. LBR has been described as a "non-core" component of the nuclear envelope, and showed defective or delayed recruitment to lagging chromosomes (Liu *et al.*, 2018; Orr *et al.*, 2021). The levels of LBR protein are also reported to differ at MN compared to the main nucleus (Maass *et al.*, 2018). This highlights why LBR is of particular interest in terms of the NE assembly mechanism.

In the previous chapter, we saw that proteins LBR, emerin and LAP2β, each present in the INM in interphase, show different patterns of localisation and a clearly distinct behaviour to the ER when relocalised within the cell in early mitosis. If the NE proteins were present within the ER after NEBD and freely diffusing, we would expect these proteins to behave similarly to each other, and to the ER, when they are relocalised. Our data instead suggest enrichment in subdomains or separate compartments of the ER, supporting the domain or vesicle models of mitotic NE protein localisation.

In this chapter, we set out to determine how LBR localises after NEBD in mitosis and whether this follows the vesicle or domain model. This will help us to understand the mechanism of NE reassembly later in mitosis. We began

by visualising LBR localisation in mitosis when expressed at endogenous levels and in the absence of any treatments or manipulation in the cell. When LBR was overexpresssed in different cell types, the protein showed different patterns of localisation, which suggested potential cell type variability in localisation (Giannios *et al.*, 2017). Differences in the extent of ER remodelling as cells enter mitosis have also been reported between different cell types (Lu *et al.*, 2009), which could influence the mitotic localisation of LBR. We will therefore also compare the localisation of LBR in mitosis between the different cell types used during this PhD study.

5.2 Localisation of the INM protein LBR in mitosis

Endogenous LBR localisation was visualised by indirect immunofluorescence in three cell lines (RPE-1, HCT116, HeLa) and in RPE-1 GFP-Sec61β and RPE-1 GFP-Sec61β LBR-mCherry stable cell lines described previously. LBR detected by staining in these cell lines showed a punctate pattern of localisation during interphase and mitosis, including at the reforming NE around chromatin masses (Figure 5.1A), and appeared similar in localisation between the different cell lines. In RPE-1 GFP-Sec61β cells, endogenous LBR staining was more discontinuous than the pattern of the ER marker GFP-Sec61β (Figure 5.1B). The localisation of stably expressed LBR-mCherry in the RPE-1 GFP-Sec61β LBR-mCherry cell line also appeared punctate and more discontinuous than the GFP-Sec61β (Figure 5.1C). This suggested that, unlike Sec61β, LBR does not homogeneously distribute throughout the ER and is instead concentrated into subdomains, or potentially separate compartments. These results provide further evidence to support the domain and vesicle models over the diffuse model of NE protein localisation in mitosis.

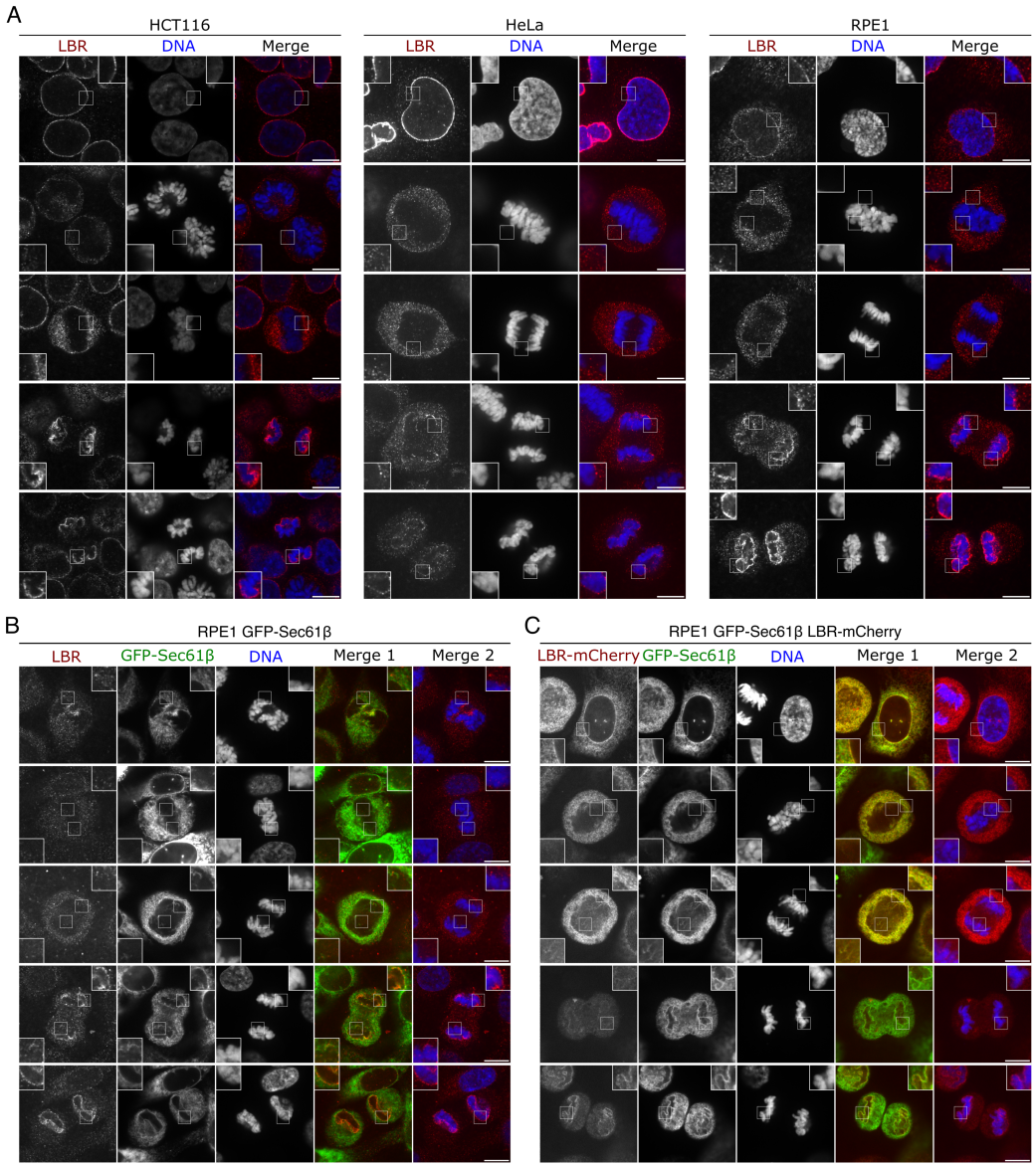

Figure 5.1. Localisation of LBR in different cell lines. (**A**-**B**) Single confocal slice images of endogenous LBR localisation in HCT116, RPE-1, HeLa or RPE-1 GFP-Sec61beta cells detected by antibody staining. (**C**) Localisation of LBR-mCherry in RPE-1 GFP-Sec61beta LBR-mCherry cell line. Cells were fixed using PTEMF fixative. DNA was labelled with DAPI. Scale bars, 10 µm. Insets are shown at 2 times magnification.

5.3 Further investigating the relocalisation pattern of LBR

The fixation process has been found to affect the visualisation of specific ER structures within cells, particularly cisternae (Lu *et al.*, 2009), and the formation of protein assemblies (Irgen-Gioro *et al.*, 2022). This could affect the appearance of any associated protein localisation when compared to live cell imaging. To first confirm that the punctate pattern of relocalised LBR we observed previously (Figure 4.9) was not an artefact of the particular fixation process, we compared relocalisation under different fixation in HCT116 cells: PTEMF (Figure 4.9 and Figure 5.2B); PLP (Figure 5.2C) and PFA (data not shown). LBR relocalisation appeared similar under each fixative type, suggesting this pattern was not induced by the particular fixation method used.

5.3.1 INM protein LBR relocalisation appears distinct from the ER

To further investigate the LBR distribution in relation to the ER in mitosis, we visualised an ER marker in cells with LBR relocalisation. We used the same inducible system to induce LBR relocalisation to the PM as previously, but with co-expression of mCherry-Sec61β to visualise the ER. HCT116 cells transiently co-expressing mCherry-Sec61β and LBR-FKBP-GFP were prepared, rapamycin was applied to induce relocalisation of LBR, and then cells were fixed after 30 min incubation.

As observed previously (Figure 4.9 and Figure 5.2), LBR relocalised to the PM in a punctate and patchy pattern with varied size (Figure 5.2). This relocalisation pattern was particularly clear when observed from a single confocal slice at the top of the cell. ER marker mCherry-Sec61β did not show the same pattern and could not clearly be observed at relocalised FKBP-GFP-LBR puncta at the PM. If we compare LBR relocalisation to Sec61β relocalisation (in Figure 4.7 and Figure 4.8), which coated continuously around structures, LBR clearly shows a very distinct pattern. Again, this suggested concentration of LBR in particular subdomains or separate compartments of the mitotic ER, but we were still unable to distinguish between these models.

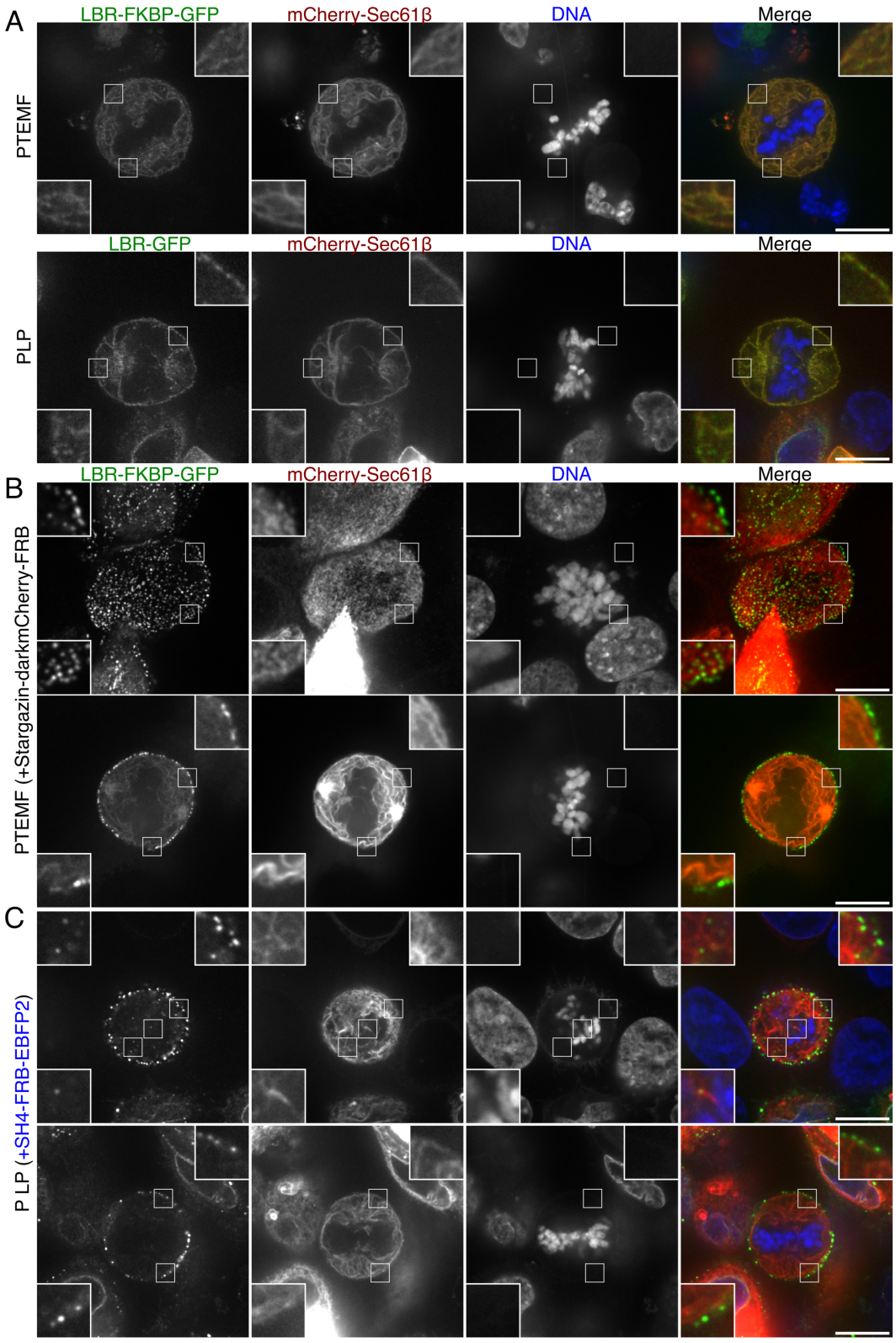

Figure 5.2. Relocalisation of the INM protein LBR in mitosis. Single confocal slices from z-stacks of HCT116 cells transiently expressing LBR-FKBP-GFP and a PM anchor (Stargazin-darkmCherry-FRB (**B**) or SH4-FRB-EBFP2 (**C**)). Controls (**A**) expressed no FKBP (LBR-GFP) or no FRB (no PM anchor) construct, as labelled. Rapamycin (200 nM) was applied to cells for 30 min before fixation. Cells were prepared with PTEMF or PLP fixative, as indicated. DNA was labelled with DAPI. Scale bars, 10 µm. Insets are 3 times expanded from specified 50 or 75 pixel region.

Next we induced relocation of LBR in live cells to visualise the relocalisation event and the formation of these large puncta, to ascertain their origin.

5.3.2 LBR relocalised in a punctate pattern under endogenous levels of expression

So far we have only studied the relocalisation pattern under conditions where LBR was overexpressed. To allow us to investigate relocalisation under endogenous levels of LBR expression, we generated a CRISPR knock-in HCT116 cell line expressing the LBR relocalisation construct (LBR-FKBP-GFP) by C-terminal PCR tagging method (Fueller *et al.*, 2020) (Figure 5.3A). HCT116 cells with incorporated insert were initially selected with puromycin and then further selected by FACS, to enhance the proportion of cells positive for expression of the fluorescent protein (Figure 5.3B). We then screened for fluorescence by microscopy and visualised the mitotic progression of the selected cells (Figure 5.3E).

Next, we characterised the genotype and protein expression of the selected pooled cells. Insertion of the FKBP-GFP tag was confirmed by genotyping PCR using primers annealing inside of the expected insert sequence within the genome (Figure 5.3D). The expression of insert at protein level was determined by western blot (Figure 5.3C). The results suggested a heterozygous (insertion at one allele) or mixed (homozygous and heterozygous for insertion) population of cells, as endogenous LBR expression was still detected in the cell pool, in addition to the tagged protein (LBR-FKBP-GFP). Note that we are currently working with a mixed population of cells. Mitotic timings have not been measured, as there is a mixed population of cell genotypes present, however no gross effect on cell division has been observed.

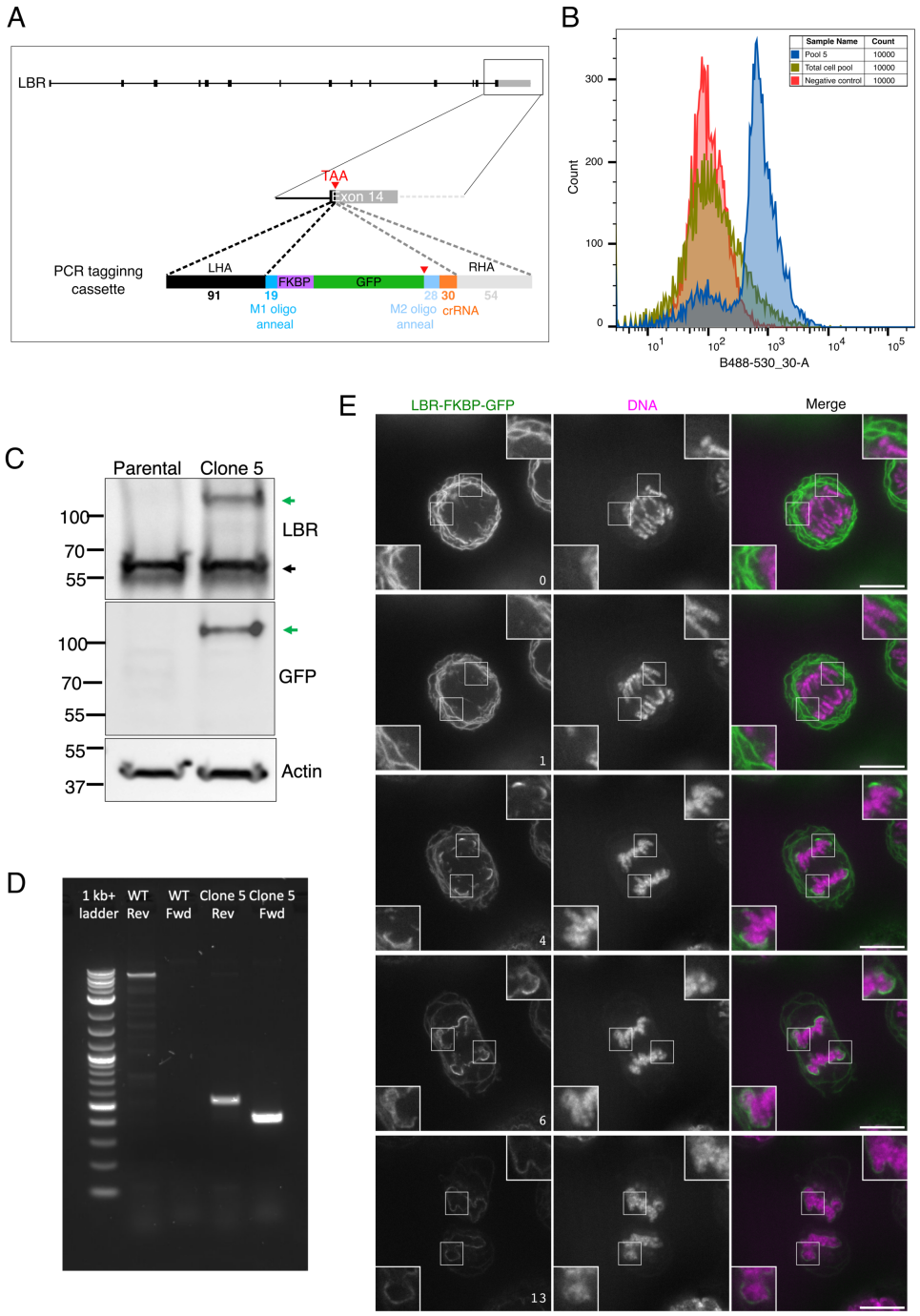

Figure 5.3. Characterisation of HCT116 LBR-FKBP-GFP cell pool. HCT116 LBR-FKBP-GFP cells were generated by C-terminal PCR tagging CRISPR method and selected for expression by puromycin and then FACS, collecting pools of cells. (**A**) Schematic of C-terminal PCR tagging of LBR. (**B**) FACS plots were generated using FlowJo v10.8.2. (**C**) Western blot of lysates collected from parental (HCT116 WT) or an edited cell pool. Proteins were detected by antibody stain for GFP or endogenous LBR protein with an actin loading control. The green arrowhead indicates the expected mass of the protein tagged (LBR-FKBP-GFP) and the black arrowhead indicates the expected mass of endogenous LBR. (**D**) Genotyping PCR of parental or edited pool using primers annealing inside of the insert sequence. (**E**) Stills of single slices from z-stack of live HCT116 LBR-FKBP-GFP cells with DNA stained by SiR-DNA dye progressing through mitosis. Labels indicate time in minutes. Insets are 2 times expanded from indicated 75 pixel region. Scale bar, 10 µm. FACS plots and western blots by Nuria Ferrandiz. Genotyping PCR by Alex Moore.

We will use this population for relocalisation experiments, as it is likely that only one tagged allele is sufficient for successful relocalisation of a compartment. While the untagged protein will still be expressed and localise in a heterozyogus cell, we expect relocalisation to reduce the protein available for NE reassembly function.

After characterising the HCT116 LBR-FKBP-GFP cells, we induced relocalisation in live mitotic cells (Figure 5.4). This allowed us to see the pattern of localisation under endogenous expression levels of LBR and to compare localisation before and after relocalisation was induced in the same cell.

HCT116 LBR-FKBP-GFP transiently expressing a mitochondrial anchor (pMito-mCherry-FRB) were prepared and the DNA was labelled with SiR-DNA dye. Relocalisation was induced in live cells on the microscope by addition of rapamycin after capture of the initial image. Again, LBR-FKBP-GFP appeared as large puncta when relocalised to the mitochondria. These puncta of LBR-FKBP-GFP after relocalisation were variable in size and were infrequent, with only one or two observed per mitochondrion. This result is very similar to that seen when transiently overexpressed LBR-FKBP-GFP was relocalised to mitochondria in HCT116 cells (Figure 4.9).

This confirmed that relocalisation observations made previously in HCT116 cells transiently expressing LBR-FKBP-GFP were not an artefact of the overexpression. Additionally, we see that the relocalised LBR-FKBP-GFP puncta did not appear to grow over time after these were initially observed on the mitochondria in live cells, which implied that LBR-FKBP-GFP was not accumulating within the regions after relocalisation. It remained difficult to distinguish the origin of the relocalised puncta, whether from ER subdomains or separate structures.

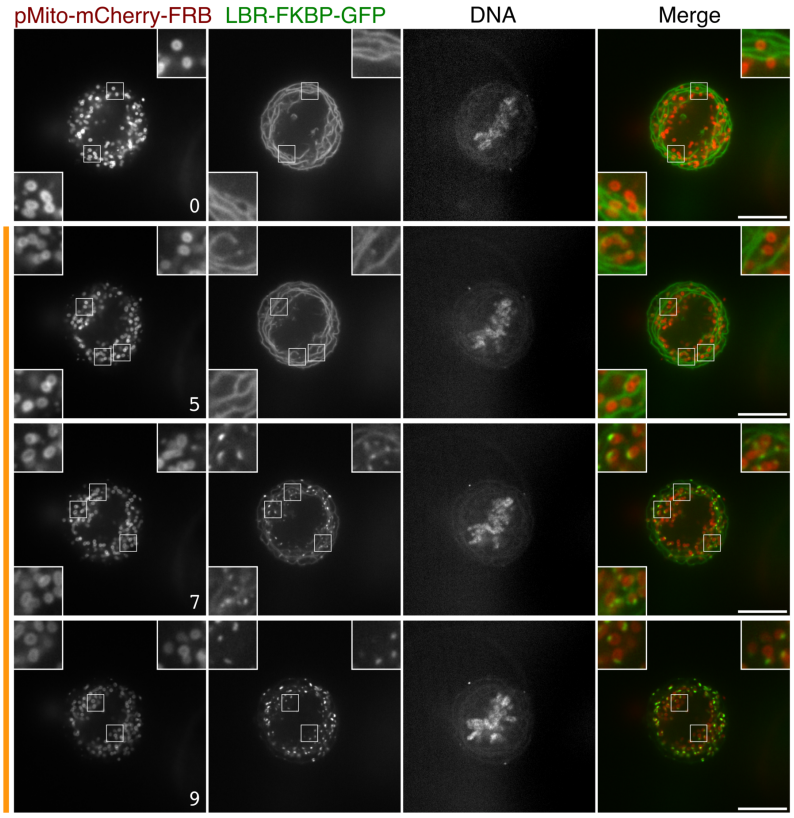

Figure 5.4. LBR relocalisation pattern at endogenous levels of expression. Single slice stills from HCT116 LBR-FKBP-GFP cells transiently expressing a mitochondrial anchor (pMito-mCherry-FRB) captured live. Relocalisation was induced through rapamycin (200 nM) addition shortly after capture of the first image, represented by the orange bar. Labels indicate time in minutes. Insets are 3 times expanded from indicated 50 pixel region. Scale bar, 10 µm.

5.4 Identifying other components enriched with LBR in mitosis

We next wanted to determine what other proteins are enriched with LBR at these subdomains or structures of higher concentration. This information may inform as to whether or not these are within, or separate to, the ER. Therefore allowing us to differentiate between domain or vesicle models.

5.4.1 INM protein LAP2β shows partial association with relocalised LBR

First, we examined the localisation of LAP2β, Lamin A and Nup133 following LBR relocalisation to the PM. HCT116 cells transiently expressing constructs to allow induced relocalisation of LBR (LBR-FKBP-GFP and SH4-FRB-EBFP2) or no relocalisation control (LBR-FKBP-GFP only, no FRB construct) were prepared, with co-expression of LAP2β-mCherry or mRuby2-laminA-C. Relocalisation of LBR-FKBP-GFP was induced through application of rapamycin to the cells for 30 min before fixation. The nucleoporin Nup133 was labelled with a fluorescently-conjugated antibody in a subset of samples.

Under these conditions, LBR formed large puncta at the PM after relocalisation, as in previous experiments. We saw no clear localisation of Nup133 (Figure 5.5) or A-type lamin proteins (mRuby2-laminA-C, data not shown) at the relocalised puncta. However, LAP2β-mCherry expressed in these cells could be observed at a proportion of LBR-FKBP-GFP puncta at the PM (example indicated with filled magenta arrowhead in Figure 5.5). This suggested a partial association between the pattern of the two INM proteins in mitosis. In control cells with no relocalisation, LBR-FKBP-GFP and LAP2β-mCherry each appeared discontinuous in pattern, with some regions of more concentrated, but nonoverlapping signal of each. These observations may support the existence of domains of distinct protein profiles or behaviours within the ER during mitosis, which we were interested to further investigate.

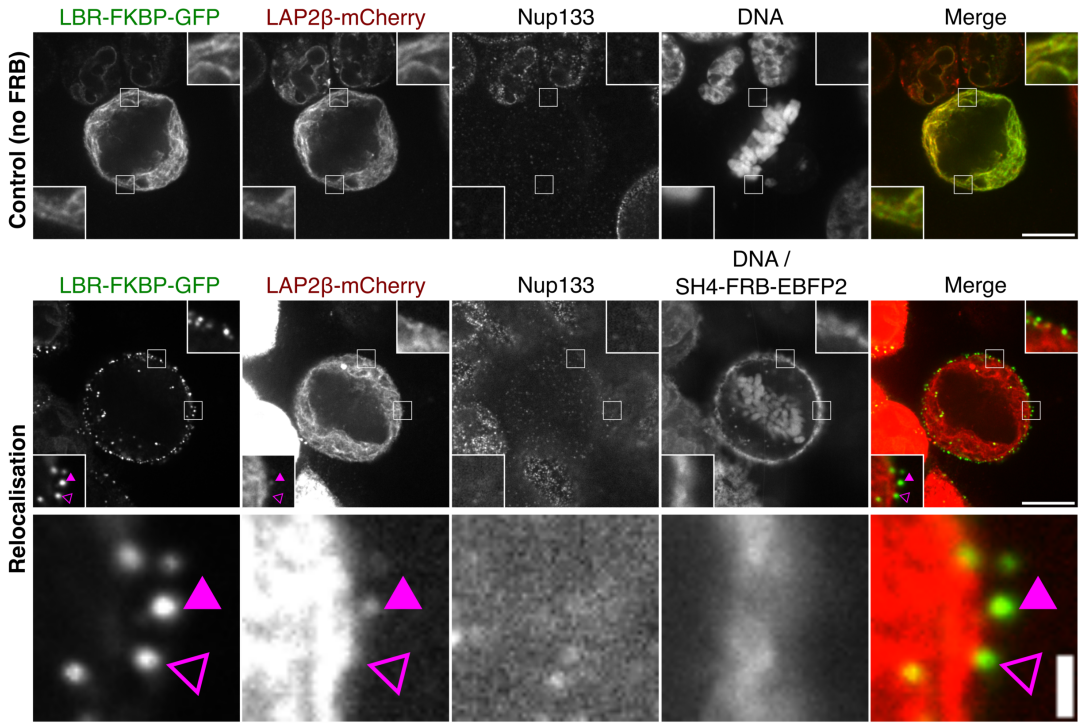

Figure 5.5. LAP2β shows a partial association with relocalised LBR. Single confocal slices from z-stacks of HCT116 cells transiently expressing LBR-FKBP-GFP and a plasma membrane anchor (SH4-FRB-EBFP2) or no relocalisation control (no FRB construct), and LAP2β-mCherry, as labelled. Rapamycin (200 nM was applied for 30 min before fixation with PTEMF fixative. The display range has been adjusted in the expanded images to better allow visualisation of LAP2β-mCherry. Filled magenta arrowheads indicate examples of LAP2β localising at LBR-FKBP-GFP relocalised puncta, while arrowheads with no fill indicate LBR-FKBP-GFP puncta with no clear LAP2β signal. Scale bars, 10 µm or 1 µm on expanded images. Insets are 3 times expanded from the specified 50 pixel region. Expanded images below are 12 times expanded from the same 50 pixel region.

5.4.2 LBR shows an association with relocalised LAP2β

We were then interested to see the pattern of LBR in a reciprocal relocalisation experiment, where LAP2β was relocalised within the cell. The constructs to allow relocalisation of LAP2β to the mitochondria (FKBP-GFP-LAP2β and pMito-mCherry-FRB) were transiently expressed in HCT116 cells. Control cells with no anchor expressed (no FRB construct) were prepared alongside. As in previous experiments, rapamycin was applied for 30 min before cells were fixed to induce relocalisation. Endogenous LBR was then labelled by antibody staining of the fixed samples.

In a similar experiment, LAP2β had previously shown a distinct pattern when relocalised to the PM or mitochondria, with a more complete and continuous coating than relocalised LBR (Figure 4.9). Here we observe similar relocalisation pattern of LAP2β as previously, with continuous, but incomplete, coating of mitochondria (Figure 5.6B). In control samples with no relocalisation, LBR had a more discontinuous pattern than LAP2β-GFP (Figure 5.6A). In relocalised samples, endogenous LBR was detected at sites of LAP2β relocalised around the mitochondria, but LBR signal did not overlap with LAP2β. Instead, LBR appeared at the ends of LAP2β coated regions (Figure 5.6B).

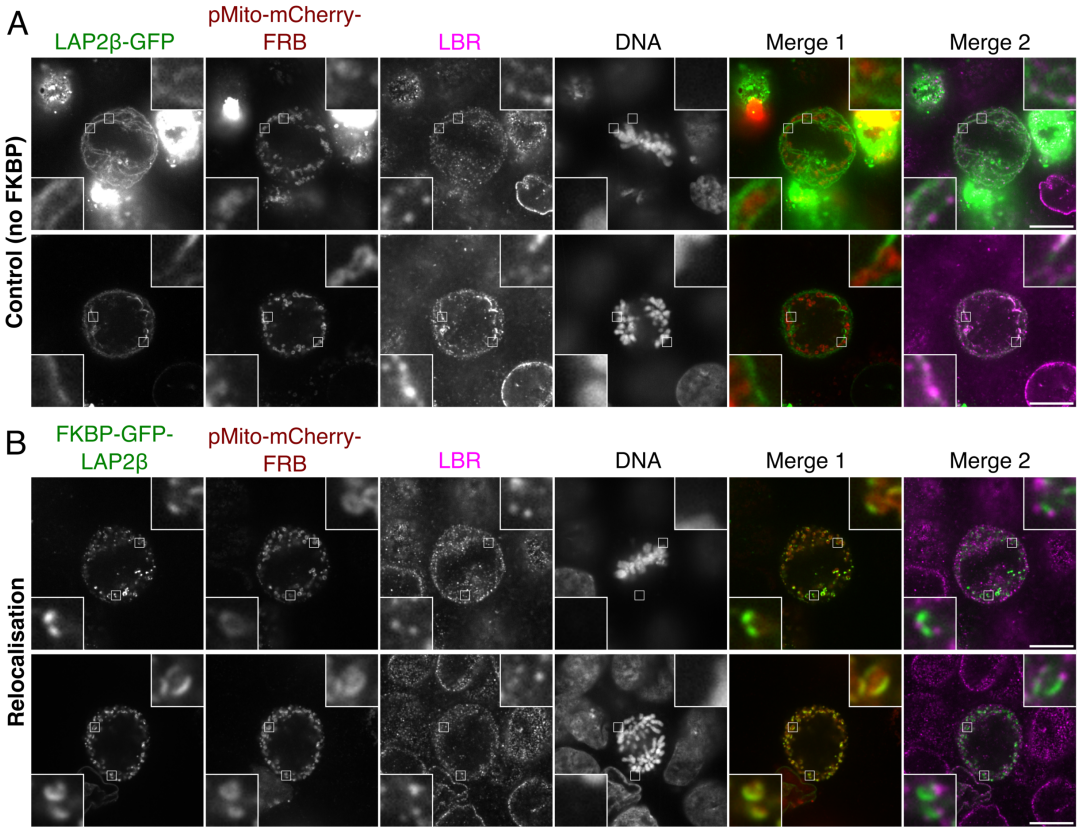

Figure 5.6. LBR shows an association with relocalised LAP2β. Single confocal slices from z-stacks of HCT116 cells transiently expressing FKBP-GFP-LAP2β and a mitochondrial anchor (pMito-mCherry-FRB) or controls cells (no FKBP construct, expressing LAP2β-GFP), as labelled. Rapamycin (200 nM) was applied for 30 min before fixation with PTEMF fixative. Scale bars, 10 µm. Insets are 6 times expanded from specified 30 pixel region.

We have identified that the protein LAP2β shows a partial association with LBR enriched regions in mitosis. LAP2β was present at a proportion of relocalised LBR puncta and when LAP2β itself was relocalised, LBR was detected at relocalised sites. However, in each case the proteins appear distinct in their localisation, without any clear overlap. LBR and LAP2β each localise to the INM in interphase. If NE proteins were freely diffusing within the ER in mitosis, as proposed in the diffusion model, we would expect to see some overlap of signal. The results tend to support enrichment of particular INM proteins in subdomains of the ER, over the presence of these proteins in shared vesicle.

Of note, LAP2β has been described as a "core" localising protein and LBR as a "non-core" protein in the transient subdomains formed at the NE during reassembly later in mitosis. The association of LBR and LAP2β observed by relocalisation at this earlier mitotic stage may also inform the reassembly mechanism.

We wanted to identify other proteins which may be similarly enriched with either protein. Using immunofluorescence to determine if individual proteins relocalise with LBR is a low throughput approach and also limited by the available antibodies and expression constructs. We therefore next moved to a using a higher throughput approach to identify proteins enriched in the LBR enriched subdomains or structures in mitosis. From the results, we can then verify interesting proteins within the cell context.

5.4.3 Identifying proteins in mitotic membrane fractions containing LBR

To isolate LBR-containing membrane compartments, stable RPE-1 GFP-Sec61β LBR-mCherry cells (or RPE-1 GFP-Sec61β cells as a control) were synchronised and subcellular fractionation used to separate membranes (as shown in Figure 5.7A).

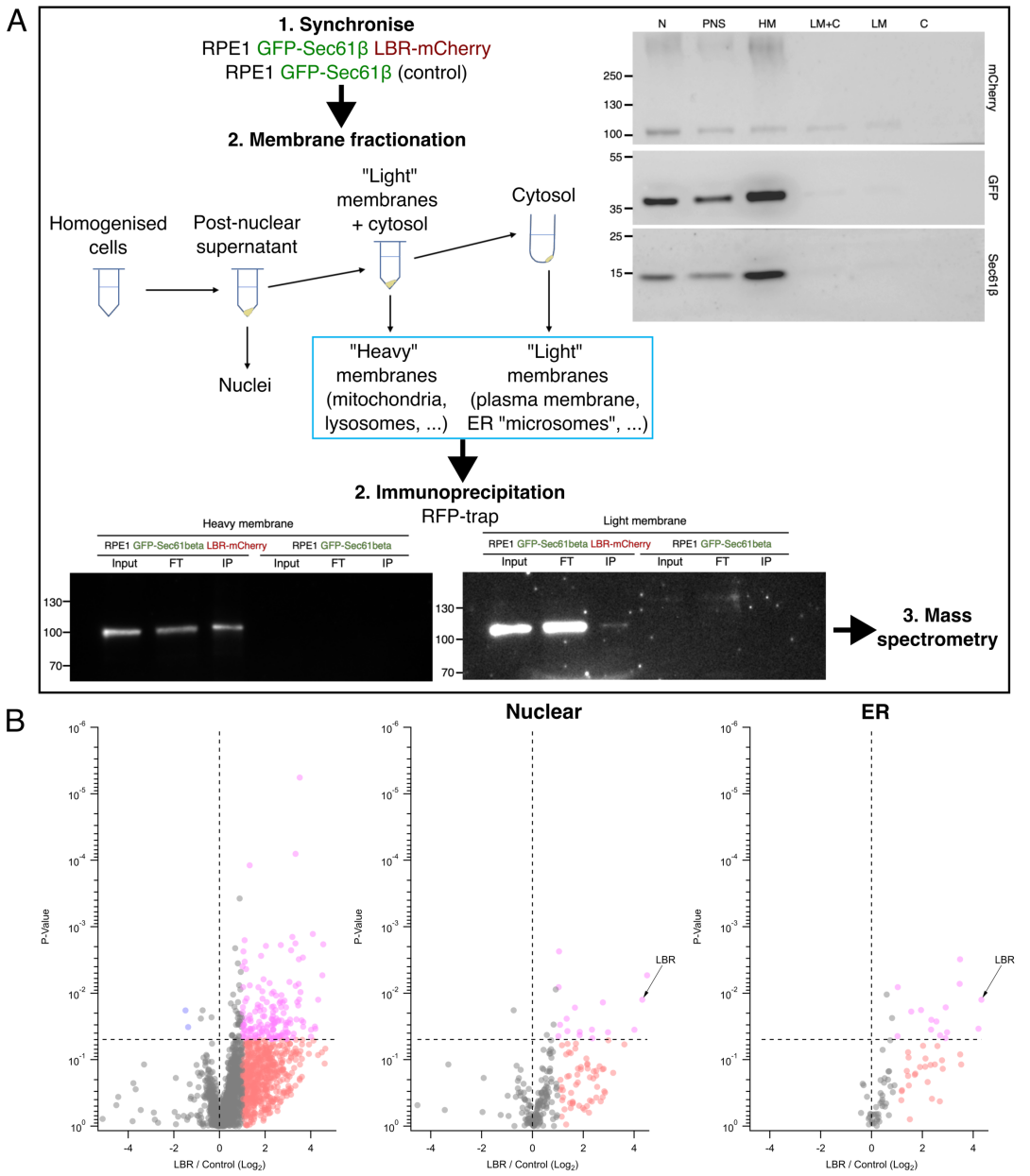

Figure 5.7. Isolating LBR containing compartments from mitotic cells. (**A**) Schematic of mitotic cell fraction and immunoprecipitation method to isolate LBR-mCherry membrane compartments. RPE-1 GFP-Sec61β/LBR-mCherry cells were synchronised (thymidine/nocodazole). Membranes were fractionated from synchronised mitotic cells by sequential centrifugation. Upper western blots show isolated fractions (equivalent to input stage for membrane fractions to immunoprecipitaton) with proteins detected by antibody stain for mCherry, GFP or Sec61β, as indicated, to check for presence of proteins of interest in each fraction (nuclei (N), post-nuclear supernatant (PNS), "heavy" membrane (HM), "light" membrane (LM) and cytosol (C)). Lower western blots shows input, flow through and IP product from HM and LM fractions stained with antibody against mCherry protein. HM and LM fractions were analysed by mass spectrometry. (**B**) Volcano plot of comparing LFQ intensities from mass spectrometry results after MaxQuant processing and presented using Igor. Horizontal dashed line indicates the log fold change threshold (1.5 fold) used to determine significantly enriched proteins in LBR sample relative to control (with HM and LM results combined in each condition). The left plot shows all results after processing raw data in MaxQuant. Middle and right plots show results filtered by GO terms for nuclear or ER proteins (Methods Table 2.5 and 2.6).

We confirmed which membrane fractions contained LBR-mCherry and Sec61β by western blot (Figure 5.7A). The results indicated presence of LBR-mCherry, but not Sec61β, in the "light" membrane fraction, which would suggest separate compartments. However we cannot rule out that this may be as a result of differences in antibody detection.

LBR-mCherry was immunoprecipitated (IP) from the "heavy" and "light" membrane fractions. We confirmed successful IP of LBR-mCherry from membrane fractions by western blot (Figure 5.7A). The remaining IP sample was then prepared for "in-gel" digest and mass spectrometry analysis.

The mass spectrometry results processed using MaxQuant confirmed successful enrichment of LBR-mCherry in RPE-1 GFP-Sec61β/LBR-mCherry cells samples relative to the control, presented in Figure 5.7B. A complex mix of proteins was significantly enriched, so we needed a way to rationalise the results.

We filtered the results by subcellular localisation using Gene Ontology (GO) terms. Isolated compartments enriched in LBR also contained other markers of the NE and ER (Figure 5.7). Of note, LEMD3 (MAN1) was significantly enriched in IP of RPE-1 GFP-Sec61β/LBR-mCherry cell samples relative to the control. LEMD3 originates from the interphase INM, and contains a LEM domain, as do LAP2β and emerin for which we have observed mitotic localisation. LEM domain proteins, including MAN1, are concentrated at the "core" region of chromatin during NE reassembly through interaction with BAF (Mansharamani and Wilson, 2005), whereas LBR is initially recruited and concentrated at the peripheral ends ("non-core") regions of chromatin (Haraguchi *et al.*, 2008). Interestingly, MAN1 has been reported to be recruited to chromatin with similar timing to LBR in live mammalian cells (Haraguchi *et al.*, 2008), which implies it could have similar temporal, but distinct spatial, regulation of recruitment.

LAP2β was not identified as significantly enriched in the LBR containing membrane fractions, despite our observation that this protein partially associated with relocalised LBR in cells. We suspect therefore that our proteomic method may not be optimal for isolating specifically the structures or subdomains of ER that are enriched for LBR.

GO terms describe interphase localisation, and this is a significant limitation, particularly for NE proteins in which localisation is not characterised in mitosis. Entry into mitosis is associated with loss, but also gain of many interactions, some of which affect subcellular localisation. Particularly as NEBD allows interaction of components previously separated by the NE in interphase. As we have seen, nuclear and NE proteins can also have transient interactions and localisations at

different mitotic stages, also not accounted for by GO term analysis.

5.4.4 Identifying proteins relocalised with LBR

The membrane fractionation approach isolated total LBR containing compartments from mitotic RPE-1 GFP-Sec61β LBR-mCherry cells and did not select for the concentrated LBR subdomains or structures of interest that we can observe by relocalisation. To address this shortfall we devised a way to purify material which would allow us to characterise the components present specifically within the LBR-FKBP-GFP containing compartments which are relocalised. To isolate these compartments, we induced LBR-FKBP-GFP relocalisation to the mitochondria in synchronised mitotic cells, isolated the mitochondria, and then released the LBR-FKBP-GFP-containing compartments from the mitochondria by proteolysis and then separated them for analysis (as summarised in Figure 5.8A).

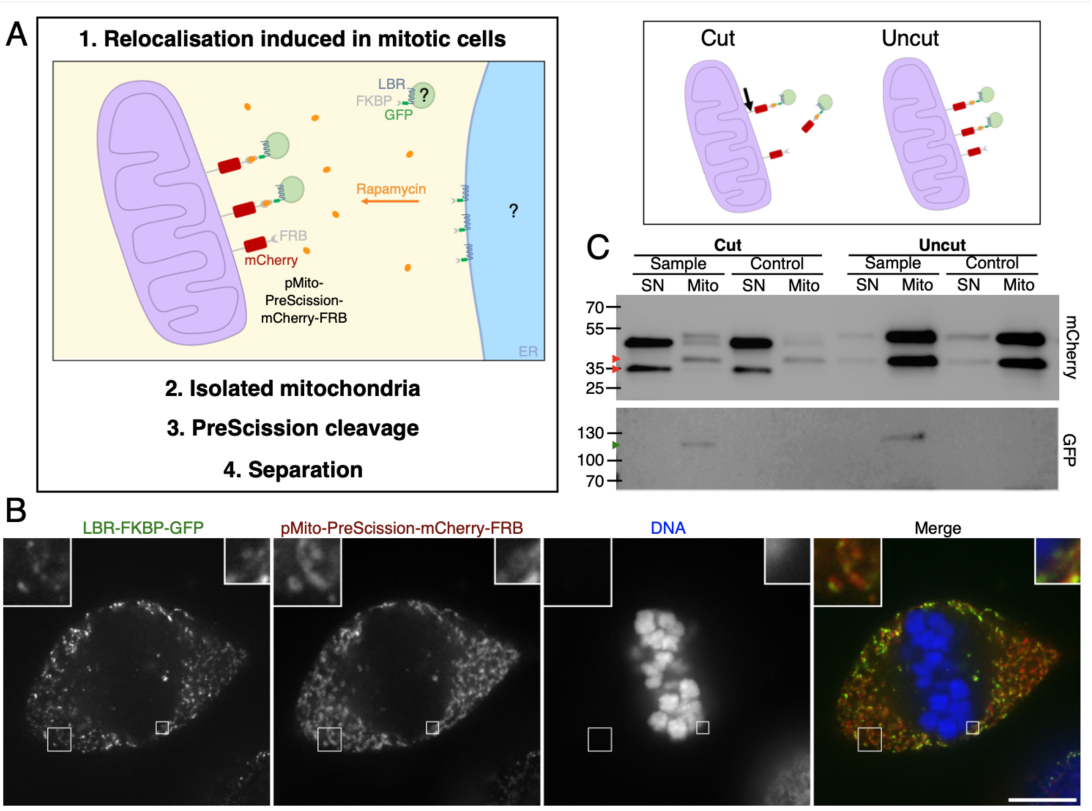

Figure 5.8. Isolating relocalised LBR containing compartments from mitotic cells. (**A**) Schematic of method used to isolate LBR containing compartments relocalised to the mitochondria in mitosis. (**B**) Wild-type HeLa transiently expressing LBR-FKBP-GFP and pMito-PreScission-mCherry-FRB treated with rapamycin (200 nM)for 30 min to induce heterodimerisation before PTEMF fixation. DNA was labelled with DAPI. Insets are 3 times expanded from a 50 pixel region or 4 times expanded from a 25 pixel region. Scale bar, 10 µm. (**C**) Western blot of mitochondrial pellet (mito) or supernatant (SN) from mitochondria isolated from synchronised mitotic HCT116 cells transiently expressing cleavable mitotrap (pMito-PreScission-mCherry-FRB) and LBR-FKBP-GFP (or LBR-GFP in control) with rapamycin treatment to induce heterodimerisation and then incubation with PreScission protease (cut) or uncut. Red arrowheads indicate the expected mass could represent PreScission cleaved and uncut pMito-PreScission-mCherry-FRB. Proteins were detected by antibody stain for mCherry or GFP.

We first designed a construct that allowed release and separation of relocalised LBR-FKBP-GFP from the mitochondria after relocalisation, which was important to minimise mitochondrial protein noise (and increased protein complexity) of samples for mass spectrometry. A short fragment encoding a protease recognition site was introduced into the mitochondrial anchor construct (pMito-PreScission-mCherry-FRB). Following proteolytic cleavage, we expect the mCherry-FRB fragment of the mitochondrial anchor to be released from the mitochondria and therefore any bound FKBP-tagged protein that heterodimerised to the FRB after rapamycin treatment to also be released.

We then confirmed that LBR-FKBP-GFP relocalised to the cleavable mitochondrial anchor similar to as the anchor before the cleavage site was introduced. LBR-FKBP-GFP relocalised to the cleavable anchor (pMito-PreScission-mCherry-FRB) in a punctate pattern when the constructs were transiently expressed in WT HeLa (Figure 5.8B), similar to previous patterns with non-cleavable mitochondrial anchor (pMito-mCherry-FRB) in HCT116 (Figure 4.9). LRB-FKBP-GFP puncta of variable size were observed at mitochondria, with only one or two puncta visible per mitochondrion. This also demonstrated that the relocalisation pattern of LBR is not likely cell type specific.

Next we induced relocalisation of LBR-FKBP-GFP to the mitochondria in synchronised mitotic HeLa cells transiently expressing the cleavable mitochondrial anchor through application of rapamycin. The mitochondria were then isolated, as shown in Figure 5.8A. PreScission protease was added to the isolated mitochondria to cleave the recognition site of the mitochondrial anchor, releasing any FKBP-tagged protein heterodimerised with the FRB tag of the anchor from the mitochondria. The isolated mitochondria sample was incubated with protease (or no cleavage control) after which the supernatant and mitochondria were separated by centrifugation. The success of cleavage and release of relocalised protein was assessed by western blot of each fraction (Figure 5.8C).

The main advantage of this approach over the mitotic membrane fraction method described in the above section is that we should enrich for the relocalising compartment containing LBR-FKBP-GFP. Also that we may better maintain ER structures and minimise the formation of "microsomes", which are small vesicles formed by mechanical fragmentation of the ER, through use of fewer and lower force centrifugation steps than in the membrane fraction method.

Protease cleavage of the mitochondrial anchor was successful, as determined by the presence of a band of lower mass detected in staining for mCherry protein in the supernatant of cut compared to uncut samples (Figure 5.8C).

However, a band of mass expected for LBR-FKBP-GFP was detected only in sample mitochondrial fractions in both cut and uncut conditions (GFP staining, Figure 5.8C). As we have shown that we have successful cleavage of the mitochondrial tag in the cut samples, we expected LBR-FKBP-GFP would be released into supernatant in this sample. We suspect that the centrifugation step used to separate mitochondria and supernatant at this final step may also pellet membranes structures other than mitochondria, which may include LBR-FKBP-GFP containing structures, especially as these appeared by microscopy to be large and protein dense.

We aim to further optimise the system to improve the purity of the mitochondria isolated and to increase the concentration of the final product for mass spectrometry analysis. In future, these experiments will be conducted at endogenous levels of LBR expression in the HCT116 LBR-FKBP-GFP cells we have generated, which will improve transfection efficiency (require only to transfect single construct) and therefore the mass of relocalised material isolated from a similar number of cells compared to transient transfection of two constructions.

5.5 Structure of relocalised LBR compartments in mitosis

Our investigations so far have suggested that LBR is concentrated in particular subdomains of the ER or in separate structures, supporting either the domain or vesicle model of mitotic NE protein distribution. However, we have so far been unable to conclude through our relocalisation experiments which of these models describes mitotic LBR localisation.

To determine between vesicle and domain models, we next visualised the nanoscale structure of the relocalised LBR-FKBP-GFP membranes at the mitochondria by SBF-SEM.

The images revealed ER-like structures in close proximity to the mitochondria in cells with relocalised LBR-FKBP-GFP (Figure 5.9). These structures were elongated and connected over several z-sections. At some of the close contacts we see electron density at the apparent contact site (examples indicated by red arrowheads in Figure 5.9B and D). This density is due to concentration of protein

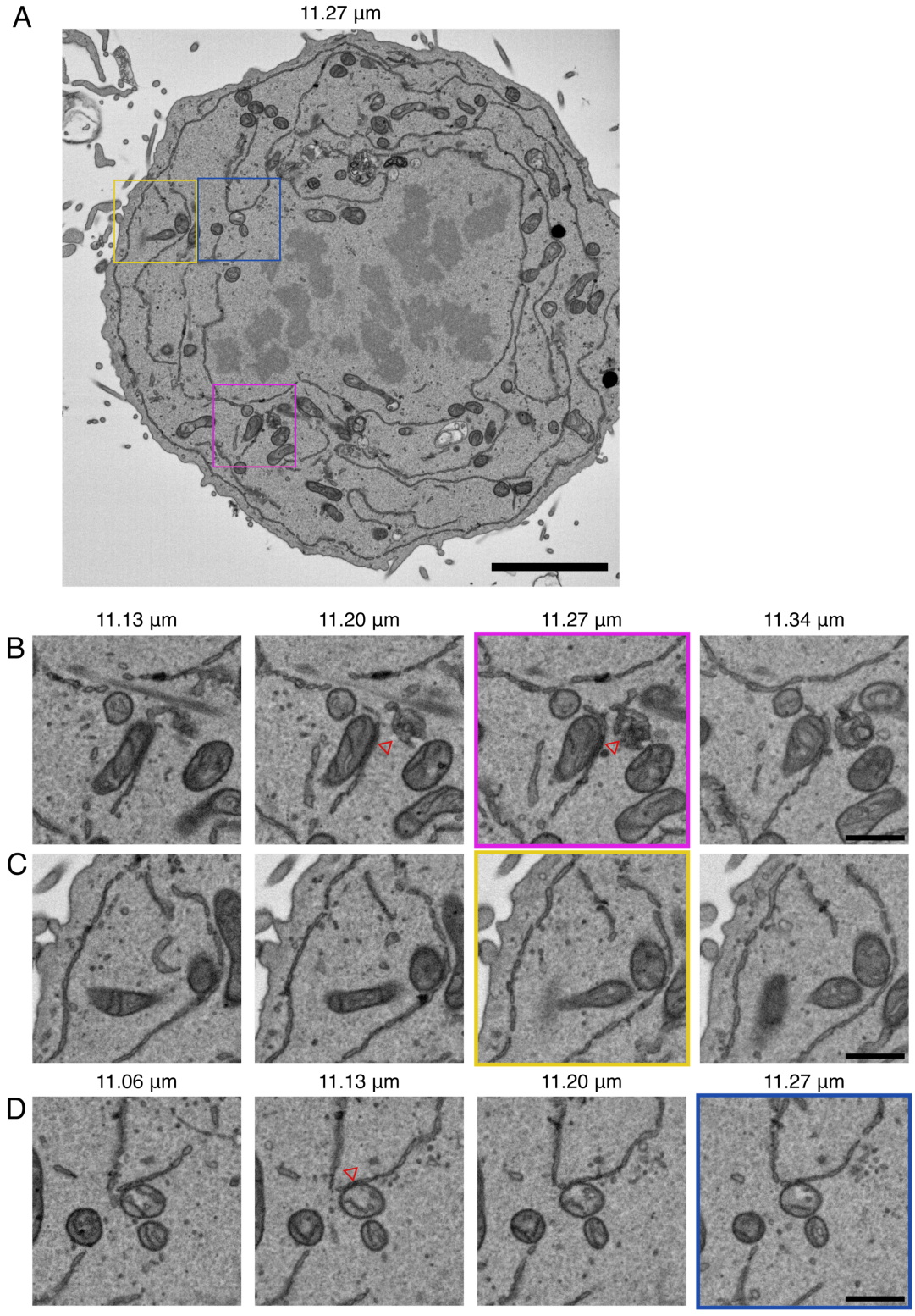

Figure 5.9. Relocalised LBR-FKBP-GFP compartments are not vesicular. (**A**) Single slice from SBF-SEM imaging of a HCT116 cell transiently expressing LBR-FKBP-GFP and pMito-mCherry-FRB. Rapamycin was applied for 30 min before fixation. Steps (70 nm) Depth (µm) indicated. Scale bar, 5 µm.(**B-D**) Expanded from selected regions indicated in **A**. Scale bars, 1 µm. Red arrowheads indicate examples of density at the contacts between SBF-SEM samples prepared by Nuria Ferrandiz.

at the site which accumulates heavy metal stain. The likely identity of this protein is LBR-FKBP-GFP. However, a change in density at the ER region closest to mitochondria was not seen at all ER structures close to mitochondria (example Figure 5.9C), suggesting that the density appears only at very high protein concentrations and that not all contacts meet those levels.

We are working to segment structures in single z-sections of the image stack and to render these in 3D to compare ER and mitochondria contacts in the LBR-FKBP-GFP relocalised cell compared to a control cell with no relocalisation. This will allow us to quantify the changes in ER-mitochondria contacts after LBR-FKBP-GFP relocalisation in mitosis and to further characterise the structure and connections of relocalised compartments. We are unsure currently whether we induce any change or fragmentation of ER structure through LBR-FKBP-GFP relocalisation, which could also explain the possible variable size of relocalised puncta. In addition, through relocalising LBR-FKBP-GFP we could preferentially move particular ER structure types, which we are also interested to further investigate.

The major observation in these experiments was that we did not observe vesicular structures present at the mitochondria after LBR-FKBP-GFP relocalisation. Our results therefore support the model that LBR is enriched in subdomains within the ER during mitosis.

5.6 Disrupting LBR function in NE reassembly

So far, we have utilised the induced relocalisation system to study LBR localisation pattern in mitosis in relation to the ER. Whatever the normal localisation, the relocalisation of LBR sequesters the protein away from its endogenous location within the cell and prevents or hinders its recruitment to chromatin for NE reassembly during late mitosis. This manipulation therefore allows us to determine the function of LBR specifically during in NE reassembly in mitosis.

LBR-FKBP-GFP relocalisation affected recruitment to chromatin in HCT116

Our aim was to induce relocalisation of LBR in early mitotic cells to observe any effects on recruitment of LBR to chromatin for NE reassembly later in mitosis and on the mitotic progression of cells after relocalisation. As previously, we induced relocalisation of LBR to the mitochondria, as we expect relocalisation to be most efficient at these organelles compared to the PM.

HCT116 cells transiently expressing constructs for induced LBR relocalisation to the mitochondria (LBR-FKBP-GFP and pMito-mCherry-FRB) and control cells (no FKBP construct, expressing LBR-GFP and pMito-mCherry-FRB) were prepared. Relocalisation was induced by addition of rapamycin to live cells on the microscope. The progression of cells after LBR-FKBP-GFP relocalisation was then captured at 1 min intervals (Figure 5.10).

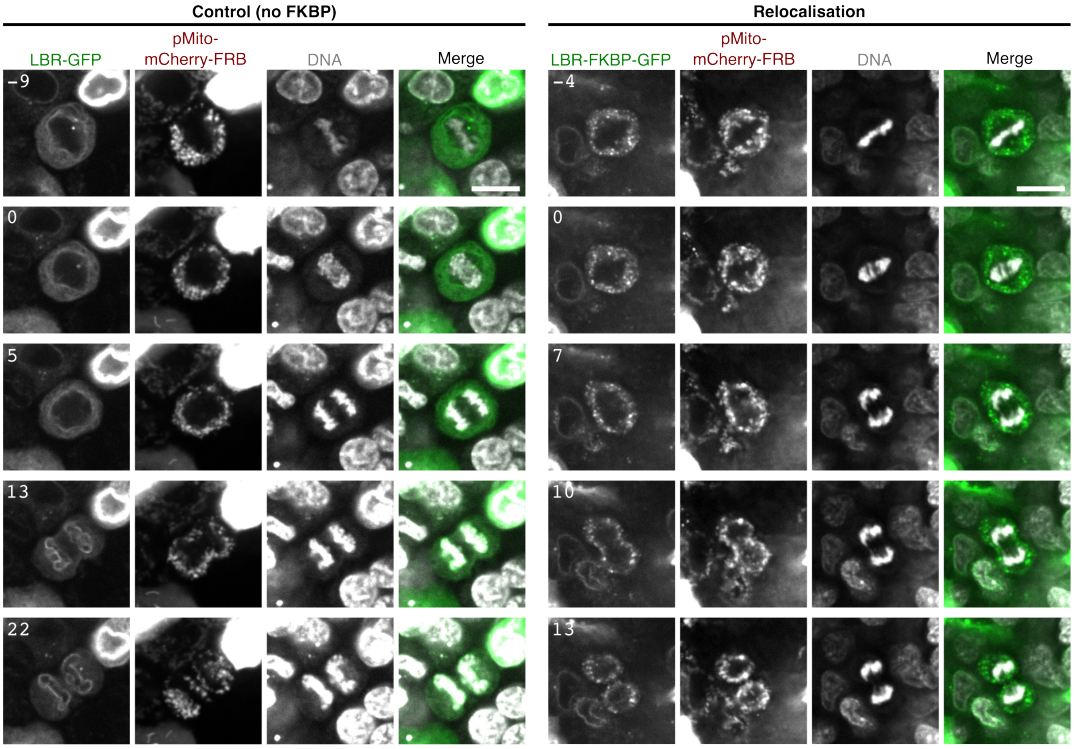

Figure 5.10. LBR-FKBP-GFP relocalisation affected recruitment to chromatin in HCT116. Single confocal slices from z-stacks of live HCT116 cells transiently expressing LBR-FKBP-GFP (or LBR-GFP in control) and a mitochondrial anchor (pMito-mCherry-FRB), as labelled. DNA was stained with SiR-DNA. Rapamycin (200 nM) was applied for around 30 min before the first image was captured. Images were captured at 1 min intervals. Time is indicated in minutes, with a time 0 representing the first frame in anaphase. Scale bars, 5 µm.

In the live cell example shown, relocalisation of LBR-FKBP-GFP to mitochondria was clear in metaphase. Some faint coating of LBR-FKBP-GFP on the outer edges of chromatin was seen as cells progressed through mitosis, but appeared with delay in recruitment to chromatin compared to in control cells. In the examples shown (Figure 5.10), in control cells, LBR-FKBP-GFP was first observed coating the peripheral ends of chromatin in early anaphase (14 min frame), around 5 min after the first anaphase frame was captured. Whereas in the LBR-FKBP-GFP relocalised cell, no coating was clear until around 10 min after the onset of anaphase, at which stage there was furrow ingression, and so appears at a later stage than the initial coating observed in the control. The coating was very faint and appeared around the outer edge of the chromatin mass, rather than being limited to the peripheral ends as was seen when first coating in control samples.

At later stages of mitosis, no recruitment of LBR-FKBP-GFP to the inner face of chromatin (facing the opposite chromatin mass) was observed in relocalised samples. Whereas, at a similar stage, LBR-FKBP-GFP coated around the chromatin masses in the control cells.

Mitotic defects were observed in a proportion of cells which progressed after relocalisation in early mitosis, often manifested as bridging or lagging chromosomes. This suggests that the NE reassembly at the inner face of the chromatin mass is disrupted or delayed after LBR-FKBP-GFP relocalisation in early mitosis. It also implies a distinct mechanism of LBR coating within this central "core" region compared to the peripheral ends. Whether this could be as a result of insufficient recruitment of LBR containing structures to this region or spreading of existing coating around the chromatin mass requires further investigation.

The faint coating that was still observed after relocalisation suggested the potential presence of LBR in multiple compartments or incomplete relocalisation. It is important to consider that endogenous, untagged LBR protein could still be functioning in NE reassembly in these cells, even where no clear coating of LBR-FKBP-GFP was observed on chromatin. Indeed this was confirmed by antibody staining endogenous LBR in fixed samples (data not shown). Also LBR is overexpressed, which can have effects on membrane production (Ma *et al.*, 2007) and timing of NE reassembly (Anderson *et al.*, 2009). Although this is also true of the control sample, the level of overexpression may differ between individual cells.

In future, quantification of the completeness of recoating and timing of mitotic

events in a larger number of cells would be required to confirm if observed mitotic defects were as a result of the relocalisation.

A further confounding factor is that mitochondrial aggregates form at relatively high levels of expression of the mitochondrial anchor. This means that any effects seen could be a result of unequal distribution of mitochondria and protein relocalised too the mitochondria to daughter cells after division, rather than resulting from LBR relocalisation. To address this issue, we repeated the experiment using a HeLa cell line where pMito-mCherry-FRB is stably expressed. This gives more consistent expression levels of the mitochondrial anchor, and therefore controls for potential effects of aggregation.

LBR-FKBP-GFP relocalisation induced mitotic defects

To set up this experiment, LBR-FKBP-GFP was transiently expressed in the HeLa pMito-mCherry-FRB stable cells. Cells were synchronised to allow more control over the mitotic stage at which relocalisation was induced (synchronised with thymidine/RO-3306, as shown in Figure 5.11A). Cells were released from the G2/M boundary by washout of treatment. At release, the DNA was labelled with SiR-DNA dye and rapamycin was applied to induce relocalisation. Note that rapamycin and SiR-DNA dye were both washed off after 30 min incubation to minimise possible effects during the longer term imaging used in this experiment. Both compounds are also applied to control cells and so this is controlled for.

Around 1 h after release of cells from synchronisation, many cells were observed in metaphase. Sample dishes were transferred to the microscope and cells in metaphase with relocalised LBR-FKBP-GFP were selected for imaging of progression through mitosis.

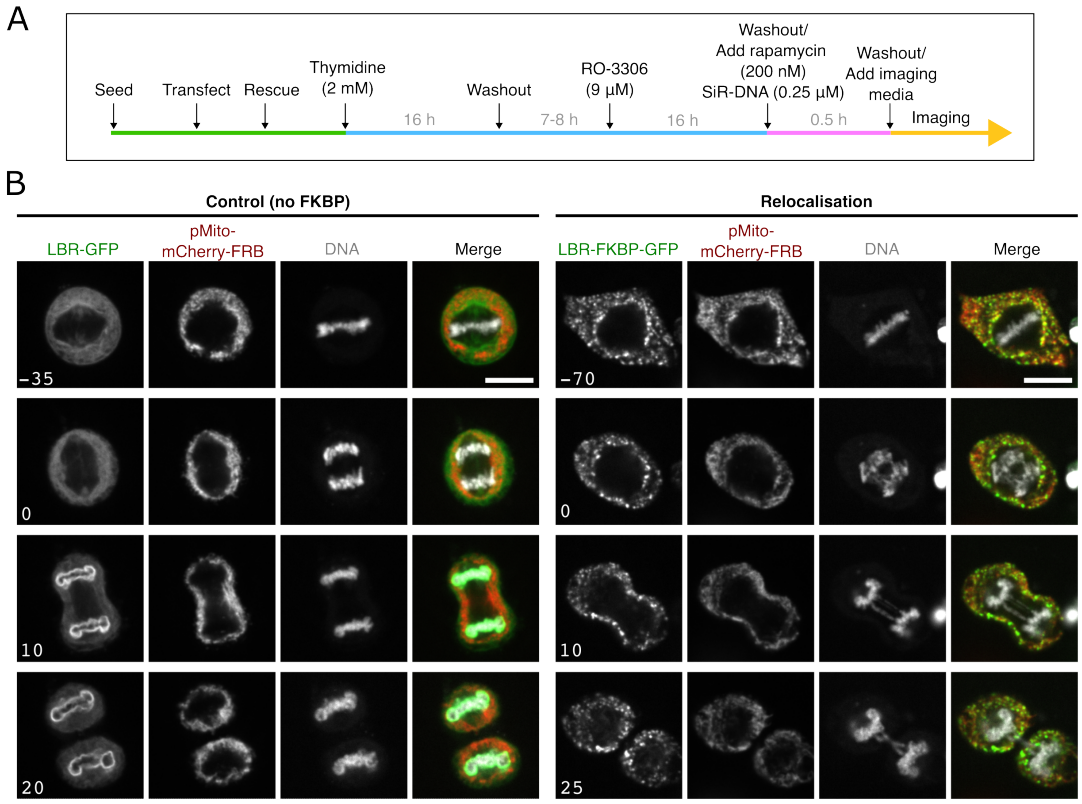

Figure 5.11. Mitotic progression after LBR relocalisation in mitosis. (**A**) Schematic of method used to synchronise, release, induce relocalisation and stain DNA in transiently transfected cells. Final concentrations of reagents used are indicated. In washout steps, cells were washed gently three times with sterile PBS and then media was replaced. (**B**) Single confocal slices of HeLa pMito-mCherry-FRB cells transiently expressing LBR-FKBP-GFP (or LBR-GFP in control) synchronised, released and with rapamycin added to induce relocalisation and DNA labelled with SiR-DNA using method as shown in **A**. Imaging was started at around 1 h after release and the addition of rapamycin (200 nM) and DNA stain (both treatments were washed off after 30 min incubation). Time is indicated in minutes, with a time 0 representing the first frame in anaphase. Images were captured at 5 min intervals. Scale bars, 5 μm.

After LBR-FKBP-GFP was relocalised to the mitochondria in HeLa pMito-mCherry-FRB, only faint recoating of chromatin with LBR-FKBP-GFP was observed. Relocalised cells were still able to progress from metaphase through mitosis. However, many examples of bridging or lagging chromosomes were observed in relocalised cells, as shown for a representative cell in Figure 5.11B. This defect did not appear as obvious or as high frequency in control cells also overexpressing LBR (Figure 5.11B). Again this implied defects in the recruitment of LBR-FKBP-GFP to chromatin for NE reassembly and, similar to LBR-FKBP-GFP relocalisation in HCT116 cells, that this induced chromosome segregation errors.

However, while we have now controlled for the level of expression of the pMito-mCherry-FRB construct, which gave mitochondrial aggregation at high levels of expression, there are several limitations to the inducible relocalisation of LBR-FKBP-GFP in HeLa pMito-mCherry-FRB cells, particularly to determine the effects of the relocalisation. HeLa are cells have high chromosomal instability and are prone to segregation defects and changes in ploidy. Often lagging and bridging chromosomes were observed in the absence of relocalisation in control cells. Ideally, we would study relocalisation effects in stable diploid cell types, where defects in segregation arise at low frequency.

An additional limitation is that the inducible system required LBR to be overexpressed in the HeLa pMito-mCherry-FRB cells. While we had some control in our sample expressing LBR-GFP, the level of expression may vary to that of LBR-FKBP-GFP in relocalised cells and also between individual cells. LBR overexpression is described to affect membrane production (Ma *et al.*, 2007) and NE reassembly timings (Anderson *et al.*, 2009), and will be an important consideration in further investigations.

To address these issues, we next conducted similar synchronisation, relocalisation and release experiments, but in HCT116 LBR-FKBP-GFP CRISPR knock-in cells, described above. These cells allow relocalisation to be induced under endogenous levels of LBR expression in a near diploid cell type.

Similar mitotic defects after LBR-FKBP-GFP relocalisation under endogenous expression levels

We have edited HCT116 cells to stably express LBR-FKBP-GFP, to allow relocalisation under endogenous levels of expression of LBR (Figure 5.3). HCT116 LBR-FKBP-GFP cells were characterised as mixed pool of cells homo- or hetero-zygous for insertion of the tag at the endogenous LBR locus (see Figure 5.3C). We have so far observed the pattern of induced relocalisation of stably expressed LBR-FKBP-GFP in HCT116 LBR-FKBP-GFP cells (Figure 5.4), but have not yet looked at any effects of relocalisation on the recruitment of LBR to chromatin for NE reassembly or on mitotic progression after relocalisation.

To investigate the mitotic progression and recruitment to chromatin in HCT116 LBR-FKBP-GFP after relocalisation of the stably expressed construct, we followed the same approach as previously in HeLa pMito-mCherry-FRB cells (shown in Figure 5.11A). HCT116 LBR-FKBP-GFP cells were transiently transfected with the mitochondrial anchor construct (pMito-mCherry-FRB), synchronised, released and then rapamycin was applied to induce relocalisation and DNA labelled.

No clear coating of LBR-FKBP-GFP was observed on chromatin after relocalisation in early mitosis in HCT116 LBR-FKBP-GFP cells (Figure 5.12), suggesting that the relocalisation completely inhibited (homozyogous cells) or reduced (heterozygous cells) LBR recruitment to the chromatin mass for NE reassembly. Mitotic defects were observed in relocalised cells, often bridging and lagging chromosomes were seen at anaphase and telophase.

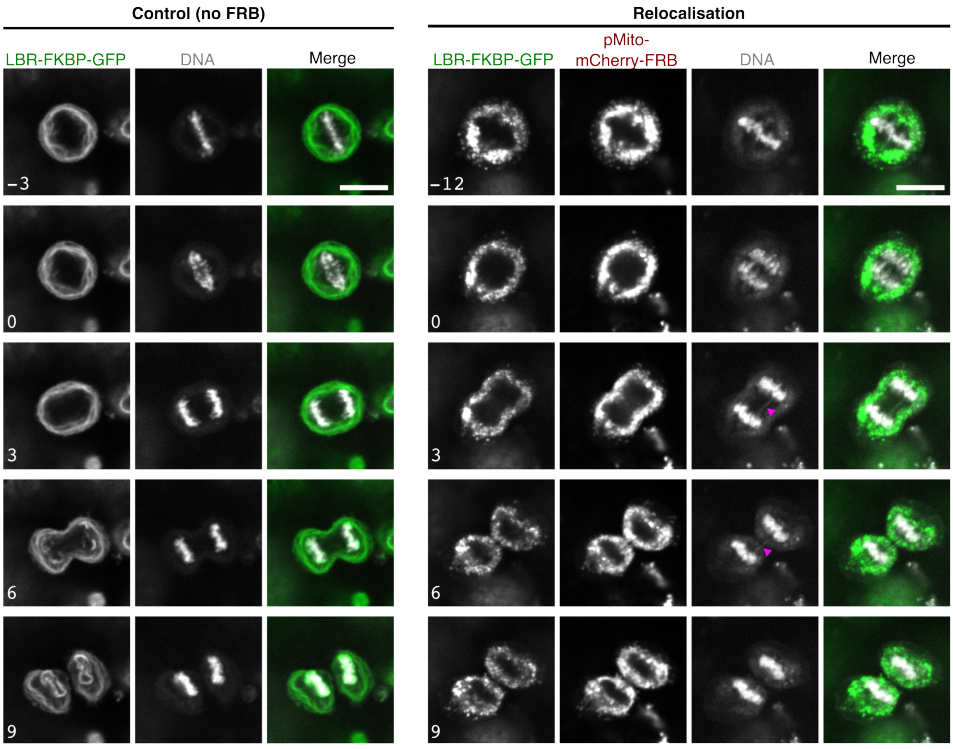

Figure 5.12. Mitotic progression after LBR relocalisation in HCT116 LBR-FKBP-GFP. Single confocal slices of HCT116 LBR-FKBP-GFP cells transiently expressing pMito-mCherry-FRB (or no FRB construct in control). Cells were synchronised, released and incubated with rapamycin to induce relocalisation and SiR-DNA to label the DNA, following method as shown in Figure 5.11**A**. Imaging was started at around 1 h after release and the addition of rapamycin (200 nM) and DNA stain (both treatments were washed off after 30 min incubation). Time is indicated in minutes, with a time 0 representing the first frame in anaphase. Images were captured at 3 min intervals. Magenta arrowheads indicate bridging chromosomes. Scale bars, 5 µm.

Our results capturing mitotic progression after induced relocalisation of LBR-FKBP-GFP to mitochondria during early mitosis in three different cell lines (HCT116, HeLa pMito-mCherry-FRB and HCT116 LBR-FKBP-GFP) suggested that we have disrupted NE reassembly. While cells frequently progressed after relocalisation of LBR-FKBP-GFP to the mitochondria was induced in early mitosis, before the stage of NE reassembly, chromosome segregation defects in the area between the separating chromatin masses later occurred. This implied a function of the relocalised compartment in recoating particularly in the "core" region of chromatin, and that different mechanisms of NE reassembly may occcur at the chromatin peripheral ends and "core" regions. Defect or delay in coating of the central "core" of chromatin was also induced after Sec61β relocalisation.

In future work, we will look at the recruitment dynamics and pattern of other nuclear and NE components to the chromatin "core" region after reduced/inhibited LBR recruitment to chromatin through relocalisation in HCT116 LBR-FKBP-GFP. This will attempt to explain the observed chromatin segregation defect and how this relates to coating of this region.

5.7 Discussion

In this chapter we further investigated the distribution of LBR relative to the ER in mitosis, in order to determine the localisation and dynamics of NE proteins after NEBD. Our relocalisation experiments suggested that LBR was present in separate compartments or concentrated within subdomains of the ER. The protein LAP2β was found to show a partial association with relocalised LBR puncta, which is of particular interest, as each protein originates from the INM in interphase but have different mechanisms and pattern of recruitment to chromatin for NE reassembly (LAP2β is concentrated at the "core" region, whereas LBR initial coats at the "non-core" peripheral ends).

Proteomic work revealed that some ER components are found together with LBR in mitosis, which argued against a localisation in vesicles. Ultrastructural analysis of LBR-FKBP-GFP relocalised to the mitochondria in mitotic cells confirmed that the protein relocalised was not present within vesicle structures, and instead appears as concentrated subdomains within the ER. We have developed a system that will allow us to purify specifically relocalised compartments which we will optimise further to determine the proteomic profile of these mitotic LBR subdomains.

Overall, our results support the domain model of NE protein localisation after NEBD during mitosis.

Finally, our functional data suggest that LBR recoating of chromatin is important for mitotic progression and that inhibition of this process causes problems in NE reassembly and chromosome segregation. This implies that the subdomains may have important function in the NE reassembly process.

Chapter 6

Discussion

The overall aim of the PhD project was to investigate the mechanisms of NE reassembly in mitosis using inducible relocalisation strategies.

6.1 Enrichment of NE proteins within subdomains of the ER after NEBD

Three models have been proposed for the fate of NE proteins after break down of the NE in early mitosis (Collas and Courvalin, 2000). The vesicle model proposes that NE proteins are sequestered into vesicles formed specifically from the NE. The more widely accepted diffusion models state that NE proteins disperse into the ER at NEBD, with two different behaviours of NE proteins proposed, either freely diffusing or concentrated within subdomains enriched in particular NE proteins.

Overall, our results support the domain model of NE protein localisation after NEBD during mitosis. We could immediately disfavour the free diffusion model, due to the distinct behaviour of NE proteins relative to the ER when our inducible relocalisation strategy was used to relocalise the ER in mitosis. In addition, different NE proteins originating from the INM each showed different relocalisation behaviours. Differentiating between vesicle and subdomain models was more difficult because our results, observing the relocalisation pattern and behaviours by confocal microscopy, were compatible with either model. Finally, direct observation of relocalised LBR-containing structures by SBF-SEM allowed us to rule out the vesicle model and provided evidence for the presence of subdomains within the ER enriched in NE proteins during mitosis.

We hypothesise that these subdomains may have a role in NE reassembly,

through concentrating proteins within the ER, primed for coating chromatin. In particular these subdomains may later establish the transient "core" and "non-core" domains during telophase NE reassembly. We observed an interesting relation between proteins that appear to be in distinct subdomains of the ER in early mitosis and those proteins described as "core" and "non-core" localising during NE reassembly in telophase. Relocalisation of different proteins originating from the INM revealed a partial association between LAP2β (described by Haraguchi *et al.* (2008) and Liu *et al.* (2018) as "core") and LBR (described by Haraguchi *et al.* (2000), Dechat *et al.* (2004), Haraguchi *et al.* (2008) and Liu *et al.* (2018) as "non-core") in mitosis. After LAP2β was relocalised, LBR appeared concentrated at particular regions of relocalised LAP2β patches at the mitochondria. When LBR was similarly relocalised within the cell, LAP2β was observed only at a proportion of relocalised LBR puncta. This suggested that the relocalised ER structures may contain distinct, but associated, subdomains enriched in NE proteins later forming "core" and "non-core" regions at NE reassembly. Emerin, another LEM domain protein described as "core" localising (Haraguchi *et al.*, 2000, 2001) and localising to the INM, has been reported to be present within subdomains with a different protein profile to LBR in interphase cells (Cheng *et al.*, 2022). This supports a relation between subdomains in the ER and proteins described as "core" and "non-core" at the telophase NE, as suggested by our results.

The subdomains may be organised by the activity and interactions of the proteins enriched within the subdomains and their differential regulation. Another explanation could be that the structure of the ER could organise the subdomains. The concentrated subdomains of NE proteins could be contained within particular ER structure types or regions of higher curvature. This would mean that when we induce relocalisation of proteins enriched in these subdomains, we are specifically, or preferentially, relocalising particular ER structures. Different ER structure types have also been proposed to contribute to reassembly of the NE at the "core" and "non-core" chromatin regions, for example as a result of differential access of structures to the spindle region. Our data implies there may be some relation in the mechanism of reassembly in the different chromatin regions.

Our functional data suggest that recoating in the "core" chromatin region is affected by relocalisation of compartments containing a "non-core" protein LBR in early mitosis. This suggests a role of proteins initially localising to "non-core" regions in the recruitment or concentration of proteins in the "core" regions. This has been reported for the nucleoporin ELYS, which regulates and recruits LBR to the peripheral ends of chromatin, but depletion of which also affected the

concentration of BAF and other proteins to the "core" region (Clever *et al.*, 2012). Overall, the mitotic ER subdomains could have a role in forming the transient "core" and "non-core" subdomains around chromatin during NE reassembly in telophase.

The mechanism that concentrates proteins within particular subdomains of the ER and how these subdomains are maintained is unclear. There is the potential that these could persist from domains of concentrated INM proteins described at the interphase NE (Makatsori *et al.*, 2004; Chmielewska *et al.*, 2011; Giannios *et al.*, 2017). These are likely formed at sites where proteins in the INM contact the nuclear lamina, chromatin or chromatin bound proteins, concentrating protein and affecting motility within the membrane.

However, we cannot exclude that a freely diffusing pool may exist, in addition to the subdomains. A generic ER population of LBR could be seen after LBR relocalisation within the cell. Although, our results suggest that the majority of protein is concentrated within subdomains of the ER. Further studies of protein dynamics with the cell will be needed to confirm this observation. However, we did not see a noticeable accumulation of protein after the initial relocalisation of LBR. The relocalised puncta seemed variable in size, but did not grow larger over time. We hypothesise that the puncta may represent accumulations of a small number of associated subdomains. These accumulations may occur at particular relocalised sites on the mitochondria (curved ends compared to flat surface), which could affect the ER structures recruited, leading to variable size, and also affect the subsequent remodelling of structures to coat across the mitochondrial surface. The puncta may additionally be limited in size by the available surface area on an individual mitochondrion, although similar puncta were seen after relocalisation to the PM, where there are no such restrictions.

Our aim now is to visualise subdomains of the ER enriched in NE proteins and to better understand the function in the NE reassembly process.

6.2 Induced relocalisation strategy

The induced relocalisation strategy has been utilised within our lab to study the rescue of chromosomes ensheathed in ER membrane in mitotic cells (Ferrandiz *et al.*, 2022) and in the identification and characterisation of intracellular nanovesicles (Larocque *et al.*, 2020). We have now demonstrated that this method can be used to distinguish between protein distributions within membrane compartments in the cell and can be used to probe protein microscale organisation in live cells.

We are in the process of further optimising the method for isolation of relocalised compartments to achieve purified sample that can be applied in future proteomic characterisation of relocalised compartments.

A significant limitation of the induced relocalisation strategy is that overexpression is usually required. Since overexpression has the potential for artefacts, this method must be used carefully. However, in this study, we overcame this limitation by generating a knock-in CRISPR cell line expressing endogenously tagged protein for relocalisation. We predict that the compartment relocalisation method and subsequent proteomic characterisation have great potential for a range of biological questions in the future.

6.3 Defective MNE formed at misaligned chromosomes

Disrupted MN were frequently observed in interphase following treatment to induce polar misaligned chromosomes in mitotic cells. We expect a large proportion of these MN to have formed from polar chromosomes situated outside of the mitotic membrane EZ, and consequently ensheathed in endomembranes, promoting missegregation (Ferrandiz *et al.*, 2022). This suggested that, in addition to promoting missegregation and MN formation, ensheathing of a chromosome in membrane may affect the stability of the MNE formed. There could be several explanations for this, for example the formation mechanism itself, with ensheathing forming multiple layers that does not mimic the ordered and controlled NE assembly process at the main chromosome mass. Also, the timing of the recruitment of nuclear components and membranes could be affected by the position of the misaligned chromosome outside of the spindle region where the regulatory mechanisms preventing premature membrane recruitment to chromatin operate.

The profile of proteins incorporated at the MNE forming at misaligned chromosomes influences stability and function, and may differ at polar compared to lagging chromosomes. In future we will isolate MN to allow proteomic characterisation of the full protein profile of the MNE, to compare MN formed from each misaligned chromosome type. However, we should consider the limitation that polar misaligned chromosomes induced by the CENP-E inhibitor treatment occur very rarely under endogenous conditions in the RPE-1 cell type used, as these are stable diploid cells. In future work we will also conduct similar experiments with spontaneously arising polar chromosomes in cancer cell lines.

At disrupted MN, ER structures were observed within the micronuclear DNA, as previously described (Hatch *et al.*, 2013). Disrupted MN also had increased levels of BAF and LBR recruitment relative to the main nucleus. BAF could be functioning to recruit components for DNA damage response to the exposed DNA at the disrupted MN (Halfmann *et al.*, 2019). MN disruption has been reported to alter chromatin compaction (Hatch *et al.*, 2013) and our observations also imply a role of BAF in mediating this effect. BAF could be acting to compact chromatin exposed to the cytosol at disrupted MN and this compaction may protect the DNA from damage by limiting the activities of, for example the inflammatory response activated by detection of DNA in the cytosol, to the surface of the chromatin.

Formation of the NE is usually limited to surface of chromatin by compaction through the DNA crosslinking action of BAF (Samwer *et al.*, 2017). The order of recruitment of BAF relative to membrane to chromatin could be important to the disrupted fate, and it is possible that at polar misaligned chromosomes outside of the exclusion zone this order is not controlled. Membranes may be recruited to these polar misaligned chromosomes prior to BAF compaction of chromatin, which could as a result trap ER structures inside the MN. The disruption at MN is rarely repaired (Hatch *et al.*, 2013), and the potential compaction of chromatin by BAF may inhibit access of components that allow repair.

In the future, we will follow misaligned chromosomes in live cells from the assembly of the MNE, to the fate of the MN in the following interphase, to visualise the stage at which disruption occurs and that ER membranes access inside chromatin, with increased levels of BAF/LBR recruitment. This will allow us to determine if these observations are a cause or consequence of disruption and also how disrupted fate of MN is affected by misaligned chromosome position (lagging or polar).

Bibliography

Afonso, O., **Matos, I.**, **Pereira, A. J.**, **Aguiar, P.**, **Lampson, M. A.**, and **Maiato, H.** (2014). Feedback control of chromosome separation by a midzone Aurora B gradient. *Science (New York, N.Y.)*, 345(6194):332–336. doi: 10.1126/science.1251121.

Akiyoshi, B., **Nelson, C. R.**, **Ranish, J. A.**, and **Biggins, S.** (2009). Analysis of Ipl1-mediated phosphorylation of the Ndc80 kinetochore protein in Saccharomyces cerevisiae. *Genetics*, 183(4):1591–1595. doi: 10.1534/genetics.109.109041.

Anderson, D. J. and **Hetzer, M. W.** (2008). Reshaping of the endoplasmic reticulum limits the rate for nuclear envelope formation. *The Journal of Cell Biology*, 182(5):911–924. doi: 10.1083/jcb.200805140.

Anderson, D. J., **Vargas, J. D.**, **Hsiao, J. P.**, and **Hetzer, M. W.** (2009). Recruitment of functionally distinct membrane proteins to chromatin mediates nuclear envelope formation in vivo. *The Journal of Cell Biology*, 186(2):183–191. doi: 10.1083/jcb.200901106.

Araújo, M., **Tavares, A.**, **Vieira, D. V.**, **Telley, I. A.**, and **Oliveira, R. A.** (2023). Endoplasmic reticulum membranes are continuously required to maintain mitotic spindle size and forces. *Life Science Alliance*, 6(1):e202201540. doi: 10.26508/lsa.202201540.

Arzt, M., **Deschamps, J.**, **Schmied, C.**, **Pietzsch, T.**, **Schmidt, D.**, **Tomancak, P.**, **Haase, R.**, and **Jug, F.** (2022). LABKIT: Labeling and Segmentation Toolkit for Big Image Data. *Frontiers in Computer Science*, 4.

Asencio, C., **Davidson, I. F.**, **Santarella-Mellwig, R.**, **Ly-Hartig, T. B. N.**, **Mall, M.**, **Wallenfang, M. R.**, **Mattaj, I. W.**, and **Gorjánácz, M.** (2012). Coordination of kinase and phosphatase activities by Lem4 enables nuclear envelope reassembly during mitosis. *Cell*, 150(1):122–135. doi: 10.1016/j.cell.2012.04.043.

Auckland, P. and **McAinsh, A. D.** (2015). Building an integrated model

of chromosome congression. *Journal of Cell Science*, 128(18):3363–3374. doi: 10.1242/jcs.169367.

Auckland, P., **Clarke, N. I.**, **Royle, S. J.**, and **McAinsh, A. D.** (2017). Congressing kinetochores progressively load Ska complexes to prevent force-dependent detachment. *Journal of Cell Biology*, 216(6):1623–1639. doi: 10.1083/jcb.201607096.

Audhya, A., **Desai, A.**, and **Oegema, K.** (2007). A role for Rab5 in structuring the endoplasmic reticulum. *The Journal of Cell Biology*, 178(1):43–56. doi: 10.1083/jcb.200701139.

Bahmanyar, S., **Biggs, R.**, **Schuh, A. L.**, **Desai, A.**, **Müller-Reichert, T.**, **Audhya, A.**, **Dixon, J. E.**, and **Oegema, K.** (2014). Spatial control of phospholipid flux restricts endoplasmic reticulum sheet formation to allow nuclear envelope breakdown. *Genes & Development*, 28(2):121–126. doi: 10.1101/gad.230599.113.

Bajer, A. (1957). Ciné-micrographic studies on mitosis in endosperm. III. The origin of the mitotic spindle. *Experimental Cell Research*, 13(3):493–502. doi: 10.1016/0014-4827(57)90078-2.

Bajer, A. and **Molè-Bajer, J.** (1955). Cine-micrographic studies on mitosis in endosperm. *Chromosoma*, 7(1):558–607. doi: 10.1007/BF00329742.

Beaudouin, J., **Gerlich, D.**, **Daigle, N.**, **Eils, R.**, and **Ellenberg, J.** (2002). Nuclear envelope breakdown proceeds by microtubule-induced tearing of the lamina. *Cell*, 108(1):83–96. doi: 10.1016/s0092-8674(01)00627-4.

Bonne, G., **Di Barletta, M. R.**, **Varnous, S.**, **Bécane, H. M.**, **Hammouda, E. H.**, **Merlini, L.**, **Muntoni, F.**, **Greenberg, C. R.**, **Gary, F.**, **Urtizberea, J. A.**, **Duboc, D.**, **Fardeau, M.**, **Toniolo, D.**, and **Schwartz, K.** (1999). Mutations in the gene encoding lamin A/C cause autosomal dominant Emery-Dreifuss muscular dystrophy. *Nature Genetics*, 21(3):285–288. doi: 10.1038/6799.

Buch, C., **Lindberg, R.**, **Figueroa, R.**, **Gudise, S.**, **Onischenko, E.**, and **Hallberg, E.** (2009). An integral protein of the inner nuclear membrane localizes to the mitotic spindle in mammalian cells. *Journal of Cell Science*, 122(Pt 12):2100–2107. doi: 10.1242/jcs.047373.

Buendia, B. and **Courvalin, J. C.** (1997). Domain-specific disassembly and reassembly of nuclear membranes during mitosis. *Experimental Cell Research*, 230(1):133–144. doi: 10.1006/excr.1996.3395.

Capalbo, L., **D'Avino, P. P.**, **Archambault, V.**, and **Glover, D. M.** (2011). Rab5 GTPase controls chromosome alignment through Lamin disassembly and relocation of the NuMA-like protein Mud to the poles during mitosis. *Proceedings of the National Academy of Sciences*, 108(42):17343–17348. doi: 10.1073/pnas.1103720108. Publisher: Proceedings of the National Academy of Sciences.

Carlton, J. G., **Jones, H.**, and **Eggert, U. S.** (2020). Membrane and organelle dynamics during cell division. *Nature Reviews. Molecular Cell Biology*, 21(3): 151–166. doi: 10.1038/s41580-019-0208-1.

Champion, L., **Pawar, S.**, **Luithle, N.**, **Ungricht, R.**, and **Kutay, U.** (2019). Dissociation of membrane–chromatin contacts is required for proper chromosome segregation in mitosis. *Molecular Biology of the Cell*, 30(4): 427–440. doi: 10.1091/mbc.E18-10-0609.

Cheeseman, I. M., **Chappie, J. S.**, **Wilson-Kubalek, E. M.**, and **Desai, A.** (2006). The conserved KMN network constitutes the core microtubule-binding site of the kinetochore. *Cell*, 127(5):983–997. doi: 10.1016/j.cell.2006.09.039.

Chen, S., **Novick, P.**, and **Ferro-Novick, S.** (2012). ER network formation requires a balance of the dynamin-like GTPase Sey1p and the Lunapark family member Lnp1p. *Nature Cell Biology*, 14(7):707–716. doi: 10.1038/ncb2523.

Cheng, L.-C., **Zhang, X.**, **Abhinav, K.**, **Nguyen, J. A.**, **Baboo, S.**, **Martinez-Bartolomé, S.**, **Branon, T. C.**, **Ting, A. Y.**, **Loose, E.**, **Yates, J. R.**, and **Gerace, L.** (2022). Shared and Distinctive Neighborhoods of Emerin and Lamin B Receptor Revealed by Proximity Labeling and Quantitative Proteomics. *Journal of Proteome Research*, 21(9):2197–2210. doi: 10.1021/acs.jproteome.2c00281.

Chmielewska, M., **Dubińska-Magiera, M.**, **Sopel, M.**, **Rzepecka, D.**, **Hutchison, C. J.**, **Goldberg, M. W.**, and **Rzepecki, R.** (2011). Embryonic and adult isoforms of XLAP2 form microdomains associated with chromatin and the nuclear envelope. *Cell and Tissue Research*, 344(1):97–110. doi: 10.1007/s00441-011-1129-2.

Christodoulou, A., **Santarella-Mellwig, R.**, **Santama, N.**, and **Mattaj, I. W.** (2016). Transmembrane protein TMEM170A is a newly discovered regulator of ER and nuclear envelope morphogenesis in human cells. *Journal of Cell Science*, 129(8):1552–1565. doi: 10.1242/jcs.175273.

Christodoulou, A., **Maimaris, G.**, **Makrigiorgi, A.**, **Charidemou, E.**, **Lüchtenborg, C.**, **Ververis, A.**, **Georgiou, R.**, **Lederer, C. W.**, **Haffner,**

C., **Brügger, B.**, and **Santama, N.** (2020). TMEM147 interacts with lamin B receptor, regulates its localization and levels, and affects cholesterol homeostasis. *Journal of Cell Science*, 133(16):jcs245357. doi: 10.1242/jcs.245357.

Chu, Q., **Wang, J.**, **Du, Y.**, **Zhou, T.**, **Shi, A.**, **Xiong, J.**, **Ji, W.-K.**, and **Deng, L.** (2022). Oligomeric CHMP7 mediates three-way ER junctions and ER-mitochondria interactions. *Cell Death & Differentiation*, pages 1–17. doi: 10.1038/s41418-022-01048-2. Publisher: Nature Publishing Group.

Cimini, D., **Fioravanti, D.**, **Salmon, E. D.**, and **Degrassi, F.** (2002). Merotelic kinetochore orientation versus chromosome mono-orientation in the origin of lagging chromosomes in human primary cells. *Journal of Cell Science*, 115(Pt 3):507–515. doi: 10.1242/jcs.115.3.507.

Cimini, D., **Moree, B.**, **Canman, J. C.**, and **Salmon, E. D.** (2003). Merotelic kinetochore orientation occurs frequently during early mitosis in mammalian tissue cells and error correction is achieved by two different mechanisms. *Journal of Cell Science*, 116(Pt 20):4213–4225. doi: 10.1242/jcs.00716.

Cimini, D., **Wan, X.**, **Hirel, C. B.**, and **Salmon, E. D.** (2006). Aurora kinase promotes turnover of kinetochore microtubules to reduce chromosome segregation errors. *Current biology: CB*, 16(17):1711–1718. doi: 10.1016/j.cub.2006.07.022.

Clarke, P. R. and **Zhang, C.** (2008). Spatial and temporal coordination of mitosis by Ran GTPase. *Nature Reviews. Molecular Cell Biology*, 9(6):464–477. doi: 10.1038/nrm2410.

Clements, L., **Manilal, S.**, **Love, D. R.**, and **Morris, G. E.** (2000). Direct interaction between emerin and lamin A. *Biochemical and Biophysical Research Communications*, 267(3):709–714. doi: 10.1006/bbrc.1999.2023.

Clever, M., **Funakoshi, T.**, **Mimura, Y.**, **Takagi, M.**, and **Imamoto, N.** (2012). The nucleoporin ELYS/Mel28 regulates nuclear envelope subdomain formation in HeLa cells. *Nucleus*, 3(2):187. doi: 10.4161/nucl.19595. Publisher: Taylor & Francis.

Collas, P. and **Courvalin, J. C.** (2000). Sorting nuclear membrane proteins at mitosis. *Trends in Cell Biology*, 10(1):5–8. doi: 10.1016/s0962-8924(99)01697-9.

Crasta, K., **Ganem, N. J.**, **Dagher, R.**, **Lantermann, A. B.**, **Ivanova, E. V.**, **Pan, Y.**, **Nezi, L.**, **Protopopov, A.**, **Chowdhury, D.**, and

Pellman, D. (2012). DNA breaks and chromosome pulverization from errors in mitosis. *Nature*, 482(7383):53–58. doi: 10.1038/nature10802.

Davidson, P. M. and **Lammerding, J.** (2014). Broken nuclei–lamins, nuclear mechanics, and disease. *Trends in Cell Biology*, 24(4):247–256. doi: 10.1016/j.tcb.2013.11.004.

de Leeuw, R., **Gruenbaum, Y.**, and **Medalia, O.** (2018). Nuclear Lamins: Thin Filaments with Major Functions. *Trends in Cell Biology*, 28(1):34–45. doi: 10.1016/j.tcb.2017.08.004.

de Regt, A. K., **Clark, C. J.**, **Asbury, C. L.**, and **Biggins, S.** (2022). Tension can directly suppress Aurora B kinase-triggered release of kinetochore-microtubule attachments. *Nature Communications*, 13(1):2152. doi: 10.1038/s41467-022-29542-8.

Dechat, T., **Gajewski, A.**, **Korbei, B.**, **Gerlich, D.**, **Daigle, N.**, **Haraguchi, T.**, **Furukawa, K.**, **Ellenberg, J.**, and **Foisner, R.** (2004). LAP2alpha and BAF transiently localize to telomeres and specific regions on chromatin during nuclear assembly. *Journal of Cell Science*, 117(Pt 25): 6117–6128. doi: 10.1242/jcs.01529.

DeLuca, J. G., **Gall, W. E.**, **Ciferri, C.**, **Cimini, D.**, **Musacchio, A.**, and **Salmon, E. D.** (2006). Kinetochore microtubule dynamics and attachment stability are regulated by Hec1. *Cell*, 127(5):969–982. doi: 10.1016/j.cell.2006.09.047.

Dohadwala, M., **da Cruz e Silva, E. F.**, **Hall, F. L.**, **Williams, R. T.**, **Carbonaro-Hall, D. A.**, **Nairn, A. C.**, **Greengard, P.**, and **Berndt, N.** (1994). Phosphorylation and inactivation of protein phosphatase 1 by cyclin-dependent kinases. *Proceedings of the National Academy of Sciences of the United States of America*, 91(14):6408–6412.

Drummond, S., **Ferrigno, P.**, **Lyon, C.**, **Murphy, J.**, **Goldberg, M.**, **Allen, T.**, **Smythe, C.**, and **Hutchison, C. J.** (1999). Temporal differences in the appearance of NEP-B78 and an LBR-like protein during Xenopus nuclear envelope reassembly reflect the ordered recruitment of functionally discrete vesicle types. *The Journal of Cell Biology*, 144(2):225–240. doi: 10.1083/jcb.144.2.225.

Dubińska-Magiera, M., **Kozioł, K.**, **Machowska, M.**, **Piekarowicz, K.**, **Filipczak, D.**, and **Rzepecki, R.** (2019). Emerin Is Required for Proper Nucleus Reassembly after Mitosis: Implications for New Pathogenetic

Mechanisms for Laminopathies Detected in EDMD1 Patients. *Cells*, 8(3):240. doi: 10.3390/cells8030240.

Ellenberg, J., **Siggia, E. D.**, **Moreira, J. E.**, **Smith, C. L.**, **Presley, J. F.**, **Worman, H. J.**, and **Lippincott-Schwartz, J.** (1997). Nuclear Membrane Dynamics and Reassembly in Living Cells: Targeting of an Inner Nuclear Membrane Protein in Interphase and Mitosis. *Journal of Cell Biology*, 138 (6):1193–1206. doi: 10.1083/jcb.138.6.1193.

Fernandez, A. G. and **Piano, F.** (2006). MEL-28 is downstream of the Ran cycle and is required for nuclear-envelope function and chromatin maintenance. *Current biology: CB*, 16(17):1757–1763. doi: 10.1016/j.cub.2006.07.071.

Ferrandiz, N., **Downie, L.**, **Starling, G. P.**, and **Royle, S. J.** (2022). Endomembranes promote chromosome missegregation by ensheathing misaligned chromosomes. *The Journal of Cell Biology*, 221(6):e202203021. doi: 10.1083/jcb.202203021.

Fonseca, C. L., **Malaby, H. L.**, **Sepaniac, L. A.**, **Martin, W.**, **Byers, C.**, **Czechanski, A.**, **Messinger, D.**, **Tang, M.**, **Ohi, R.**, **Reinholdt, L. G.**, and **Stumpff, J.** (2019). Mitotic chromosome alignment ensures mitotic fidelity by promoting interchromosomal compaction during anaphase. *The Journal of Cell Biology*, 218(4):1148–1163. doi: 10.1083/jcb.201807228.

Franz, C., **Walczak, R.**, **Yavuz, S.**, **Santarella, R.**, **Gentzel, M.**, **Askjaer, P.**, **Galy, V.**, **Hetzer, M.**, **Mattaj, I. W.**, and **Antonin, W.** (2007). MEL-28/ELYS is required for the recruitment of nucleoporins to chromatin and postmitotic nuclear pore complex assembly. *EMBO reports*, 8(2):165–172. doi: 10.1038/sj.embor.7400889.

Fueller, J., **Herbst, K.**, **Meurer, M.**, **Gubicza, K.**, **Kurtulmus, B.**, **Knopf, J. D.**, **Kirrmaier, D.**, **Buchmuller, B. C.**, **Pereira, G.**, **Lemberg, M. K.**, and **Knop, M.** (2020). CRISPR-Cas12a-assisted PCR tagging of mammalian genes. *The Journal of Cell Biology*, 219(6):e201910210. doi: 10.1083/jcb.201910210.

Fuller, B. G., **Lampson, M. A.**, **Foley, E. A.**, **Rosasco-Nitcher, S.**, **Le, K. V.**, **Tobelmann, P.**, **Brautigan, D. L.**, **Stukenberg, P. T.**, and **Kapoor, T. M.** (2008). Midzone activation of aurora B in anaphase produces an intracellular phosphorylation gradient. *Nature*, 453(7198):1132–1136. doi: 10.1038/nature06923. Number: 7198 Publisher: Nature Publishing Group.

Gao, G., **Zhu, C.**, **Liu, E.**, and **Nabi, I. R.** (2019). Reticulon and CLIMP-63

regulate nanodomain organization of peripheral ER tubules. *PLoS biology*, 17 (8):e3000355. doi: 10.1371/journal.pbio.3000355.

Gatta, A. T. and **Carlton, J. G.** (2019). The ESCRT-machinery: closing holes and expanding roles. *Current Opinion in Cell Biology*, 59:121–132. doi: 10.1016/j.ceb.2019.04.005.

Gatta, A. T., **Olmos, Y.**, **Stoten, C. L.**, **Chen, Q.**, **Rosenthal, P. B.**, and **Carlton, J. G.** (2021). CDK1 controls CHMP7-dependent nuclear envelope reformation. *eLife*, 10:e59999. doi: 10.7554/eLife.59999.

Giannios, I., **Chatzantonaki, E.**, and **Georgatos, S.** (2017). Dynamics and Structure-Function Relationships of the Lamin B Receptor (LBR). *PloS One*, 12(1):e0169626. doi: 10.1371/journal.pone.0169626.

Glotzer, M., **Murray, A. W.**, and **Kirschner, M. W.** (1991). Cyclin is degraded by the ubiquitin pathway. *Nature*, 349(6305):132–138. doi: 10.1038/349132a0.

Golchoubian, B., **Brunner, A.**, **Bragulat-Teixidor, H.**, **Neuner, A.**, **Akarlar, B. A.**, **Ozlu, N.**, and **Schlaitz, A.-L.** (2022). Reticulon-like REEP4 at the inner nuclear membrane promotes nuclear pore complex formation. *The Journal of Cell Biology*, 221(2):e202101049. doi: 10.1083/jcb.202101049.

Gomes, A. M., **Orr, B.**, **Novais-Cruz, M.**, **De Sousa, F.**, **Macário-Monteiro, J.**, **Lemos, C.**, **Ferrás, C.**, and **Maiato, H.** (2022). Micronuclei from misaligned chromosomes that satisfy the spindle assembly checkpoint in cancer cells. *Current biology: CB*, 32(19):4240–4254.e5. doi: 10.1016/j.cub.2022.08.026.

Goyal, U. and **Blackstone, C.** (2013). Untangling the web: mechanisms underlying ER network formation. *Biochimica Et Biophysica Acta*, 1833(11): 2492–2498. doi: 10.1016/j.bbamcr.2013.04.009.

Gu, M., **LaJoie, D.**, **Chen, O. S.**, **von Appen, A.**, **Ladinsky, M. S.**, **Redd, M. J.**, **Nikolova, L.**, **Bjorkman, P. J.**, **Sundquist, W. I.**, **Ullman, K. S.**, and **Frost, A.** (2017). LEM2 recruits CHMP7 for ESCRT-mediated nuclear envelope closure in fission yeast and human cells. *Proceedings of the National Academy of Sciences of the United States of America*, 114(11):E2166–E2175. doi: 10.1073/pnas.1613916114.

Guo, X., **Ni, J.**, **Liang, Z.**, **Xue, J.**, **Fenech, M. F.**, and **Wang, X.** (2019). The molecular origins and pathophysiological consequences of micronuclei:

New insights into an age-old problem. *Mutation Research. Reviews in Mutation Research*, 779:1–35. doi: 10.1016/j.mrrev.2018.11.001.

Halfmann, C. T., **Sears, R. M.**, **Katiyar, A.**, **Busselman, B. W.**, **Aman, L. K.**, **Zhang, Q.**, **O'Bryan, C. S.**, **Angelini, T. E.**, **Lele, T. P.**, and **Roux, K. J.** (2019). Repair of nuclear ruptures requires barrier-to-autointegration factor. *Journal of Cell Biology*, 218(7):2136–2149. doi: 10.1083/jcb.201901116.

Hanahan, D. and **Weinberg, R. A.** (2000). The Hallmarks of Cancer. *Cell*, 100(1):57–70. doi: 10.1016/S0092-8674(00)81683-9. Publisher: Elsevier.

Haraguchi, T., **Koujin, T.**, **Hayakawa, T.**, **Kaneda, T.**, **Tsutsumi, C.**, **Imamoto, N.**, **Akazawa, C.**, **Sukegawa, J.**, **Yoneda, Y.**, and **Hiraoka, Y.** (2000). Live fluorescence imaging reveals early recruitment of emerin, LBR, RanBP2, and Nup153 to reforming functional nuclear envelopes. *Journal of Cell Science*, 113 (Pt 5):779–794. doi: 10.1242/jcs.113.5.779.

Haraguchi, T., **Koujin, T.**, **Segura-Totten, M.**, **Lee, K. K.**, **Matsuoka, Y.**, **Yoneda, Y.**, **Wilson, K. L.**, and **Hiraoka, Y.** (2001). BAF is required for emerin assembly into the reforming nuclear envelope. *Journal of Cell Science*, 114(Pt 24):4575–4585. doi: 10.1242/jcs.114.24.4575.

Haraguchi, T., **Kojidani, T.**, **Koujin, T.**, **Shimi, T.**, **Osakada, H.**, **Mori, C.**, **Yamamoto, A.**, and **Hiraoka, Y.** (2008). Live cell imaging and electron microscopy reveal dynamic processes of BAF-directed nuclear envelope assembly. *Journal of Cell Science*, 121(Pt 15):2540–2554. doi: 10.1242/jcs.033597.

Hatch, E. M., **Fischer, A. H.**, **Deerinck, T. J.**, and **Hetzer, M. W.** (2013). Catastrophic nuclear envelope collapse in cancer cell micronuclei. *Cell*, 154(1): 47–60. doi: 10.1016/j.cell.2013.06.007.

Heller, S. A., **Shih, R.**, **Kalra, R.**, and **Kang, P. B.** (2020). Emery-Dreifuss muscular dystrophy. *Muscle & Nerve*, 61(4):436–448. doi: 10.1002/mus.26782.

Hirano, Y., **Iwase, Y.**, **Ishii, K.**, **Kumeta, M.**, **Horigome, T.**, and **Takeyasu, K.** (2009). Cell cycle-dependent phosphorylation of MAN1. *Biochemistry*, 48(7):1636–1643. doi: 10.1021/bi802060v.

Holy, T. E. and **Leibler, S.** (1994). Dynamic instability of microtubules as an efficient way to search in space. *Proceedings of the National Academy of Sciences of the United States of America*, 91(12):5682–5685.

Hu, C.-K., **Coughlin, M.**, and **Mitchison, T. J.** (2012). Midbody assembly

and its regulation during cytokinesis. *Molecular Biology of the Cell*, 23(6): 1024–1034. doi: 10.1091/mbc.E11-08-0721.

Hu, J., **Shibata, Y.**, **Zhu, P.-P.**, **Voss, C.**, **Rismanchi, N.**, **Prinz, W. A.**, **Rapoport, T. A.**, and **Blackstone, C.** (2009). A class of dynamin-like GTPases involved in the generation of the tubular ER network. *Cell*, 138(3): 549–561. doi: 10.1016/j.cell.2009.05.025.

Irgen-Gioro, S., **Walling, V.**, and **Chong, S.** Fixation Can Change the Appearance of Phase Separation in Living Cells, (2022). URL https://www.biorxiv.org/content/10.1101/2022.05.06.490956v1. Pages: 2022.05.06.490956 Section: New Results.

Ito, H., **Koyama, Y.**, **Takano, M.**, **Ishii, K.**, **Maeno, M.**, **Furukawa, K.**, and **Horigome, T.** (2007). Nuclear envelope precursor vesicle targeting to chromatin is stimulated by protein phosphatase 1 in Xenopus egg extracts. *Experimental Cell Research*, 313(9):1897–1910. doi: 10.1016/j.yexcr.2007.03.015.

Karoutas, A. and **Akhtar, A.** (2021). Functional mechanisms and abnormalities of the nuclear lamina. *Nature Cell Biology*, 23(2):116–126. doi: 10.1038/s41556-020-00630-5.

King, J. and **Nicklas, R.** (2000). Tension on chromosomes increases the number of kinetochore microtubules but only within limits. *Journal of Cell Science*, 113(21):3815–3823. doi: 10.1242/jcs.113.21.3815.

Kiyomitsu, T. and **Cheeseman, I. M.** (2013). Cortical dynein and asymmetric membrane elongation coordinately position the spindle in anaphase. *Cell*, 154 (2):391–402. doi: 10.1016/j.cell.2013.06.010.

Klopfenstein, D. R., **Kappeler, F.**, and **Hauri, H. P.** (1998). A novel direct interaction of endoplasmic reticulum with microtubules. *The EMBO journal*, 17(21):6168–6177. doi: 10.1093/emboj/17.21.6168.

Koshland, D. E., **Mitchison, T. J.**, and **Kirschner, M. W.** (1988). Polewards chromosome movement driven by microtubule depolymerization in vitro. *Nature*, 331(6156):499–504. doi: 10.1038/331499a0. Number: 6156 Publisher: Nature Publishing Group.

Kumar, D., **Golchoubian, B.**, **Belevich, I.**, **Jokitalo, E.**, and **Schlaitz, A.-L.** (2019). REEP3 and REEP4 determine the tubular morphology of the endoplasmic reticulum during mitosis. *Molecular Biology of the Cell*, 30(12): 1377–1389. doi: 10.1091/mbc.E18-11-0698.

Kuniyasu, K., **Iemura, K.**, and **Tanaka, K.** (2018). Delayed Chromosome Alignment to the Spindle Equator Increases the Rate of Chromosome Missegregation in Cancer Cell Lines. *Biomolecules*, 9(1):10. doi: 10.3390/biom9010010.

Larocque, G., **La-Borde, P. J.**, **Clarke, N. I.**, **Carter, N. J.**, and **Royle, S. J.** (2020). Tumor protein D54 defines a new class of intracellular transport vesicles. *The Journal of Cell Biology*, 219(1):e201812044. doi: 10.1083/jcb.201812044.

Lityagina, O. and **Dobreva, G.** (2021). The LINC Between Mechanical Forces and Chromatin. *Frontiers in Physiology*, 12:710809. doi: 10.3389/fphys.2021.710809.

Liu, S. and **Pellman, D.** (2020). The coordination of nuclear envelope assembly and chromosome segregation in metazoans. *Nucleus*, 11(1):35–52. doi: 10.1080/19491034.2020.1742064.

Liu, S., **Kwon, M.**, **Mannino, M.**, **Yang, N.**, **Renda, F.**, **Khodjakov, A.**, and **Pellman, D.** (2018). Nuclear envelope assembly defects link mitotic errors to chromothripsis. *Nature*, 561(7724):551–555. doi: 10.1038/s41586-018-0534-z.

Lu, L., **Ladinsky, M. S.**, and **Kirchhausen, T.** (2009). Cisternal organization of the endoplasmic reticulum during mitosis. *Molecular Biology of the Cell*, 20 (15):3471–3480. doi: 10.1091/mbc.e09-04-0327.

Lu, L., **Ladinsky, M. S.**, and **Kirchhausen, T.** (2011). Formation of the postmitotic nuclear envelope from extended ER cisternae precedes nuclear pore assembly. *The Journal of Cell Biology*, 194(3):425–440. doi: 10.1083/jcb.201012063.

Lu, Q., **Lu, Z.**, **Liu, Q.**, **Guo, L.**, **Ren, H.**, **Fu, J.**, **Jiang, Q.**, **Clarke, P. R.**, and **Zhang, C.** (2012). Chromatin-bound NLS proteins recruit membrane vesicles and nucleoporins for nuclear envelope assembly via importin-α/β. *Cell Research*, 22(11):1562–1575. doi: 10.1038/cr.2012.113.

Lu, X., **Shi, Y.**, **Lu, Q.**, **Ma, Y.**, **Luo, J.**, **Wang, Q.**, **Ji, J.**, **Jiang, Q.**, and **Zhang, C.** (2010). Requirement for Lamin B Receptor and Its Regulation by Importin β and Phosphorylation in Nuclear Envelope Assembly during Mitotic Exit. *The Journal of Biological Chemistry*, 285(43):33281–33293. doi: 10.1074/jbc.M110.102368.

Ma, Y., **Cai, S.**, **Lv, Q.**, **Jiang, Q.**, **Zhang, Q.**, **Sodmergen, n.**, **Zhai,**

Z., and **Zhang, C.** (2007). Lamin B receptor plays a role in stimulating nuclear envelope production and targeting membrane vesicles to chromatin during nuclear envelope assembly through direct interaction with importin beta. *Journal of Cell Science*, 120(Pt 3):520–530. doi: 10.1242/jcs.03355.

Maass, K. K., **Rosing, F.**, **Ronchi, P.**, **Willmund, K. V.**, **Devens, F.**, **Hergt, M.**, **Herrmann, H.**, **Lichter, P.**, and **Ernst, A.** (2018). Altered nuclear envelope structure and proteasome function of micronuclei. *Experimental Cell Research*, 371(2):353–363. doi: 10.1016/j.yexcr.2018.08.029.

Machado, S., **Mercier, V.**, and **Chiaruttini, N.** (2019). LimeSeg: a coarse-grained lipid membrane simulation for 3D image segmentation. *BMC Bioinformatics*, 20(1):2. doi: 10.1186/s12859-018-2471-0.

Maison, C., **Horstmann, H.**, and **Georgatos, S. D.** (1993). Regulated docking of nuclear membrane vesicles to vimentin filaments during mitosis. *The Journal of Cell Biology*, 123(6 Pt 1):1491–1505. doi: 10.1083/jcb.123.6.1491.

Maison, C., **Pyrpasopoulou, A.**, and **Georgatos, S. D.** (1995). Vimentin-associated mitotic vesicles interact with chromosomes in a lamin B- and phosphorylation-dependent manner. *The EMBO Journal*, 14(14): 3311–3324.

Maison, C., **Pyrpasopoulou, A.**, **Theodoropoulos, P. A.**, and **Georgatos, S. D.** (1997). The inner nuclear membrane protein LAP1 forms a native complex with B-type lamins and partitions with spindle-associated mitotic vesicles. *The EMBO journal*, 16(16):4839–4850. doi: 10.1093/emboj/16.16.4839.

Makatsori, D., **Kourmouli, N.**, **Polioudaki, H.**, **Shultz, L. D.**, **McLean, K.**, **Theodoropoulos, P. A.**, **Singh, P. B.**, and **Georgatos, S. D.** (2004). The inner nuclear membrane protein lamin B receptor forms distinct microdomains and links epigenetically marked chromatin to the nuclear envelope. *The Journal of Biological Chemistry*, 279(24):25567–25573. doi: 10.1074/jbc.M313606200.

Malhas, A., **Goulbourne, C.**, and **Vaux, D. J.** (2011). The nucleoplasmic reticulum: form and function. *Trends in Cell Biology*, 21(6):362–373. doi: 10.1016/j.tcb.2011.03.008.

Mall, M., **Walter, T.**, **Gorjánácz, M.**, **Davidson, I. F.**, **Nga Ly-Hartig, T. B.**, **Ellenberg, J.**, and **Mattaj, I. W.** (2012). Mitotic lamin disassembly is triggered by lipid-mediated signaling. *The Journal of Cell Biology*, 198(6): 981–990. doi: 10.1083/jcb.201205103.

Mammel, A. E., **Huang, H. Z.**, **Gunn, A. L.**, **Choo, E.**, and **Hatch, E. M.** (2022). Chromosome length and gene density contribute to micronuclear membrane stability. *Life Science Alliance*, 5(2):e202101210. doi: 10.26508/lsa.202101210.

Mansharamani, M. and **Wilson, K. L.** (2005). Direct binding of nuclear membrane protein MAN1 to emerin in vitro and two modes of binding to barrier-to-autointegration factor. *The Journal of Biological Chemistry*, 280 (14):13863–13870. doi: 10.1074/jbc.M413020200.

McCleland, M. L., **Kallio, M. J.**, **Barrett-Wilt, G. A.**, **Kestner, C. A.**, **Shabanowitz, J.**, **Hunt, D. F.**, **Gorbsky, G. J.**, and **Stukenberg, P. T.** (2004). The vertebrate Ndc80 complex contains Spc24 and Spc25 homologs, which are required to establish and maintain kinetochore-microtubule attachment. *Current biology: CB*, 14(2):131–137. doi: 10.1016/j.cub.2003.12.058.

McCullough, S. and **Lucocq, J.** (2005). Endoplasmic reticulum positioning and partitioning in mitotic HeLa cells. *Journal of Anatomy*, 206(5):415–425. doi: 10.1111/j.1469-7580.2005.00407.x.

McIntosh, J. R. (2021). Anaphase A. *Seminars in Cell & Developmental Biology*, 117:118–126. doi: 10.1016/j.semcdb.2021.03.009.

Merta, H., **Carrasquillo Rodríguez, J. W.**, **Anjur-Dietrich, M. I.**, **Vitale, T.**, **Granade, M. E.**, **Harris, T. E.**, **Needleman, D. J.**, and **Bahmanyar, S.** (2021). Cell cycle regulation of ER membrane biogenesis protects against chromosome missegregation. *Developmental Cell*, 56(24):3364–3379.e10. doi: 10.1016/j.devcel.2021.11.009.

Mierzwa, B. and **Gerlich, D. W.** (2014). Cytokinetic abscission: molecular mechanisms and temporal control. *Developmental Cell*, 31(5):525–538. doi: 10.1016/j.devcel.2014.11.006.

Mimura, Y., **Takagi, M.**, **Clever, M.**, and **Imamoto, N.** (2016). ELYS regulates the localization of LBR by modulating its phosphorylation state. *Journal of Cell Science*, 129(22):4200–4212. doi: 10.1242/jcs.190678.

Mudumbi, K. C., **Czapiewski, R.**, **Ruba, A.**, **Junod, S. L.**, **Li, Y.**, **Luo, W.**, **Ngo, C.**, **Ospina, V.**, **Schirmer, E. C.**, and **Yang, W.** (2020). Nucleoplasmic signals promote directed transmembrane protein import simultaneously via multiple channels of nuclear pores. *Nature Communications*, 11(1):2184. doi: 10.1038/s41467-020-16033-x. Number: 1 Publisher: Nature Publishing Group.

Musacchio, A. (2015). The Molecular Biology of Spindle Assembly Checkpoint Signaling Dynamics. *Current biology: CB*, 25(20):R1002–1018. doi: 10.1016/j.cub.2015.08.051.

Nabetani, A., **Koujin, T.**, **Tsutsumi, C.**, **Haraguchi, T.**, and **Hiraoka, Y.** (2001). A conserved protein, Nuf2, is implicated in connecting the centromere to the spindle during chromosome segregation: a link between the kinetochore function and the spindle checkpoint. *Chromosoma*, 110(5):322–334. doi: 10.1007/s004120100153.

Nagano, A., **Koga, R.**, **Ogawa, M.**, **Kurano, Y.**, **Kawada, J.**, **Okada, R.**, **Hayashi, Y. K.**, **Tsukahara, T.**, and **Arahata, K.** (1996). Emerin deficiency at the nuclear membrane in patients with Emery-Dreifuss muscular dystrophy. *Nature Genetics*, 12(3):254–259. doi: 10.1038/ng0396-254.

Nichols, R. J., **Wiebe, M. S.**, and **Traktman, P.** (2006). The vaccinia-related kinases phosphorylate the N' terminus of BAF, regulating its interaction with DNA and its retention in the nucleus. *Molecular Biology of the Cell*, 17(5):2451–2464. doi: 10.1091/mbc.e05-12-1179.

Nicklas, R. B. and **Ward, S. C.** (1994). Elements of error correction in mitosis: microtubule capture, release, and tension. *The Journal of Cell Biology*, 126(5):1241–1253. doi: 10.1083/jcb.126.5.1241.

Nixon, F. M., **Honnor, T. R.**, **Clarke, N. I.**, **Starling, G. P.**, **Beckett, A. J.**, **Johansen, A. M.**, **Brettschneider, J. A.**, **Prior, I. A.**, and **Royle, S. J.** (2017). Microtubule organization within mitotic spindles revealed by serial block face scanning electron microscopy and image analysis. *Journal of Cell Science*, 130(10):1845–1855. doi: 10.1242/jcs.203877.

Nixon-Abell, J., **Obara, C. J.**, **Weigel, A. V.**, **Li, D.**, **Legant, W. R.**, **Xu, C. S.**, **Pasolli, H. A.**, **Harvey, K.**, **Hess, H. F.**, **Betzig, E.**, **Blackstone, C.**, and **Lippincott-Schwartz, J.** (2016). Increased spatiotemporal resolution reveals highly dynamic dense tubular matrices in the peripheral ER. *Science*, 354(6311):aaf3928. doi: 10.1126/science.aaf3928. Publisher: American Association for the Advancement of Science.

Okamoto, A., **Utani, K.-i.**, and **Shimizu, N.** (2012). DNA replication occurs in all lamina positive micronuclei, but never in lamina negative micronuclei. *Mutagenesis*, 27(3):323–327. doi: 10.1093/mutage/ger082.

Olmos, Y., **Perdrix-Rosell, A.**, and **Carlton, J. G.** (2016). Membrane Binding by CHMP7 Coordinates ESCRT-III-Dependent Nuclear Envelope

Reformation. *Current biology: CB*, 26(19):2635–2641. doi: 10.1016/j.cub.2016.07.039.

Orr, B., **De Sousa, F.**, **Gomes, A. M.**, **Afonso, O.**, **Ferreira, L. T.**, **Figueiredo, A. C.**, and **Maiato, H.** (2021). An anaphase surveillance mechanism prevents micronuclei formation from frequent chromosome segregation errors. *Cell Reports*, 37(6):109783. doi: 10.1016/j.celrep.2021.109783.

Orso, G., **Pendin, D.**, **Liu, S.**, **Tosetto, J.**, **Moss, T. J.**, **Faust, J. E.**, **Micaroni, M.**, **Egorova, A.**, **Martinuzzi, A.**, **McNew, J. A.**, and **Daga, A.** (2009). Homotypic fusion of ER membranes requires the dynamin-like GTPase atlastin. *Nature*, 460(7258):978–983. doi: 10.1038/nature08280.

Patel, J. T., **Bottrill, A.**, **Prosser, S. L.**, **Jayaraman, S.**, **Straatman, K.**, **Fry, A. M.**, and **Shackleton, S.** (2014). Mitotic phosphorylation of SUN1 loosens its connection with the nuclear lamina while the LINC complex remains intact. *Nucleus (Austin, Tex.)*, 5(5):462–473. doi: 10.4161/nucl.36232.

Pawar, S., **Ungricht, R.**, **Tiefenboeck, P.**, **Leroux, J.-C.**, and **Kutay, U.** (2017). Efficient protein targeting to the inner nuclear membrane requires Atlastin-dependent maintenance of ER topology. *eLife*, 6:e28202. doi: 10.7554/eLife.28202.

Polioudaki, H., **Kourmouli, N.**, **Drosou, V.**, **Bakou, A.**, **Theodoropoulos, P. A.**, **Singh, P. B.**, **Giannakouros, T.**, and **Georgatos, S. D.** (2001). Histones H3/H4 form a tight complex with the inner nuclear membrane protein LBR and heterochromatin protein 1. *EMBO reports*, 2(10):920–925. doi: 10.1093/embo-reports/kve199.

Prinz, W. A., **Toulmay, A.**, and **Balla, T.** (2020). The functional universe of membrane contact sites. *Nature Reviews Molecular Cell Biology*, 21(1):7–24. doi: 10.1038/s41580-019-0180-9. Number: 1 Publisher: Nature Publishing Group.

Puhka, M., **Vihinen, H.**, **Joensuu, M.**, and **Jokitalo, E.** (2007). Endoplasmic reticulum remains continuous and undergoes sheet-to-tubule transformation during cell division in mammalian cells. *The Journal of Cell Biology*, 179(5):895–909. doi: 10.1083/jcb.200705112.

Puhka, M., **Joensuu, M.**, **Vihinen, H.**, **Belevich, I.**, and **Jokitalo, E.** (2012). Progressive sheet-to-tubule transformation is a general mechanism for endoplasmic reticulum partitioning in dividing mammalian cells. *Molecular Biology of the Cell*, 23(13):2424–2432. doi: 10.1091/mbc.E10-12-0950.

Romanauska, A. and **Köhler, A.** (2018). The Inner Nuclear Membrane Is a Metabolically Active Territory that Generates Nuclear Lipid Droplets. *Cell*, 174(3):700–715.e18. doi: 10.1016/j.cell.2018.05.047.

Salina, D., **Bodoor, K.**, **Eckley, D. M.**, **Schroer, T. A.**, **Rattner, J. B.**, and **Burke, B.** (2002). Cytoplasmic Dynein as a Facilitator of Nuclear Envelope Breakdown. *Cell*, 108(1):97–107. doi: 10.1016/S0092-8674(01)00628-6. Publisher: Elsevier.

Samwer, M., **Schneider, M. W. G.**, **Hoefler, R.**, **Schmalhorst, P. S.**, **Jude, J. G.**, **Zuber, J.**, and **Gerlich, D. W.** (2017). DNA Cross-Bridging Shapes a Single Nucleus from a Set of Mitotic Chromosomes. *Cell*, 170(5):956–972.e23. doi: 10.1016/j.cell.2017.07.038.

Santos, M., **Costa, P.**, **Martins, F.**, **da Cruz e Silva, E. F.**, **da Cruz e Silva, O. A. B.**, and **Rebelo, S.** (2015). LAP1 is a crucial protein for the maintenance of the nuclear envelope structure and cell cycle progression. *Molecular and Cellular Biochemistry*, 399(1-2):143–153. doi: 10.1007/s11010-014-2241-x.

Schlaitz, A.-L., **Thompson, J.**, **Wong, C. C. L.**, **Yates, J. R.**, and **Heald, R.** (2013). REEP3/4 ensure endoplasmic reticulum clearance from metaphase chromatin and proper nuclear envelope architecture. *Developmental Cell*, 26(3):315–323. doi: 10.1016/j.devcel.2013.06.016.

Schneider, M. W. G., **Gibson, B. A.**, **Otsuka, S.**, **Spicer, M. F. D.**, **Petrovic, M.**, **Blaukopf, C.**, **Langer, C. C. H.**, **Batty, P.**, **Nagaraju, T.**, **Doolittle, L. K.**, **Rosen, M. K.**, and **Gerlich, D. W.** (2022). A mitotic chromatin phase transition prevents perforation by microtubules. *Nature*, 609(7925):183–190. doi: 10.1038/s41586-022-05027-y.

Schroeder, L. K., **Barentine, A. E. S.**, **Merta, H.**, **Schweighofer, S.**, **Zhang, Y.**, **Baddeley, D.**, **Bewersdorf, J.**, and **Bahmanyar, S.** (2019). Dynamic nanoscale morphology of the ER surveyed by STED microscopy. *The Journal of Cell Biology*, 218(1):83–96. doi: 10.1083/jcb.201809107.

Schweizer, N., **Pawar, N.**, **Weiss, M.**, and **Maiato, H.** (2015). An organelle-exclusion envelope assists mitosis and underlies distinct molecular crowding in the spindle region. *The Journal of Cell Biology*, 210(5):695–704. doi: 10.1083/jcb.201506107.

Serio, G., **Margaria, V.**, **Jensen, S.**, **Oldani, A.**, **Bartek, J.**, **Bussolino, F.**, and **Lanzetti, L.** (2011). Small GTPase Rab5 participates in chromosome congression and regulates localization of the centromere-associated protein

CENP-F to kinetochores. *Proceedings of the National Academy of Sciences*, 108(42):17337–17342. doi: 10.1073/pnas.1103516108. Publisher: Proceedings of the National Academy of Sciences.

Shibata, Y., **Shemesh, T.**, **Prinz, W. A.**, **Palazzo, A. F.**, **Kozlov, M. M.**, and **Rapoport, T. A.** (2010). Mechanisms determining the morphology of the peripheral ER. *Cell*, 143(5):774–788. doi: 10.1016/j.cell.2010.11.007.

Shimizu, N., **Itoh, N.**, **Utiyama, H.**, and **Wahl, G. M.** (1998). Selective entrapment of extrachromosomally amplified DNA by nuclear budding and micronucleation during S phase. *The Journal of Cell Biology*, 140(6):1307–1320. doi: 10.1083/jcb.140.6.1307.

Smoyer, C. J., **Katta, S. S.**, **Gardner, J. M.**, **Stoltz, L.**, **McCroskey, S.**, **Bradford, W. D.**, **McClain, M.**, **Smith, S. E.**, **Slaughter, B. D.**, **Unruh, J. R.**, and **Jaspersen, S. L.** (2016). Analysis of membrane proteins localizing to the inner nuclear envelope in living cells. *The Journal of Cell Biology*, 215 (4):575–590. doi: 10.1083/jcb.201607043.

Smyth, J. T., **Beg, A. M.**, **Wu, S.**, **Putney, J. W.**, and **Rusan, N. M.** (2012). Phosphoregulation of STIM1 leads to exclusion of the endoplasmic reticulum from the mitotic spindle. *Current biology: CB*, 22(16):1487–1493. doi: 10.1016/j.cub.2012.05.057.

Soto, M., **García-Santisteban, I.**, **Krenning, L.**, **Medema, R. H.**, and **Raaijmakers, J. A.** (2018). Chromosomes trapped in micronuclei are liable to segregation errors. *Journal of Cell Science*, 131(13):jcs214742. doi: 10.1242/jcs.214742.

Strambio-De-Castillia, C., **Niepel, M.**, and **Rout, M. P.** (2010). The nuclear pore complex: bridging nuclear transport and gene regulation. *Nature Reviews Molecular Cell Biology*, 11(7):490–501. doi: 10.1038/nrm2928. Number: 7 Publisher: Nature Publishing Group.

Tijhuis, A. E., **Johnson, S. C.**, and **McClelland, S. E.** (2019). The emerging links between chromosomal instability (CIN), metastasis, inflammation and tumour immunity. *Molecular Cytogenetics*, 12:17. doi: 10.1186/s13039-019-0429-1.

Uhlmann, F., **Lottspeich, F.**, and **Nasmyth, K.** (1999). Sister-chromatid separation at anaphase onset is promoted by cleavage of the cohesin subunit Scc1. *Nature*, 400(6739):37–42. doi: 10.1038/21831.

Ulbert, S., **Platani, M.**, **Boue, S.**, and **Mattaj, I. W.** (2006).

Direct membrane protein-DNA interactions required early in nuclear envelope assembly. *The Journal of Cell Biology*, 173(4):469–476. doi: 10.1083/jcb.200512078.

Ungricht, R. and **Kutay, U.** (2015). Establishment of NE asymmetry—targeting of membrane proteins to the inner nuclear membrane. *Current Opinion in Cell Biology*, 34:135–141. doi: 10.1016/j.ceb.2015.04.005.

Vagnarelli, P. (2021). Back to the new beginning: Mitotic exit in space and time. *Seminars in Cell & Developmental Biology*, 117:140–148. doi: 10.1016/j.semcdb.2021.03.010.

Vagnarelli, P., **Hudson, D. F.**, **Ribeiro, S. A.**, **Trinkle-Mulcahy, L.**, **Spence, J. M.**, **Lai, F.**, **Farr, C. J.**, **Lamond, A. I.**, and **Earnshaw, W. C.** (2006). Condensin and Repo-Man-PP1 co-operate in the regulation of chromosome architecture during mitosis. *Nature Cell Biology*, 8(10):1133–1142. doi: 10.1038/ncb1475.

Vagnarelli, P., **Ribeiro, S.**, **Sennels, L.**, **Sanchez-Pulido, L.**, **de Lima Alves, F.**, **Verheyen, T.**, **Kelly, D. A.**, **Ponting, C. P.**, **Rappsilber, J.**, and **Earnshaw, W. C.** (2011). Repo-Man coordinates chromosomal reorganization with nuclear envelope reassembly during mitotic exit. *Developmental Cell*, 21(2):328–342. doi: 10.1016/j.devcel.2011.06.020.

Vedrenne, C., **Klopfenstein, D. R.**, and **Hauri, H.-P.** (2005). Phosphorylation controls CLIMP-63-mediated anchoring of the endoplasmic reticulum to microtubules. *Molecular Biology of the Cell*, 16(4):1928–1937. doi: 10.1091/mbc.e04-07-0554.

Vietri, M., **Schink, K. O.**, **Campsteijn, C.**, **Wegner, C. S.**, **Schultz, S. W.**, **Christ, L.**, **Thoresen, S. B.**, **Brech, A.**, **Raiborg, C.**, and **Stenmark, H.** (2015). Spastin and ESCRT-III coordinate mitotic spindle disassembly and nuclear envelope sealing. *Nature*, 522(7555):231–235. doi: 10.1038/nature14408.

Vigneron, S., **Brioudes, E.**, **Burgess, A.**, **Labbé, J.-C.**, **Lorca, T.**, and **Castro, A.** (2009). Greatwall maintains mitosis through regulation of PP2A. *The EMBO journal*, 28(18):2786–2793. doi: 10.1038/emboj.2009.228.

Voeltz, G. K., **Prinz, W. A.**, **Shibata, Y.**, **Rist, J. M.**, and **Rapoport, T. A.** (2006). A class of membrane proteins shaping the tubular endoplasmic reticulum. *Cell*, 124(3):573–586. doi: 10.1016/j.cell.2005.11.047.

von Appen, A., **LaJoie, D.**, **Johnson, I. E.**, **Trnka, M. J.**, **Pick, S. M.**,

Burlingame, A. L., **Ullman, K. S.**, and **Frost, A.** (2020). LEM2 phase separation promotes ESCRT-mediated nuclear envelope reformation. *Nature*, 582(7810):115–118. doi: 10.1038/s41586-020-2232-x. Number: 7810 Publisher: Nature Publishing Group.

Vukušić, K. and **Tolić, I. M.** (2021). Anaphase B: Long-standing models meet new concepts. *Seminars in Cell & Developmental Biology*, 117:127–139. doi: 10.1016/j.semcdb.2021.03.023.

Vukušić, K. and **Tolić, I. M.** (2022). Polar Chromosomes-Challenges of a Risky Path. *Cells*, 11(9):1531. doi: 10.3390/cells11091531.

Wang, S., **Tukachinsky, H.**, **Romano, F. B.**, and **Rapoport, T. A.** (2016). Cooperation of the ER-shaping proteins atlastin, lunapark, and reticulons to generate a tubular membrane network. *eLife*, 5:e18605. doi: 10.7554/eLife.18605.

Warecki, B. and **Sullivan, W.** (2018). Micronuclei Formation Is Prevented by Aurora B-Mediated Exclusion of HP1a from Late-Segregating Chromatin in Drosophila. *Genetics*, 210(1):171–187. doi: 10.1534/genetics.118.301031.

Waterman-Storer, C. M., **Gregory, J.**, **Parsons, S. F.**, and **Salmon, E. D.** (1995). Membrane/microtubule tip attachment complexes (TACs) allow the assembly dynamics of plus ends to push and pull membranes into tubulovesicular networks in interphase Xenopus egg extracts. *The Journal of Cell Biology*, 130(5):1161–1169. doi: 10.1083/jcb.130.5.1161.

Westrate, L. M., **Lee, J. E.**, **Prinz, W. A.**, and **Voeltz, G. K.** (2015). Form follows function: the importance of endoplasmic reticulum shape. *Annual Review of Biochemistry*, 84:791–811. doi: 10.1146/annurev-biochem-072711-163501.

Wiese, C., **Goldberg, M. W.**, **Allen, T. D.**, and **Wilson, K. L.** (1997). Nuclear envelope assembly in Xenopus extracts visualized by scanning EM reveals a transport-dependent 'envelope smoothing' event. *Journal of Cell Science*, 110 (Pt 13):1489–1502. doi: 10.1242/jcs.110.13.1489.

Wilson, K. L. and **Newport, J.** (1988). A trypsin-sensitive receptor on membrane vesicles is required for nuclear envelope formation in vitro. *The Journal of Cell Biology*, 107(1):57–68. doi: 10.1083/jcb.107.1.57.

Wood, K. W., **Lad, L.**, **Luo, L.**, **Qian, X.**, **Knight, S. D.**, **Nevins, N.**, **Brejc, K.**, **Sutton, D.**, **Gilmartin, A. G.**, **Chua, P. R.**, **Desai, R.**, **Schauer, S. P.**, **McNulty, D. E.**, **Annan, R. S.**, **Belmont, L. D.**,

Garcia, C., **Lee, Y.**, **Diamond, M. A.**, **Faucette, L. F.**, **Giardiniere, M.**, **Zhang, S.**, **Sun, C.-M.**, **Vidal, J. D.**, **Lichtsteiner, S.**, **Cornwell, W. D.**, **Greshock, J. D.**, **Wooster, R. F.**, **Finer, J. T.**, **Copeland, R. A.**, **Huang, P. S.**, **Morgans, D. J.**, **Dhanak, D.**, **Bergnes, G.**, **Sakowicz, R.**, and **Jackson, J. R.** (2010). Antitumor activity of an allosteric inhibitor of centromere-associated protein-E. *Proceedings of the National Academy of Sciences*, 107(13):5839–5844. doi: 10.1073/pnas.0915068107. Publisher: Proceedings of the National Academy of Sciences.

Wood, L. A., **Larocque, G.**, **Clarke, N. I.**, **Sarkar, S.**, and **Royle, S. J.** (2017). New tools for "hot-wiring" clathrin-mediated endocytosis with temporal and spatial precision. *The Journal of Cell Biology*, 216(12):4351–4365. doi: 10.1083/jcb.201702188.

Worman, H. J., **Yuan, J.**, **Blobel, G.**, and **Georgatos, S. D.** (1988). A lamin B receptor in the nuclear envelope. *Proceedings of the National Academy of Sciences of the United States of America*, 85(22):8531–8534. doi: 10.1073/pnas.85.22.8531.

Woźniak, M. J., **Bola, B.**, **Brownhill, K.**, **Yang, Y.-C.**, **Levakova, V.**, and **Allan, V. J.** (2009). Role of kinesin-1 and cytoplasmic dynein in endoplasmic reticulum movement in VERO cells. *Journal of Cell Science*, 122(Pt 12): 1979–1989. doi: 10.1242/jcs.041962.

Wurzenberger, C. and **Gerlich, D. W.** (2011). Phosphatases: providing safe passage through mitotic exit. *Nature Reviews Molecular Cell Biology*, 12(8): 469–482. doi: 10.1038/nrm3149. Number: 8 Publisher: Nature Publishing Group.

Ye, Q. and **Worman, H. J.** (1996). Interaction between an integral protein of the nuclear envelope inner membrane and human chromodomain proteins homologous to Drosophila HP1. *The Journal of Biological Chemistry*, 271(25): 14653–14656. doi: 10.1074/jbc.271.25.14653.

Zhang, C. and **Clarke, P. R.** (2001). Roles of Ran-GTP and Ran-GDP in precursor vesicle recruitment and fusion during nuclear envelope assembly in a human cell-free system. *Current biology: CB*, 11(3):208–212. doi: 10.1016/s0960-9822(01)00053-7.

Zhang, C.-Z., **Spektor, A.**, **Cornils, H.**, **Francis, J. M.**, **Jackson, E. K.**, **Liu, S.**, **Meyerson, M.**, and **Pellman, D.** (2015). Chromothripsis from DNA damage in micronuclei. *Nature*, 522(7555):179–184. doi: 10.1038/nature14493.

Zhang, S., **Chang, L.**, **Alfieri, C.**, **Zhang, Z.**, **Yang, J.**, **Maslen, S.**,

Skehel, M., and **Barford, D.** (2016). Molecular mechanism of APC/C activation by mitotic phosphorylation. *Nature*, 533(7602):260–264. doi: 10.1038/nature17973.

Zheng, R., **Ghirlando, R.**, **Lee, M. S.**, **Mizuuchi, K.**, **Krause, M.**, and **Craigie, R.** (2000). Barrier-to-autointegration factor (BAF) bridges DNA in a discrete, higher-order nucleoprotein complex. *Proceedings of the National Academy of Sciences of the United States of America*, 97(16):8997–9002. doi: 10.1073/pnas.150240197.

Zhou, L., **Jilderda, L. J.**, and **Foijer, F.** (2020). Exploiting aneuploidy-imposed stresses and coping mechanisms to battle cancer. *Open Biology*, 10(9):200148. doi: 10.1098/rsob.200148.

Zhuang, X., **Semenova, E.**, **Maric, D.**, and **Craigie, R.** (2014). Dephosphorylation of barrier-to-autointegration factor by protein phosphatase 4 and its role in cell mitosis. *The Journal of Biological Chemistry*, 289(2): 1119–1127. doi: 10.1074/jbc.M113.492777.

Zuleger, N., **Kelly, D. A.**, **Richardson, A. C.**, **Kerr, A. R. W.**, **Goldberg, M. W.**, **Goryachev, A. B.**, and **Schirmer, E. C.** (2011). System analysis shows distinct mechanisms and common principles of nuclear envelope protein dynamics. *The Journal of Cell Biology*, 193(1):109–123. doi: 10.1083/jcb.201009068.

Zwerger, M., **Jaalouk, D. E.**, **Lombardi, M. L.**, **Isermann, P.**, **Mauermann, M.**, **Dialynas, G.**, **Herrmann, H.**, **Wallrath, L. L.**, and **Lammerding, J.** (2013). Myopathic lamin mutations impair nuclear stability in cells and tissue and disrupt nucleo-cytoskeletal coupling. *Human Molecular Genetics*, 22(12):2335–2349. doi: 10.1093/hmg/ddt079.

Supplementary Data

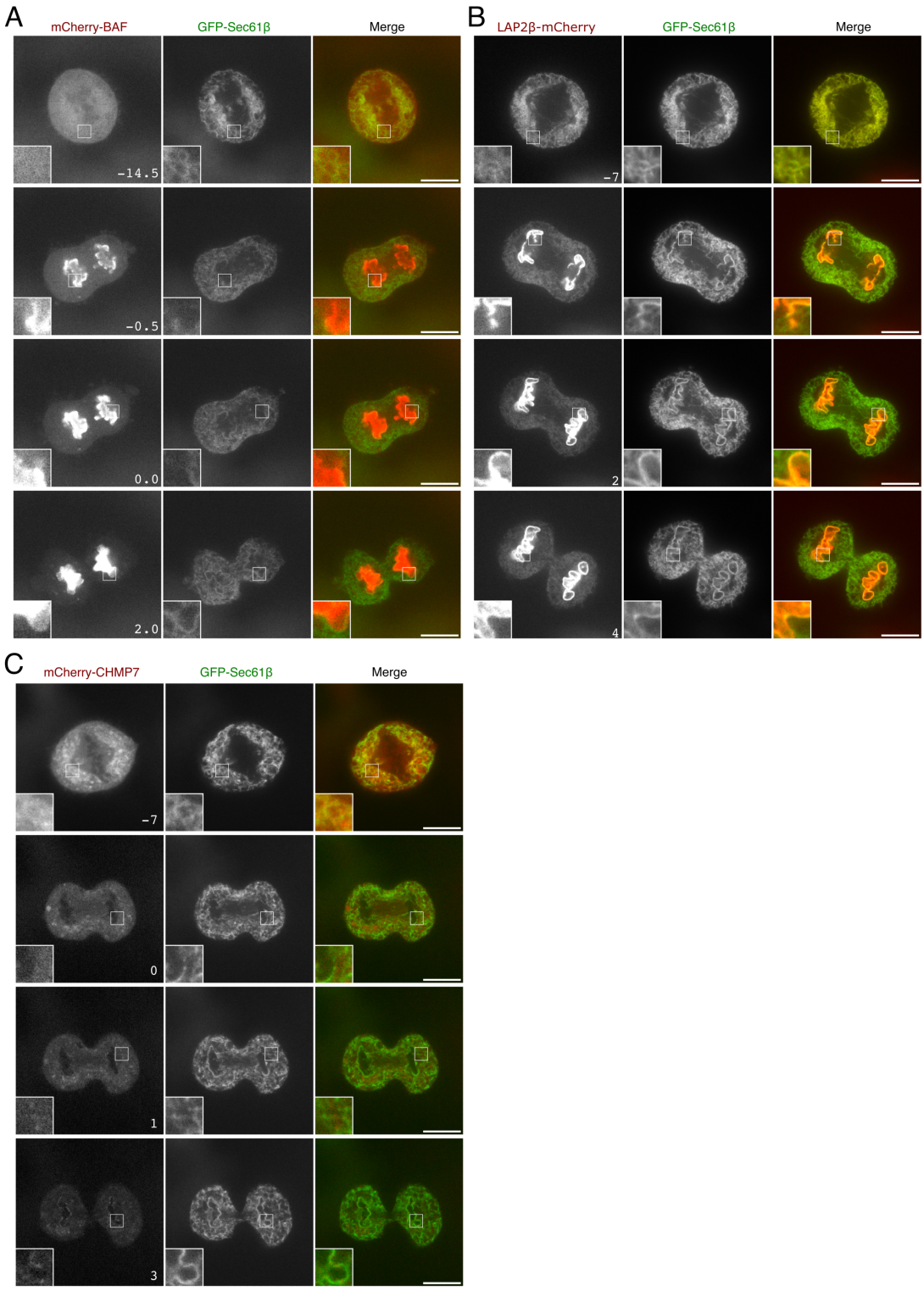

Figure 6.1. Mitotic localisation of nuclear, NE and ER proteins in RPE-1 stable cell lines. RPE-1 cell lines stably expressing the indicated mCherry-tagged nuclear or NE protein (BAF, CHMP7, emerin, LAP2β or LBR) and the ER marker GFP-Sec61β were made by lentiviral transduction. Shown are single slices of cell lines captured live with an imaging interval of 0.5 min (BAF and emerin) or 1 min (LBR, LAP2β and CHMP7). Time is indicated in minutes. ROIs are 3 times expanded from 50 pixel region. Scale bars, 10 µm.

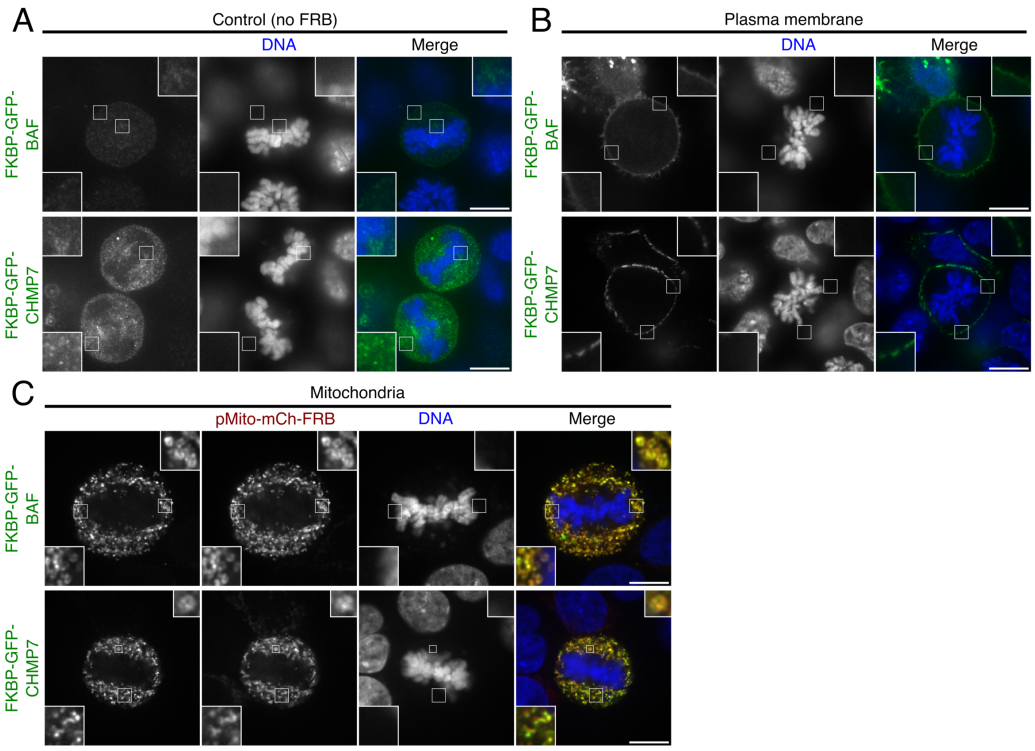

D

Relocalised protein	Plasma membrane	Mitochondria
BAF	Continuous, complete coating	Continuous, complete coating
CHMP7	Puncta and patches, near complete coating	Puncta and patches, near complete coating

Figure 6.2. Differing pattern of relocalisation of nuclear/nuclear envelope proteins in mitosis. (**A-B**) Representative single slice micrographs from z-stacks of HCT116 cells transiently expressing indicated FKBP-GFP-tagged nuclear/NE protein (FKBP-GFP-BAF or FKBP-GFP-CHMP7) and no FRB anchor control (**A**) or with plasma membrane anchor (Stargazin-darkmCherry-FRB or Stargazin-mCherry-FRB, **B**)) or a mitochondrial anchor (pMito-mCherry-FRB, **C**). Rapamycin was applied for 30 min before PTEMF fixation and staining of DNA with DAPI. Scale bars, 10 µm. ROI are 3 times expanded from 50 pixel region, or 4 times expanded from 25 pixel region. (**C**) Summary table of relocalisation patterns of INM proteins observed in **A-C**.

Appendix

JCB Journal of Cell Biology

ARTICLE

Endomembranes promote chromosome missegregation by ensheathing misaligned chromosomes

Nuria Ferrandiz[1], Laura Downie[1], Georgina P. Starling[1], and Stephen J. Royle[1]

Errors in mitosis that cause chromosome missegregation lead to aneuploidy and micronucleus formation, which are associated with cancer. Accurate segregation requires the alignment of all chromosomes by the mitotic spindle at the metaphase plate, and any misalignment must be corrected before anaphase is triggered. The spindle is situated in a membrane-free "exclusion zone"; beyond this zone, endomembranes (mainly endoplasmic reticulum) are densely packed. We investigated what happens to misaligned chromosomes localized beyond the exclusion zone. Here we show that such chromosomes become ensheathed in multiple layers of endomembranes. Chromosome ensheathing delays mitosis and increases the frequency of chromosome missegregation and micronucleus formation. We use an induced organelle relocalization strategy in live cells to show that clearance of endomembranes allows for the rescue of chromosomes that were destined for missegregation. Our findings indicate that endomembranes promote the missegregation of misaligned chromosomes that are outside the exclusion zone and therefore constitute a risk factor for aneuploidy.

Introduction

Accurate chromosome segregation during mitosis is essential to prevent aneuploidy, a cellular state of abnormal chromosome number (Duijf and Benezra, 2013). Errors in mitosis that lead to aneuploidy can occur via different mechanisms. These mechanisms include mitotic spindle abnormalities (Ghadimi et al., 2000), incorrect kinetochore-microtubule attachments (Cimini et al., 2001), dysfunction of the spindle assembly checkpoint (Kalitsis et al., 2000), defects in cohesion (Daum et al., 2011), and failure of cytokinesis (Fujiwara et al., 2005). Some of these error mechanisms result in the missegregation of whole chromosomes, a process termed chromosomal instability (CIN). The majority of solid tumors are aneuploid, with higher rates of CIN, and so understanding the mechanisms of chromosome missegregation is an important goal of cancer cell biology. In addition, chromosome missegregation is associated with micronucleus formation, which is linked to genomic rearrangements that may drive tumor progression (Crasta et al., 2012; Ly et al., 2017; Liu et al., 2018).

While the mitotic spindle has logically been the focus of efforts to understand chromosome missegregation, there has been less attention on other features of mitotic cells such as intracellular membranes. In eukaryotic cells, entry into mitosis constitutes a large-scale reorganization of intracellular membranes. The nuclear envelope (NE) breaks down, while the ER and Golgi apparatus disperse to varying extents (Hepler and Wolniak, 1984; Warren, 1993). These organelle remnants—collectively termed "endomembranes"—are localized toward the cell periphery, while the mitotic spindle itself is situated in an "exclusion zone" that is largely free of membranes and organelles (Bajer, 1957; Porter and Machado, 1960; Nixon et al., 2017). The endomembranes beyond the exclusion zone are densely packed, although the details of their ultrastructure vary between cell lines (Puhka et al., 2007; Lu et al., 2009, 2011; Puhka et al., 2012; Champion et al., 2017). This arrangement means that, although mitosis is open in mammalian cells, the spindle operates within a partially closed system. Several lines of evidence suggest that endomembranes must be cleared from the exclusion zone for the mitotic spindle to function normally (Vedrenne et al., 2005; Schlaitz et al., 2013; Champion et al., 2019; Kumar et al., 2019; Merta et al., 2021). In addition, it is thought that this arrangement is required to concentrate factors needed for spindle formation (Schweizer et al., 2015).

[1]Centre for Mechanochemical Cell Biology, Warwick Medical School, Coventry, UK.

Correspondence to Nuria Ferrandiz: n.ferrandiz@warwick.ac.uk; Stephen J. Royle: s.j.royle@warwick.ac.uk

G.P. Starling's present address is The Francis Crick Institute, London, UK.

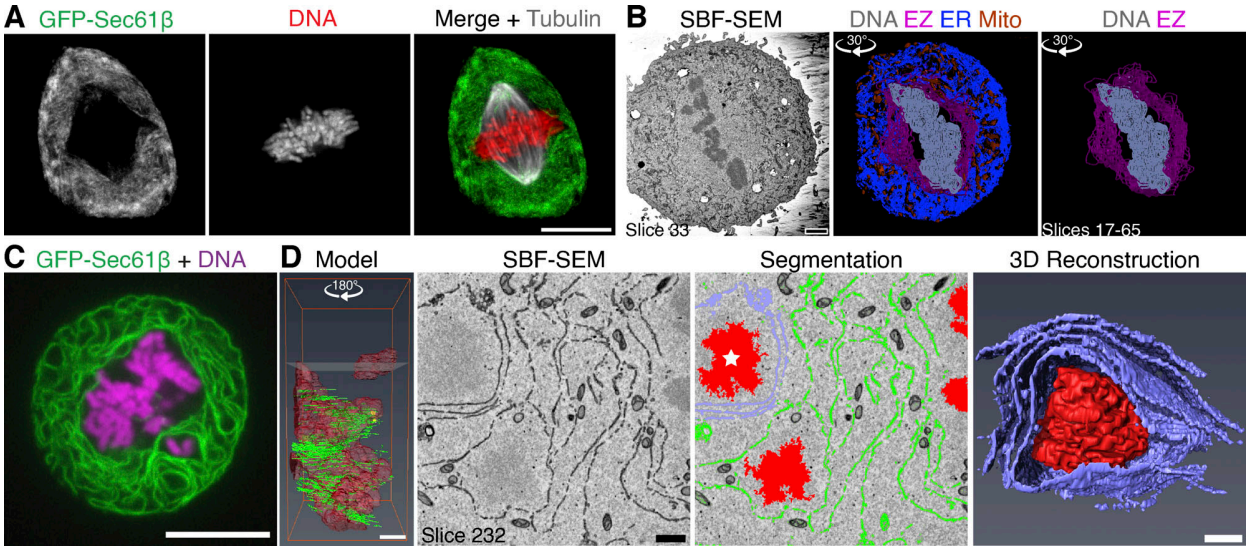

Figure 1. **Misaligned chromosomes outside the exclusion zone are ensheathed in endomembranes. (A)** Confocal image of a mitotic RPE-1 cell stably coexpressing GFP-Sec61β (green) Histone H3.2-mCherry (DNA, red) and stained with SiR-Tubulin (gray). Scale bar, 10 µm. **(B)** SBF-SEM imaging of mitotic cells and subsequent segmentation reveals the endomembranes (ER, blue) and mitochondria (Mito, orange) beyond the exclusion zone boundary (EZ, pink), with the chromosomes (DNA, gray) within. Angle of rotation about y axis is shown. Scale bar, 2 µm. **(C)** Confocal image of an untreated HeLa cell coexpressing GFP-Sec61β (green) and Histone H2B-mCherry (magenta) with a spontaneously occurring ensheathed chromosome. **(D)** SBF-SEM imaging of an untreated HeLa cell with a spontaneously occurring ensheathed chromosome. Model shows the position of two ensheathed chromosomes (red) away from the metaphase plate; height of slice 232 is indicated. Scale bar, 2 µm. Segmentation shows endomembranes (green and lilac surrounding the chromosome marked with a star), rendered in 3D (reconstruction). Scale bars, 1 µm. See Videos 1 and 2.

This study was prompted by a simple question: What happens to misaligned chromosomes that find themselves beyond the exclusion zone? We show that such chromosomes become "ensheathed" in multiple layers of endomembranes. Chromosome ensheathing delays mitosis and increases the frequency of chromosome missegregation and subsequent formation of micronuclei. Using an induced organelle relocalization strategy, we demonstrate that clearance of endomembranes allows the rescue of chromosomes that were destined for missegregation. Our findings indicate that endomembranes are a risk factor for CIN if the misaligned chromosomes go beyond the exclusion zone boundary during mitosis.

Results

Misaligned chromosomes outside the exclusion zone are ensheathed in endomembranes

During mitosis, the spindle apparatus is situated in a membrane-free exclusion zone. Outside the exclusion zone, the ER and NE—collectively called endomembranes—surround the mitotic spindle. We investigated the organization of endomembranes in mitotic cells using light microscopy and EM. First, we carried out live-cell imaging of mitotic RPE-1 cells that stably coexpress GFP-Sec61β and Histone H3.2-mCherry, stained with SiR-tubulin to mark the ER, DNA, and microtubules. These images revealed a mitotic spindle-sized exclusion zone from which GFP-Sec16β signal was absent (Fig. 1 A). Second, serial block face scanning electron microscopy (SBF-SEM) of mitotic RPE-1 cells showed that the ellipsoid exclusion zone is largely devoid of endomembranes, including mitochondria and other organelles. Outside the exclusion zone, endomembranes are tightly packed, and the border between these two regions is clearly delineated and could be segmented (Fig. 1 B).

Misaligned chromosomes are those that fail to attach or lose their attachment to the mitotic spindle. What happens to misaligned chromosomes that end up among the endomembranes beyond the exclusion zone? HeLa cells have high rates of chromosome misalignment, and live-cell imaging showed that misaligned chromosomes could be situated beyond the exclusion zone (Fig. 1 C). Reconstruction of SBF-SEM data from HeLa cells showed that three to four layers of endomembranes ensheath the chromosomes beyond the exclusion zone (Fig. 1 D and Videos 1 and 2). We use the term ensheathed to describe how these chromosomes are surrounded by endomembranes but not fully enclosed in any one layer, as though in a vesicle.

To study chromosome ensheathing in diploid cell lines, we needed to artificially increase the frequency of misaligned chromosomes in mitosis. Our main model was RPE-1 cells pretreated with 150 nM GSK923295, a centromere protein E (CENP-E) inhibitor (Wood et al., 2010), before washing out the drug for 1 h (Fig. 2 A). In parallel, we also used a system of targeted Y-chromosome spindle detachment in DLD-1 cells (Ly et al., 2017; Fig. S1). Using live-cell imaging in both cell types, we observed that misaligned chromosomes beyond the exclusion zone are submerged in endomembranes (Figs. 2 B and S1 E). Next, we used an image analysis method to determine the location of kinetochores in 3D space and map these positions relative to the exclusion zone boundary (see Materials and methods; Fig. 2, C and D; and Fig. S1, F and G). Kinetochores of chromosomes that were not aligned at the metaphase plate therefore fell into two categories: those that were surrounded by

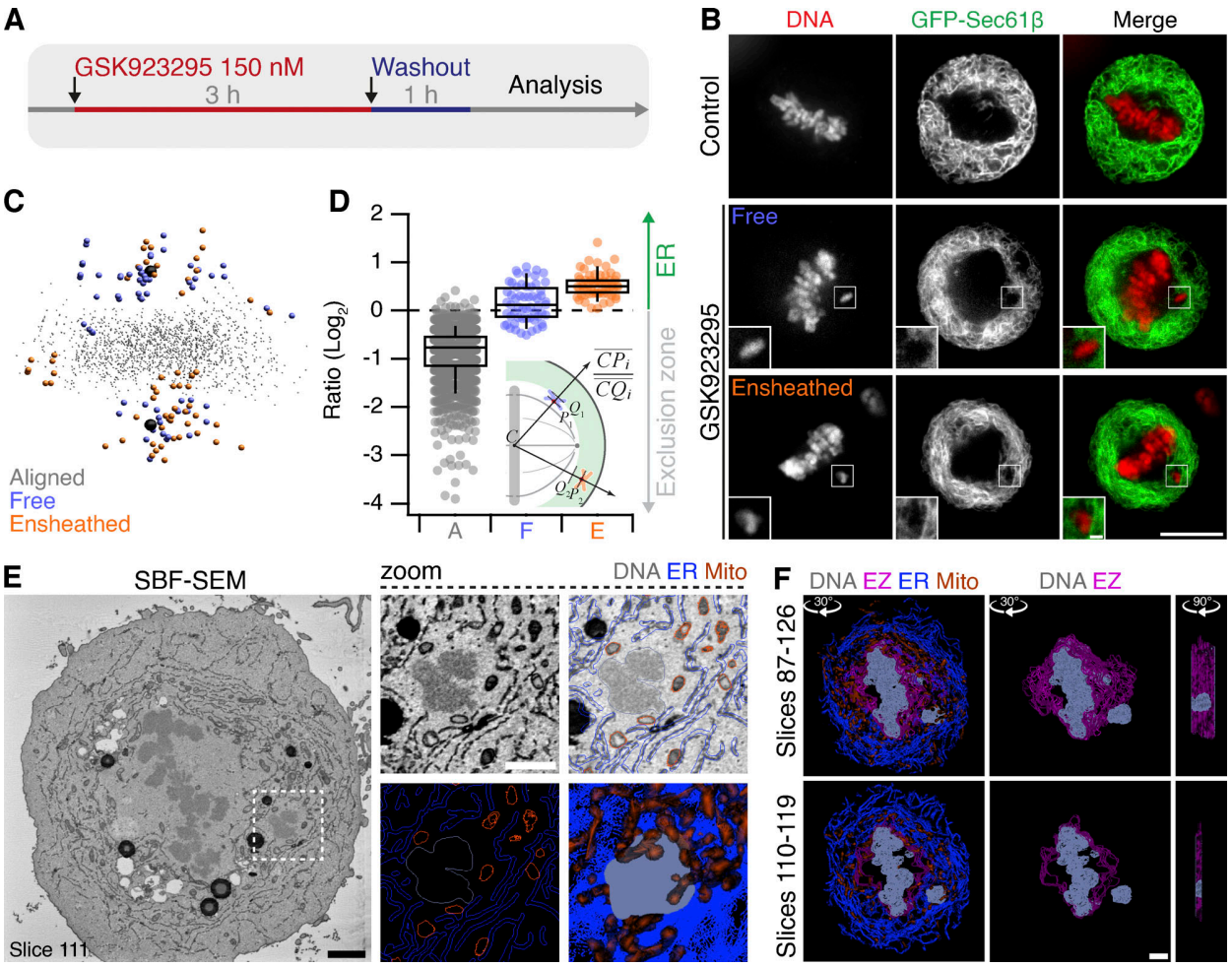

Figure 2. **Induction of misaligned chromosomes in stably diploid RPE1 cells by pretreatment with a CENP-E inhibitor. (A)** Polar, misaligned chromosomes can be induced by treatment with CENP-E inhibitor GSK923295 (150 nM, 3 h) and subsequent washout (1 h). **(B)** Confocal micrographs to show that these misaligned chromosomes (SiR-DNA, red) are either outside the exclusion zone delineated by GFP-Sec61β (green), termed ensheathed, or at the boundary and inside the exclusion zone, termed free. Scale bars, 10 µm; 1 µm (inset). **(C)** Spatially averaged 3D view of all CENP-C–positive kinetochores in the dataset; see Materials and methods). Small gray points represent kinetochores at the metaphase plate. Colored points represent misaligned chromosomes that were ensheathed (orange) and those that were not (free, blue). Spindle poles are shown in black. **(D)** Box plot to show the relative position of each kinetochore relative to the exclusion zone boundary. Chromosome misalignment was induced by pretreatment with GSK923295 (150 nM). Ratio of kinetochores within the exclusion zone are <0 and those within the ER are >0 on a log2 scale. Dots represent kinetochore ratios from 31 RPE-1 cells at metaphase. Boxes show IQR, bar represents the median, and whiskers show 9th and 91st percentiles. Inset: Schematic diagram to show how the position of kinetochores relative to the exclusion zone boundary was calculated. *C* is the centroid of aligned kinetochores, *P* is a kinetochore, and *Q* is the point along the 3D path (*CP*) that intersects the exclusion zone boundary. The ratio of *CP* to *CQ* is taken for each kinetochore (aligned kinetochores, gray; free, blue; and ensheathed, orange). **(E)** Single SBF-SEM image showing an ensheathed chromosome. Boxed region is shown expanded and modeled (zoom). Single slice and a 3D model (bottom right) of slices 87–126 are shown. Scale bar, 2 µm (black) and 500 nm (white). **(F)** Modeled substacks from SBF-SEM images showing a chromosome outside the exclusion zone, ensheathed in ER. Slices shown and angles and axes of rotation are indicated (see Video 3). Scale bar, 2 µm.

GFP-Sec61β signal, termed ensheathed, and those that were not, termed free (Fig. 2, B and D). Spatial analysis revealed that the kinetochores of ensheathed chromosomes were beyond the exclusion zone, whereas kinetochores of free chromosomes lay at the boundary in RPE-1 cells (Fig. 2 D). In DLD-1 cells, the distinction was even more clear, with the kinetochores of free chromosomes positioned inside the exclusion zone S1F. The exclusion zone therefore approximately defines chromosome misalignment, with those chromosomes beyond the exclusion zone likely to be ensheathed by endomembranes. However, imaging GFP-Sec61β was required to verify that a chromosome was fully ensheathed.

We again used SBF-SEM to observe how chromosomes beyond the exclusion zone interact with endomembranes in RPE-1 cells. Cells observed by fluorescence microscopy to have at least one ensheathed chromosome were selected for 3D EM analysis (Fig. 2 E). Segmentation of these datasets confirmed that the chromosome was fully beyond the exclusion zone boundary (Fig. 2 F and Video 3) and was ensheathed in several layers of endomembranes (Fig. 2 E). The observation of ensheathed chromosomes raised immediate questions about their fate and whether ensheathing leads to aberrant mitosis.

Ensheathed chromosomes delay mitotic progression

To determine the impact of ensheathed chromosomes on cell division, we first analyzed mitotic progression in RPE-1 cells stably expressing GFP-Sec61β with induction of ensheathed chromosomes using GSK923295 pretreatment. Cells that had at least one ensheathed chromosome showed prolonged mitosis (median NE breakdown [NEB]-to-anaphase timing of 66 min compared with 27 min in GSK923295 pretreated cells in which all chromosomes were aligned). The time to align the majority of chromosomes (NEB-to-metaphase) was delayed for cells with either a free or an ensheathed chromosome, but cells with an ensheathed chromosome had an additional delay to progress to anaphase (Fig. 3 A). Given these delays, we next confirmed that the spindle assembly checkpoint was active in these cells. The amount of Mad2 and Bub1 detected by immunofluorescence at CENP-C–positive kinetochores of free or ensheathed chromosomes was similar and was four-fold higher than at kinetochores of aligned chromosomes (Fig. 3, B and C; and Fig. S2, A and B, for DLD-1 cells). Using live-cell imaging, we found that GFP-Mad2 was recruited to kinetochores of ensheathed chromosomes (Fig. 3, D and E; and Video 4). Semiautomated 4D tracking of chromosomes allowed us to monitor their GFP-Mad2 status over time, relative to anaphase onset. These data revealed that GFP-Mad2 is lost from ensheathed chromosomes with similar kinetics to the signals at misaligned chromosomes that successfully congress to the metaphase plate (Fig. 3 E).

The failure of ensheathed chromosomes to congress is likely due to a lack of microtubule attachment, suggesting that endomembranes inhibit chromosome–microtubule interactions. We confirmed that ensheathed chromosomes have no stable end-on kinetochore-microtubule attachments by detecting colocalization of kinastrin, a marker for stable end-on attachment (Dunsch et al., 2011), with kinetochores of aligned and misaligned chromosomes (Fig. S3, A–C). Live-cell imaging of RPE-1 cells stably coexpressing Histone H3.2-mCherry and GFP-Sec61β, stained with SiR-Tubulin, showed that ensheathed chromosomes that failed to congress had no detectable microtubule contacts; free chromosomes that had microtubule contacts could be rescued and aligned at the metaphase plate, albeit after a delay (Fig. S3, D and E).

These results suggest that ensheathed chromosomes hinder mitotic progression in a spindle assembly checkpoint–dependent manner. Lack of microtubule contact is sensed by the spindle assembly checkpoint, but ultimately, the checkpoint is extinguished in the absence of congression after a long delay. The cells then proceed to anaphase, resulting in missegregation of the ensheathed chromosome.

Ensheathed chromosomes promote formation of micronuclei

To understand the fate of cells with an ensheathed chromosome, we next examined mitosis in control or GSK923295-pretreated RPE-1 cells stably expressing GFP-Sec61β using live-cell spinning disc microscopy (Fig. 4 A). In cells with an ensheathed chromosome, we observed the long delay in mitosis relative to control cells, and that mitosis was often resolved by missegregation and formation of a micronucleus (Figs. 4 A and S2 C for DLD-1 cells). These experiments suggested that ensheathed chromosomes are potentially a precursor to micronuclei. We therefore followed the fate of mitotic cells by long-term live-cell imaging to understand the likelihood of mitotic outcomes. Our sample of cells pretreated with GSK923295 included the three metaphase classes: aligned (25.8%), free (5.4%), and ensheathed (65.6%). The most frequent fate of cells with an ensheathed chromosome was micronucleus formation (39%). Of the 47 cells that formed a micronucleus after division in the dataset, 46 were from the ensheathed class (Fig. 4 B). This promotion of micronucleus formation was significant in cells with an ensheathed chromosome compared to free ($P = 1.3 \times 10^{-3}$, Fisher's exact test). A smaller proportion of cells with an ensheathed chromosome exited mitosis normally, albeit with a delay (34%), with the remainder showing other defects or death (20% or 8%). Cells pretreated with GSK923295, that had aligned all their chromosomes, had similar fates to parental and control cells (Fig. 4 B; and Videos 5 and 6). These fate-mapping experiments suggest that ensheathing of chromosomes by endomembranes promotes the formation of micronuclei.

Micronuclei formed from ensheathed chromosomes have a disrupted NE

Micronuclei can undergo a collapse of their NE, which manifests as ER tubules invading the micronuclear space (Hatch et al., 2013). We therefore asked if micronuclei that formed from ensheathed chromosomes were similarly defective. Using confocal imaging of RPE-1 cells stably coexpressing GFP-Sec61β and either mCherry-BAF or LBR-mCherry that were fixed 8 h after washout of GSK923295 to examine micronucleus integrity, we found that the majority of micronuclei have ER inside the micronucleus (Fig. 5). The fluorescence of GFP-Sec61β was higher at the micronucleus compared with the main nucleus (Fig. 5 B). Moreover, the levels of either mCherry-BAF or LBR-mCherry were correlated with GFP-Sec61β. To confirm that these micronuclei had disrupted NEs, we stained for H3K27Ac, a modification to Histone H3 that is removed by exposure to the cytoplasm (Mammel et al., 2021). Intact micronuclei had H3K27Ac signals similar to those of the corresponding main nucleus, whereas in micronuclei that were disrupted, the signal was lost (Fig. 5 A). The ratio of H3K27Ac signal at the micronucleus compared with the main nucleus was anticorrelated with the ratios of GFP-Sec61β, mCherry-BAF, and LBR-mCherry (Fig. 5 B). Since the majority of micronuclei formed after pretreatment of RPE-1 cells with GSK923295 are derived from ensheathed chromosomes (Fig. 4 B), these data suggest that the ensheathing process may contribute to the formation of defective micronuclear envelope. However, due to the low rates of missegregation of free chromosomes, it was not possible to conclude whether disruption was specific to chromosome ensheathing.

Induced relocalization of ER enables the rescue of ensheathed chromosomes

Does ensheathing of misaligned chromosomes cause chromosome missegregation? To answer this question, we sought a way to clear the mitotic ER and test whether this enabled subsequent rescue of misaligned chromosomes to the metaphase plate. To

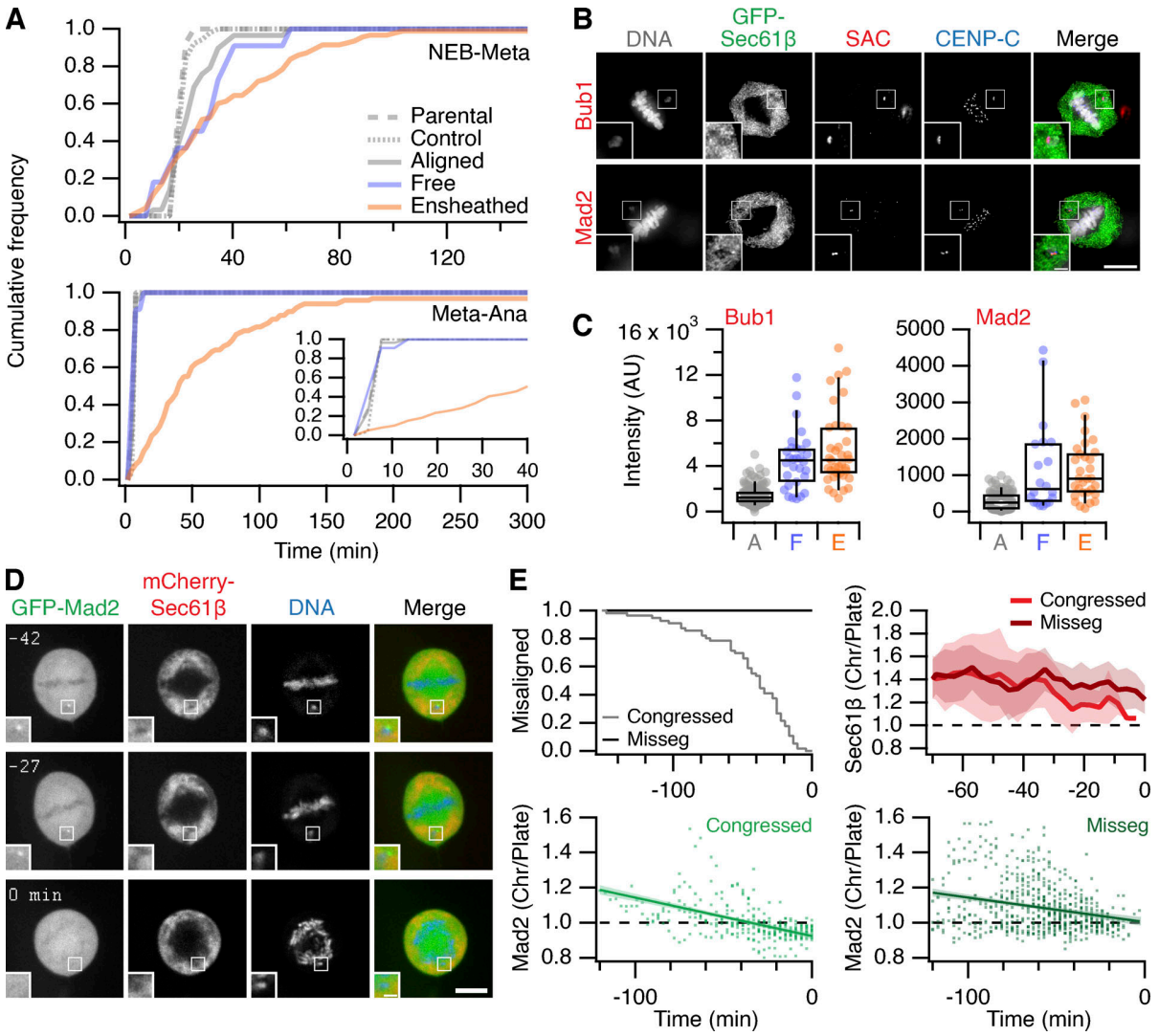

Figure 3. **Impact of ensheathed chromosomes on cell division. (A)** Mitotic timing of RPE-1 cells. Cumulative frequencies for NEB to metaphase (NEB-Meta) and metaphase to anaphase (Meta-Ana) are shown. RPE-1 stably expressing GFP-Sec61β were treated with 150 nM GSK923295 for 3 h before washout. Three classes of metaphase were seen: all chromosomes aligned (Aligned, n = 29), cells with one or more free chromosomes (Free, n = 11), and cells with one or more ensheathed chromosome (Ensheathed, n = 107). Timing of untreated parental (Parental, n = 69) and stable RPE-1 (Control, n = 52) cells is also shown. Inset in Meta-Ana shows same data on an expanded time scale. Comparison of NEB-Meta and Meta-Ana timing distributions for ensheathed vs. control, $P = 1.9 \times 10^{-57}$ and 7.8×10^{-23}, Kolmogorov–Smirnov test. **(B)** Micrographs of immunofluorescence experiments to detect Bub1 or Mad2 (SAC, red) at kinetochores (CENP-C, blue) in cells stably expressing GFP-Sec61β (green); DAPI-stained DNA is shown in gray. Scale bars, 10 µm; 2 µm (insets). **(C)** Quantification of Bub1 and Mad2 immunofluorescence at kinetochores marked by CENP-C. Ensheathed chromosomes were classified using the GFP-Sec61β signal. Dots represent kinetochores, boxes show IQR, bar represents the median, and whiskers show 9th and 91st percentiles (Bub1: n_A = 132, n_F = 30, n_E = 37; (Mad2: n_A = 103, n_F = 20, n_E = 31). **(D)** Stills from live-cell imaging experiments to track Mad2 levels at kinetochores of ensheathed chromosomes. A GSK923295-pretreated RPE-1 cell is shown, stably coexpressing GFP-Mad2 (green) and mCherry-Sec61β (red); DNA is stained using SiR-DNA (blue). Time relative to anaphase is shown in minutes. Insets show 2× zoom of the indicated ROI. Scale bars, 10 µm; 2 µm (insets). **(E)** Quantification of live Mad2 imaging experiments. Kaplan–Meier plot to show congression times of the last misaligned chromosome to align. Measurement of mCherry-Sec61β (mean ± SD) and GFP-Mad2 is shown for the misaligned that congressed and those that were missegregated (misseg). A linear regression fit with 95% confidence intervals is shown for GFP-Mad2. All plots are shown in time (minutes) relative to anaphase onset. Total cells with misaligned chromosomes, n = 72; cells where all chromosomes congressed, n = 56; and where there was missegregation, n = 16.

clear the mitotic ER, we used an induced relocalization strategy (Fig. 6 A). Induced relocalization of small organelles has been demonstrated for Golgi, intracellular nanovesicles, and endosomes, typically using heterodimerization of FKBP-rapamycin-FRB with the FKBP domain fused to the organelle and the FRB domain at the mitochondria (Dunlop et al., 2017; Hirst et al., 2015; Larocque et al., 2020; van Bergeijk et al., 2015). We reasoned that a large organellar network, such as the ER, may be cleared by inducing its relocalization to the cell boundary. Our strategy therefore comprised an ER-resident hook (FKBP-GFP-Sec61β) and a plasma membrane anchor (stargazin-mCherry-FRB) with application of rapamycin predicted to induce the

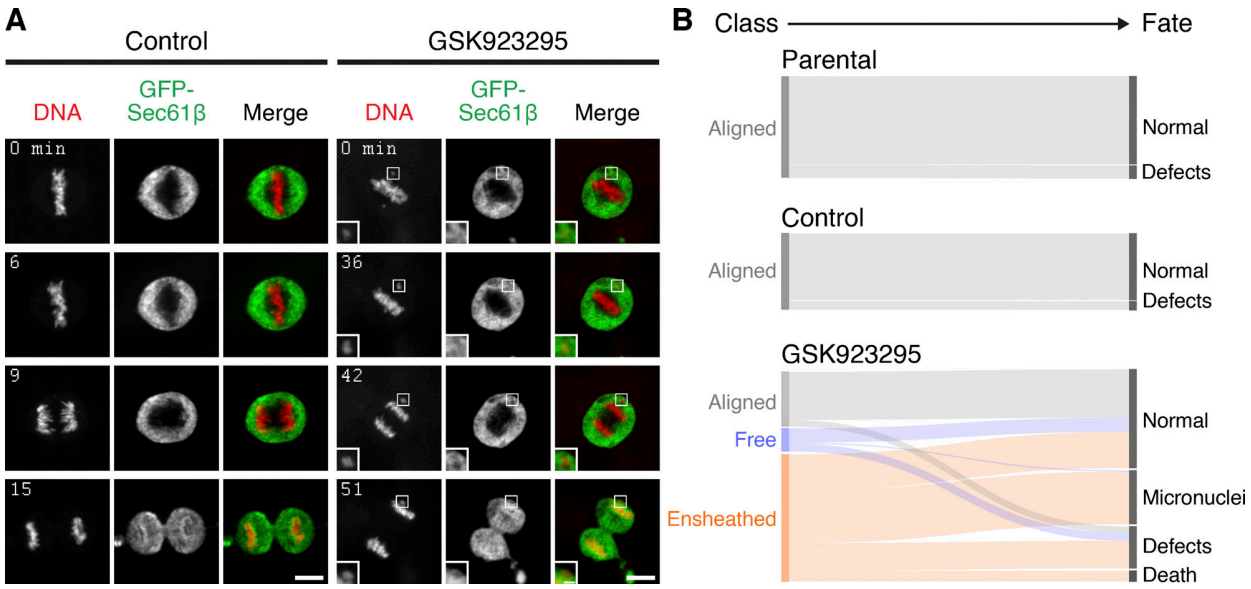

Figure 4. **Ensheathed chromosomes promote formation of micronuclei. (A)** Stills from live-cell imaging experiments to track the fate of ensheathed chromosomes. A control or GSK923295-pretreated GFP-Sec61β RPE-1 cell is shown; DNA is stained using SiR-DNA (red). Scale bars, 10 µm; 2 µm (insets). Shown in Videos 5 and 6. **(B)** Sankey diagram to show the fate (right) of cells in each of the three metaphase classes (left). Fates include normal division, micronucleus formation, death, and other defects (lagging chromosome, cytokinesis failure). Note that the fate of cells (and not chromosomes) is tracked. A cell with three misaligned chromosomes, only one of which is ensheathed, is classified as ensheathed. Parental RPE-1 cells (Parental, *n* = 92) and untreated RPE-1 stably expressing GFP-Sec61β (Control, *n* = 69) are from two and three independent overnight experiments, respectively. Fates of GSK923295-pretreated GFP-Sec61β cells (*n* = 186) were compiled from seven experiments. Fates of individual chromosomes are shown in Fig. S5 B.

relocalization of ER to the plasma membrane (Fig. 6 A). HCT116 cells were used for these experiments, as they are near diploid and easy to transfect and showed a fate and mitotic response to GSK923925 pretreatment similar to those of RPE-1 (Fig. S4).

We found that the clearance of ER in mitotic cells with this strategy was efficient, occurring in 89.2% of HCT116 cells expressing the system after treatment with 200 nM rapamycin. Onset was variable, with a median time to maximum clearance of 15 min (interquartile range [IQR], 12–24 min; Fig. 6 B). Importantly, induced relocalization of FKBP-GFP-Sec61β to the plasma membrane represented the clearance of ER and not the extraction of the protein. First, immunostaining of two other endogenous ER-resident proteins, KDEL and calnexin, also showed relocalization to the plasma membrane (Fig. 6 C). Second, SBF-SEM imaging allowed us to observe the relocalization of ER to the plasma membrane (Fig. 6 D). Here, the expansion of the exclusion zone and the direct attachment of hundreds of ER tubules to the plasma membrane could be unambiguously visualized.

We next tested whether ER clearance could be used as an intervention in cells with ensheathed chromosomes. To do this, HCT116 cells expressing FKBP-GFP-Sec61β and stargazin-mCherry-FRB, pretreated with 150 nM GSK923295 to induce ensheathed chromosomes, were imaged as 200 nM rapamycin was applied to induce clearance of the ER. In control cells where no rapamycin was applied, the cells were arrested in mitosis for prolonged periods. In cells where the ER had been cleared, congression of the ensheathed chromosome was clearly seen after clearance had occurred (Fig. 7 A and Video 7). We used automated image analysis to track the 3D position of the misaligned chromosome over time, in an unbiased manner (Fig. 7, B–C). Congression of the ensheathed chromosome within 80 min was seen in 86.7% of cells with induced ER clearance. In control cells, the majority (66.7%) were unable to resolve the ensheathed chromosome in the same time (Fig. 7, A–C). These data suggest that ER clearance is an effective intervention in cells with ensheathed chromosomes and points to a causal role for endomembranes in chromosome missegregation.

Discussion

This study demonstrates that misaligned chromosomes located beyond the exclusion zone are liable to become ensheathed by endomembranes. The fate of cells with ensheathed chromosomes is biased toward missegregation, aneuploidy, and micronucleus formation. We showed that if the ER was cleared by induced relocalization in live mitotic cells, these chromosomes could be rescued by the mitotic spindle, an intervention which suggests that chromosome ensheathing by endomembranes is a risk factor for chromosome missegregation and subsequent aneuploidy.

Chromosomes can become misaligned during mitosis for a number of reasons, but we show here that those that transit out of the exclusion zone become ensheathed in endomembranes. We demonstrated this with four different cell models: RPE-1 or HCT116 cells pretreated with a CENP-E inhibitor, DLD-1 cells with targeted disconnection of the Y-chromosome, and HeLa cells with spontaneously arising misaligned chromosomes. In each case, misaligned chromosomes beyond the exclusion zone typically became ensheathed in endomembranes. Although the

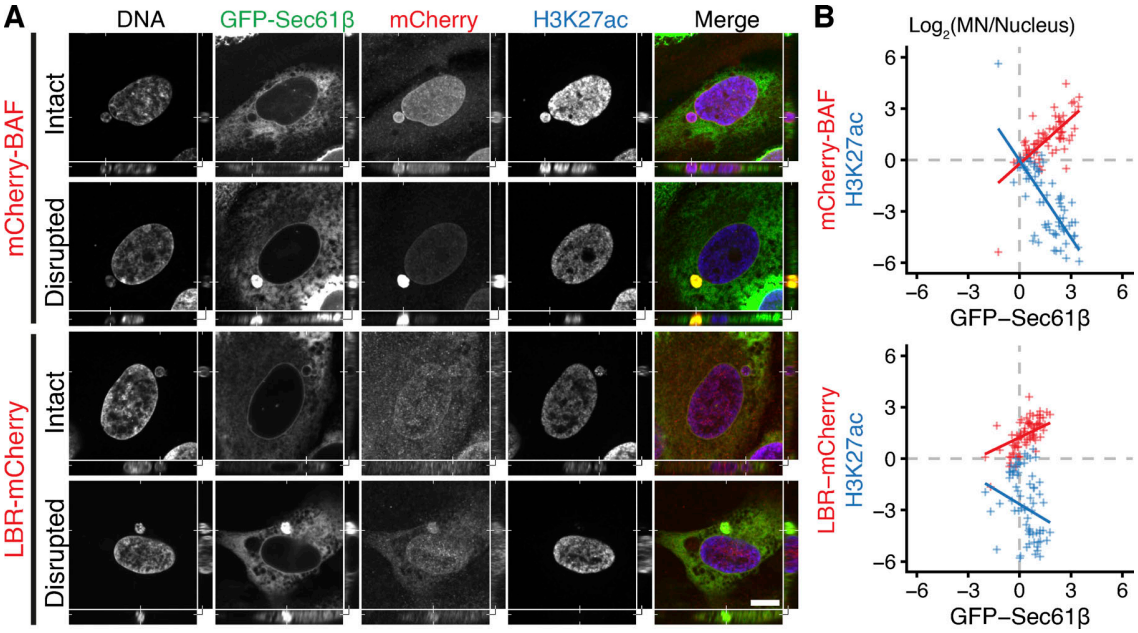

Figure 5. **Missegregation of an ensheathed chromosome results in a micronucleus with a disrupted NE. (A)** Confocal images showing examples of an intact or a disrupted micronucleus as indicated. Images show mCherry-BAF or LBR-mCherry (red) stably coexpressed with GFP-Sec61β (green) in RPE-1 cells; H3K27ac was detected by immunofluorescence (blue), and DNA was stained with DAPI. XY view is through the center of the micronucleus; YZ (right) and XZ (below) are orthogonal views at the positions indicated. Scale bar, 10 µm. **(B)** Scatter plots to show the fluorescence intensity of H3K27ac (blue) and either mCherry-BAF or LBR-mCherry (red) vs. GFP-Sec61β intensity. Data are plotted as the $\log_2$ ratio of intensity at the micronucleus vs. main nucleus. For RPE1 GFP-Sec61β mCherry-BAF, *n* = 71 cells, and LBR-mCherry, *n* = 73 cells, from three independent experiments in each cell type.

morphology of mitotic endomembranes varies between cell lines (Puhka et al., 2007; Lu et al., 2009, 2011; Puhka et al., 2012; Champion et al., 2017), all ensheathed chromosomes were draped in several layers of endomembranes. We use the term ensheathed to describe how these chromosomes are surrounded by endomembranes but not fully enclosed in any one layer as though in a vesicle. The ensheathing membrane follows the contours of the chromosome closely. Our SBF-SEM analysis did not uncover any obvious electron-dense connections between the ensheathed chromosome and its surrounding membranes, although a previous report indicated that exogenous DNA clusters may physically interact with mitotic ER (Wang et al., 2016).

A major finding of our work is that ensheathing promotes missegregation and micronucleus formation. Our 3D EM images of ensheathed chromosomes show that microtubules face a difficult task to negotiate several layers of endomembranes to make the contact between kinetochore and spindle that is necessary for rescue and alignment. In cases where contact is made, endomembranes are also likely to impair the congression of the chromosome, as suggested by a recent study in which excess ER was shown to slow chromosome motions (Merta et al., 2021). Since endomembranes are a risk factor for missegregation, their precise organization—for example the sheet-to-tubule ratio of the ER—may influence the likelihood for missegregation (Champion et al., 2017). The lack of attachment is sufficient to prolong spindle assembly checkpoint signaling and delay mitosis. Ultimately, the cells progress to anaphase and missegregate, likely due to checkpoint exhaustion after prolonged metaphase (Uetake and Sluder, 2010; Yang et al., 2008). Whatever the mechanism, the role of endomembranes in promoting missegregation may be important for tumor progression. It is possible that in tumor cells that are aneuploid, endomembranes may contribute to the higher rates of CIN observed (Funk et al., 2016; Nicholson and Cimini, 2015). In non-transformed cells, misaligned chromosomes that arise spontaneously are more often of the free class, suggesting that the ensheathing mechanism described here is most relevant in a cancer context.

The fate of cells with ensheathed chromosomes was biased toward missegregation and formation of micronuclei. Interestingly, a previous study found that artificially tethering endomembranes to aligned chromosomes within the exclusion zone caused mitotic errors, although the outcome was dependent on at what stage tethering was induced (Champion et al., 2019). Tethering before mitotic entry resulted in segregation errors and multilobed nuclei, whereas tethering during metaphase had little consequence. Although conceptually similar, the ensheathing process reported here is a natural consequence of a misaligned chromosome becoming entangled in endomembranes. Key differences include the position of the ensheathed chromosome, the lack of microtubule attachments, no direct membrane-chromosome tethering, and multiple vs. single endomembrane layers; these likely explain the different observed mitotic phenomena. We found that the micronuclei that result from ensheathed chromosomes had disrupted envelopes 8 h after release from CENP-E inhibition. Rupture of micronuclei has been shown to lead to DNA damage and activation of innate immune and cell invasion pathways (Ly et al., 2017; Hatch et al., 2013; Mammel et al., 2021; Bakhoum et al., 2018). The presence

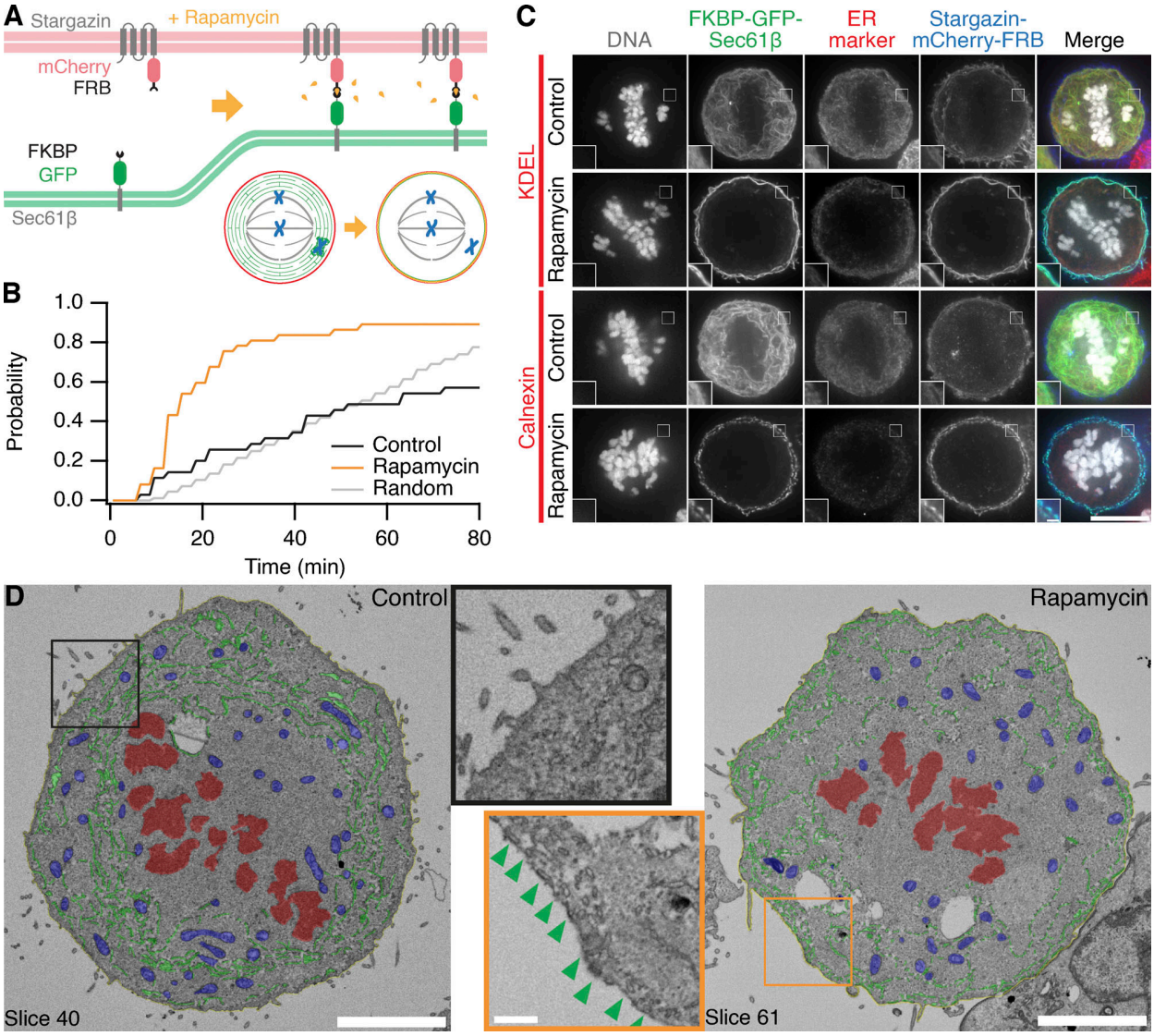

Figure 6. **Inducible relocalization of ER in mitotic cells. (A)** Schematic diagram of the ER clearance procedure. Rapamycin induces the heterodimerization of the ER-resident FKBP-GFP-Sec61β and the plasma-membrane localized Stargazin-mCherry-FRB. **(B)** Cumulative histogram showing the time to detection of ER clearance. An automated segmentation procedure was used to monitor ER localization in mitotic cells. The time at which the largest decrease in ER localization occurred was taken (n = 35–37, see Materials and methods). Random occurrence is shown for comparison. The median (IQR) ER clearance time in rapamycin-treated cells was 15 (12–24) min; rapamycin is applied after the first frame (T = 0). **(C)** Induced relocalization of FKBP-GFP-Sec61β to the plasma membrane causes ER clearance. Typical immunofluorescence micrographs of mitotic HCT116 cells pretreated with GSK923295, expressing FKBP-GFP-Sec61β (green) and Stargazin-mCherry-FRB (blue), treated or not with rapamycin (200 nM). Cells were stained for ER markers KDEL or Calnexin as indicated (red), DNA was stained with DAPI (gray). Insets are 2× expansions of the ROI shown. Scale bars, 10 µm; 1 µm (insets). **(D)** SBF-SEM imaging of control or ER-cleared (rapamycin) mitotic HCT116 cells. A single slice is shown with segmentation of ER (green), plasma membrane (yellow), mitochondria (blue), and chromosomes (red). Scale bars, 5 µm; 1 µm (insets). Insets are 2× expansions of the indicated ROI shown without segmentation; green arrowheads indicate ER attachment to the plasma membrane.

of ER in the micronuclear space of disrupted micronuclei indicates that ensheathing may increase the likelihood of rupture. We speculate that this may occur by endomembranes physically interfering with envelope reformation at the micronucleus, although it is possible that ER is present in the micronuclear space as a consequence, rather than a cause, of disruption.

Mitosis in human cells is open, yet we have known for >60 yr that the spindle exists in a membrane-free ellipsoid exclusion zone (Bajer, 1957; Porter and Machado, 1960; Nixon et al., 2017). It seems intuitive that the spindle must operate in a membrane-free area to avoid errors, but recent work suggests that the exclusion zone is actively maintained and that this arrangement is important for concentrating factors for spindle assembly (Schweizer et al., 2015) or for maintenance of spindle structure (Kumar et al., 2019; Schlaitz et al., 2013). We found that ER clearance, via an induced relocalization strategy, could be used as an intervention to improve the outcome for mitotic cells with ensheathed chromosomes. Induced relocalization of small

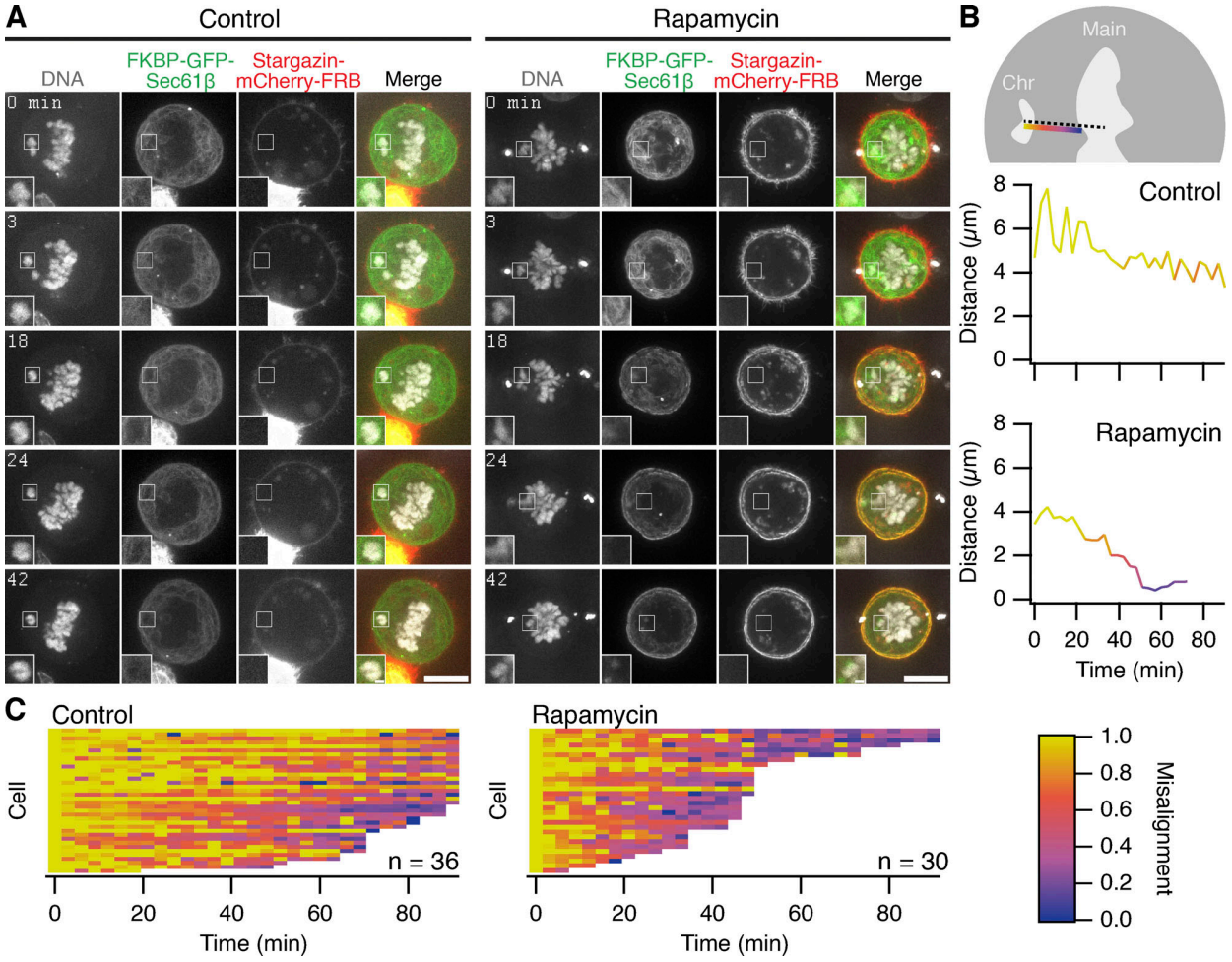

Figure 7. **Rescue of ensheathed chromosomes by the induced relocalization of ER. (A)** Stills from live-cell imaging of ER clearance experiments. FKBP-GFP-Sec61β (green), Stargazin-mCherry-FRB (red), and SiR-DNA (gray) are shown. Insets are 2× expansions of the ROI shown. Scale bars, 10 µm; 1 µm (insets). See Video 7. **(B)** Semiautomated 4D tracking of misaligned chromosome location is used to monitor congression. Two tracks from the cells in A are shown. The shortest Euclidean distance from the centroid of the misaligned chromosome to the edge of the main chromosome plate is plotted as a function of time. **(C)** Fate of misaligned chromosomes in control or rapamycin-treated cells. Rescue of misaligned chromosomes was detected in 26 of 30 rapamycin-treated cells. Coloring in B and C is with the color scale shown. Tracks terminate at 90 min or when the chromosome merges with the plate. Median termination time was 93 min (control, n = 36) and 45 min (rapamycin, n = 30); P = 7.1 × 10^{-9}, Wilcoxon rank test. Rapamycin is applied after the first frame (T = 0).

organelles has previously been demonstrated (Dunlop et al., 2017; Hirst et al., 2015; Larocque et al., 2020; van Bergeijk et al., 2015), but the movement of a large organellar network by similar means had not been attempted previously. Surprisingly, ER clearance in mitotic cells was efficient, although it was much slower than the relocalization of intracellular nanovesicles, taking tens of minutes rather than tens of seconds (Larocque et al., 2020). We speculate that the efficiency of clearance is due to cooperativity of relocalization, since the FKBP-GFP-Sec61β molecules are dispersed in the ER, which is interconnected. These experiments were important to show that ensheathing was causal for chromosome missegregation. We note that this method has many future applications: to selectively perturb mitotic structures, at defined times, during cell division. For example, ER clearance and concomitant expansion of the exclusion zone is an ideal manipulation to probe the function of this enigmatic cellular region.

Materials and methods

Molecular biology

The following plasmids were gifts, available from Addgene, or from previous work as indicated: Histone H3.2-mCherry (A. Bowman, University of Warwick), pAc-GFPC1-Sec61β (#15108; Addgene), psPAX2 (#12260; Addgene), pMD2.G (#12259; Addgene), pWPT-GFP (#12255; Addgene), Stargazin-GFP-LOVpep (#80406; Addgene), LBR pEGFP-N1 (#61996; Addgene), EGFP-BAF (#101772; Addgene), pMito-mCherry-FRB (#59352; Addgene), Histone H2B-mCherry (Cheeseman et al., 2013), and pFKBP-GFP-C1 (Clarke and Royle, 2018).

To generate a plasmid to express mCherry-Sec61β, EcoRI-BglII digestion product of pAc-GFPC1-Sec61β was ligated into pmCherry-C1 vector (made by substituting mCherry for EGFP in pEGFP-C1 [Clontech] by AgeI-XhoI digestion). LBR-mCherry was made by amplifying the LBR insert from LBR in pEGFP-N2 using (5′-AAGCTTGGTACCCATGCCAAGTAGGAAATTTGC-3′ and 5′-TC

GAGGGATCCGTGTAGATGTATGGAAATATACGG-3′) and ligating into pmCherry-N1 using KpnI and BamHI. The mCherry-BAF construct was amplified from EGFP-BAF using oligonucleotides (5′-AAGCTTAGATCTATGACAACCTCCCAAAAGC-3′ and 5′-TCG AGAAGCTTCTACAAGAAGGCATCACACC-3′) and inserted into pmCherry-C1 using BglII and HindIII.

For lentivirus transfer plasmids, constructs for expression (mCherry-BAF, GFP-Mad2, mCherry-Sec61β) were cloned into pWPT-GFP using MluI-SalI sites or MluI-BstBI for LBR-mCherry. Plasmids for ER clearance were generated as follows. For FKBP-GFP-Sec61β, a BglII-EcoRI fragment from pAc-GFP-C1-Sec61β was ligated into pFKBP-GFP-C1. Stargazin-mCherry-FRB construct was made by PCR of Stargazin encoding region from Stargazin-GFP-LOVpep using (5′-GCGGCTAGCATGGGGCTGTTT GATCGAGGTGTTCAAATGCTTTT-3′ and 5′-TTTACTCATGGA TCCTTTACGGGCGTGGTCCGG-3′) and insertion into pMito-mCherry-FRB at NheI-BamHI sites. Plasmids are available from Addgene.

Cell biology

HCT116 (CCL-247; ATCC) and HEK293T (CRL-11268; ATCC) cells were maintained in DMEM supplemented with 10% FBS and 100 U ml^{-1} penicillin/streptomycin. DLD-1-WT and DLD-1-C-H3 (Ly et al., 2017) cell lines were gifts from Don Cleveland (University of California San Diego, San Diego, CA). These cell lines and their derivatives were maintained in DMEM supplemented with 10% Tetra-Free FBS (D2-118, SLS), 2 mM L-glutamine, 100 U ml^{-1} penicillin/streptomycin, and 100 µg ml^{-1} hygromycin. RPE-1 (Horizon Discovery) and derived cell lines were maintained in DMEM/F-12 Ham supplemented with 10% FBS, 2 mM L-glutamine, 100 U ml^{-1} penicillin/streptomycin, and 0.26% sodium bicarbonate ($NaHCO_3$). All cell lines were kept in a humidified incubator at 37°C and 5% CO_2. Cells were routinely tested for mycoplasma contamination by a PCR-based method.

RPE-1 GFP-Sec61β stable cell line was generated by Fugene-HD (Promega) transfection of pAc-GFPC1-Sec61β. DLD-1-WT mCherry-Sec61β and DLD-1-C-H3 mCherry-Sec61β stable cell lines were generated by GeneJuice (Merck Millipore) transfection of mCherry-Sec61β into the respective parental lines. Individual clones were isolated by G418 treatment (500 µg ml^{-1}) and validated using a combination of Western blot, FACS, and fluorescence microscopy. Stable coexpression of Histone H3.2-mCherry, mCherry-BAF, or LBR-mCherry with GFP-Sec61β in RPE-1 cells was achieved by lentiviral transduction of cells stably expressing GFP-Sec61β. For stable expression of GFP-Mad2 with mCherry-Sec61β, dual lentivirus transduction was used. Individual cells positive for GFP and mCherry signal were sorted by FACS, and single cell clones were validated by fluorescence microscopy. Note that the transgenic expression of GFP-Sec61β is associated with downregulation of endogenous Sec61β (Fig. S5 A). Transient transfections of HCT116, RPE-1, and HeLa were done using Fugene-HD or GeneJuice according to the manufacturer's instructions.

For lentiviral transduction, HEK293T packaging cells were incubated in DMEM supplemented with 10% FBS, 2 mM L-glutamine, and 25 µM chloroquine diphosphate (C6628; Sigma-Aldrich) for 3 h. Transfection constructs were prepared at 1.3 pM psPAX2, 0.72 pM pMD2.G, and 1.64 pM transfer plasmid (encoding the tagged protein to be expressed) in Opti-Pro SFM. Polyethylenimine dilution in OptiPro SFM was prepared separately at 1:3 ratio with DNA (wt/wt, DNA: polyethylenimine) in the transfection mixture. Transfection mixes were combined, incubated at room temperature for 15–20 min, and then added to the packaging cells. Cells were incubated for 18 h, after which the medium was replaced with DMEM supplemented with 10% FBS and 100 U ml^{-1} penicillin/streptomycin. Viral particles were harvested 48 h after transfection. Viral supernatant was centrifuged and filtered before applying to target cells. Target cells were infected through incubation in medium containing 8 µg ml^{-1} polybrene (408727; Sigma-Aldrich) for 16–20 h. Medium was replaced with complete medium, and cells were screened after 24 h. All incubations were in a humidified incubator at 37°C and 5% CO_2.

To induce misaligned chromosomes in RPE-1 or HCT116 cell lines, cells were incubated in complete medium containing 150 nM GSK923295 (Selleckchem) for 3 h before release of cells from treatment. For fixed cell experiments, release was for 1 h. To induce the auxin-degron system in DLD-1 cells, 500 µM indole-3-acetic (A10556; Thermo Fisher Scientific) and 500 µg ml^{-1} doxycycline (D9891; Sigma-Aldrich) were added to the medium, and cells were incubated for 24 h.

ER clearance was induced through application of rapamycin (Alfa Aesar) to a final concentration of 200 nM, to HCT116 cells expressing FKBP-GFP-Sec61β and stargazin-mCherry-FRB. For fixed cell experiments, rapamycin treatment was for 30 min.

Fluorescence methods

For immunofluorescence, cells were fixed at room temperature using PFA solution (3% formaldehyde and 4% sucrose in PBS) for 15 min and permeabilized at room temperature in 0.5% (vol/vol) Triton X-100 in PBS for 10 min. Cells were blocked in 3% BSA in PBS for 60 min at room temperature. Cells were then incubated for 60 min at room temperature with primary antibody dilutions prepared in 3% BSA in PBS as follows: mouse anti-Bub1 (ab54893, 1:500; Abcam); mouse anti-Mad2 (sc-65492, 1:200; Santa Cruz); rabbit anti-calnexin (ab22595, 1:200; Abcam); guinea pig anti-CENP-C (PD030, 1:2,000; Medical and Biological Labs Company); rabbit anti-H3K27ac (ab4729, 1:1,000; Abcam); rabbit anti-KDEL (PA1-013, 1:200; Invitrogen); and rabbit anti-kinastrin (HPA042027, 1:1,000; Atlas Antibodies). After three PBS washes, cells were incubated with secondary antibodies for 60 min and Alexa Fluor 568– or Alexa Fluor 647–conjugated antibody in 3% BSA/PBS (1:500; Invitrogen). After three PBS washes, coverslips were rinsed and mounted with Vectashield containing DAPI (Vector Laboratories) and sealed. In cases where GFP signal required amplification, cells were incubated with GFP-booster (Alexa Fluor 488, 1:200; Chromotek) at the secondary antibody step. Where amplification of mCherry was required, mouse anti-mCherry (1C51; ab125096, 1:500; Abcam) was used with Alexa Fluor 568–conjugated secondary antibody.

For FISH of DLD-1 WT and DLD-1-C-H3 cells, the degron system was induced, and cells were synchronized by doubled thymidine (2.5 mM) treatment. Samples were fixed in Carnoy's fixative (3:1 vol/vol methanol:glacial acetic acid) for 5 min at

room temperature, rinsed in fixative before addition of fresh fixative, and incubated for a further 10 min. Samples were rinsed in distilled water before FISH probe denaturation and hybridization following the manufacturer's protocol (Xcyting Centromere Enumeration Probe, XCE Y green, D-0824-050-FI; MetaSystems Probes). To dye chromosomes or microtubules in fixed- or live-cell imaging, cells were incubated for 30 min with 0.5 µM SiR-DNA or SiR-Tubulin (Spirochrome), respectively.

Biochemistry

For Western blot, cells were harvested, and lysates were prepared by sonication of cells in UTB buffer (8 M urea, 50 mM Tris, and 150 mM β-mercaptoethanol). Lysates were incubated on ice for 30 min, clarified in a benchtop centrifuge (20,800 *g*) for 15 min at 4°C, boiled in Laemmli buffer for 10 min, and resolved on a precast 4–15% polyacrylamide gel (Bio-Rad). Proteins were transferred to nitrocellulose using a Trans-Blot Turbo Transfer System (Bio-Rad). Primary antibodies were diluted in 4% BSA in PBS and used as follows: rabbit anti-Sec61β (PA3-015, 1:1,000; Invitrogen); HRP-conjugated mouse anti-β-actin (sc-47778, 1:20,000; Santa Cruz); rabbit anti-mCherry (ab183628, 1:2,000; Abcam); anti-GAPDH (G9545, 1:5,000; Sigma-Aldrich); rabbit anti-CENP-A (2186, 1:1,000; Cell Signaling); mouse anti-BAF (A-11, 1:500; Santa Cruz); and mouse anti-LBR (SAB1400151, 1:500; Sigma-Aldrich). Secondary antibodies of anti-mouse, anti-rabbit, and anti-rat IgG HRP conjugates were prepared in 5% milk in PBS. For detection, enhanced chemiluminescence detection reagent (GE Healthcare) and manual exposure of Hyperfilm (GE Healthcare) was performed.

Microscopy

For fixed-cell imaging experiments, a Personal DeltaVision microscope system (Applied Precision), based on an IX-71 microscope body (Olympus) was used with a CoolSNAP HQ2 interline charge-coupled device camera (Photometrics) and a 60× oil-immersion 1.42-NA oil PlanApo N objective and equipped with Precision Control microscope incubator, Tokai Hit stage top incubator, and Applied Precision motorized xyz stage. Illumination was via a Lumencor SPECTRA X light engine (DAPI, 395/25; GFP, 470/24; mCherry, 575/25; CY-5, 640/30), dichroics (quad: reflection 381-401:464-492:531-556:619-644; transmission 409-456:500-523:564-611:652-700; GFP/mCh: reflection 464-492:561-590; transmission 500-553:598-617) and filter sets (DAPI: excitation 387/11, emission 457/50; GFP: excitation 470/40, emission 525/50; TRITC: excitation 575/25, emission 597/45; mCherry: excitation 572/28, emission 632/60; and CY-5: excitation 640/14, emission 685/40). Image capture was by softWoRx 5.5.1 (Applied Precision). Images were deconvolved using softWoRx 3.0 with the following settings: conservative ratio, 15 cycles, and high noise filtering.

For live-cell imaging, cells were plated onto fluorodishes (WPI) and imaged in complete medium in an incubated chamber at 37°C and 5% CO_2. Most live-cell imaging was done using a Nikon CSU-W1 spinning disc confocal system; SoRa upgrade (Yokogawa) was used with either a Nikon 100×, 1.49 NA, oil, CFI SR HP Apo TIRF or 63×, 1.40 NA, oil, CFI Plan Apo objective with optional 2.3× intermediate magnification and 95B Prime camera (Photometrics). The system has a CSU-W1 (Yokogawa) spinning disk unit with 50 µm and SoRa disks (SoRa disk used), Nikon Perfect Focus autofocus, Okolab microscope incubator, Nikon motorized xy stage, and Nikon 200-µm z-piezo. Excitation was via 405-, 488-, 561-, and 638-nm lasers with 405/488/561/640-nm dichroic and blue, 446/60; green, 525/50; red, 600/52; and FRed, 708/75 emission filters. Acquisition and image capture was via NiS Elements (Nikon).

For mitotic progression and fate experiments, the DeltaVision system described above was used. For live-cell imaging of HeLa cells, a spinning disc confocal system (UltraView VoX; PerkinElmer) with a 60×, 1.40 NA, oil, Plan Apo VC objective (Nikon) was used. Images were captured using an ORCA-R2 digital charge-coupled device camera (Hamamatsu) after excitation with 488- and 561-nm lasers and 405/488/561/640-nm dichroic and 525/50, 615/70 filter sets. Images were captured using Volocity 6.3.1. All microscopy data were stored in an OMERO database in native file formats.

SBF-SEM

To prepare samples for SBF-SEM, RPE-1 GFP-Sec61β cells on gridded dishes were first incubated with 150 nM GSK923295 (Selleckchem) for 3 h to induce misaligned chromosomes, before release of cells from treatment and incubation for ∼30 min with 0.5 µM SiR-DNA (Spirochrome) to visualize DNA. HeLa cells on gridded dishes were not treated and were not stained. Using live-cell light microscopy, cells with an ensheathed chromosome were selected for SBF-SEM. Fluorescent and bright-field images of the selected cell were captured, and the coordinate position was recorded. Cells were washed twice with phosphate buffer (PB) before fixing (2.5% glutaraldehyde, 2% paraformaldehyde, 0.1% tannic acid [low molecular weight] in 0.1 M phosphate buffer, pH 7.4) for 1 h at room temperature. Samples were washed three times with PB and then postfixed in 2% reduced osmium (equal volume of 4% OsO_4 prepared in water and 3% potassium ferrocyanide in 0.1 M PB solution) for 1 h at room temperature, followed by a further three washes with PB. Cells were then incubated for 5 min at room temperature in 1% (wt/vol) thiocarbohydrazide solution, followed by three PB washes. A second osmium staining step was included, incubating cells in a 2% OsO_4 solution prepared in water for 30 min at room temperature, followed by three washes with PB. Cells were then incubated in 1% uranyl acetate solution at 4°C overnight. This was followed by a further three washes with PB. Walton's lead aspartate was prepared adding 66 mg lead nitrate (TAAB) to 9 ml 0.03 M aspartic acid solution at pH 4.5, and then adjusting to final volume of 10 ml with 0.03 M aspartic acid solution and to pH 5.5 (pH adjustments with KOH). Cells were incubated in Walton's lead aspartate for 30 min at room temperature and then washed three times in PB. Samples were dehydrated in an ethanol dilution series (30, 50, 70, 90, and 100% ethanol, 5-min incubation in each solution) on ice, and then incubated for a further 10 min in 100% ethanol at room temperature. Finally, samples were embedded in an agar resin (AGAR 100 R1140; Agar Scientific).

SBF-SEM data were segmented using Microscopy Image Browser v2.60, and the resulting 3D model was visualized in

IMOD v4.10.49 (Belevich et al., 2016; Kremer et al., 1996). HeLa SBF-SEM data was segmented and reconstructed in Amira 6.7 (Thermo Fisher Scientific).

Data analysis

Kinetochore position analysis was in two parts. First, the positions of kinetochores and spindle poles in hyperstacks were manually mapped using Cell Counter in Fiji. The kinetochore point sets were classified into three categories: those aligned at the metaphase plate and those that were misaligned, with the latter group subdivided into kinetochores of chromosomes that were ensheathed and those that were not (free). Second, the ER channel of the hyperstack was segmented in Fiji to delineate the exclusion zone. Next, the Cell Counter XML files and their respective binarized ER stacks were read by program written in Igor Pro (WaveMetrics). To analyze the position of points relative to the exclusion zone in each cell, the ratio of two Euclidean distances was calculated (see Eq. 1). Where C is the centroid of all aligned kinetochores, P_i is the position of a kinetochore and Q_i is the point on the path from C through P, where the exclusion zone/ER boundary intersects with the path.

$$\frac{\overline{CP_i}}{\overline{CQ_i}}. \quad (1)$$

The ratio of these two distances gave a measure of how deep the point was placed inside or outside the exclusion zone (0 being on the boundary and 1 being as far outside of the exclusion zone as from the centroid to the boundary, on a $\log_2$ scale).

For analysis of live-cell GFP-Mad2 and mCherry-Sec61β imaging, a semiautomated 4D tracking procedure was used. Briefly, the DNA channel from these videos was used for segmentation of chromosomes and metaphase plate as discrete 3D objects over time. The centroid-to-centroid distance was found for each chromosome relative to the plate (congression was taken as the merging of chromosome and plate objects), and the time of anaphase onset was determined. Fluorescence signals were taken from each chromosome object using a 3-pixel expansion of the region of interest (ROI). For mCherry-Sec61β, the mean voxel density was used. For GFP-Mad2, the maximum pixel intensity at each z position was taken from the expanded ROI and averaged per time point; this method gave a more accurate measure of Mad2 recruitment than the mean voxel density. Signals from each channel are expressed as a ratio of chromosome to plate. Mad2 signals were grouped by whether the chromosome congressed, and then measurements from all chromosomes relative to anaphase were used to fit a line by linear regression. Only the last chromosome to congress (or not) was analyzed per cell. Data processing was via Fiji/ImageJ followed by analysis in Igor Pro.

Automated kinetochore-kinastrin colocalization was using a script that located the 3D position of kinetochores (CENP-C) and kinastrin puncta from thresholded images using 3D Object Counter in Fiji. These positions were loaded into Igor, and the Euclidean distance to the nearest kinastrin punctum from each kinetochore was found. ER clearance experiments were quantified using two automated procedures. First, ER, DNA, and plasma membrane were segmented separately, the plasma membrane segments were used to define the cell, and the total area of segmented ER within this region was measured for all z-positions over time using a Fiji macro. Data were read by Igor, and the ER volume over time was calculated. ER clearance manifested as a rapid decrease in ER volume, but the onset was variable. The derivative of ER volume over time was used to find the point of rapid decrease, and this point was used to define the time to ER clearance. Random fluctuations in otherwise constant ER volume over time also resulted in minima that occurred randomly. This process was modeled and plotted for comparison with the control group, where no clearance was seen. Second, the segmented DNA was classified into misaligned chromosome and main chromosome mass by a user blind to the conditions of the experiment. 3D coordinates of these two groups were fed into Igor, where the centroids and boundaries of the chromosome and main chromosome mass were defined. The closest Euclidean distance between the centroid of the chromosome and edge of the main chromosome mass was used as the distance. Misalignment, shown as a colorscale, is this distance normalized to the starting distance. Figures were made with Fiji, R, or Igor Pro and assembled using Adobe Illustrator.

Statistical testing

Comparison of mitotic timing distributions was done using a Kolmogorov–Smirnov test (P values are $P_n[\varepsilon]$). The effect of presence of ensheathed chromosome on mitotic fate (frequency of micronucleus formation) was examined using Fisher's exact test with no correction. Chromosome congression times were not normally distributed, and so the effect of ER clearance was determined using Wilcoxon rank test. Exact P values for all tests are quoted, rather than using arbitrary levels of significance.

Online supplemental material

Fig. S1 shows ensheathed chromosomes in DLD-1 cells. Fig. S2 shows spindle assembly checkpoint activation and micronucleus formation in DLD-1 cells. Fig. S3 shows lack of microtubule attachments of ensheathed chromosomes. Fig. S4 shows mitotic timing and fate of HCT116 cells pretreated with CENP-E inhibitor. Fig. S5 shows stable transgene expression in RPE1 cells. Video 1 shows a 3D reconstruction of an ensheathed chromosome in a HeLa cell. Video 2 shows a 3D reconstruction of an ensheathed chromosome in a HeLa cell. Video 3 shows a 3D reconstruction of an ensheathed chromosome in an RPE-1 cell. Video 4 shows an example of GFP-Mad2 at an ensheathed chromosome. Video 5 shows an example of mitotic outcome of a cell with aligned chromosomes. Video 6 shows an example of mitotic outcome of a cell with an ensheathed chromosome. Video 7 shows an example of ER clearance and subsequent rescue of an ensheathed chromosome.

Data availability

All code used in the manuscript is available at https://github.com/quantixed/Misseg.

Acknowledgments

We thank Claire Mitchell and Laura Cooper from the Computing and Advanced Microscopy Unit (CAMDU) for their help and

support. Faye Nixon, Alison Beckett and Ian Prior at the Liverpool Biomedical EM Unit provided SBF-SEM imaging. We are grateful to Richard Bayliss, Vishakha Karnawat, Jonathan Millar, Alonso Pardal and James Shelford for feedback on the project and manuscript.

This work was supported by a Pioneer Award and Programme Award from Cancer Research UK (C25425/A24167 and C25425/A27718). L. Downie was supported by a studentship from BBSRC Midlands Integrative Biosciences Training Partnership (BB/M01116X/1).

The authors declare no competing financial interests.

Author contributions: Conceptualization—N. Ferrandiz; investigation and resources—N. Ferrandiz and L. Downie; formal analysis—L. Downie and S.J. Royle; funding acquisition and software—S.J. Royle; supervision and writing—original draft—M. Ferrandiz and S.J. Royle; visualization—G.P. Starling and S.J. Royle; writing—review & editing—N. Ferrandiz, L. Downie and S.J. Royle.

Submitted: 5 March 2022
Revised: 29 March 2022
Accepted: 5 April 2022

References

Bajer, A. 1957. Ciné-micrographic studies on mitosis in endosperm. III. The origin of the mitotic spindle. *Exp. Cell Res.* 13:493–502. https://doi.org/10.1016/0014-4827(57)90078-2

Bakhoum, S.F., B. Ngo, A.M. Laughney, J.-A. Cavallo, C.J. Murphy, P. Ly, P. Shah, R.K. Sriram, T.B.K. Watkins, N.K. Taunk, et al. 2018. Chromosomal instability drives metastasis through a cytosolic DNA response. *Nature.* 553:467–472. https://doi.org/10.1038/nature25432

Belevich, I., M. Joensuu, D. Kumar, H. Vihinen, and E. Jokitalo. 2016. Microscopy image browser: A platform for segmentation and analysis of multidimensional datasets. *PLoS Biol.* 14:e1002340. https://doi.org/10.1371/journal.pbio.1002340

van Bergeijk, P., M. Adrian, C.C. Hoogenraad, and L.C. Kapitein. 2015. Optogenetic control of organelle transport and positioning. *Nature.* 518:111–114. https://doi.org/10.1038/nature14128

Champion, L., M.I. Linder, and U. Kutay. 2017. Cellular reorganization during mitotic entry. *Trends Cell Biol.* 27:26–41. https://doi.org/10.1016/j.tcb.2016.07.004

Champion, L., S. Pawar, N. Luithle, R. Ungricht, and U. Kutay. 2019. Dissociation of membrane-chromatin contacts is required for proper chromosome segregation in mitosis. *Mol. Biol. Cell.* 30:427–440. https://doi.org/10.1091/mbc.E18-10-0609

Cheeseman, L.P., E.F. Harry, A.D. McAinsh, I.A. Prior, and S.J. Royle. 2013. Specific removal of TACC3-ch-TOG-clathrin at metaphase deregulates kinetochore fiber tension. *J. Cell Sci.* 126:2102–2113. https://doi.org/10.1242/jcs.124834

Cimini, D., B. Howell, P. Maddox, A. Khodjakov, F. Degrassi, and E.D. Salmon. 2001. Merotelic kinetochore orientation is a major mechanism of aneuploidy in mitotic mammalian tissue cells. *J. Cell Biol.* 153:517–527. https://doi.org/10.1083/jcb.153.3.517

Clarke, N.I., and S.J. Royle. 2018. FerriTag is a new genetically-encoded inducible tag for correlative light-electron microscopy. *Nat. Commun.* 9:2604. https://doi.org/10.1038/s41467-018-04993-0

Crasta, K., N.J. Ganem, R. Dagher, A.B. Lantermann, E.V. Ivanova, Y. Pan, L. Nezi, A. Protopopov, D. Chowdhury, and D. Pellman. 2012. DNA breaks and chromosome pulverization from errors in mitosis. *Nature.* 482:53–58. https://doi.org/10.1038/nature10802

Daum, J.R., T.A. Potapova, S. Sivakumar, J.J. Daniel, J.N. Flynn, S. Rankin, and G.J. Gorbsky. 2011. Cohesion fatigue induces chromatid separation in cells delayed at metaphase. *Curr. Biol.* 21:1018–1024. https://doi.org/10.1016/j.cub.2011.05.032

Duijf, P.H.G., and R. Benezra. 2013. The cancer biology of whole-chromosome instability. *Oncogene.* 32:4727–4736. https://doi.org/10.1038/onc.2012.616

Dunlop, M.H., A.M. Ernst, L.K. Schroeder, D.K. Toomre, G. Lavieu, and J.E. Rothman. 2017. Land-locked mammalian Golgi reveals cargo transport between stable cisternae. *Nat. Commun.* 8:432. https://doi.org/10.1038/s41467-017-00570-z

Dunsch, A.K., E. Linnane, F.A. Barr, and U. Gruneberg. 2011. The astrin-kinastrin/SKAP complex localizes to microtubule plus ends and facilitates chromosome alignment. *J. Cell Biol.* 192:959–968. https://doi.org/10.1083/jcb.201008023

Fujiwara, T., M. Bandi, M. Nitta, E.V. Ivanova, R.T. Bronson, and D. Pellman. 2005. Cytokinesis failure generating tetraploids promotes tumorigenesis in p53-null cells. *Nature.* 437:1043–1047. https://doi.org/10.1038/nature04217

Funk, L.C., L.M. Zasadil, and B.A. Weaver. 2016. Living in CIN: Mitotic infidelity and its consequences for tumor promotion and suppression. *Dev. Cell.* 39:638–652. https://doi.org/10.1016/j.devcel.2016.10.023

Ghadimi, B.M., D.L. Sackett, M.J. Difilippantonio, E. Schröck, T. Neumann, A. Jauho, G. Auer, and T. Ried. 2000. Centrosome amplification and instability occurs exclusively in aneuploid, but not in diploid colorectal cancer cell lines, and correlates with numerical chromosomal aberrations. *Genes Chromosomes Cancer.* 27:183–190.

Hatch, E.M., A.H. Fischer, T.J. Deerinck, and M.W. Hetzer. 2013. Catastrophic nuclear envelope collapse in cancer cell micronuclei. *Cell.* 154:47–60. https://doi.org/10.1016/j.cell.2013.06.007

Hepler, P.K., and S.M. Wolniak. 1984. Membranes in the mitotic apparatus: Their structure and function. *Int. Rev. Cytol.* 90:169–238. https://doi.org/10.1016/s0074-7696(08)61490-4

Hirst, J., J.R. Edgar, G.H.H. Borner, S. Li, D.A. Sahlender, R. Antrobus, and M.S. Robinson. 2015. Contributions of epsinR and gadkin to clathrin-mediated intracellular trafficking. *Mol. Biol. Cell.* 26:3085–3103. https://doi.org/10.1091/mbc.E15-04-0245

Kalitsis, P., E. Earle, K.J. Fowler, and K.H. Choo. 2000. Bub3 gene disruption in mice reveals essential mitotic spindle checkpoint function during early embryogenesis. *Genes Dev.* 14:2277–2282. https://doi.org/10.1101/gad.827500

Kremer, J.R., D.N. Mastronarde, and J.R. McIntosh. 1996. Computer visualization of three-dimensional image data using IMOD. *J. Struct. Biol.* 116:71–76. https://doi.org/10.1006/jsbi.1996.0013

Kumar, D., B. Golchoubian, I. Belevich, E. Jokitalo, and A.-L. Schlaitz. 2019. REEP3 and REEP4 determine the tubular morphology of the endoplasmic reticulum during mitosis. *Mol. Biol. Cell.* 30:1377–1389. https://doi.org/10.1091/mbc.E18-11-0698

Larocque, G., P.J. La-Borde, N.I. Clarke, N.J. Carter, and S.J. Royle. 2020. Tumor protein D54 defines a new class of intracellular transport vesicles. *J. Cell Biol.* 219:e201812044. https://doi.org/10.1083/jcb.201812044

Liu, S., M. Kwon, M. Mannino, N. Yang, F. Renda, A. Khodjakov, and D. Pellman. 2018. Nuclear envelope assembly defects link mitotic errors to chromothripsis. *Nature.* 561:551–555. https://doi.org/10.1038/s41586-018-0534-z

Lu, L., M.S. Ladinsky, and T. Kirchhausen. 2009. Cisternal organization of the endoplasmic reticulum during mitosis. *Mol. Biol. Cell.* 20:3471–3480. https://doi.org/10.1091/mbc.e09-04-0327

Lu, L., M.S. Ladinsky, and T. Kirchhausen. 2011. Formation of the postmitotic nuclear envelope from extended ER cisternae precedes nuclear pore assembly. *J. Cell Biol.* 194:425–440. https://doi.org/10.1083/jcb.201012063

Ly, P., L.S. Teitz, D.H. Kim, O. Shoshani, H. Skaletsky, D. Fachinetti, D.C. Page, and D.W. Cleveland. 2017. Selective Y centromere inactivation triggers chromosome shattering in micronuclei and repair by non-homologous end joining. *Nat. Cell Biol.* 19:68–75. https://doi.org/10.1038/ncb3450

Mammel, A.E., H.Z. Huang, A.L. Gunn, E. Choo, and E.M. Hatch. 2021. Chromosome length and gene density contribute to micronuclear membrane stability. *Life Sci. Alliance.* 5:e202101210. https://doi.org/10.26508/lsa.202101210

Merta, H., J.W. Carrasquillo Rodríguez, M.I. Anjur-Dietrich, T. Vitale, M.E. Granade, T.E. Harris, D.J. Needleman, and S. Bahmanyar. 2021. Cell cycle regulation of ER membrane biogenesis protects against chromosome missegregation. *Dev. Cell.* https://doi.org/10.1016/j.devcel.2021.11.009

Nicholson, J.M., and D. Cimini. 2015. Link between aneuploidy and chromosome instability. *Int. Rev. Cell Mol. Biol.* 315:299–317https://doi.org/10.1016/bs.ircmb.2014.11.002

Nixon, F.M., T.R. Honnor, N.I. Clarke, G.P. Starling, A.J. Beckett, A.M. Johansen, J.A. Brettschneider, I.A. Prior, and S.J. Royle. 2017. Microtubule organization within mitotic spindles revealed by serial block face

scanning electron microscopy and image analysis. *J. Cell Sci.* 130: 1845–1855. https://doi.org/10.1242/jcs.203877

Porter, K.R., and R.D. Machado. 1960. Studies on the endoplasmic reticulum. IV. Its form and distribution during mitosis in cells of onion root tip. *J. Biophys. Biochem. Cytol.* 7:167–180. https://doi.org/10.1083/jcb.7.1.167

Puhka, M., M. Joensuu, H. Vihinen, I. Belevich, and E. Jokitalo. 2012. Progressive sheet-to-tubule transformation is a general mechanism for endoplasmic reticulum partitioning in dividing mammalian cells. *Mol. Biol. Cell.* 23:2424–2432. https://doi.org/10.1091/mbc.E10-12-0950

Puhka, M., H. Vihinen, M. Joensuu, and E. Jokitalo. 2007. Endoplasmic reticulum remains continuous and undergoes sheet-to-tubule transformation during cell division in mammalian cells. *J. Cell Biol.* 179:895–909. https://doi.org/10.1083/jcb.200705112

Schlaitz, A.-L., J. Thompson, C.C.L. Wong, J.R. Yates, and R. Heald. 2013. REEP3/4 ensure endoplasmic reticulum clearance from metaphase chromatin and proper nuclear envelope architecture. *Dev. Cell.* 26: 315–323. https://doi.org/10.1016/j.devcel.2013.06.016

Schweizer, N., N. Pawar, M. Weiss, and H. Maiato. 2015. An organelle-exclusion envelope assists mitosis and underlies distinct molecular crowding in the spindle region. *J. Cell Biol.* 210:695–704. https://doi.org/10.1083/jcb.201506107

Uetake, Y., and G. Sluder. 2010. Prolonged prometaphase blocks daughter cell proliferation despite normal completion of mitosis. *Curr. Biol.* 20: 1666–1671. https://doi.org/10.1016/j.cub.2010.08.018

Vedrenne, C., D.R. Klopfenstein, and H.-P. Hauri. 2005. Phosphorylation controls CLIMP-63-mediated anchoring of the endoplasmic reticulum to microtubules. *Mol. Biol. Cell.* 16:1928–1937. https://doi.org/10.1091/mbc.e04-07-0554

Wang, X., N. Le, A. Denoth-Lippuner, Y. Barral, and R. Kroschewski. 2016. Asymmetric partitioning of transfected DNA during mammalian cell division. *Proc. Natl. Acad. Sci. USA.* 113:7177–7182. https://doi.org/10.1073/pnas.1606091113

Warren, G. 1993. Membrane partitioning during cell division. *Annu. Rev. Biochem.* 62:323–348. https://doi.org/10.1146/annurev.bi.62.070193.001543

Wood, K.W., L. Lad, L. Luo, X. Qian, S.D. Knight, N. Nevins, K. Brejc, D. Sutton, A.G. Gilmartin, P.R. Chua, et al. 2010. Antitumor activity of an allosteric inhibitor of centromere-associated protein-E. *Proc. Natl. Acad. Sci. USA.* 107:5839–5844. https://doi.org/10.1073/pnas.0915068107

Yang, Z., J. Loncarek, A. Khodjakov, and C.L. Rieder. 2008. Extra centrosomes and/or chromosomes prolong mitosis in human cells. *Nat. Cell Biol.* 10: 748–751. https://doi.org/10.1038/ncb1738

Supplemental material

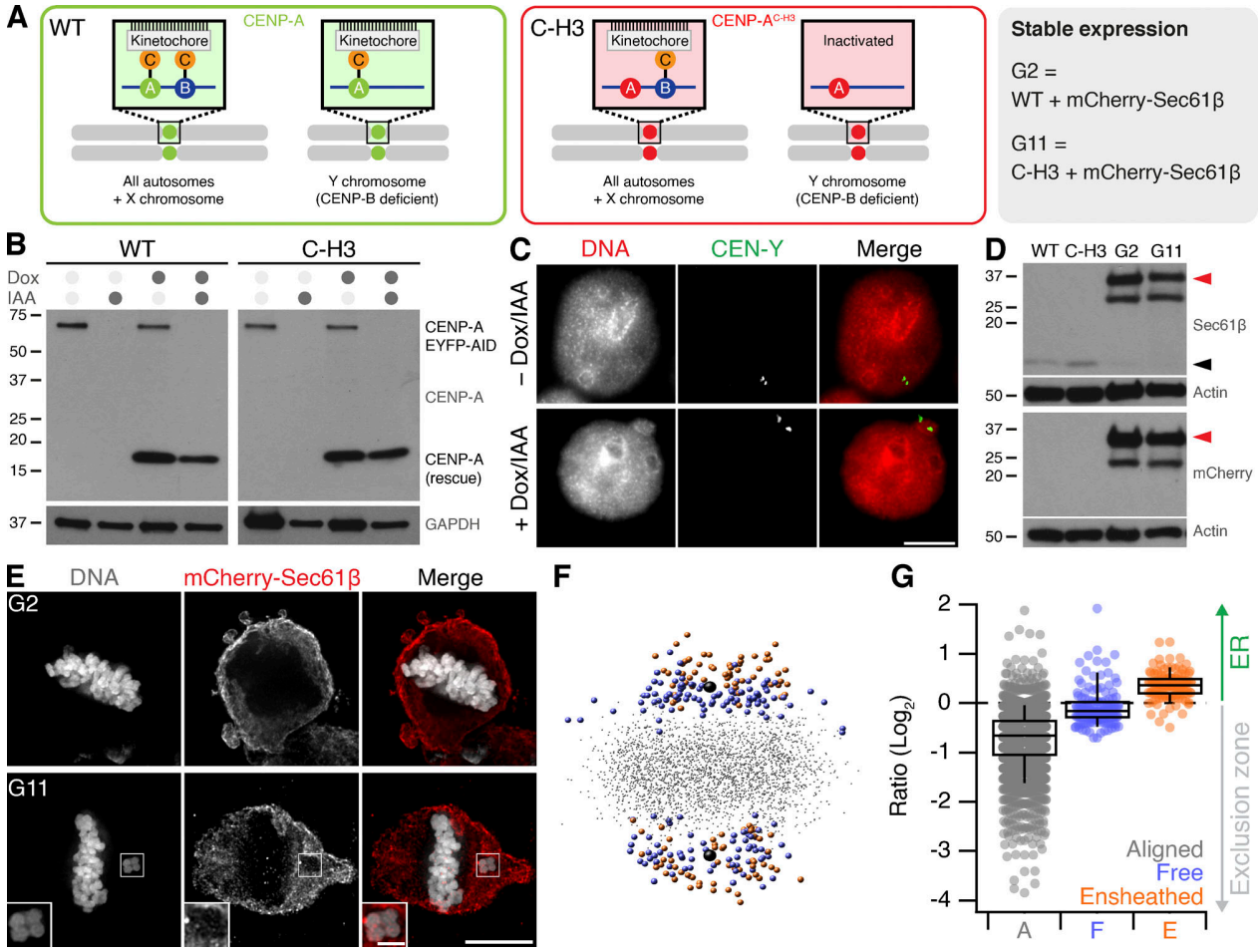

Figure S1. **Ensheathed chromosomes in DLD-1 cells after targeted missegregation of Y-chromosome. (A)** Schematic diagram after Ly et al. (2017), showing how reexpression of a CENP-A mutant (C-H3) in DLD-1 cells where CENP-A is degraded causes selective misalignment of the Y-chromosome. WT and C-H3 lines were further modified to express mCherry-Sec61β. **(B)** Western blot of lysates from WT or C-H3 DLD-1 cells treated with doxycycline (Dox) and/or indole-3-acetic acid (IAA) as indicated. Upper blot shows anti-CENP-A detection of endogenous CENP-A fused to EYFP-AID tag (66 kD) and expression of untagged CENP-A (either WT or C-H3). Lower blot shows GAPDH loading control. **(C)** Typical FISH images locating the Y-chromosome in the main nucleus in control cells and in a micronucleus in cells expressing C-H3 CENP-A. Scale bar, 10 µm. **(D)** Western blot of lysates from stable cell lines expressing mCherry-Sec61β derived from WT (G2) or C-H3 (G11). Detection of Sec61β or mCherry is shown as indicated with actin loading controls. Migration of Sec61β and mCherry-Sec61β is indicated by black and red arrowheads, respectively. Note that the expression of mCherry-Sec61β downregulates endogenous Sec61β. **(E)** Deconvolved wide-field microscopy images showing an ensheathed chromosome in G11 cells but not in G2 cells treated with Dox/IAA. Scale bars, 10 µm; 2 µm (insets). **(F)** Spatially averaged view of all kinetochores in the G11 DLD-1 Dox/IAA dataset (see Materials and methods). Small gray points represent kinetochores at the metaphase plate. Colored points represent misaligned chromosomes that were ensheathed (orange) and those that were not (blue). Spindle poles are shown in black. **(G)** Box plot to show the relative position of each kinetochore relative to the exclusion zone boundary. Ratio of kinetochores within the exclusion zone are <0 and those within the ER are >0 on a $\log_2$ scale. Dots represent kinetochore ratios from 50 DLD-1 cells at metaphase. Boxes show IQR, bar represents the median, and whiskers show 9th and 91st percentiles. Source data are available for this figure: SourceData FS1.

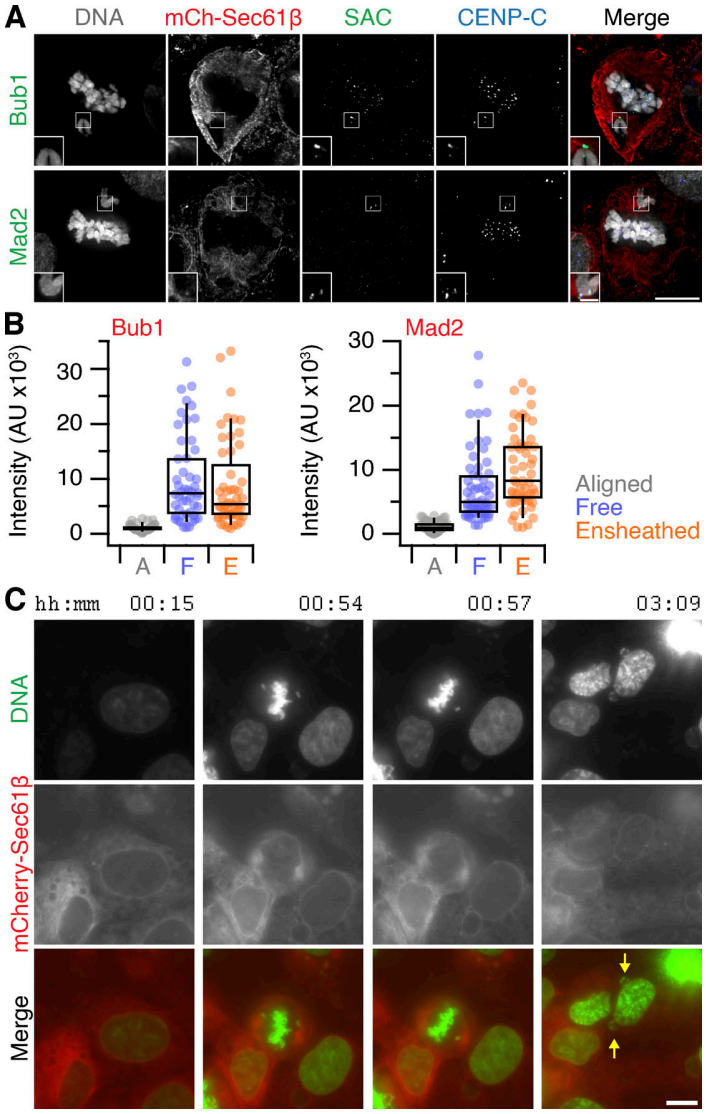

Figure S2. **Spindle assembly checkpoint and micronucleus formation in DLD-1 cells. (A)** Micrographs of immunofluorescence experiments to detect Bub1 or Mad2 (SAC, green) at kinetochores (CENP-C, blue) in cells stably expressing mCherry-Sec61β (red); DAPI-stained DNA is shown in gray. Scale bars, 10 µm; 2 µm (insets). **(B)** Quantification of Bub1 and Mad2 immunofluorescence at kinetochores marked by CENP-C. Ensheathed chromosomes were classified using the mCherry-Sec61β signal. Dots show kinetochore measurements, boxes show IQR, bar represents the median, and whiskers show 9th and 91st percentiles (Bub1: n_A = 52, n_F = 49, n_E = 52; (Mad2: n_A = 55, n_F = 57, n_E = 55). **(C)** Stills from a video showing an example of ensheathed chromosomes in G11 DLD-1 cells forming micronuclei following Dox/IAA treatment. Scale, 10 µm.

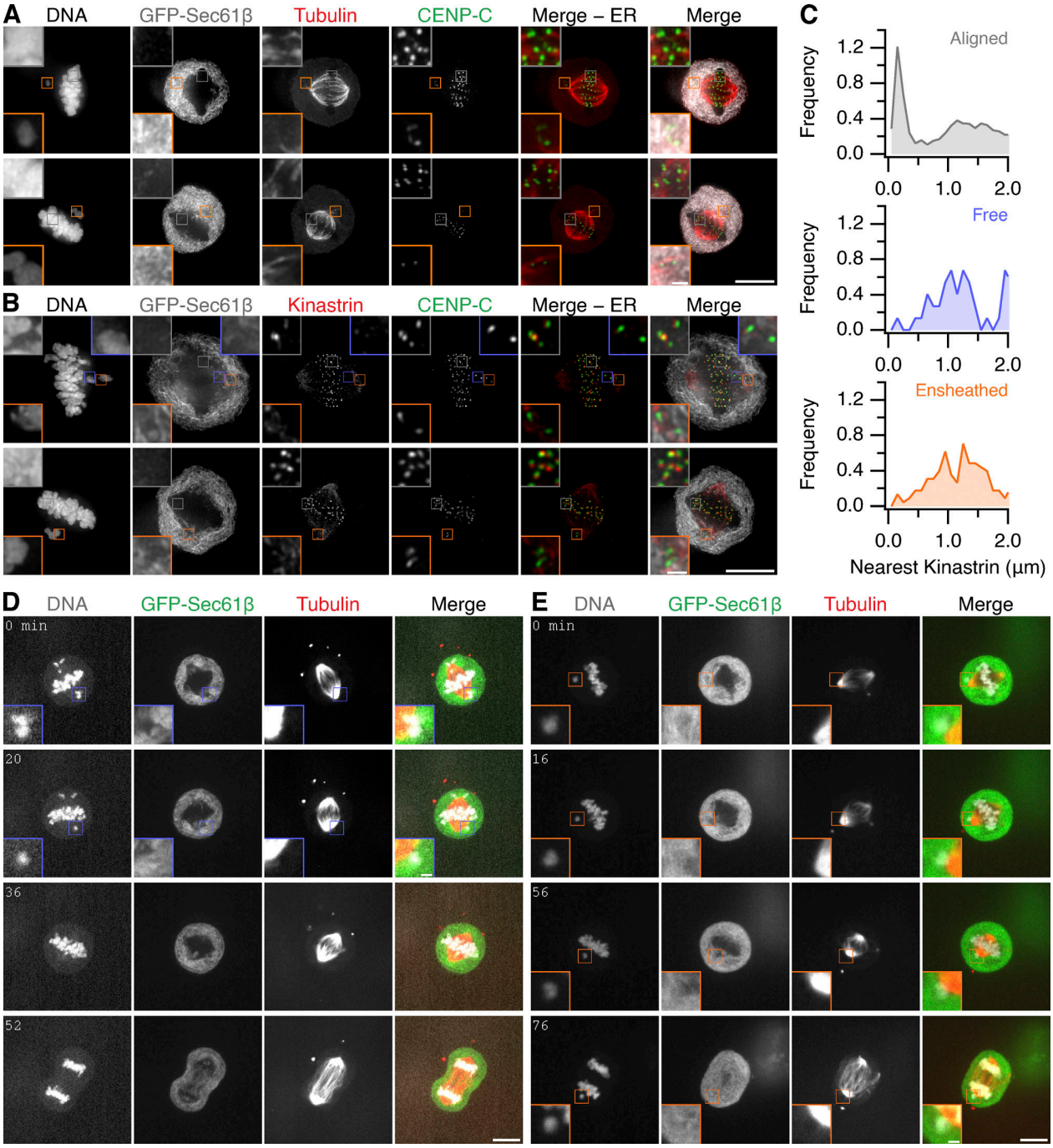

Figure S3. **Ensheathed chromosomes do not have stable microtubule-kinetochore attachment. (A)** Micrographs of RPE-1 cells stably expressing GFP-Sec61β (gray) pretreated with GSK923295 immunostained for tubulin (red) and CENP-C (green); DNA stained with DAPI. Examples show end-on attachments at aligned kinetochores and potential lateral kinetochore-MT contacts for ensheathed chromosomes. **(B)** Micrographs of RPE-1 cells stably expressing GFP-Sec61β (gray) pretreated with GSK923295 immunostained for kinastrin (red) and CENP-C (green); DNA stained by DAPI. Scale bars, 10 µm; 2 µm (insets). **(C)** Frequency distributions of the proximity of the nearest kinastrin punctum to each kinetochore (CENP-C punctum). Kinetochores (n, % with kinastrin <600 nm): aligned (3,124, 26.8%); free (74, 4.1%); ensheathed (227, 6.2%). **(D and E)** Still images from live-cell imaging experiments of RPE-1 cells stably expressing GFP-Sec61β (green) and Histone H3.2-mCherry (gray), pretreated with 150 nM GSK923295 and stained with SiR-Tubulin (red). Similar results were recorded in 25 cells with free chromosomes and 16 cells with ensheathed chromosomes. Scale bars, 10 µm; 2 µm (insets).

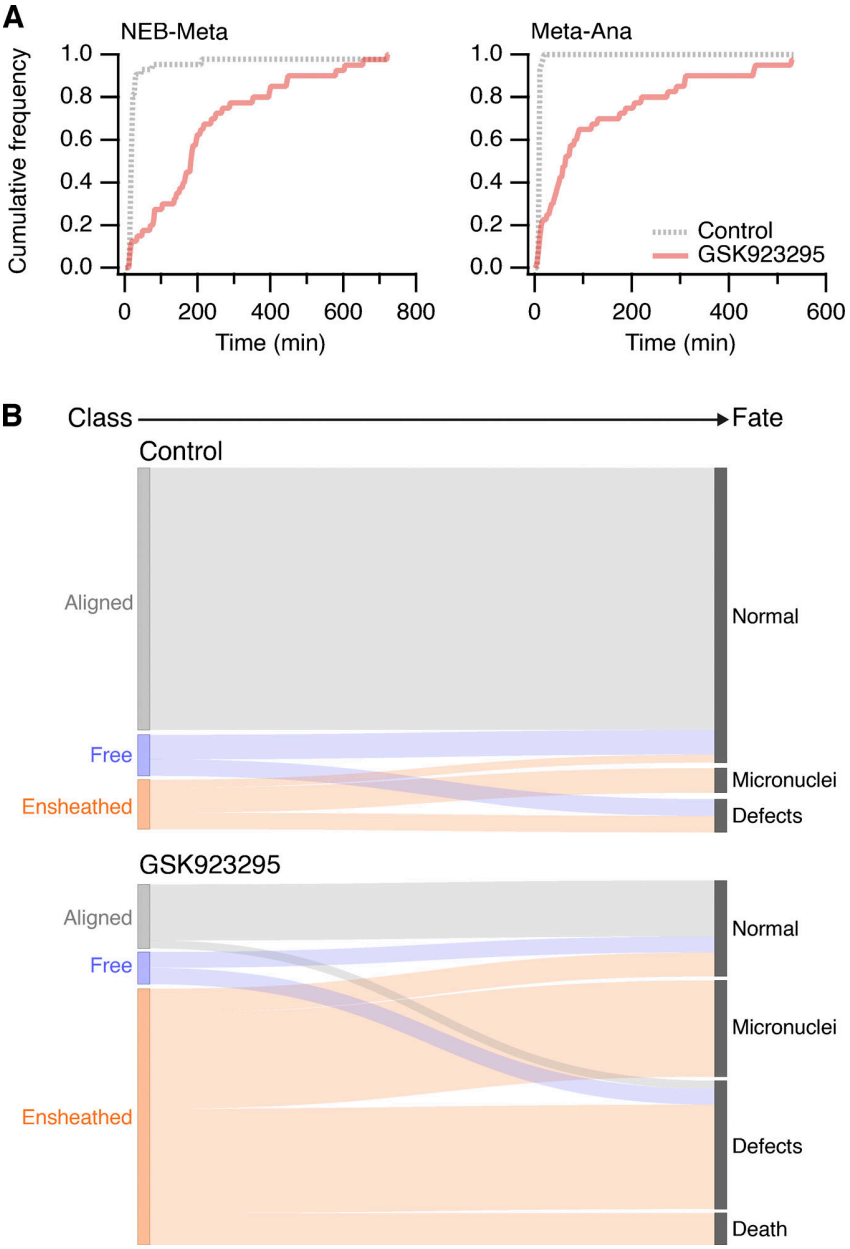

Figure S4. **Mitotic timing and fate of HCT116 cells pretreated with CENP-E inhibitor. (A)** Mitotic timing of HCT116 cells. Cumulative frequencies for NEB to metaphase (NEB-Meta) and metaphase to anaphase (Meta-Ana) are shown. Cells were treated with 150 nM GSK923295 for 3 h before washout for 1 h and subsequent imaging. Control, *n* = 43, GSK pretreatment, *n* = 40; pooled from three experiments. **(B)** Sankey diagram to show the fate (right) of cells in each of the three metaphase classes (left). Fates include normal division, micronuclei formation, death, and other defects (lagging chromosome, cytokinesis failure). Note that the fate of cells (and not chromosomes) is tracked.

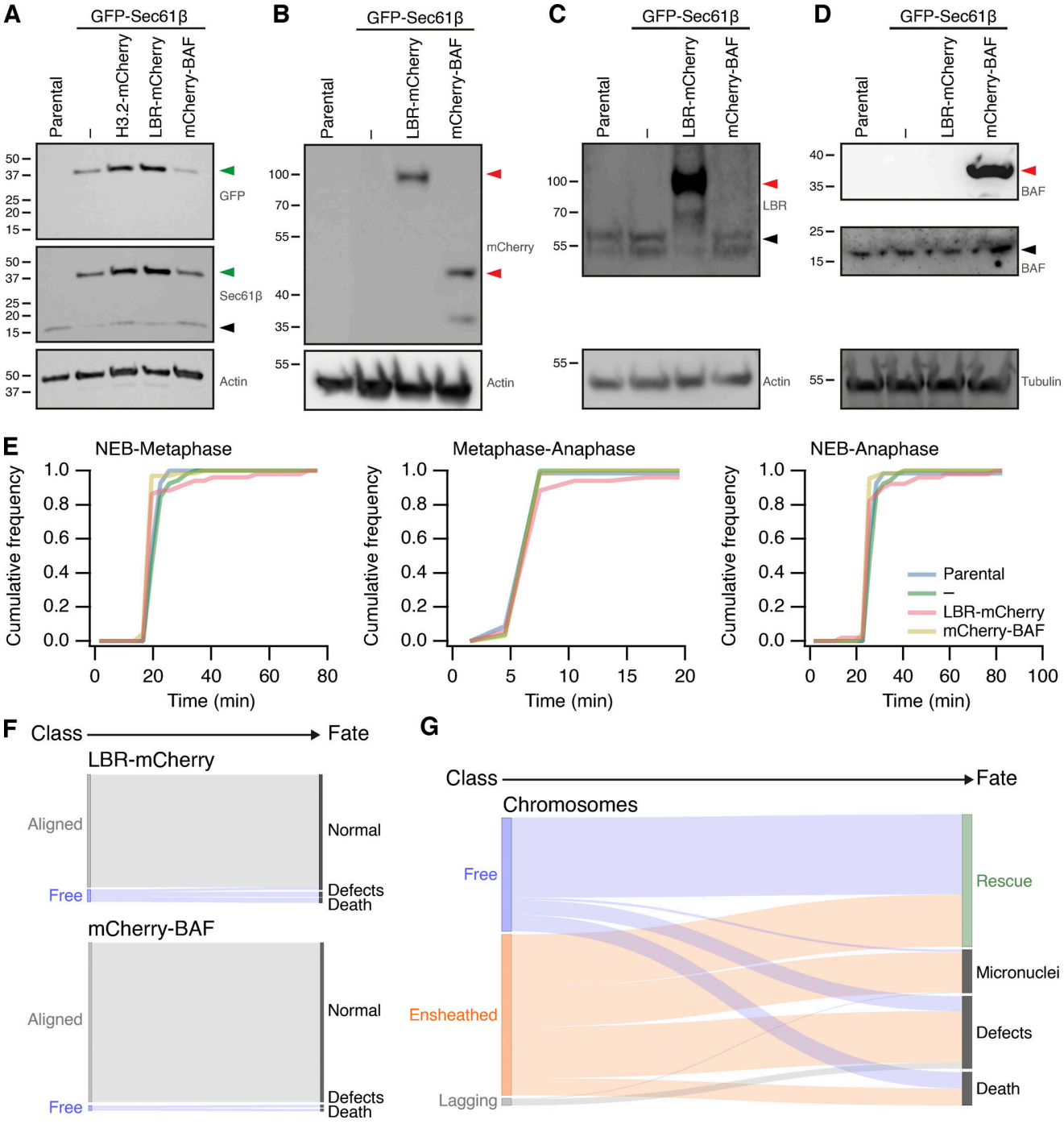

Figure S5. **Stable transgene expression in RPE1 cells and fate of misaligned chromosomes in RPE1 cells stably expressing GFP-Sec61β. (A–D)** Western blots to examine expression of proteins in parental RPE1 cells or clonal cells stably expressing GFP-Sec61β alone or with Histone3.2-mCherry, LBR-mCherry, or mCherry-BAF, as indicated. Membranes were probed for GFP, Sec61β, mCherry, LBR, BAF. Actin or tubulin is shown as a loading control. Green or red arrowheads indicate the expected position of GFP- or mCherry-tagged protein; black arrowheads indicate the untagged protein. **(E)** Mitotic timing of RPE1 cells stably expressing transgenes. Cumulative frequencies for NEB to metaphase, metaphase to anaphase, and NEB to anaphase are shown. Parental, $n = 69$; GFP-Sec61β alone, $n = 52$; GFP-Sec61β and LBR-mCherry, $n = 66$; GFP-Sec61β and mCherry-BAF, $n = 51$. **(F)** Sankey diagram to show the fate (right) of RPE1 cells in each of the three metaphase classes (left). Fates include normal division, micronuclei formation, death, and other defects (lagging chromosome, cytokinesis failure). Note that the fate of cells (and not chromosomes) is tracked. LBR-mCherry/GFP-Sec61β, $n = 51$; mCherry-BAF/GFP-Sec61β, $n = 67$; pooled from three experiments. **(G)** Sankey diagram to show the fate (right) of chromosomes in each of the three metaphase classes (left) after GSK923295 pretreatment. Fates include rescue, micronuclei formation, death, and other defects (lagging chromosome, cytokinesis failure). Number of chromosomes: free, 146; ensheathed, 207; lagging, 9. The same dataset was analyzed for the outcome of cells (classified by the final misaligned chromosome) in Fig. 4. Note that ensheathed chromosomes at metaphase that were rescued all became "free" chromosomes before rescue. Source data are available for this figure: SourceData FS5.

Video 1. **3D reconstruction of an ensheathed chromosome in a HeLa cell.** SBF-SEM data from a HeLa cell with spontaneously occurring ensheathed chromosome. The following cellular features are shown (in order of appearance): spindle microtubules (green), centrioles (yellow), DNA (red), mitochondria (multicolored then gold), endomembranes (white), plasma membrane (blue). Playback, 25 fps.

Video 2. **3D reconstruction of an ensheathed chromosome in a HeLa cell.** Same reconstruction but showing only chromosomes (red) and endomembranes (blue). Endomembranes that ensheath the chromosome of interest are shown in purple. Playback, 25 fps.

Video 3. **3D reconstruction of an ensheathed chromosome in an RPE-1 cell.** A substack from SBF-SEM imaging showing a chromosome (gray) outside the exclusion zone (pink), ensheathed in endomembranes (blue). Three complete rotations are shown with DNA only, DNA plus exclusion zone boundary, finally with endomembranes (ER and mitochondria, brown) added. Scale bar, 2 µm. Playback, 4 fps.

Video 4. **Example of GFP-Mad2 at an ensheathed chromosome.** GSK923295-pretreated RPE-1 cell stably expressing GFP-Mad2 (left) and mCherry-Sec61β (middle) with DNA stained with SiR-DNA (right). Time, hh:mm. Playback, 8 fps.

Video 5. **Example of mitotic outcome of a cell with aligned chromosomes.** Control RPE-1 cell expressing GFP-Sec61β (green) stained with SiR-DNA (red). Cell has all chromosomes aligned and divides normally. Time, hh:mm. Playback, 8 fps.

Video 6. **Example of mitotic outcome of a cell with an ensheathed chromosome.** GSK923295-pretreated RPE-1 cell expressing GFP-Sec61β (green) stained with SiR-DNA (red). Cell has an ensheathed chromosome and missegregates, leading to a micronucleus. Time, hh:mm. Playback, 8 fps.

Video 7. **Example of ER clearance and subsequent rescue of an ensheathed chromosome.** Control (left) and ER clearance (right) in mitotic HCT116 cells expressing FKBP-GFP-Sec61β (green) and Stargazin-mCherry-FRB (red). DNA is stained with SiR-DNA (magenta). Scale bar, 10 µm. Playback, 10 fps.